TOWARDS EFFICIENT AND ROBUST CONTROL OF BIPEDAL WALKING

BASIC MODELS OF POSTURE AND RHYTHMIC MOVEMENT

Bart Verdaasdonk

De promotiecommissie is als volgt samengesteld:

Voorzitter en Secretaris:	
Prof. dr. F. Eising	Universiteit Twente
Promotoren:	
Prof. dr. F.C.T. van der Helm	Universiteit Twente
Prof. dr. ir. H.F.J.M. Koopman	Universiteit Twente
Referent:	
Dr. ir. M. Wisse	TU Delft
Leden:	
Prof. dr. S.A. van Gils	Universiteit Twente
Prof. dr. J.S. Rietman	Universiteit Twente
Prof. dr. E. Otten	RU Groningen
Prof. dr. ir. S. Stramigioli	Universiteit Twente
Dr. J.B. Dingwell, Ph.D.	University of Texas

The publication of this Ph.D. thesis was financially supported by:

Anna Fonds, Leiden
Nefit BV, Deventer

Printed by Gildeprint Drukkerijen, Enschede, The Netherlands

Cover design: Gea Bisschop
Cover photo: edited version of the original by Lodewijk van Dongen

ISBN 978-90-365-2608-1

TOWARDS EFFICIENT AND ROBUST CONTROL OF BIPEDAL WALKING

BASIC MODELS OF POSTURE AND RHYTHMIC MOVEMENT

Proefschrift

ter verkrijging van
de graad van doctor aan de Universiteit Twente
op gezag van de rector magnificus,
prof. dr. W.H.M. Zijm,
volgens het besluit van het College voor Promoties
in het openbaar te verdedigen
op vrijdag 8 februari 2008 om 16:45 uur

door

Bart Willem Verdaasdonk

geboren op 12 januari 1975
te Groenlo

Dit proefschrift is goedgekeurd door promotoren:

Prof. dr. F.C.T. van der Helm
Prof. dr. ir. H.F.J.M. Koopman

Contents

Chapter 1

Introduction

1. Motivation

The phrase 'nature knows best' most definitely applies to walking. After decades of intensive research, it is still a mystery how human walking is resilient to large perturbations, while maintaining efficiency. Researchers *have* been able to model and design bipedal walkers that are robust *or* efficient, but none that reconcile robustness and efficiency up to the level of human walking. The paradox that human walking is at the same time efficient and robust has kept researchers busy for years and probably will so for years to come. The first motivation for the research described in this thesis is to aquire fundamental insight in some of the principles that account for the reconciliation of efficiency and robustness in human walking, and by that making a step towards solving the paradox.

The second motivation for conducting this research is gaining knowledge about balance control in standing and walking to improve rehabilitation aids in the future. The Biomechanical Engineering group of the University of Twente has years of experience in making successful designs of passive orthoses and lower-limb prostheses. However, there is a limit to what can be achieved passively. Excess strain on the body makes walking a strenuous task for users of orthoses and lower-limb prostheses: they get tired much faster compared to people with a normal gait pattern. There is also the esthetic aspect. Most commercially available walking aids are passive and result in a very stiff gait, which does not look natural. There is need for improvement! Active prostheses and orthoses could take walking aids to the next level. At present, there are – as far as we know – no active orthosis and only a few fully active lower-limb prostheses on the market. Most of the latter are active dampers, including the successful C-Leg of Otto Bock. Recently, the first active knee joint prosthesis has been introduced that actually delivers additional power to the user: the POWER KNEE from Össur. This kind of application needs to take over (part of) the balance control with minimal energy consumption. Therefore, fundamental knowledge of efficient and robust gait control is indispensable to achieve progress in this field. The obtained knowledge could also be beneficial in research regarding gait rehabilitation robots, such as the one currently developed in our group, termed LOPES.

Another motivation is the field of bipedal gait robots. Although not the spearhead of the research presented in this thesis, collaboration with the BioMechanical Engineering group of the Delft University of Technology did raise the question if the gained knowledge of efficient and robust gait control could be applied to bipedal gait robots.

2. Towards efficient and robust control of bipedal walking

2.1 Introduction

There is a fundamental difference between standing and walking: standing is a posture, while walking is a rhythmic task. However, to get towards an understanding of efficient and robust control of human walking, control of posture has to be studied first, because control mechanisms such as reflexes are used in both posture and rhythmic tasks. For example, studies of human arm swinging (Abe and Yamada 2003; Hatsopoulos and Warren Jr 1996) – a rhythmic task – have suggested that the frequency of arm swinging is controlled by modulation of the reflex gains. If these reflex gains are so high that they would give postural instability, it is unlikely that these gains can be used to obtain stable controllable arm swinging. Therefore, knowledge of how limb dynamics are shaped by reflexes in posture could also prove usefull with regard to control of rhythmic movements, including walking.

Mathematically speaking, posture is associated with an *equilibrium*, while rhythmic tasks are associated with a *limit cycle*. In the chapters of this thesis the concepts equilibrium and limit cycle and the analysis of their stability are largely assumed known. Therefore, instead of giving an extensive literature review, this section will discuss some basics of spinal control (i.e. low-level control by structures seated in the spinal cord) of posture (Sect. 2.2) and rhythmic movement (Sect. 2.3) and the analysis of their stability. References to more detailed information on posture and rhythmic movement can be found in the designated chapters.

To introduce the concept of stability, a general description is displayed in Fig. 1. It depicts two balls on a mountain. The left ball is said to be in an unstable

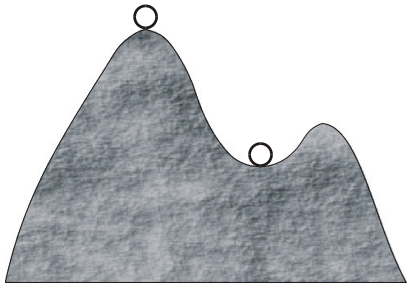

Fig. 1 General notion of stability. The left ball on top of the peak represents a mathematical solution that is unstable, while the right ball in the valley represents a stable one.

position, because the smallest perturbation (and these are always present) will cause the ball to fall down the mountain peak. The ball on the right is in a position that is said to be asymptotically stable, which means that after a small perturbation the ball will return in time to its original position. In the remainder of this thesis, we will refer to an asymptotically stable solution as being 'stable', unless mentioned otherwise.

2.2 Posture

Spinal control of posture

Posture is holding your body or in a certain position. Examples are sitting and standing. The central nervous system will notice deviations from the posture by sensors that detect motion or position, termed proprioceptors, and will tell the muscles to generate a restoring force.
In biomechanics, postural control is often studied by giving people the task to hold their body or body parts such as your hand in position while it is being perturbed (e.g. de Vlugt et al. 2002; Fitzpatrick et al. 1992; Van der Helm et al. 2002). This kind of research has shown that reflexes are the most important control mechanisms in maintaining postural stability despite perturbations. The most basic reflex is the stretch reflex, which is a monosynaptic reflex. Figure 2 shows basically how the stretch reflex works. After being perturbed, the flexor muscle lengthens and the stretch receptor inside the muscle – termed muscle spindle – translates this muscle stretch into an increased discharge rate. This signal is subsequently sent to the spinal cord, where it connects to the motoneuron synaptically. The motoneuron is now excited and will cause the muscle to increase contraction, thereby counteracting the muscle stretch. The central nervous system is able to modulate the stretch reflex – and by that the joint stiffness – in three ways. The first is by *gamma activation*. This excites specialized muscle fibers around the muscle spindle, which increases the spindle's sensitivity. The second way is by *presynaptic inhibition*. In this case another pathway reduces the amount of neurotransmitter available before the synaptic connection to the motoneuron. This causes the motoneuron's activity to become smaller. Presynaptic inhibition is especially important in rhythmic movement. The third way is by *direct activation* of the motoneurons. Reflex modulation is necessary for the central nervous system to be able to maintain different types of postures (e.g. holding your arm high or low) in different environmental circumstances (e.g. with or without added weights) with the same basic control system (i.e. the reflexes).

Analysis of posture

Posture is associated with the mathematical concept *equilibrium*. At an equilibrium of a continuous time system, the system is at rest. The equilibrium – and by that the posture – can be stable or unstable (see Fig.

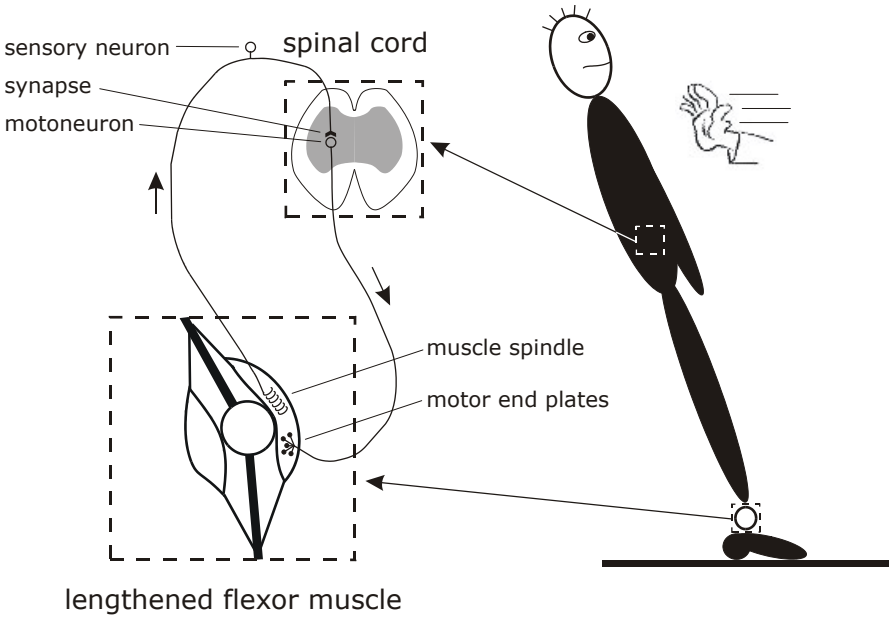

Fig. 2 The stretch reflex. Pushing a standing person lengthens his ankle's dorsal flexor muscles. This muscle lengthening is picked up by the muscle spindles, which send a signal to the spinal cord. These signals are subsequently passed onto the motor nerves and converge on the muscles by the motor end plates. The result is that the flexor muscles activate and counteract the lengthening caused by the perturbation. In other word, stretch reflexes provide robustness against perturbations.

1). To find out what the influence of reflex gains and time delays are on postural stability and dynamic response, the *eigenvalues* **λ** of the system are calculated. Eigenvalues characterize the stability and natural response of *linear* systems. Equation 1 states a general form of linear systems, termed state-space description:

$$\begin{aligned} \dot{\mathbf{x}} &= A\mathbf{x} + B\mathbf{u} \\ \mathbf{y} &= C\mathbf{x} + D\mathbf{u} \end{aligned} \tag{1}$$

In Eq. 1 **x** is the state vector of the system, **y** is the output vector and **u** is the input vector ($\dot{\mathbf{x}}$ means the time derivative of **x**). The system matrix *A* contains the system dynamics and from it the eigenvalues can be calculated by solving Eq. 2 (*I* is the unity matrix).

$$\det(A - \lambda I) = 0 \tag{2}$$

For non-linear systems like the posture model of Ch. 2, the system equations can be linearized in the equilibrium (i.e. the system states associated with the posture). Near the equilibrium, the eigenvalues of the linearized system will still be a valid estimation of the stability and dynamic properties of the real non-linear system, but for larger deviations from the equilibrium, the eigenvalues cannot predict the system's behavior anymore. For example, if you push the right ball in Fig. 1 hard enough to the right, it will topple over the shallow peak and fall down the mountain. Clearly, the eigenvalues associated with the stable equilibrium (i.e. the valley) cannot predict this.

To explain how eigenvalues can help us in determining the stability and behavior of musculo-skeletal systems, a simple model of human stance is shown in Fig. 3. The muscle pair with stretch reflexes, shown in Fig. 2, is represented by joint stiffness K and joint damping B of the ankle. Furthermore, the inertial properties of the standing person are reduced to a point mass m. The equation of motion for this model is as follows:

$$M_p = ml^2\ddot{\theta} + B\dot{\theta} + K\theta - mgl\sin\theta \tag{3}$$

with M_p the perturbation moment, g the gravity constant and l the length between the center of the head and the ankle joint.

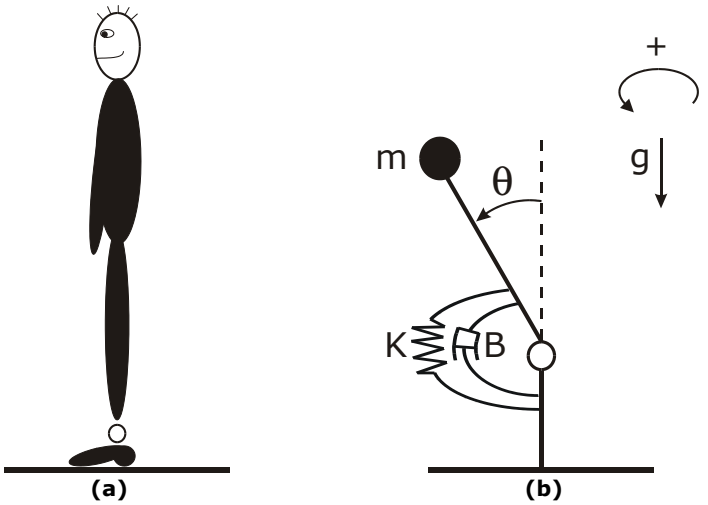

Fig. 3 A simple model of human stance. **(a)** A standing person **(b)** The dynamical model of the standing person. The ankle muscles are represented by a rotational stiffness K and damping B, the mass is represented by m and g is the gravity constant. The sway is represented by the angle θ.

If the standing person is not perturbed too hard, the angle θ will remain small and $\sin\theta$ equals θ. The equation of motion then becomes:

$$M_p = ml^2\ddot{\theta} + B\dot{\theta} + K_{tot}\theta \tag{4}$$

with $K_{tot} = K - mgl$ the total joint stiffness.

Rewriting Eq. 4 into state-space description (Eq. 1) gives (no output specified, thus no C and D matrix):

$$\dot{\mathbf{x}} = A\mathbf{x} + Bu \quad \text{with } \mathbf{x} = \begin{bmatrix} \theta \\ \omega \end{bmatrix} \text{ and } u = M_p$$

$$A = \begin{bmatrix} 0 & 1 \\ -\frac{K_{tot}}{ml^2} & -\frac{B}{ml^2} \end{bmatrix}, B = \begin{bmatrix} 0 \\ \frac{1}{ml^2} \end{bmatrix} \tag{5}$$

where ω is the angular velocity (i.e. time derivative of angle θ)

Filling system matrix A into Eq. 2 leads to:

$$\det\begin{bmatrix} -\lambda & 1 \\ -\frac{K_{tot}}{ml^2} & -\left(\lambda + \frac{B}{ml^2}\right) \end{bmatrix} = \lambda^2 + \frac{B}{ml^2}\lambda + \frac{K_{tot}}{ml^2} = 0 \tag{6}$$

Solving Eq. 6 gives the following eigenvalues:

$$\lambda = -\frac{B}{2ml^2} \pm \sqrt{\frac{B^2}{4m^2l^4} - \frac{K_{tot}}{ml^2}} \tag{7}$$

Without damping (i.e. B=0) and with positve stiffness (i.e. K_{tot}>0) the person would never stop swinging back and forth after a push, just as in an ideal mass-spring system. In this case the eigenvalues are $\lambda = \pm j\sqrt{K_{tot}/ml^2}$ (j^2=-1). Hence, imaginary eigenvalues represent *undamped oscillation*. In general, *complex* eigenvalues with both real and imaginary parts indicate *damped oscillatory* response. Joint damping will produce a force that resists movement and by that dissipates energy. The more joint damping is added, the faster the oscillatory movement will die out. In other words, the *real* (negative) part of eigenvalues indicate how *fast* the system is back at its equilibrium after a perturbation. If the total joint stiffness K_{tot} is smaller than zero, i.e. the muscular stiffness K is smaller than the negative gravitational

stiffness $-mgl$, at least one eigenvalue has a *positive* real value (i.e. one or both eigenvalues lie in the right-half plane), regardless of the damping value B (see Eq. 6). A negative joint stiffness will not produce a restoring force after the person is pushed, but a force away from the posture: the person falls. In other words, the real parts of all eigenvalues $\boldsymbol{\lambda}$ have to be *negative* for the system to be stable in its equilibrium.

Systems may show fundamentally different behavior when certain parameters are varied. Such a change in behavior is associated with a *bifurcation*, that is, a change in the qualitative structure of the solutions to the differential equations that describe the system (Arrowsmith and Place 1990; Seydel 1994). In this thesis only *local bifurcations* are studied. Local bifurcations are bifurcations that can be completely analysed by only looking at the local stability properties of equilibria, limit cycles or other invariant sets. Hence, local bifurcations are associated with loss of the local stability of invariant sets by parameter change. In case of equilibria, the type of local bifurcation that is encountered can be determined by the way the eigenvalues of the linearized system cross over to the right-half of the complex plane (with non-zero speed). The bifurcation is termed a *fold bifurcation* if the eigenvalue equals zero (Fig. 4a). It is termed a *Hopf bifurcation* in case of a pair of imaginary eigenvalues (Fig 4b). At a fold bifurcation two equilibria (or two fixed points in case of discrete time systems) collide and annihilate each other: there are two equilibria more on one side of the fold bifurcation compared to the other side. In symmetrical systems the fold bifurcation will present itself as a *pitchfork bifurcation*. If an equilibrium becomes unstable by Hopf bifurcation, a *limit cycle* will emerge. Limit cycles and their analysis will be discussed in the next section. In this thesis, both the pitchfork and the Hopf bifurcation are encountered for postural equilibria and the associated implications are discussed in the designated chapters (mainly Ch. 2). Somewhat more exotic bifurcation – i.e.

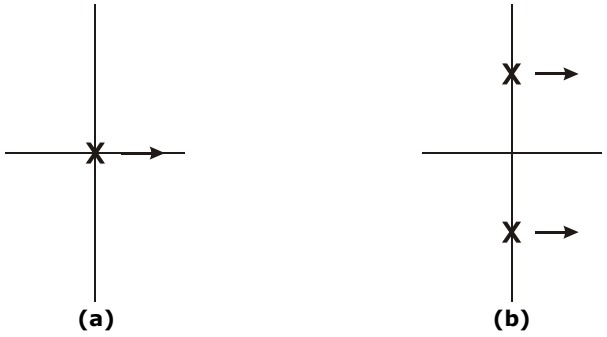

Fig. 4 The eigenvalues (marked with 'x') in the complex plane belonging to **(a)** a fold bifurcation and **(b)** a Hopf bifurcation.

the Bognadov-Takens bifurcation and the fold-Hopf bifurcation – are also encountered (Ch. 2), but it is outside the scope of this thesis to discuss all the possible behaviors beyond these types of bifurcation. More information on these types of bifurcations can be found in Kuznetsov (1998).

2.3 Rhythmic movement

Spinal control of rhythmic movement

Rhythmic movements are commonplace in nature. Examples are scratching, chewing, walking, running, swimming and flying. A lot of those rhythmic movements are controlled by neural networks in the spinal cord, termed central pattern generators (CPGs). CPGs excite the muscles periodically to provide the basic motor pattern to perform the rhythmic task at hand. In most rhythmic movements the CPGs alternately excite the flexor and extensor muscles – i.e. the muscles that respectively flex and extend the joint around which they are wrapped – and by that induce rhythmic movement. A well-known CPG model is the half-center model (Brown 1914). Figure 5 shows a half-center model, which is derived from the models of Matsuoka (1985; 1987).

The assumption that CPGs are important in human gait is for the most part based on abundant evidence of CPGs in the animal world (reviews in Duysens and Van de Crommert 1998; MacKay-Lyons 2002). For example, cats that have their afferent and efferent pathways to the brain transected (i.e. the brain does not receive sensory information from the body, nor is it able to send information back) are still able to walk when they are put on a treadmill (see Van de Crommert et al. (1998) for a lot of references to treadmill walking in spinal cats). When the speed of the treadmill is increased, the CPGs adapt their motor pattern to match this speed. This adaptive behavior originates from reflexive input from the paws (pressure information) and the muscles (length and velocity information). The increase in treadmill velocity increases the rate at which the sensory information changes and the CPGs adapt their output pattern to this new input pattern in such a way that a faster gait is obtained. It is noted that the sense of balance of the transected cats is much weaker that that of normal cats, since these cats lack integration of sensory information by the cerebellum, motor control by the motor cortex and sensory information of their orientation and movement in space by the vestibular system. However, the fact that they are still able to walk and adapt their gait pattern to the environment *despite these deficits* shows the key role CPGs and reflexes play in walking. Other clear examples of the existence of CPGs are provided by studies on isolated spinal cords of rats(Cazalets et al. 1995; Clarac et al. 2004; Juvin et al. 2007; Marchetti et al. 2001). Chemical stimulation (bath-applied neurotransmitters), electrical

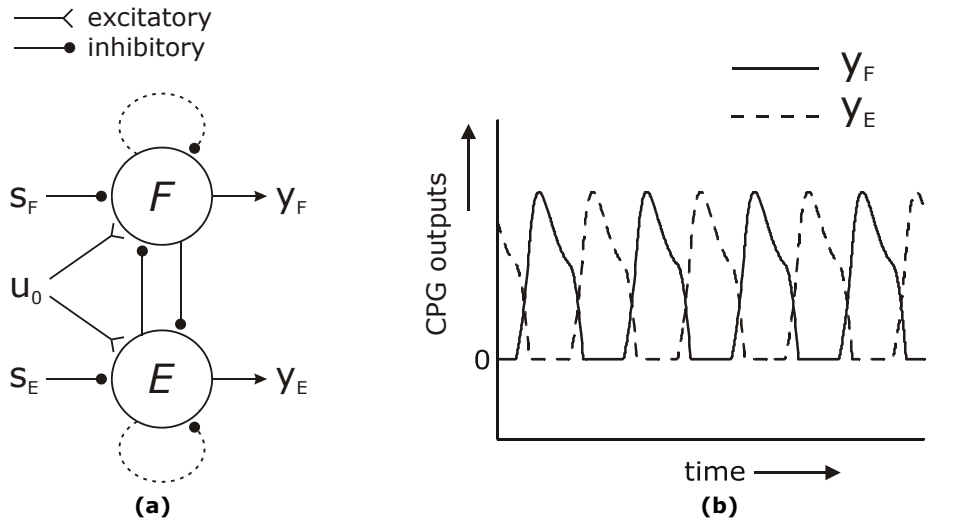

Fig. 5 (a) The half-center model is a well-known CPG model. Two groups of neurons termed the flexor center (denoted '*F*') and extensor center (denoted '*E*') provide motor patterns for the flexor and extensor muscles, respectively. Both receive constant excitatory supra-spinal input u_0. However, as both centers inhibit each other, only one of the centers can be firing at the same time. A center can only fire for some time, because it possesses adaptation dynamics (shown by *dashed lines*). Subsequently, the other center will start firing, as it is no longer inhibited. Hence, the CPG exhibits an oscillation, even without reflexive input (i.e. intrinsic oscillation). However, if reflexive input (s_F and s_E) is present, the CPG will entrain to it by altering its output pattern.
(b) Typical output pattern of the CPG (y_F and y_E are the firing rates), which leads to alternating flexion and extension of a limb.

stimulation of the dorsal roots (i.e. spinal nerves that contain sensory information) and electrical stimulation of the brainstem evoke alternating rhythmic patterns in the ventral roots that are normally connected to the flexor and extensor muscles. This is termed *fictive locomotion*.
Although there is no direct evidence of the existence of CPGs in the human spine, there *are* indications and indirect evidence of their presence. Newborn babies make coordinated stepping movements when their feet touch the ground (Borvendeg and de Groot 2000; Davis et al. 1994; Forssberg 1985; Yang et al. 1998). This stepping behavior is thought to be controlled by spinal structures, because anencephalic babies – having a brain stem but no cerebellum or cerebrum – still display this stepping behavior (Peiper 1961). In normal babies this 'spinal stepping' disappears when they develop, probably because the importance of supraspinal control of locomotion is larger in adult humans than in animals (i.e. cortical dominance). Nonetheless, these observations strongly advocate the existence of spinal control structures used in human walking. Further indications are provided by studies

showing that tonic electrical stimulation of the lumbar spinal cord induces locomotion stepping in paraplegic patients (Dimitrijevic et al. 1998; Shapkov and Shapkova 1999; Shapkov et al. 1996; Wickelgren 1998). Finally, studies on reflex modulation during rhythmic arm (Zehr et al. 2004; Zehr and Chua 2000; Zehr et al. 2003; Zehr and Kido 2001) and leg movements (for reviews see Brooke et al. 1997; Zehr and Stein 1999) suggest the presence of CPGs in the human spine, since the observed subcortical neural control is similar to that in animals for which CPGs are already discovered.

Analysis of rhythmic movement

Rhythmic movement is associated with the mathematical concept *limit cycle*. A limit cycle is a closed orbit in state space. Limit cycles can only exist for *non-linear* systems. Figure 6 shows how replacing a viscous damper with a non-linear damper changes the equilibrium of the mass-spring-damper system into a limit cycle. The limit cycle is called stable if a small perturbation leads to an orbit that approaches the limit cycle (see Fig 6b). It is unstable if arbitrary small perturbations lead to orbits leaving the

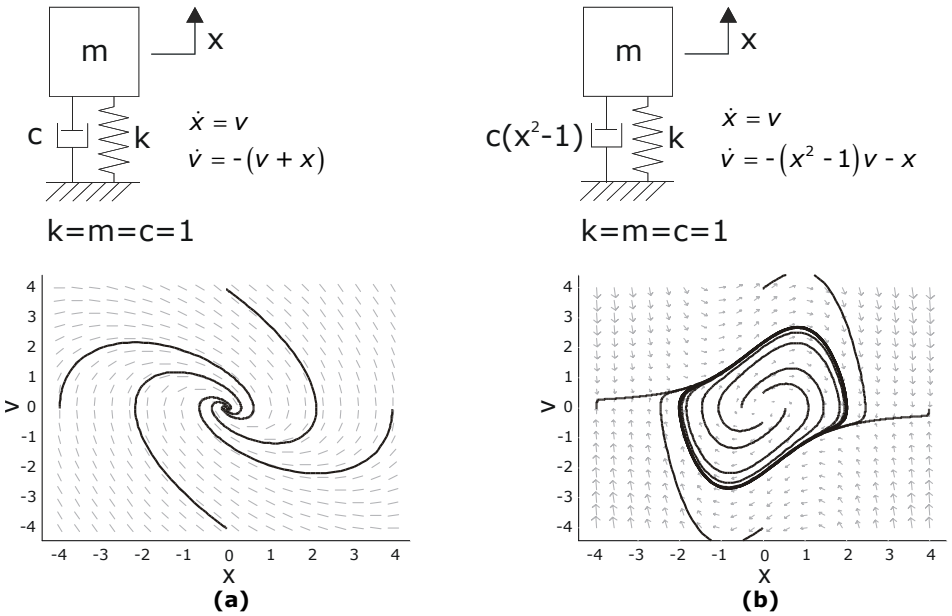

Fig. 6 Phase potraits of the mass-spring-damper system with **(a)** a viscous damper **(b)** a non-linear damper. The non-linear damper causes presence of a stable limit cycle, because it dissipates energy when x>|1|, but it supplies energy when x< |1|. Loss and supply of energy are always necessary components for the existence of stable limit cycles.

neighborhood of the limit cycle. A *stable limit cycle* implies self sustained oscillations. For example, the gait cycle in walking is represented by a stable limit cycle (Holt et al. 1990). If the walker is not pushed or tripped too hard, he will be able to maintain balance. Some time after the perturbation he will walk again with the same velocity, periodic muscle activations and joint angles etcetera. In other words, the walker will return to its original gait cycle, that is, to its limit cycle.

Besides the system's non-linearity, there are two necessary conditions for stable limit cycles to exist in physical systems. The first is the presence of energy buffers that enable the existence of oscillations by exchanging energy from one buffer to another. The second is the presence of loss and supply of energy. The latter generally requires a control mechanism that regulates the supply (and possibly part of the loss) of energy. For example, in walking the masses act as kinetic and potential energy buffers that will exchange energy during walking. The main part of the energy loss during walking comes from the impact at heel strike. The central nervous system controls the muscles in such a way that this loss of energy is compensated so that sustained walking is obtained.

Equation 8 states a general form of autonomous non-linear systems consisting of ordinary differential equations, in which $\mathbf{x}$ is the state vector of the system, $\mathbf{F}(\mathbf{x})$ is the set of non-linear equations in $\mathbf{x}$ and and $\mathbf{c}$ is a vector consisting of constants.

$$\dot{\mathbf{x}} = \mathbf{F}(\mathbf{x}) + \mathbf{c} \tag{8}$$

Assume this system possesses a limit cycle. To determine if the limit cycle is stable, a (hyper)surface Ω is placed transverse to the limit cycle (see Fig. 7). This surface is termed a *Poincaré section*. The crossings of the orbit with this surface in a given direction can be seen as a discrete representation of the flow near the limit cycle. The mapping from surface to surface is called the *Poincaré map* $P(\mathbf{x})$ (see Eq. 9a) and has a state space whose dimension is reduced by one relative to the original continuous time system. The limit cycle is represented by the *fixed point* $\tilde{\mathbf{x}}$ of the Poincaré map (see Eq. 9b and Fig. 7). A fixed point is a rest point of a discrete time system, analogous to an equilibrium in continuous time systems. Thus, the limit cycle in state space is represented by fixed point $\tilde{\mathbf{x}}$ in reduced state space.

$$\mathbf{x} \mapsto P(\mathbf{x}) \tag{9a}$$

$$P(\tilde{\mathbf{x}}) = \tilde{\mathbf{x}} \tag{9b}$$

The limit cycle will be locally stable if the fixed point of the Poincaré map is locally stable. This is determined by calculating the eigenvalues of the

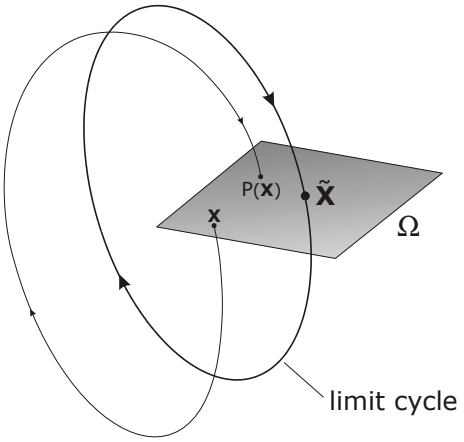

Fig. 7 The Poincaré map displays a stroboscopic view of the system's dynamics. It maps from surface to surface (from **x** to P(**x**)). The surface is placed tranverse to the limit cycle and is termed a Poincaré section. The limit cycle is represented by the point $\tilde{\mathbf{x}}$ on the Poincaré section.

Poincaré map, which are termed *Floquet multipliers*. The Floquet multipliers $\boldsymbol{\lambda}$ can be calculated by solving Eq. 10, in which J is the jacobian of the Poincaré map and I is the unity matrix.

$$\det\left(J - \lambda I\right) = 0 \tag{10a}$$

$$J = DP(\mathbf{x}) = \begin{bmatrix} \frac{\partial P_1}{\partial x_1} & \cdots & \frac{\partial P_1}{\partial x_{n-1}} \\ \vdots & \vdots & \vdots \\ \frac{\partial P_{n-1}}{\partial x_1} & \cdots & \frac{\partial P_{n-1}}{\partial x_{n-1}} \end{bmatrix}_{\tilde{\mathbf{x}}} \tag{10b}$$

The Floquet multipliers can be seen as growth factors of small deviations from the limit cycle. The system will return to the limit cycle if the largest absolute value of the Floquet multipliers is smaller than 1 (i.e. all multipliers lie within the unit circle), because the deviation from the limit cycle becomes smaller every time the orbit hits the surface Ω: the limit cycle is locally asymptotically stable. If the largest multiplier (in absolute value) is larger than 1, deviations from the limit cycle will grow and thus the limit cycle is unstable.

The event that a parameter change causes the limit cycle to change stability is termed a *local bifurcation* (see Sect. 2.2). The type of local bifurcation is

determined by the way the multipliers cross the unit circle (with non-zero speed), as shown in Fig. 8. The types of bifurcation encountered in the research of the current thesis are *the pitchfork and the period doubling bifurcation*. The pitchfork bifurcation is a type of fold bifurcation (see Sect. 2.2). Beyond a period doubling bifurcation the system exhibits behavior with twice the period of before the bifurcation. An example of multiple period doubling bifurcations undergone by a simple gait model is shown in Fig. 9. Figure 9a shows the normal gait cycle, while Fig. 9b shows the altered gait due to multiple period doubling bifurcations. A well-known route to *chaos* (Feigenbaum 1978) consists of subsequent period doubling bifurcations, finally leading to behavior without any periodicity, that is, chaos. This route is exhibited by the passive dynamic walker in Ch. 5.

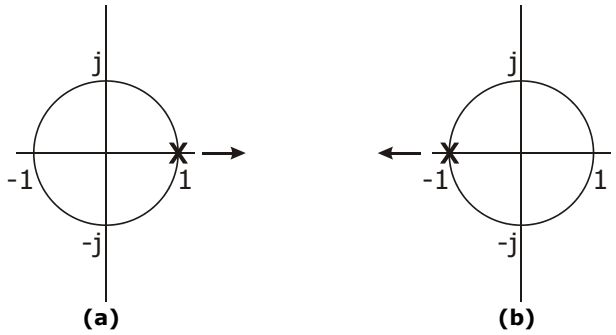

Fig. 8 The Floquet multipliers (marked with 'x') in the complex plane belonging to **(a)** a pitchfork bifurcation and **(b)** a period doubling bifurcation.

The Floquet multipliers are often determined by the perturbation method. The following example illuminates the concept limit cycle and shows how the perturbation method works in a simple model of a boy jumping on a trampoline (see Fig. 10a). Jumping the trampoline is associated with a stable limit cycle. Potential energy (i.e. heigth) is transformed into kinetic energy while falling down towards the trampoline. After the trampoline is hit, part of the kinetic energy will be lost by damping and part will be buffered by the spring action of the trampoline. The energy loss is compensated by the boy who – while on the trampoline – uses his muscles to supply the necessary force. A higher force F_m will lead to a limit cycle with greater jumping height. When the boy leaves the trampoline to go up, kinetic energy is transformed back into potential energy and the cycle is complete. The equation of motion of this model is stated in Eq. 11, where y is the boy's height, m is the boy's mass, g is the gravity constant, $B(y)$ is a non-linear damping and $K(y)$ is a non-linear stiffness. Perturbations are represented by the force F_p.

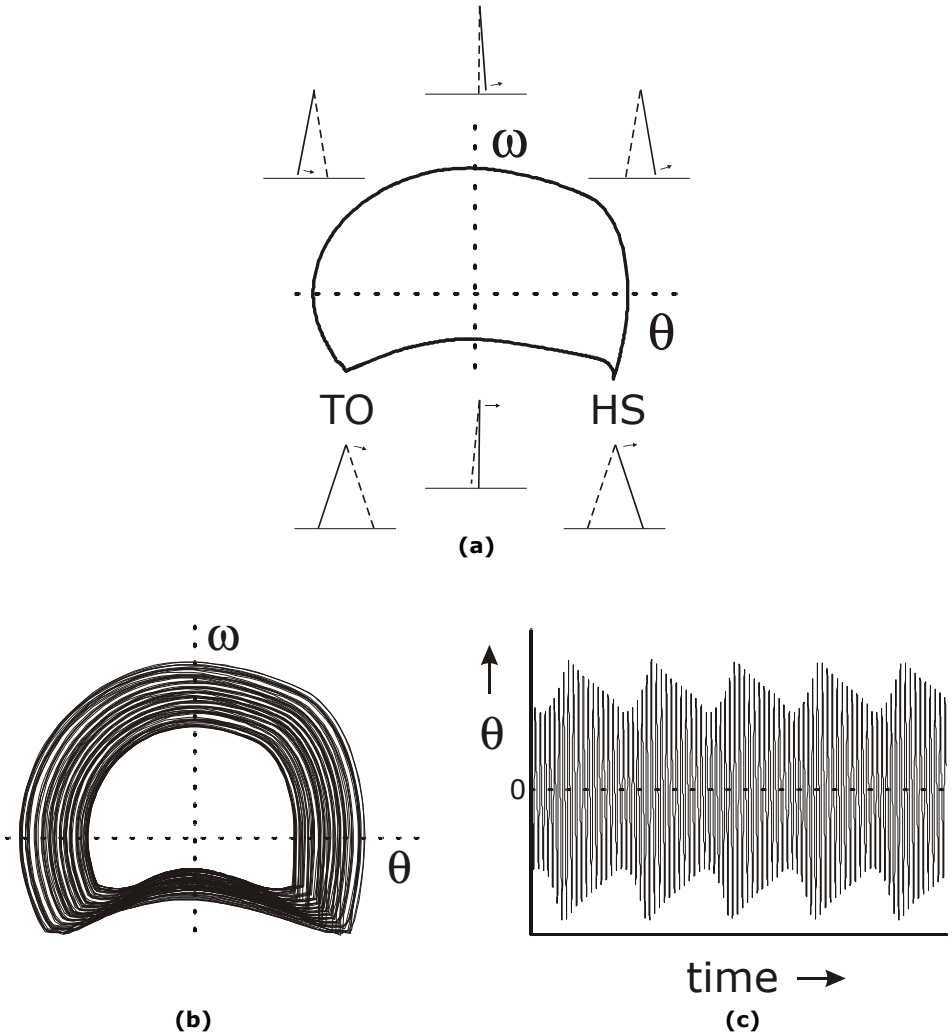

Fig. 9 Multiple period doubling bifurcations in a simple gait model **(a)** Phase plane of right limb angle θ versus angular velocity ω of the normal gait cycle, that is, *before* the series of period doubling bifurcations. HS means heel strike and TO means toe off. The small figures next to the phase plane plot show the configuration of the walker's legs at several points in the gait cycle (*solid* line is right leg, *dashed* line is left leg) **(b)** The phase plane *after* multiple period doubling bifurcations **(c)** The time series of the *angle* θ of the right leg *after* multiple period doubling bifurcations

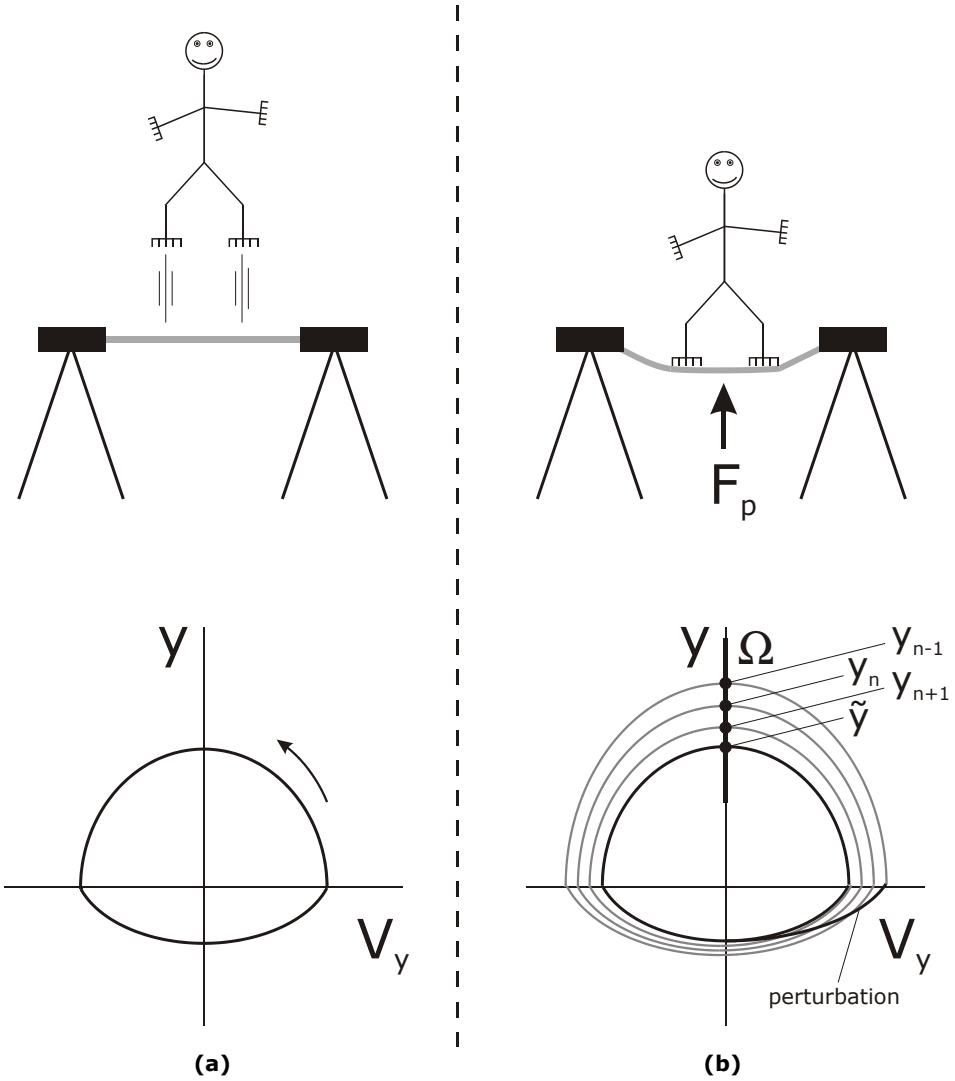

Fig. 10 Boy jumping a trampoline is a limit cycle **(a)** Phase portrait of heigth y versus velocity v_y of the jumping **(b)** Perturbation leads to a deviation of the boy's trajectory relative to the limit cycle. The crossing from positive velocity to a negative velocity (v_y=0) is chosen as the Poincaré section Ω. The boy returns back to the limit cycle in time and the subsequent crossings with Ω are shown (y_{n-1}, y_n and y_{n+1}). The limit cycle itself is represented by the point $\tilde{y}$ on Ω.

$$F_m - mg + F_p = m\ddot{y} + B(y)\dot{y} + K(y)y \tag{11}$$

The model has two states, namely y and the velocity v_y (v_y is the time derivative of y, i.e. $\dot{y}$). The stiffness $K(y)$ is dependent on the height y, because the boy only experiences spring action when on the trampoline and not in mid air. The damping $B(y)$ is dependend on the height y, because the damping on the trampoline is far greater than that provided by air resistence. These non-linearities in the stiffness and damping together with the intermittent control of the boy's muscles – compensating the damper's energy loss – and the exchange of energy between height, spring and kinetic energy buffers fulfill the necessary conditions for the existence of a limit cycle. Figure 10a shows the phase portrait – plotting both states against each other – of the limit cycle associated with the trampoline jumping. Figure 10b shows that a deviation from the limit cycle will occur if the boy is perturbed. The boy will return to its limit cycle and in this simple one-dimensional case the Floquet multipliers can be determined from this recovery (in general, however, all the state variables of a system have to be perturbed to fill the jacobian J (Eq. 10b) before the multipliers $\boldsymbol{\lambda}$ can be calculated (Eq. 10a)). The phase portrait shows how the boy returns to its original jump height, i.e. its limit cycle. To be able to calculate the multipliers the dynamics are discretized by taking a surface tranverse to the limit cycle. As the original state-space of this model is two-dimensional, the Poincaré section is in fact a line. If the boy's trajectory is in the vicinity of the limit cycle, data from its crossings with this line can be used to calculate the jacobian J (Eq. 10b). This data is shown in Fig. 10b and gives the following jacobian:

$$J = \left.\frac{\partial P}{\partial y}\right|_{\tilde{y}} = \frac{\Delta P}{\Delta y} = \frac{y_{n+1} - \tilde{y}}{y_n - \tilde{y}} \tag{12}$$

with n representing the number of the cycle.

Filling the jacobian J into Eq. 10a gives the Floquet multipliers. Since the reduced state-space of the system on the Poincaré section is one-dimensional, there is only one Floquet multiplier, which therefore equals the jacobian:

$$\begin{aligned} &\det(J - \lambda I) = 0 \\ &\Leftrightarrow J - \lambda = 0 \\ &\Leftrightarrow \lambda = J = \frac{y_{n+1} - \tilde{y}}{y_n - \tilde{y}} = \frac{\Delta y_{n+1}}{\Delta y_n} \end{aligned} \tag{13}$$

From Eq. 13 it is easily seen that the Floquet multiplier represents the grow factor of deviations from the limit cycle:

$$\begin{aligned} &\Delta y_{n+1} = \lambda \Delta y_n \\ &\Leftrightarrow \Delta y_{n+k} = \lambda^k \Delta y_n \end{aligned} \tag{14}$$

Hence, the multiplier's absolute value has to be smaller than one, because else the deviation from the limit cycle would grow: the limit cycle would be unstable. Equation 14 also shows that for stable limit cycles a smaller multiplier λ means a faster recovery from small perturbations. It is noted that Floquet multipliers – like the eigenvalues of an equilibrium – represent the behavior of the linearised system. Thus, the multipliers are only valid representations of the limit cycle's stability and the grow factors of deviations in the vicinity of the limit cycle. Large perturbations can lead to trajectories away from the limit cycle and towards another invariant set (e.g. a stable equilibrium), despite the fact that the limit cycle is *locally stable*.

Stable limit cycles and equilibria are examples of attractors. The *global stability* of attractors is shown by their *basin of attraction*. This is the part of state-space from which the system will converge to the attractor. Thus, in principle, the global stability of stance and gait could be determined by obtaining the basin of attraction. Unfortunaly, neuro-musculo-skeletal models of stance and gait tend to be high dimensional systems. This makes it virtually impossible to calculate the basin of attraction numerically, let alone find an analytical expression for it.

3. Goal and approach

The goal of the research presented in this thesis is to find the principles of neural control that make human walking both efficient and robust. Modeling is used to achieve this goal, because – in contrast to experimental research – one can isolate the interesting parts of the system from the rest, leaving a model that contains the essential dynamics of the system under investigation. With such a model, the influence of important neural parameters on the quality of walking – such as dynamic gait stability – can be assessed. Modeling is necessary, because there are a number of problems with experimental gait research that make it very hard – if not impossible – to get a reliable estimation of the dynamic properties of walking. Firstly, it is difficult to separate the contributions of different parts of the system to the dynamics of walking. Secondly, repeatability is never perfect. It is therefore common practice to average between different gait cycles to obtain the 'normal' gait cycle. By averaging, however, the variations between subsequent gait cycles are thrown away, while these could contain valuable information about the dynamic properties of walking. Repeatability becomes even more of a problem when trying to discover the dynamic response to perturbations. Learning effects change the response, so objective measurements are hard to make. Thirdly, one cannot measure – or even know – all the states of the system. Fourthly, the neural parameters under investigation cannot be physically changed to the desired extent or cannot be changed at all. In other words, with experimental research alone, it is virtually impossible to ascertain the influence of neural parameters on the dynamical properties of walking. Modeling – fed with data from experimental research – is needed to find the principles behind robust and efficient human walking.

Instead of starting with a large control scheme with a huge amount of variables and parameters, a bottom-up approach was chosen to fully understand each step taken and appreciate the influence of low-level neural control, starting off with investigating the influence of reflexes on the quality of posture and working towards efficient and robust spinal gait control. With the bottom-up approach in mind, the following research questions are deduced from the goal:

- What is the influence of different components of reflexive feedback on postural stability and associated dynamical behavior?

- Can the co-existence of CPGs and reflexes explain observed efficient and robust rhythmic limb movement?

- Can both efficiency and robustness be achieved in CPG-controlled walking or is there a trade-off between these gait qualities?

The research described in this thesis is qualitative in nature, since the goal is *not* to develop predictive models, but to acquire fundamental knowledge of the influence of low-level neural control on posture and rhythmic movement. Therefore, minimalistic neuro-musculo-skeletal models of posture, rhythmic limb movement and walking are developed, which nonetheless possess enough of the the essential dynamics to evaluate the influence of important neural parameters on the quality of their behavior.

Changes in the behavior of dynamical systems correspond to changes in the qualitative structure of their solutions, which are termed bifurcations. Bifurcation analysis and continuation methods are therefore valuable mathematical tools for determining the influence of parameters on the qualitative behavior of the system under investigation. They are used in this thesis to evaluate the stability margins regarding neural parameters and to discriminate different biomechanical behaviors. Examples of the latter are stable posture versus clonus (see Ch. 2, Sect. 3.1) and symmetrical gait versus limping (e.g. Ch. 5, Sect. 3.1).

4 Thesis outline

The scientific contribution produced during fulfillment of the PhD assignment consists of five articles on the subjects of posture, rhythmic limb movement and gait, which make up for the chapters of the present thesis. The research questions are addressed in the following chapters:

- What is the influence of different components of reflexive feedback on postural stability and associated dynamical behavior?

  Chapter 2 introduces bifurcation and stability analysis as a way of identifying different behaviors of neuro-musculo-skeletal models and functions as a framework for later chapters. In this chapter the influence of reflexive feedback of muscle lengthening, muscle velocity, force and time delay on the behavior and stability in musculoskeletal systems is assessed using a model of human stance.

- Can the co-existence of CPGs and reflexes explain observed efficient and robust rhythmic limb movement?

  Chapter 3 presents a CPG model that shows flexible, efficient and robust control of rhythmic limb movement and determines the necessary and sufficient types of afferent feedback to do so.

  Chapter 4 presents a neuro-musculo-skeletal model of the forearm, in which the local reflex loop co-exists with the CPG and both receive afferent input from the muscles. This model achieves energy efficient rhythmic arm movement by resonance tuning, a feature also observed in human arm swinging.

- Can both efficiency and robustness be achieved in CPG-controlled walking or is there a trade-off between these gait qualities?

  Chapter 5 presents a comparison of passive-dynamic walking – i.e. walking passively down a slope – with CPG-controlled walking. The CPG hardly changes the natural limit cycle of the passive walker; it only compensates the energy lost at heel strike and draws the walker back to the limit cycle when perturbed. This way, robust walking is achieved, while retaining the energy efficiency of passive dynamic walking.

Chapter 6 shows that in a simple CPG-controlled gait model with human mass distribution – i.e. unable to walk passively down a slope – walking is achieved, which is both efficient and robust against perturbations. However, a strict trade-off between these gait qualities is present.

Finally, **Chapter 7** presents discussion, conclusions and future directions.

References

Abe MO, Yamada N (2003) Modulation of elbow joint stiffness in a vertical plane during cyclic movement at lower or higher frequencies than natural frequency. Exp Brain Res 153:394-9

Arrowsmith DK, Place CM (1990) An introduction to dynamical systems. In. Cambridge University Press, Cambridge, pp 423

Borvendeg K, de Groot L (2000) The stepping response in early infancy. Neuropediatrics 31:180-5

Brooke JD, Cheng J, Collins DF, McIlroy WE, Misiaszek JE, Staines WR (1997) Sensori-sensory afferent conditioning with leg movement: gain control in spinal reflex and ascending paths. Prog Neurobiol 51:393-421

Brown TG (1914) On the nature of the fundamental activity of the nervous centres; together with an analysis of the conditioning of rhythmic activity in progression, and a theory of the evolution of function in the nervous system. J Physiol 48:18-46

Cazalets JR, Borde M, Clarac F (1995) Localization and organization of the central pattern generator for hindlimb locomotion in newborn rat. J Neurosci 15:4943-51

Clarac F, Pearlstein E, Pflieger JF, Vinay L (2004) The in vitro neonatal rat spinal cord preparation: a new insight into mammalian locomotor mechanisms. J Comp Physiol A Neuroethol Sens Neural Behav Physiol 190:343-57

Davis DW, Thelen E, Keck J (1994) Treadmill stepping in infants born prematurely. Early Hum Dev 39:211-23

de Vlugt E, Schouten AC, van der Helm FC (2002) Adaptation of reflexive feedback during arm posture to different environments. Biol Cybern 87:10-26

Dimitrijevic MR, Gerasimenko Y, Pinter MM (1998) Evidence for a spinal central pattern generator in humans. Ann N Y Acad Sci 860:360-76.

Duysens J, Van de Crommert HW (1998) Neural control of locomotion; The central pattern generator from cats to humans. Gait Posture 7:131-141.

Feigenbaum MJ (1978) Quantitative universality for a class of non-linear transformations. J. Stat. Phys. 19:25-52

Fitzpatrick RC, Taylor JL, McCloskey DI (1992) Ankle stiffness of standing humans in response to imperceptible perturbation: reflex and task-dependent components. J Physiol 454:533-47

Forssberg H (1985) Ontogeny of human locomotor control. I. Infant stepping, supported locomotion and transition to independent locomotion. Exp Brain Res 57:480-93

Hatsopoulos NG, Warren Jr WH (1996) Resonance Tuning in Rhythmic Arm Movements. J Mot Behav 28:3-14

Holt KG, Hamill J, Andres RO (1990) The force-driven harmonic oscillator as a model for human locomotion. Human Movement Science 9:55

Juvin L, Simmers J, Morin D (2007) Locomotor rhythmogenesis in the isolated rat spinal cord: a phase-coupled set of symmetrical flexion extension oscillators. J Physiol 583:115-28

Kuznetsov YA (1998) Elements of Applied Bifurcation Theory. In: Marsden JE, Sirovich L (eds) Applied mathematical sciences. Vol. 112. Springer-Verlag, New York, pp 591

MacKay-Lyons M (2002) Central pattern generation of locomotion: a review of the evidence. Phys Ther 82:69-83.

Marchetti C, Beato M, Nistri A (2001) Alternating rhythmic activity induced by dorsal root stimulation in the neonatal rat spinal cord in vitro. J Physiol 530:105-12

Matsuoka K (1985) Sustained oscillations generated by mutually inhibiting neurons with adaptation. Biol Cybern 52:367-76

Matsuoka K (1987) Mechanisms of frequency and pattern control in the neural rhythm generators. Biol Cybern 56:345-53

Peiper A (1961) Cerebral functions in infancy and childhood. In, Consultants Bureau, New York

Seydel R (1994) Practical bifurcation and stability analysis: from equilibrium to chaos. In: Interdisciplinary Applied Mathematics. Vol. 5. Springer-Verlag, New York, pp 407

Shapkov YT, Shapkova EY (1999) Human spinal locomotor generators: Problems of assessment of stimulation efficiency. Biomedical Engineering 32:211

Shapkov YT, Shapkova EY, Mushkin AY (1996) Spinal electrostimulation as an approach to locomotor activity induction in children: Clinical aspects and technological problems. Biomedical Engineering 30:177

Van de Crommert HW, Mulder T, Duysens J (1998) Neural control of locomotion: sensory control of the central pattern generator and its relation to treadmill training. Gait Posture 7:251-263.

Van der Helm FC, Schouten AC, de Vlugt E, Brouwn GG (2002) Identification of intrinsic and reflexive components of human arm dynamics during postural control. J Neurosci Methods 119:1-14.

Wickelgren I (1998) Teaching the spinal cord to walk. Science 279:319-21

Yang JF, Stephens MJ, Vishram R (1998) Infant stepping: a method to study the sensory control of human walking. J Physiol 507 (Pt 3):927-37

Zehr EP, Carroll TJ, Chua R, Collins DF, Frigon A, Haridas C, Hundza SR, Thompson AK (2004) Possible contributions of CPG activity to the control of rhythmic human arm movement. Can J Physiol Pharmacol 82:556-68

Zehr EP, Chua R (2000) Modulation of human cutaneous reflexes during rhythmic cyclical arm movement. Exp Brain Res 135:241-50

Zehr EP, Collins DF, Frigon A, Hoogenboom N (2003) Neural control of rhythmic human arm movement: phase dependence and task modulation of hoffmann reflexes in forearm muscles. J Neurophysiol 89:12-21

Zehr EP, Kido A (2001) Neural control of rhythmic, cyclical human arm movement: task dependency, nerve specificity and phase modulation of cutaneous reflexes. J Physiol 537:1033-45

Zehr EP, Stein RB (1999) What functions do reflexes serve during human locomotion? Prog Neurobiol 58:185-205.

Chapter 2

Bifurcation and stability analysis in musculo-skeletal systems: a study into human stance

B.W. VERDAASDONK, H.F.J.M. KOOPMAN, S.A. VAN GILS, F.C.T. VAN DER HELM

Biological Cybernetics 91: 48-62, 2004

Abstract

Reflexes are important in the control of such daily activities as standing and walking. The goal of this study is to establish how reflexive feedback of muscle length, velocity and force can lead to stable equilibria (i.e. posture) and limit cycles (e.g. ankle clonus and gait). The influence of stretch reflexes on the behavior and stability of musculo-skeletal systems was examined using a model of human stance. We computed branches of fold and Hopf bifurcations by numerical bifurcation analysis of the model. These fold and Hopf branches divide the parameter space, constructed by the reflexive feedback gains, into regions of different behavior: unstable posture, stable posture and stable limit cycles. These limit cycles correspond to a neural deficiency, termed ankle clonus. We also linked bifurcation analysis to known biomechanical concepts by linearizing the model: the fold branch corresponds to zero ankle stiffness and defines the minimal muscle length feedback necessary for stable posture; the Hopf branch is related to unstable reflex loops. Crossing the Hopf branch can lead to the above mentioned stable limit cycles. The Hopf branch reduces with increasing time delays, making the subject's posture more susceptible to unstable reflex loops. This might be one of the reasons why elderly people, or those with injuries to the central nervous system, often have trouble with standing and other posture tasks. The influence of co-contraction and force feedback on the behavior of the posture model was also investigated. An increase in co-contraction leads to an increase in ankle stiffness (i.e. intrinsic muscle stiffness) and a decrease in the effective reflex loop gain. On the one hand, positive force feedback increases the ankle stiffness (i.e. intrinsic and reflexive muscle stiffness); on the other hand it makes the posture more susceptible to unstable reflex loops. For negative force feedback, the opposite is true. Finally, we calculated areas of reflex gains for perturbed stance and quiet stance in healthy subjects by fitting the model to data from the literature. The overlap of these areas of reflex gains could indicate that stretch reflexes are the major control mechanisms in both quiet and perturbed stance. In conclusion, this study has successfully combined bifurcation analysis with the more common biomechanical concepts and tools to determine the influence of reflexes on the stability and quality of stance. In the future, we will develop this line of research to look at rhythmic tasks, such as walking.

1. Introduction

For healthy people, walking seems an easy task, since for them it is an effortless and robust way of locomotion. However, people with an orthosis or prosthesis and people with a decreased capacity of the central nervous system (e.g. older people, CVA patients) often find walking difficult. They need to put more effort in each step, become tired more quickly and are less able to deal with perturbations (e.g. a push). To help these groups, the principles that make normal walking such a robust and efficient form of locomotion must be discovered first.

If people are slightly perturbed by their environment during walking, they tend to return to their original periodic movement. This periodic orbit that gait approaches each time it is perturbed can be described by a *stable* limit cycle (e.g. Garcia et al. 1998; Hurmuzlu and Basdogan 1994). A limit cycle is termed *stable* if the system under consideration returns towards this cycle after small perturbations. The mathematical description of walking as approaching a stable limit cycle gives us the opportunity to explore the influence of physiological parameters on the qualitative behavior and stability of gait. Simplified segment models of humans show unactuated walking down a shallow slope (Garcia et al. 1998; McGeer 1989; Schwab and Wisse 2001), which McGeer termed *passive dynamic walking* (McGeer 1990). Such models can be seen as damped mechanical non-linear oscillators, maintaining oscillation by a small supply of gravitational energy (by means of the slope), which compensates for energy losses due to friction and heel strike. It is this interaction between energy loss and energy supply that creates the limit cycle to which the model returns after small perturbations. The drawback of passive dynamic walking is its poor robustness against perturbations. Schwab and Wisse (2001) have quantified the robustness by computation of the *basin of attraction* of the simplest walking model of Garcia et al. (1998); they showed that the basin was very small.

Humans exploit the natural dynamics of their body during walking. At a certain velocity they walk with minimum effort per unit distance traveled (Inman et al. 1981; McMahon 1984). It is this velocity people mostly adopt, exploiting natural dynamics to the maximum and resembling passive dynamic walking most closely. However, unlike the passive dynamic walking models, humans can adapt their speed (i.e. change to another limit cycle) and are robust against larger perturbations. A major contribution to this adaptability and robustness comes from reflexes and probably from central pattern generators. The functional role of muscle, load receptor (probably Golgi tendon organs) and cutaneous reflexes in gait is discussed in depth by Zehr and Stein (1999). They conclude that stretch reflexes are important, among other factors, in providing stability against perturbations in the swing phase,

and in providing both weight support and stability in the stance phase. Load receptor reflexes could be important in the stance and stance-to-swing phase and affect the period of the limit cycle, although it is unclear to what extent. To fulfill their functional role during gait, reflexes are modulated (i.e. phase dependent), but the mechanisms that cause this modulation are not yet known precisely. A central pattern generator (CPG) could play an important part in the phase modulation of reflexes during walking. A CPG is a neural oscillator that entrains to the 'mechanical oscillator' (i.e. segment model), thus providing an activation pattern that in turn leads to stable locomotion. Evidence for the existence of CPGs was found, for example, in lampreys (Cohen and Wallen 1980; Grillner et al. 1981) and cats (Amemiya and Yamaguchi 1984; Brown 1911; Shik et al. 1966). Although there is no direct evidence of CPGs in humans, there is a growing number of observations suggesting their presence in the human spine (reviews by Duysens and Van de Crommert 1998; MacKay-Lyons 2002). Taga (1995a,b, 1998) and Taga et al. (1991) have successfully used simple CPGs in their neuro-musculo-skeletal models of human locomotion in order to achieve robust locomotion.

In this paper, we investigate the qualitative influence of reflexes on the behavior and stability of musculo-skeletal systems. The goal is to establish how reflexive feedback of muscle lengthening, velocity and force, and the time delays, present in these reflex arcs, can lead to stable equilibria (i.e. posture) and limit cycles (e.g. ankle clonus, gait). As reflex gains or time delays are varied, changes may occur in the qualitative structure of the solutions to the delayed differentials equations that describe the model. These changes are termed *bifurcations* and may reveal significant behavior of the musculo-skeletal system. This study considers stance (i.e. posture), but also provides a framework for future research into the influence of certain types of reflexes on the behavior and stability of physiologically based gait models.

In the next section, the model is outlined. It is a model of stance, consisting of an inverted pendulum with an antagonistic muscle pair around the ankle joint and reflexive feedback of muscle lengthening, velocity and force. The model is complex enough to demonstrate some basic influences of reflexes on the qualitative behavior of musculo-skeletal systems. Necessary conditions for stable and unstable equilibria to become stable limit cycles are discussed and mathematical concepts from the bifurcation analysis are linked to known biomechanical concepts such as stiffness. The influence of reflex gains, delays and co-contraction on the qualitative behavior of the model is investigated by using bifurcation analysis. Finally, the model is fitted to data of perturbed and quiet stance.

2. Methods

2.1 Musculo-skeletal model of stance

A simple posture model is used to investigate the influence of reflex gains, delays and co-contraction on the qualitative behavior and stability of musculo-skeletal systems. The model consists of an inverted pendulum with an antagonistic muscle pair, as shown in Fig. 1. The inverted pendulum represents a person who tries to maintain an upright position by flexing and extending the ankles. Stance is assumed to be a perturbed equilibrium (e.g. by measurement errors of muscle spindles), thus producing sway. The only joint in this model represents the ankle joints, and the two muscles represent the Tibialis anterior muscle and the Soleus muscle for both legs. The lumped Hill-type muscle model is based on the work of Winters and Stark (1985; 1987) and models both activation and contraction dynamics. It consists of a contractile element (CE) and a serial elastic element (SE), which is modeled as non-linear spring. The frequently used parallel elastic element has been omitted, because it has no influence on the local stability of the considered posture (i.e. eigenvalues). Two types of feedback are incorporated in the model: intrinsic feedback (force-length and force-velocity relationships of the muscle) and reflexive feedback. This feedback defines the visco-elastic properties of the muscle pair.

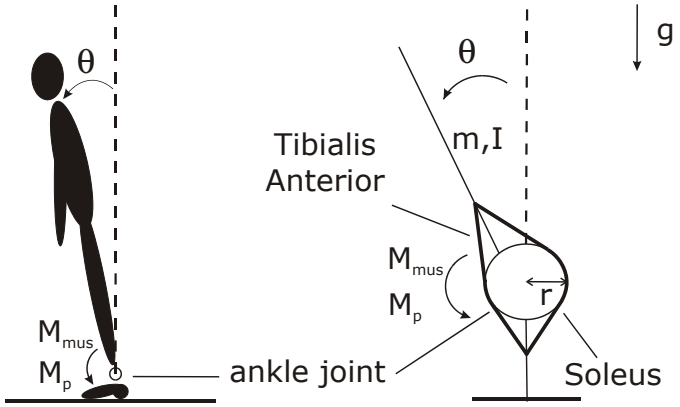

Fig. 1 Simplified human posture (*left*) and dynamic model representation as inverted pendulum with muscles (*right*). Parameters are mass m, moment of inertia I, moment arm r. The muscle moment M_{mus} tries to keep the angle θ to a minimum, despite the destabilizing actions of the perturbation moment M_p and gravity g.

The equation of motion for the inverse pendulum with mass m, moment of inertia around the ankles I, distance from ankles to center of mass l_{com} and gravitational constant g, is written as

$$I\ddot{\theta} = mgl_{com}\sin\theta + M_{mus} + M_{p} \tag{1}$$

in which θ is the angle of the pendulum with respect to the vertical position, M_{mus} is the moment around the ankles produced by the muscle forces $\mathbf{F_{mus}}$ via their constant moment arms r, and M_{p} is the perturbation moment imposed by the environment. The activation and contraction dynamics of the Hill-type muscles are presented in Eqs. 2 and 3, respectively. Both muscles are parameterized as a Soleus muscle (Thunnissen 1993; Yamaguchi et al. 1990) for simplicity (i.e. symmetric model).

$$\dot{\mathbf{a}} = f_{a}\left(\mathbf{a}, \mathbf{u_{ss}}, \Delta\mathbf{l_{mus}}\left(t-\tau\right), \mathbf{v_{mus}}\left(t-\tau\right), \mathbf{F_{mus}}\left(t-\tau\right), k_{p}, k_{v}, k_{f}\right) \tag{2}$$

$$\dot{\mathbf{l}}_{\mathbf{ce}} = f_{c}\left(\mathbf{Fv_{ce}}\left(\mathbf{a}, \mathbf{Fl_{ce}}, \mathbf{F_{se}}\right)\right) \tag{3}$$

Equation 2 is a delay differential equation (DDE). The dependence on time t is only written explicitly in case of a delay, because else the equations could be mistaken to be non-autonomous. The vector $\mathbf{a}$ represents the active states of both muscles, and $\mathbf{u_{ss}}$ is the supra-spinal neural input vector. The vectors $\Delta\mathbf{l_{mus}}$ and $\mathbf{v_{mus}}$ represent the muscle lengths (relative to the rest lengths) and the muscle velocities, respectively. They are fed back by the reflexive gains k_{p} and k_{v}, respectively, with a time delay τ. This feedback of muscle lengths and velocities represents the stretch reflexes and reciprocal inhibition found in all antagonistic muscle pairs. Force feedback by Golgi tendon organs is represented by an ipsilateral feedback of each muscle force by a reflex gain k_{f}, with time delay τ.
Equation 3 is an inverse force-velocity relationship. The vector $\mathbf{Fv_{ce}}(\mathbf{a},\mathbf{Fl_{ce}},\mathbf{F_{se}})$ represents the momentary values of the force-velocity relationships of the CEs of both muscles, which is obtained by recognizing that the force in the SE must be equal to the force in the CE in this muscle model. These force-velocity relationships are expressed in terms of the momentary values of the force-length relationships of the CEs $\mathbf{Fl_{ce}}$ and the forces in the SEs $\mathbf{F_{se}}$. The elaborate form of Eqs. 1, 2 and 3 is found in App. A.1.

The model contains a total of 6 state variables: the angle θ, the angular velocity ω, the active states of the Tibialis anterior and the Soleus, a_{ta} and a_{sol}, and the lengths of the CEs of both muscles, $l_{ce,ta}$ and $l_{ce,sol}$. However, because of reflexive feedback, the angle and angular velocity also appear in delayed form, $\theta(t\text{-}\tau)$ and $\omega(t\text{-}\tau)$, respectively. Thus, the system is of infinite order. The considered equilibrium is standing upright, which corresponds to zero angle, zero angular velocity, and for both muscles constant, equal, active states and lengths of the CEs. The muscles have different time

constants for increasing and decreasing muscle activation and there is a discontinuity in the slope of the force-velocity curve of the CEs at zero velocity. These discontinuities are exactly in the equilibrium and render bifurcation analysis difficult. Therefore, they have been approximated with the help of a 'sharp' tangent hyperbolic function (i.e. steep slope), as shown in App. A.2. Numerical simulations showed no significant change in behavior between the model with real discontinuities and the one with the smoothed discontinuities.

2.2 Bifurcation analysis

The purpose of the performed bifurcation analysis is to identify the influence of those parameters that can be adjusted by the central nervous system. These are assumed to be the supra-spinal neural input vector $\mathbf{u_{ss}}$ and the reflexive feedback gains of the muscle length, velocity and force, k_p, k_v and k_f, respectively. The supra-spinal input for both muscles is assumed to be equal, thus $\mathbf{u_{ss}} = [u_{ss,ta}\ u_{ss,sol}]^T = [u_{ss}\ u_{ss}]^T$. The influence of a time delay τ, inevitably present in all reflex arcs, is also analyzed. Time delays limit the maximum reflex gains possible for a stable posture, as is known from control engineering. However, the influence of time delays on the occurrence and stability of limit cycles is less clear.

A bifurcation is the appearance of a topologically nonequivalent phase portrait under parameter variation (Kuznetsov 1998). Local bifurcations of a continuous time system, to which we confine ourselves in this paper, may occur when eigenvalues of the linearization about an equilibrium pass the imaginary axis as parameters vary. The two most common bifurcations for such systems are the fold and the Hopf bifurcation, which are conventional textbook paradigms (e.g. Arrowsmith and Place 1990; Iooss and Joseph 1990; Kuznetsov 1998; Seydel 1988). The *fold* bifurcation is associated with the appearance or disappearance of two equilibria. In symmetric systems, such as the musculo-skeletal model, the fold bifurcation often manifests itself as a *pitchfork* bifurcation (Kuznetsov 1998 pp 280-282). Beyond this type of fold bifurcation, an additional third equilibrium appears or disappears, which changes stability at the bifurcation point (eigenvalue of the considered equilibrium passes through zero with non-zero speed). It is this type of fold bifurcation that is associated with the stability of posture in the musculo-skeletal model, with the third equilibrium representing the posture. A *Hopf* bifurcation occurs when a conjugated pair of eigenvalues passes the imaginary axis with non-zero speed. The Andronov-Hopf theorem gives conditions that guarantee that a limit cycle will appear or disappear after a Hopf bifurcation (Arrowsmith and Place 1990). Note that there are two different scenarios, namely the subcritical and the supercritical Hopf bifurcation, but only the latter leads to stable limit cycles. The local stability of encountered limit cycles can be assessed by placing a (hyper)surface

transverse to the flow near the limit cycle. The crossings of the orbit with this surface in a given direction can be seen as a discrete representation of the flow near the limit cycle. This discrete map is called a Poincaré map – or first return map – and has a state space whose dimension is reduced by one relative to the original continuous time system. The limit cycle is represented by a *fixed point* (i.e. rest point) of the Poincaré map. The limit cycle will be locally stable if the fixed point of the Poincaré map is locally stable. This is determined by calculating the eigenvalues of the Poincaré map, which are called *Floquet multipliers*. All multipliers have to be within the unit circle (i.e. in absolute value smaller than 1) for the limit cycle to be locally asymptotically stable (Kuznetsov 1998 pp 27).

Stretch reflexes (position and velocity feedback) are generally known to have an important regulatory function in posture as well as in locomotion (Houk 1979). Co-contraction is an effective – but also very energy-consuming – way of regulating the visco-elastic properties of muscles and is probably only used when necessary. Therefore, our analysis is started by looking at the influence of the stretch reflex at a low co-contraction level. A parameter space is constructed with the positional gain k_p on the horizontal axis and the velocity gain k_v on the vertical axis. In such a space, the dependence of existing bifurcations on those parameters can be shown. The functional role of force feedback is less clear and will be analyzed subsequently in the same parameter space. The steps of the analysis are described in the paragraph below.

Firstly, the equilibria of the DDEs (Eqs. 1, 2 and 3) are calculated for a reference set of parameters. At these equilibria, the system is linearized and, at least, the rightmost eigenvalues – that is, the eigenvalues with the largest real-parts (Lyapunov exponents) – have to be calculated, because these play a dominant role in the system's behavior and stability. Secondly, one of the parameters is changed so that the rightmost eigenvalue(s) crosses the imaginary axis. If it concerns a single eigenvalue with zero imaginary part, a fold bifurcation is encountered, whereas if it concerns a conjugated pair of eigenvalues, a Hopf bifurcation has occurred. From a fold point a whole branch of fold points can be followed through parameter space spanned by k_p and k_v. Similarly, from a Hopf point a branch of Hopf points can be computed, which is represented by a set of combinations of k_p and k_v.

The calculated fold and Hopf branches, with the reflex gains k_p and k_v as parameters, will be used as reference branches for determination of the influence of the other parameters. The influence of time delay τ, supra-spinal input level u_{ss} (i.e. level of co-contraction) and force feedback gain k_f will be determined by calculation of the fold and Hopf branches in the same parameter space, in the same way as described above. Only the parameter whose influence is to be determined is changed relative to the reference parameter set. The influence of those deviating parameters can be observed

by comparing the reference bifurcation branches with the ones with deviating parameter sets. Choosing the same parameter space, instead of constructing new ones with the deviating parameter on one of the axis, is important since it allows the influence of parameters to be compared.

The intersections of fold and Hopf branches can lead to mathematically intriguing bifurcations points, such as the Bognadov-Takens bifurcation and the fold-Hopf bifurcation (Kuznetsov 1998). These bifurcations were indeed encountered in the analysis (Sect. 3.1), but are only discussed as far as is considered relevant. It is not within the scope of this paper to review all possible behaviors in the neighborhood of such points. More significant is the subdivision of parameter space by fold and Hopf branches. This leads to different regions in parameter space, each representing a different qualitative behavior of the model.

In analyzing musculo-skeletal models, the delays present in the reflex arcs result in delayed differential equations (DDEs). The state space for a DDE is infinite-dimensional. The 'DDE-BIFTOOL' Matlab package (Engelborghs et al. 2001) is used in order to perform bifurcation analysis for the DDEs. This package approximates the most dominant eigenvalues, which allows the user to determine the type of bifurcation. Subsequently, DDE-BIFTOOL tests the necessary conditions for the bifurcation to be generic. The Floquet multipliers of limit cycles, emerging beyond the Hopf branch, are numerically calculated by DDE-BIFTOOL by time integration of the variational equation around the periodic solution (for details, see Engelborghs et al. 2001).

2.3 Biomechanical interpretation of fold and Hopf bifurcations by linearization of the stance model

Bifurcation analysis is relatively unknown in the field of biomechanics, whereas it can be of great assistance in understanding the influence of certain parameters on the behavior and stability of biological systems. In the previous subsection (Sect. 2.2), fold and Hopf bifurcations were discussed. In this section, a linearized model is constructed in the form of a block diagram, which makes it possible to link the fold and Hopf bifurcations to some well-known biomechanical and control engineering concepts. The musculo-skeletal model (Sect. 2.1) is linearized in its equilibrium, which represents stance. The equilibrium states are entirely determined by the level of co-contraction a_{co}. The active states of the muscles in equilibrium are equal to the level of co-contraction (a_{ta}=a_{sol}=a_{co}), and co-contraction also determines the length of the contractile elements (CE), $l_{ce,ta}$ and $l_{ce,sol}$. Higher co-contraction leads to a decreased length of the CEs such that a new force equilibrium with the SEs is established, with higher force and generally higher muscle stiffness and viscosity. The angle θ and angular velocity ω are both zero in the equilibrium, because both muscles have the same rest length and supra-spinal input level

u_{ss}. The level of co-contraction is mainly determined by the supra-spinal input, but can also be increased or decreased by force feedback. Positive force feedback will increase the level of co-contraction, while negative force feedback will decrease it. Feedback of the muscle lengths and velocities does *not* change the level of co-contraction a_{co}. The stability of the equilibrium depends on the level of co-contraction and on the reflexive feedback of muscle lengths, velocities and forces. The feedback of muscle lengths and velocities is proven to be especially important in keeping the posture stable (Van der Helm et al. 2002). Time delays in these reflex arcs limit the maximum possible feedback gains, because the gain and phase margin of the reflex loop is decreased by the extra phase lag introduced by time delays. In other words, time delays jeopardize the stability of the posture at high reflex gains.

The linearized model is shown in Fig. 2. The scheme is similar to the linearized musculo-skeletal models used by van der Helm and Rozendaal for analyzing shoulder posture tasks (Van der Helm and Rozendaal 2000). However, in our model, the influence of the SEs of the muscles is not discarded, because the Soleus and Tibialis Anterior have long tendons.

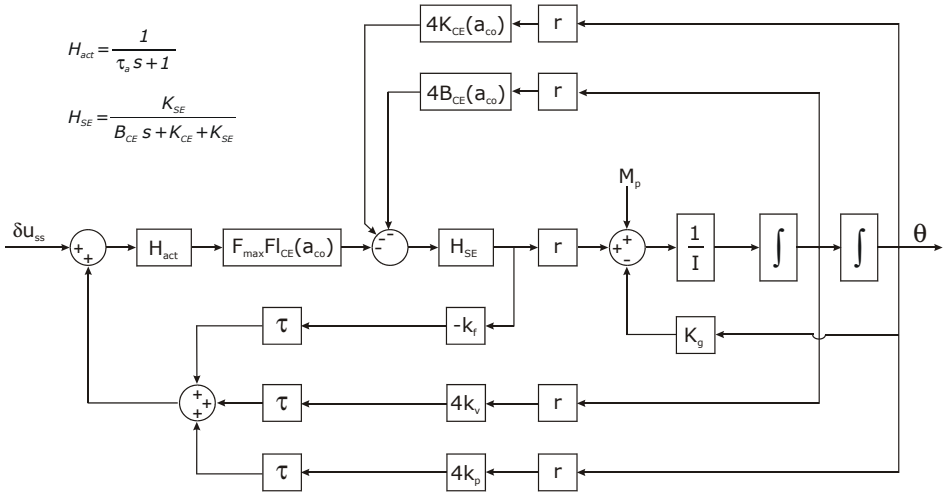

Fig. 2 Linearized model of the musculo-skeletal system including intrinsic visco-elastic properties of the muscle (K_{CE} is stiffness of CE, B_{CE} is viscosity of CE, and H_{SE} is visco-elastic properties due to SE) and delayed reflexive feedback of muscle length, velocity and force with gains k_p, k_v and k_f, respectively. The delay τ is modeled by a Padé approximation. Segment model parameters are moment of inertia I, moment arm r and gravitational stiffness K_g. Muscle parameters are maximal force F_{max} and the value of the force-length relationship in equilibrium $Fl_{CE}(a_{co})$. H_{act} represents the muscle activation dynamics. Inputs are supra-spinal input fluctuations $\delta u_{ss}=u_{ss}-a_{co}$, and perturbation moment M_p. Output is angle of inverse pendulum relative to vertical θ.

Therefore, the SEs of the modeled muscles are compliant (relative to, for example, shoulder muscles) and have a large influence on the behavior and stability of the posture. In the linearized model, this influence is represented by the transfer function H_{SE}. This is recognized as the visco-elastic behavior of the SE in series with the CE. In most muscles of the upper extremity, the SE is very stiff because the tendons are relatively short. In such cases, the influence of the SE in the muscle model can be neglected, but this is generally not true for muscles in the lower extremities.

Gravity has a destabilizing effect on the posture of the inverted pendulum and is modeled as a negative stiffness. This negative gravitational stiffness $K_g=-mgl_{com}$ must be compensated by intrinsic and reflexive feedback so as to achieve a stable posture.

Intrinsic feedback is achieved by co-contraction a_{co}. This co-contraction results in a certain stiffness K_{CE} and viscosity B_{CE} of the CE of each muscle. The stiffness K_{CE} of the muscle model is proportional to the co-contraction and the derivative of the force-length relationship at the equilibrium length of the CE. The viscosity B_{CE} of the muscle model is proportional to the co-contraction, the force-length relationship at the equilibrium length of the CE and the derivative of the force-velocity relationship at zero velocity of the CE. As the length of the CEs is determined by the co-contraction, K_{CE} and B_{CE} only depend on the level of co-contraction.

Reflexive feedback is achieved by feedback of muscle length, velocity and force with gains k_p, k_v and k_f, respectively. All reflexive feedback is proportional to the value of the force-length relationship in the equilibrium $Fl_{ce}(a_{co})$, as shown in the block diagram. The time delay τ is modeled as a third-order Padé approximation (see App. A.3) in the linearized block diagram, which gives good results regarding prediction of the eigenvalues of the model (at least up to the transition from linear stability to linear instability). The stretch reflex is modeled as the feedback of angle θ and angular velocity ω, because these are directly related to muscle length and velocity (see App. A.1). Ideally, the feedback of muscle length would purely define muscle stiffness and the feedback of muscle velocity would purely define muscle viscosity. However, the activation dynamics H_{act}, visco-elastic dynamics H_{SE} and especially the delay τ ($H_\tau=e^{-j\omega\tau}$) add a considerable phase lag to the reflex loop, endangering the stability of posture. The visco-elastic dynamic properties due to the SE, H_{SE}, not only introduces phase lag, but also reduces the total muscle stiffness. It becomes $K_{mus}=K_{SE}(K_{CE}+K_R)/(K_{CE}+K_{SE})$, with K_{SE} the stiffness of the SE, K_{CE} the intrinsic stiffness of the CE and K_R the reflexive contribution to the stiffness of the CE.

The contribution of force feedback with gain k_f is twofold. Firstly, as mentioned above, force feedback changes the level of co-contraction a_{co}. Positive force feedback will increase the co-contraction and thereby increase

the intrinsic and reflexive contributions to muscle stiffness and viscosity. Negative force feedback will decrease the muscle stiffness and viscosity. Secondly, force feedback introduces some extra dynamics because it modulates the intrinsic and reflexive feedback loops, as shown in the block diagram (Fig. 2). Positive force feedback makes activation dynamics become more dominant, giving more phase lag at low frequencies. This leads to linear instability if this phase lag is not compensated by additional feedback of muscle velocity. On the other hand, negative force feedback will decrease the intrinsic and reflexive contributions to muscle stiffness and viscosity. The activation dynamics become less dominant, giving less phase lag at low frequencies in the reflexive loops, and the posture might therefore be less susceptible to instability.
It has been long known that negative force feedback exists in humans (Sherwood 1997), and at one time it was thought that its sole purpose was the protection of muscles from overload. Later, the functions of stiffness regulation (Houk 1979) and compensation for muscle fatigue (Kirsch and Rymer 1987) were hypothesized. The existence of positive force feedback in humans is still the subject of debate (Capaday 2000; Capaday 2001; Duysens 2000). The exact role of force feedback in posture and locomotion is not yet clear, although it does seem to be significant (Dietz 1998; Dietz and Duysens 2000; Duysens et al. 2000).

The linearized model of stance can predict the eigenvalues of the posture quite well. Therefore, it will be used to provide insight into the physical causes of encountered fold and Hopf bifurcations (see Sects. 3.1-3.4). A limitation of the linearized model is that the behavior will only be correctly predicted if the posture is stable and the perturbations are small. Hence, bifurcation analysis is necessary to predict the behavior of the posture when it has become linearly unstable.

3. Results of the numerical simulations

In this section, the influence of stretch reflexes (including reciprocal inhibition), time delays, co-contraction and force feedback on the behavior of the musculo-skeletal model of stance is discussed. Stability regions of posture and periodic movement in parameter space (k_p versus k_v, Sect. 2.2) will be distinguished with the help of bifurcation analysis. The linearized model described in Sect. 2.3 will be used to link these findings with known concepts in the biomechanical field. Section 3.5 describes how the model is fitted to data from literature about quiet and perturbed stance in order to get a notion of normal feedback gains in healthy people.

To begin our analysis, a reference parameter set has to be chosen. This defines the reference equilibrium in state space and accompanying eigenvalues. The reference parameter set is $[u_{ss}\ k_p\ k_v\ k_f\ \tau]^T = [0.1\ 50\ 10\ 0\ 50\cdot10^{-3}]^T$, where u_{ss} is the value of both supra-spinal neural inputs, k_p, k_v and k_f are the reflexive feedback gains of the muscle lengthening, velocity and force, respectively, and τ is the time delay present in the reflex arcs. A low level of supra-spinal input (u=0.1) is chosen, which is not enough to stabilize the posture without reflexive feedback. The influence of stretch reflexes is studied first, and thus the force feedback gain k_f is initially set to zero. The reference gains k_p=50 and k_v=10 stabilize the posture. A reference delay τ of 50 ms is chosen, because this is typical for the short latency reflexes found in human ankle flexors and extensors (Sinkjaer et al. 1988). These parameters give an equilibrium at

$$\mathbf{x_{eq,ref}} = \left[a_{ta}\ a_{sol}\ l_{ce,ta}\ l_{ce,sol}\ \theta\ \omega\right]^T = \left[0.1\ 0.1\ 0.936\ 0.936\ 0\ 0\right]^T,$$

with accompanying rightmost eigenvalues $\lambda_{rm,ref} = -1.46 \pm 4.54j$ (i.e. posture is stable). As mentioned in Sect. 2.3, the states of the equilibrium $\mathbf{x_{eq}}$ only depend on the value of the supra-spinal inputs u_{ss} and on the force feedback gain k_f. However, the stability of the equilibrium also depends on the positional feedback gain k_p, the velocity feedback gain k_v and the delay τ of the reflex arc.

3.1 Influence of stretch reflexes on model behavior and stability

The influence of stretch reflex gains on the behavior of the model is explored by looking at bifurcations in parameter space, with the positional gain k_p on one axis and the velocity gain k_v on the other. A bifurcation point is found by varying one parameter while looking at the rightmost eigenvalues of the equilibrium, because they dominate the system behavior. Figure 3 shows the

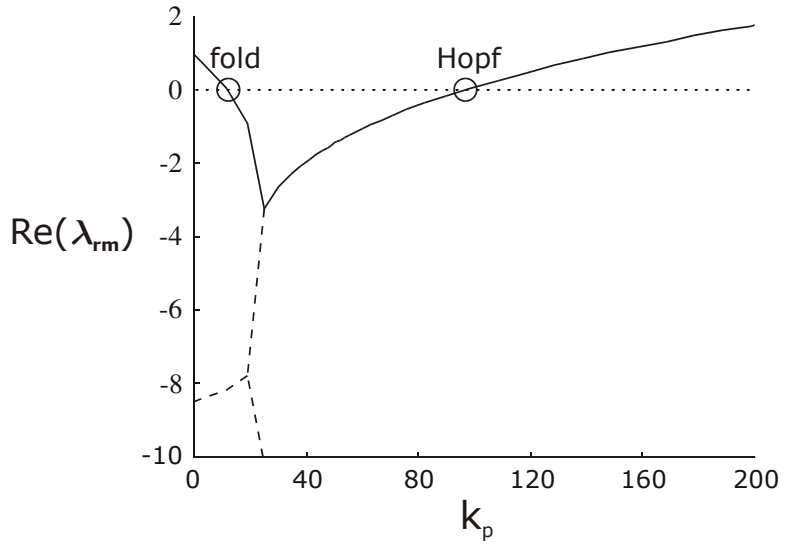

Fig. 3 The real part of the rightmost eigenvalues versus the positional feedback gain k_p. The other parameters are kept constant at reference values. The *left marking* represents a fold bifurcation (one eigenvalue through zero); the *right marking* represents a Hopf bifurcation (conjugated pair of eigenvalues through imaginary axis).

real part of the rightmost eigenvalues $\boldsymbol{\lambda}_{\mathbf{rm}}$ in dependence of k_p, while the other parameters are kept constant at their reference value.

The events for which the rightmost eigenvalues go through the imaginary axis are marked in the figure by circles and correspond to a fold and a Hopf bifurcation. Distinguishing between a Hopf and a fold bifurcation from this figure is not possible. However, looking at the imaginary part of the eigenvalues will reveal the nature of the bifurcation (Sect. 2.2).

A fold and a Hopf branch are continued in parameter space, with the previously determined bifurcation points as starting points. Figure 4 shows the fold and the Hopf branch as well as the starting points. The fold branch is a vertical line, indicating that the fold bifurcation only depends on k_p.

The fold and Hopf branches divide parameter space into four regions, marked I, II, III and IV in the figure. The intrinsic stiffness of the muscles, induced by a co-contraction of 10 percent, is too small to compensate for the negative stiffness caused by the gravitational force. Thus, without reflexive feedback ($[k_p\ k_v]^T = [0\ 0]^T$ in the figure) the pendulum will fall to $\pm\pi$, because the

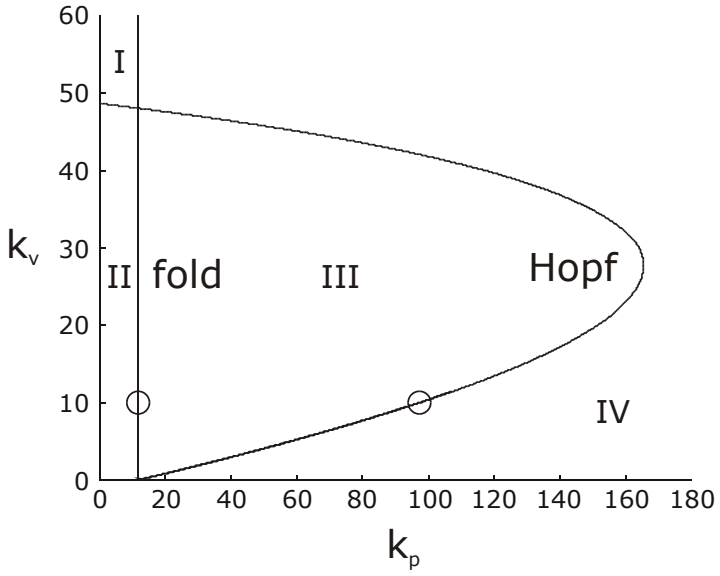

Fig. 4 Hopf and fold bifurcations in parameter space. The parameters are the positional feedback gain k_p and the velocity feedback gain k_v. The starting points of the bifurcation branches are marked and correspond to the marked points in Fig. 3. The fold and Hopf branch divide the parameter space in four different regions: I, II, III, IV. In region I and II the posture is unstable and the person will 'fall'. The posture is stable in region III and in region IV oscillatory movements are experienced (i.e. limit cycles).

muscles have no parallel element. Reflexive feedback of the muscle lengthening will increase the muscle stiffness. For a given level of co-contraction, a certain minimal positional feedback gain $k_{p,min}$ is necessary in order to compensate for the negative 'gravitational stiffness' K_g. This minimal feedback gain of the muscle length, $k_{p,min}$, is represented by the vertical fold bifurcation line in the figure. Thus, in region I and II the person falls because the total ankle stiffness, caused by muscles and gravity, is negative.

For stable posture, besides the minimal positional feedback gain $k_{p,min}$,a minimal velocity feedback gain $k_{v,min}$ is also necessary. Velocity feedback is necessary to compensate for the phase lag caused by time delay in the reflex arcs, muscle activation dynamics and the presence of a compliant SE (Sec 2.3). Figure 5 shows the minimal feedback gains to be $[k_{p,min}\ k_{v,min}]^T = [11.7\ 5.5\cdot10^{-2}]^T$. This point is an intersection of the fold and Hopf branch and has a double zero as rightmost eigenvalues. It is, in fact, a Bognadov-Takens (BT) bifurcation and it is the start of the Hopf branch in parameter space.

The lower part of the Hopf branch (Fig. 4), up to the turn ($[k_p\ k_v]^T = [165.6\ 27.6]^T$), represents all possible positional feedback gains k_p with accompanying minimal velocity feedback gains k_v. For higher velocity gains,

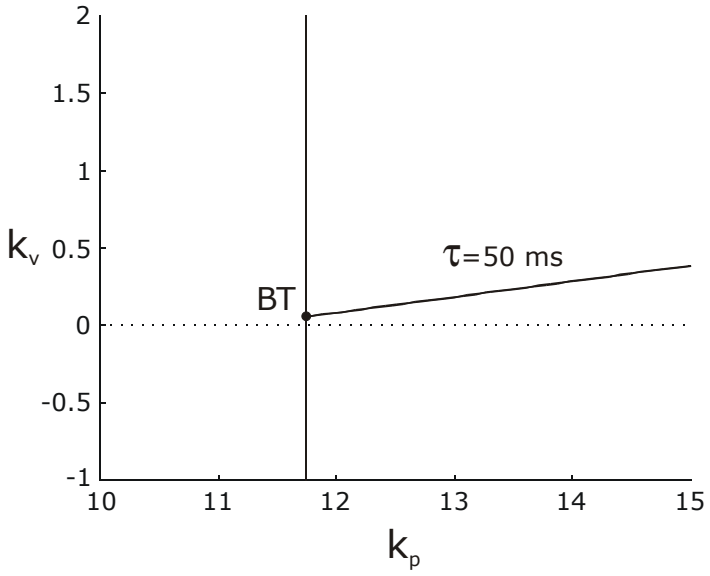

Fig. 5 Zoom-in of Fig. 4. BT is a Bognadov-Takens bifurcation, the first intersection of fold and Hopf branch and representing the minimal feedback gains $[k_{p,min}\ k_{v,min}]^T = [11.7\ 5.5{\cdot}10^{-2}]^T$ above which the posture will be stable (up to certain maximum gains).

the posture is stable; for lower gains it is unstable. However, if velocity gains increase too much the reflex loop also becomes unstable. The upper part of the Hopf branch is associated with these maximal velocity feedback gains. To the right of the turning point of the Hopf branch the posture is also unstable, because the positional feedback is too high for any velocity feedback. Thus, in region III the posture is stable because the lack of intrinsic stiffness is compensated by a large enough positional feedback. In addition, the phase lag, introduced mostly by time delay, is compensated by a velocity feedback.
If one travels from region III to IV across the Hopf branch, the phase and/or gain margin reduces and the stability of the posture vanishes. Instead, a limit cycle originates around the equilibrium states of the previously stable posture. Limit cycles can only exist for non-linear systems, and their local stability is determined by the eigenvalues of the Poincaré map (i.e. linearization about the cycle), called Floquet multipliers (Sect. 2.2). The Floquet multipliers of the limit cycles were calculated and the absolute values were always less than unity, indicating stable limit cycles just beyond the Hopf branch in all of region IV. In Fig. 6, the size of the imaginary part of the conjugated pair of eigenvalues associated with the Hopf bifurcation is shown. The size of the imaginary part *Im* is directly related to the period *T* of the sinusoidal periodic solutions just beyond these Hopf points ($T=2\pi/Im$).

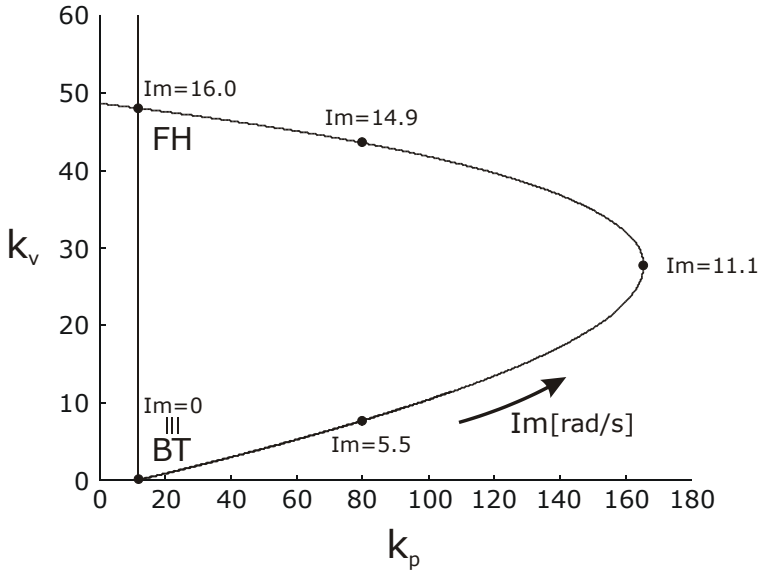

Fig. 6 Size of imaginary parts *Im* of conjugated pair of eigenvalues related to the Hopf bifurcations are plotted along the Hopf branch. The period *T* of limit cycles just beyond these Hopf points is about $T=2\pi/Im$.

Along the Hopf branch, for increasing velocity gain k_v, *Im* increases (i.e. *T* decreases) from 0 rad/s at the BT to16.0 rad/s at the second intersection of the fold and Hopf branch. This intersection has a zero and a conjugated pair of eigenvalues on the imaginary axis and is in fact a fold-Hopf (FH) bifurcation. Left from the FH, in region I, the limit cycles are unstable. In the neighborhood of the BT and FH bifurcations, complex dynamical behavior can be expected, such as homoclinic cycles (BT) and tori (FH). However, analysis of these complex behaviors is not within the scope of this paper. See Kuznetsov (1998) for more information about BT and FH bifurcations, and about the possible system behavior in their neighborhoods.

The observed limit cycles do *not* represent the sway experienced during stance, because sway is assumed to be the result of perturbations acting on a stable equilibrium (Sect. 2.1). They are more likely to be related to a pathological case termed ankle clonus. Clonus is a sustained rhythmical contraction of muscles that occurs after a sudden stretch and is often caused by injury to the central nervous system. Hidler and Rymer (1999, 2000) showed that the presence of two conditions lead to clonus, namely, the presence of significant delays in the reflex paths and an increase in effective reflex gains, caused by a reduced motoneuron firing threshold. The ankle is

one of the most distal joints, which means that there are large time delays in its reflex arcs. This is why ankle clonus is a quite common type of clonus.
The limit cycles to the right and above the Hopf branch (Figs. 4 and 6) are caused by similar mechanisms to those causing ankle clonus, namely, high reflex gains in combination with a considerable time delay in the reflex arcs. The period of the oscillations, associated with ankle clonus, depends on the feedback gains of muscle lengthening and velocity and varies between 1.8 and 2.5 Hz (Fig. 6). In literature, frequencies of about 3 to 8 Hz are reported, but these are usually assessed when the patient is seated. It is therefore not surprising that our simulated frequencies, assessed using a model of stance, are somewhat lower (the moment of inertia about the ankles is much larger in stance compared to sitting).

3.2 Influence of reflex delay on model behavior and stability

The influence of time delay τ on the behavior of the posture model is shown in Fig. 7 in parameter space. The fold branch does not change for different delays, because it represents the muscle length feedback $k_{p,min}$ for zero ankle stiffness, and stiffness is defined at zero frequency. Time delay only adds phase lag proportional to frequency ($H_\tau = e^{-j\omega\tau}$) and has no influence on

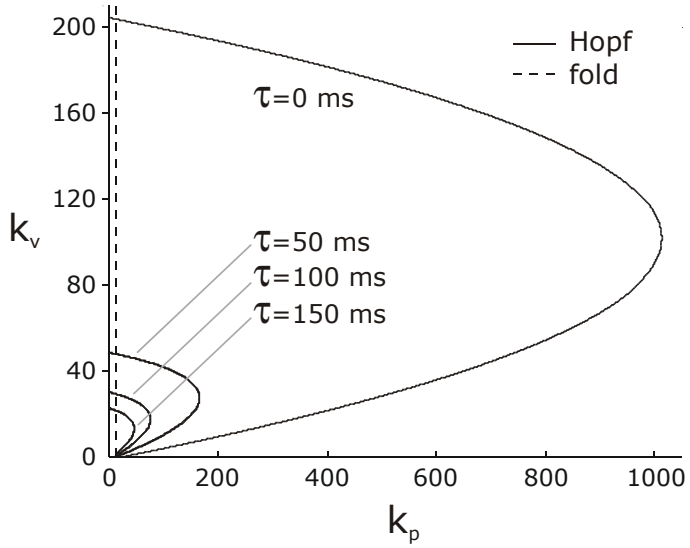

Fig. 7 Influence of time delays τ on fold and Hopf branches. Fold bifurcation branch is unaffected by delay. Hopf bifurcation branch shrinks with increasing delay.

stiffness and therefore none on the location of the fold bifurcation in parameter space either. However, time delay has a tremendous influence on the Hopf branch. For increasing delay, the Hopf branch 'shrinks' because it becomes harder to compensate for the extra phase lag introduced by this delay. This causes the region of reflex gains for which the posture is stable (region III in Fig. 4) to become smaller.
The period of the stable limit cycles, emerging beyond the Hopf branch, will increase with increasing time delay. The frequency of stable oscillations is up to 6.3 Hz for zero time delay, up to 2.5 Hz for 50 ms time delay (as mentioned in the previous section), up to 1.7 Hz for 100 ms time delay, and up to 1.2 Hz for 150 ms time delay. These maximum frequencies lie in the neighborhood of the FH.

Figure 8 shows a zoom-in of parameter space at the BT point. The minimal velocity feedback gain $k_{v,min}$ necessary for stable posture increases for increasing time delay τ, because the extra phase lag of the time delay has to be compensated by extra velocity feedback. The figure also shows that without time delay no velocity feedback would be necessary at all to obtain stable posture (though it might give better transient response).

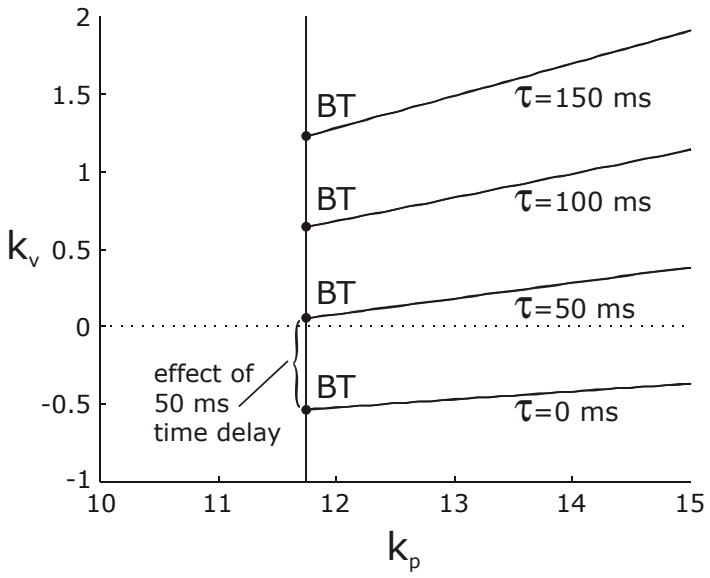

Fig. 8 Zoom-in of Fig. 7. Increasing time delay increases the minimal velocity feedback, $k_{v,min}$, necessary for stable posture.

3.3 Influence of co-contraction on model behavior and stability

Increased supra-spinal input u_{ss} leads to increased co-contraction a_{co} and so to shortened CEs. In other words, the active states and lengths of the CEs of the muscles in equilibrium change. In Fig. 9, the influence of increased supra-spinal inputs u_{ss} on the fold bifurcation in terms of positional feedback gain k_p is shown. The intrinsic stiffness of the muscles becomes greater for increasing co-contraction, and for u_{ss}>0.23 the stiffness has become so great that reflexive feedback is no longer necessary for stable posture (k_p<0 for u_{ss}>0.23 in Fig. 9). In a parameter space of k_p versus k_v (as in Fig. 4), this would manifest itself as a shift of the vertical fold branch to the left for increasing u_{ss}.

The influence of increased supra-spinal input u_{ss} on the Hopf branch is shown in Fig. 10. This figure shows that the Hopf branch grows rapidly with increasing co-contraction and thus provides stable posture for much larger

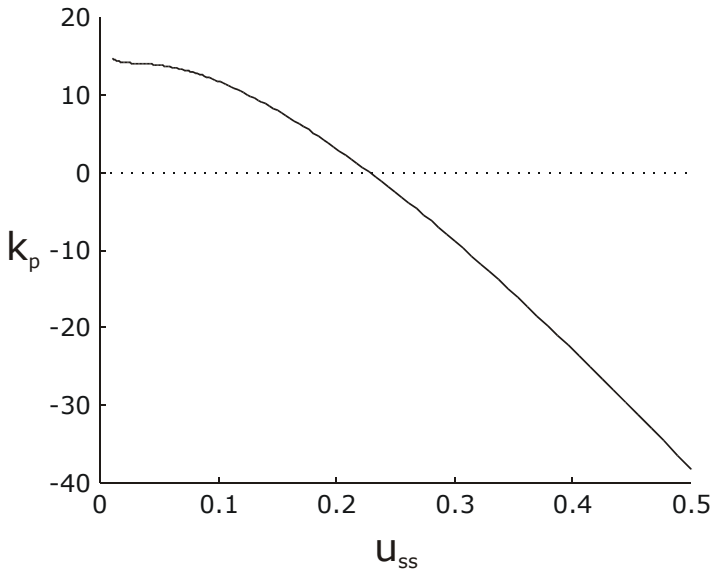

Fig. 9 Influence of supra-spinal input u_{ss}, in this case equal to the co-contraction a_{co} (no force feedback), on fold bifurcation. The fold branch represents the minimal muscle length feedback $k_{p,min}$, which exactly compensates for the negative gravitational stiffness: the total ankle stiffness is zero. Higher co-contraction increases the intrinsic muscle stiffness and therefore less muscle length feedback is necessary for stable posture. For neural inputs higher than 0.23 (23% of maximal co-contraction) the posture is stable without any reflexive feedback at all.

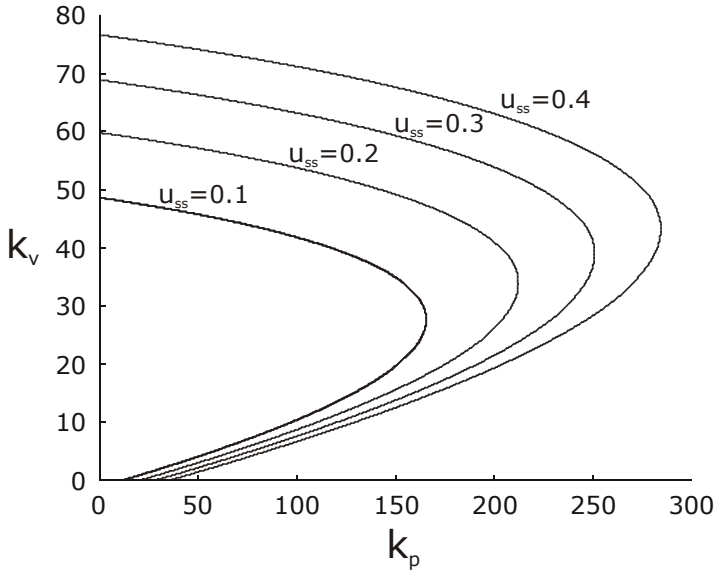

Fig. 10 Influence of neural input u_{ss}, in this case equal to the co-contraction a_{co} (no force feedback), on Hopf branches. Increased level of co-contraction lowers the effective reflex loop gain and increases the intrinsic muscle stiffness, which leads to larger Hopf branches.

feedback gains. A large part of this growth is due to the fact that for increasing co-contraction the muscles will work on a lower part of their force-length relationship (below optimum length), thereby decreasing the effective reflex loop gain. Moreover, increasing the intrinsic stiffness of the muscles decreases the loop gain further, especially at low frequencies.
The period of the stable limit cycles, emerging beyond the Hopf branches, will decrease slightly with increasing co-contraction. The frequency of the stable oscillations is up to 2.5 Hz for 10% co-contraction (as mentioned in Sect. 3.1), up to 2.7 Hz for 20-30% co-contraction, and up to 2.8 Hz for 40% co-contraction.

3.4 Influence of force feedback on model behavior and stability

The influence of force-feedback in musculo-skeletal systems is still a topic of debate. Force feedback in the model of stance has two consequences: it changes the equilibrium by changing the level of co-contraction a_{co} (Sec 3.3) and it modulates the intrinsic and reflexive feedback loops (Sec 2.3). The solid lines in Fig. 11 show the influence of force feedback with gain k_f on the fold bifurcation (positive k_f means positive force feedback). For positive force

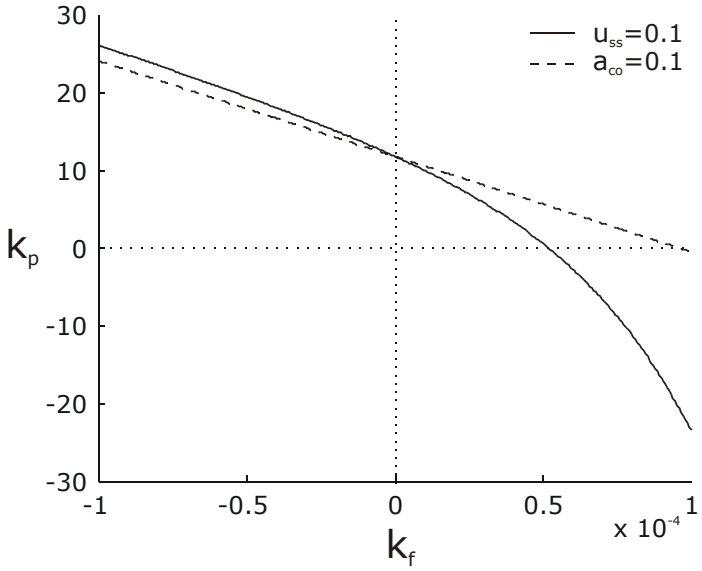

Fig. 11 Influence of force feedback k_f on fold bifurcation. Positive k_f means positive force feedback. *Solid line* shows influence of force feedback on fold bifurcation. Positive force feedback increases the co-contraction and modulates the intrinsic and reflexive feedback loops. This increases ankle stiffness, and therefore less muscle length feedback k_p is necessary. The influence of the modulation effect alone is shown by the *dashed line* (co-contraction is kept constant by adapting the supra-spinal input u_{ss}).

feedback, less or no positional feedback is necessary in terms of k_p to obtain positive ankle stiffness; for negative force feedback more positional feedback is necessary. To merely see the modulation effect of force feedback, the supra-spinal inputs were adapted such that there was no increase in co-contraction (i.e. same equilibrium for all k_f). This is represented by the dashed lines and shows a linear relation between k_p and k_f.

The influence of force feedback on the Hopf branch is shown in Fig. 12. The modulation effect (dashed lines) of positive force feedback makes the Hopf branch shrink considerably, which is compensated only slightly by the effect of increased co-contraction. Negative force feedback, on the other hand, enlarges the Hopf branch. To summarize, positive force feedback increases the muscle stiffness (intrinsic and reflexive), but the posture becomes more susceptible to an unstable reflex loop. For negative force feedback, it is precisely the other way around.

The frequency of stable oscillations is not very sensitive to increasing force feedback. It is up to 2.6 Hz for negative force feedback with gain k_f=-1.0·10^{-5}

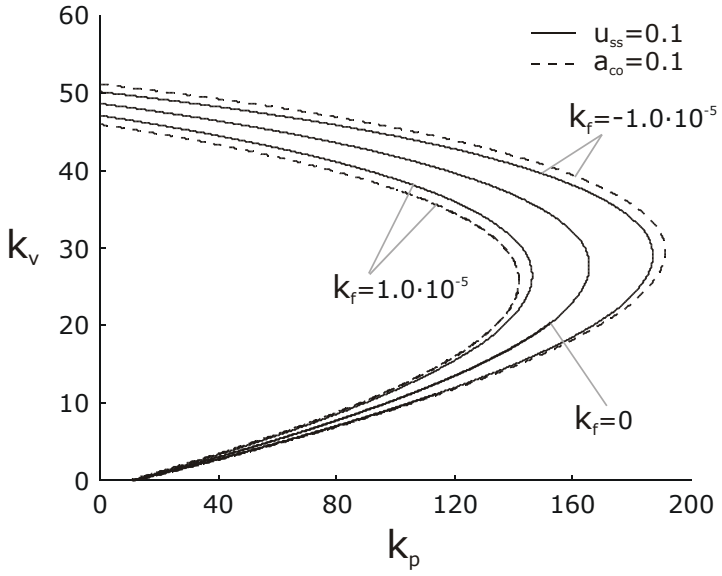

Fig. 12 Influence of force feedback k_f on Hopf branches. Positive k_f means positive force feedback. *Solid lines* show influence of force feedback on the Hopf branch (increased co-contraction and modulation of reflexive and intrinsic loops). The influence of the modulation effect alone is shown by the *dashed lines* (co-contraction is kept constant by adapting the supra-spinal input u_{ss}). The effect of modulation is dominant and causes the Hopf branch to shrink for positive force feedback.

and up to 2.5 Hz for no force feedback (as mentioned in Sect. 3.1) or positive force feedback with gain k_f=1.0·10^{-5}.

3.5 Model fit to data of quiet and perturbed stance

To get a notion about the reflex gains experienced during posture, the model was fitted to data from literature about disturbance rejection and quiet stance in the sagittal plane. Mihelj et al. (2000) measured the effective ankle stiffness (i.e. stiffness of ankle muscles plus gravitational stiffness) in the sagittal plane in response to disturbances, relying mainly on ankle strategy (i.e. counteracting perturbations with your ankle joints only). They found it to be between 9 and 12 Nm/°. We roughly estimated the relative damping factor at between 0.6 and 0.8 by taking the logarithmic decrement of the presented graphs. The combinations of reflex gains $[k_p\ k_v]^T$ reflecting these data is shown in Fig. 13 (light gray area).

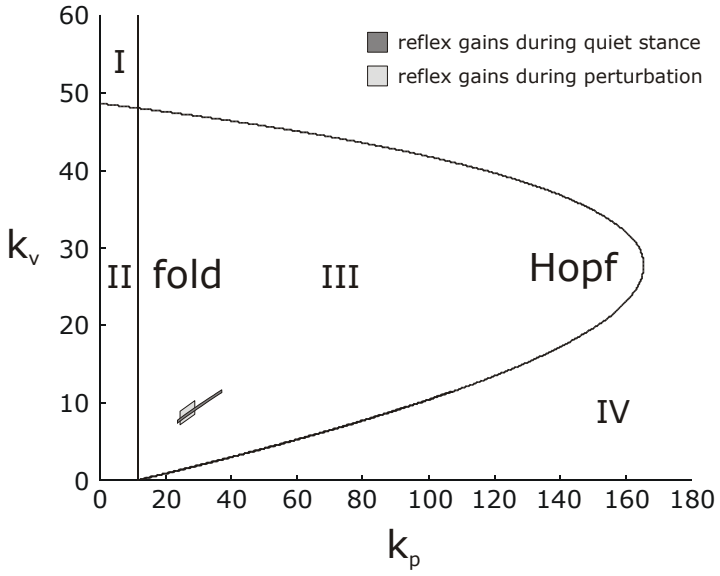

Fig. 13 Areas of reflex gains for the stance model fitted to data from the literature of perturbed stance (*light gray*) and quiet stance (*dark gray*).

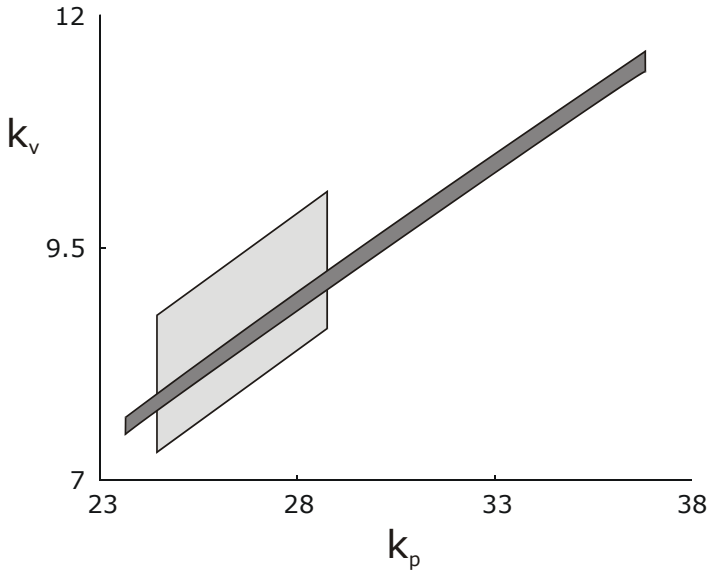

Fig. 14 Zoom-in of Fig. 13. The overlap of the areas of reflex gains, experienced during perturbed and quiet stance, could indicate that stretch reflexes play a major role in stabilizing the posture in both cases.

Whether or not ankle stiffness – reflexive stiffness in particular – is important in quiet stance remains a topic of debate. Some believe anticipatory control makes a major contribution to stability during quiet stance (Masani et al. 2003; Morasso and Sanguineti 2002). However, Fitzpatrick et al. (1994) have shown that afferent feedback from ankle muscles is sufficient for a stable upright stance. Therefore, we fitted our model to data of quiet stance in the sagittal plane with the subject's eyes closed (Winter et al. 1998) and also plotted it into Fig. 13 (dark gray area). Figure 14 zooms in on the areas of reflex gains. The figure shows that the areas of reflex gains for perturbed stance and quiet stance overlap.

Most experts agree that reflexes play a crucial role in perturbed stance. For quiet stance, it has been proposed that anticipatory control may play a key role. However, the overlap of the calculated areas of reflex gains for perturbed stance and quiet stance could be an indication that stretch reflexes are the major control mechanisms in both cases.

4. Discussion

4.1 How should stability be quantified?

The upright standing posture considered in this paper is an example of a perturbed equilibrium. Fluctuations around the equilibrium can be caused by, for example, measurement noise in muscle spindles, noise in the neural processing of the information, or environmental perturbations such as a push. If these fluctuations are small, local asymptotic stability of the posture guarantees convergence back to the equilibrium. The local stability is defined by the eigenvalues of the equilibrium. Similarly, the stability against small perturbations in walking is determined by the Floquet multipliers of the gait cycle, which Hurmuzlu et al. (1996) calculated from experimental data constructing a Poincaré map. Another method to assess local stability from experimental gait data is the calculation of maximum finite-time Lyapunov exponents (Dingwell and Cusumano 2000; Dingwell et al. 2000). Traditional measures of gait stability, based on kinematic variability, are poor predictors of local stability (Dingwell et al. 2001).

For both walking and posture tasks, the stability against larger perturbations is of great importance. In walking, for example, perturbations like tripping, stumbling and pushing are frequent in daily life (Forner Cordero 2003). Stability against these kinds of perturbation cannot be determined by the calculation of the eigenvalues, because for large perturbations linearization is in general not justified. In fact, for large perturbations the non-linear terms of the differential equations determine the stability. Thus, local stability is only a necessary condition for stability against larger perturbations.

An interesting measure of stability is the *basin of attraction*. The basin of attraction of an attractor, such as a limit cycle, is the set of all the initial conditions in state space that lead to an orbit that approaches the attractor (Seydel 1988). Schwab and Wisse (2001) calculated the basin of attraction of the gait cycle of the simplest walking model for different slopes (i.e. different gravitational energy inputs). After comparison with the Floquet multipliers at these slopes, they concluded that there is no obvious relation between the local stability and the size of the basin of attraction. In other words, a better local stability margin does not imply a better stability margin against large perturbations.

The interpretation of the basin of attraction is easy in the above case, because the basin of attraction equals all combinations of initial stance leg angles and angular velocities that lead to stable walking. If the basin of attraction is larger, the bipedal robot is easier to start up and this is

desirable. Thus, Schwab and Wisse (2001) concluded that the size of the basin of attraction is the most important stability measure in designing such bipedal robots. The question is if the basin of attraction is also a good measure of stability for human walking. In models of human walking, the basin of attraction can theoretically be computed in the same way as is done for the simplest walker, namely, by searching numerically the state-space for all initial conditions under which the system returns to the cycle. However, more realistic models of walking can only be described by high-dimensional models, and this implies two problems. The first is the high computational effort required: the computation time for calculating the basin of attraction grows exponentially with system dimension, while the computing time for the 2D basin of the simplest walker is already long. The second problem is one of interpretation. Not only is the *size* of the basin of attraction given in terms of (hyper)volume of importance, but its *shape* as well. If the basin of attraction increases substantially in some dimensions of low importance but decreases a little in a very important dimension, looking only at the (hyper)volume of the basin leads to the wrong conclusion, namely, that the stability margin has increased. Another problem concerning the interpretation of the basin of attraction is that the states of the model are often an abstraction or simplification of reality and/or are not measurable (e.g. muscle activation). Thus for many states it is not known how much they are perturbed in real-life walking.

Stability in experimental gait studies is often quantified by indices, coming from rather intuitive tests and having few predictive capabilities (Boulgarides et al. 2003). Moreover, the question remains whether the perturbations given in such tests are representative of those in everyday life. It would be useful to link the stability measures from theoretical and experimental research in the future to see how they are related and possibly to propose better ways of determining stability through experimental research.

4.2 Concluding remarks

Bifurcations analysis was performed to show the influence of stretch reflexes, time delays, co-contraction and force feedback on the behavior and stability of a model of stance. A fold and a Hopf branch divided the parameter space, in terms of muscle length and velocity feedback gains, into regions of different behavior: unstable posture, stable posture and stable limit cycles. A linearized model was constructed and provides insight in the biomechanical causes for the bifurcations. The fold bifurcation represents zero ankle stiffness, below which the posture is unstable and a person falls. Ankle stiffness is increased by extra muscle length feedback, increased co-contraction or positive force feedback. Feedback of muscle velocity is necessary to compensate for phase lag caused by time delay in the reflex arcs, muscle activation dynamics and the presence of a compliant SE. The

Hopf bifurcation represents the transition to unstable reflex loops. Beyond a Hopf bifurcation the posture becomes unstable and, in case of positive ankle stiffness, a stable limit cycle emerges. The Hopf branch shrinks for increasing time delays, making the posture more susceptible to unstable reflex loops. Older people or people with injuries to the central nervous system often have larger time delays in their reflex arcs. The fact that these groups of people often have trouble with posture tasks, such as standing, might be explained by this increased time delay. Positive force feedback also reduces the size of the Hopf branch. More co-contraction leads to a growth of the Hopf branch, causing a larger region of postural stability in terms of stretch reflex gains. The period of the limit cycles, emerging beyond the Hopf branch, is mainly dependent on muscle length and velocity feedback and on the amount of time delay present in the reflex arc. The stable limit cycles do not correspond to the sway observed in human stance, but rather to a neural deficiency termed ankle clonus. This is caused by higher effective reflex gains (i.e. reduced motoneuron firing threshold) together with the large time delay present in the reflex arcs of the ankles. A model fit to data of perturbed and quiet stance in healthy subjects shows that stretch reflexes might be the major control mechanism in both cases.
This study has considered the influence of reflexes on stance by combining bifurcation analysis with more common biomechanical concepts and tools. It provides a framework for future research: we will develop this line of research to look at rhythmic tasks such as walking.

References

Amemiya M, Yamaguchi T (1984) Fictive locomotion of the forelimb evoked by stimulation of the mesencephalic locomotor region in the decerebrate cat. Neurosci Lett 50:91-96.

Arrowsmith DK, Place CM (1990) An introduction to dynamical systems. Cambridge University Press, Cambridge, pp 423

Boulgarides LK, McGinty SM, Willett JA, Barnes CW (2003) Use of clinical and impairment-based tests to predict falls by community-dwelling older adults. Phys Ther 83:328-339

Brown TG (1911) The intrinsic factors in the act of progression in the mammal Proc Royal Soc. Vol. B84, London, pp 308-319

Capaday C (2000) Control of a 'simple' stretch reflex in humans. Trends Neurosci 23:528-529

Capaday C (2001) Force-feedback during human walking. Trends Neurosci 24:10

Cohen AH, Wallen P (1980) The neuronal correlate of locomotion in fish. "Fictive swimming" induced in an in vitro preparation of the lamprey spinal cord. Exp Brain Res 41:11-18

Dietz V (1998) Evidence for a load receptor contribution to the control of posture and locomotion. Neurosci Biobehav Rev 22:495-499.

Dietz V, Duysens J (2000) Significance of load receptor input during locomotion: a review. Gait Posture 11:102-110.

Dingwell JB, Cusumano JP (2000) Nonlinear time series analysis of normal and pathological human walking. Chaos 10:848-863

Dingwell JB, Cusumano JP, Cavanagh PR, Sternad D (2001) Local dynamic stability versus kinematic variability of continuous overground and treadmill walking. J Biomech Eng 123:27-32

Dingwell JB, Cusumano JP, Sternad D, Cavanagh PR (2000) Slower speeds in patients with diabetic neuropathy lead to improved local dynamic stability of continuous overground walking. J Biomech 33:1269-1277

Duysens J (2000) Reply. Trends Neurosci 23:529-530

Duysens J, Clarac F, Cruse H (2000) Load-regulating mechanisms in gait and posture: comparative aspects. Physiol Rev 80:83-133.

Duysens J, Van de Crommert HW (1998) Neural control of locomotion; The central pattern generator from cats to humans. Gait Posture 7:131-141.

Engelborghs K, Luzyanina T, Samaey G (2001) DDE-BIFTOOL v. 2.00: a Matlab package for bifurcation analysis of delay differential equations. Technical Report TW-330, Department of Computer Science, K.U. Leuven, LeuvenDepartment of Computer Science, Heverlee, Belgium

Fitzpatrick R, Rogers DK, McCloskey DI (1994) Stable human standing with lower-limb muscle afferents providing the only sensory input. J Physiol 480 (Pt 2):395-403

Forner Cordero A (2003) Human gait, stumble and ... fall? Mechanical limitations of the recovery from a stumble. Engineering Technology. University of Twente, Enschede, pp 196

Garcia M, Chatterjee A, Ruina A, Coleman M (1998) The simplest walking model: stability, complexity, and scaling. J Biomech Eng 120:281-288.

Grillner S, McClellan A, Perret C (1981) Entrainment of the spinal pattern generators for swimming by mechano- sensitive elements in the lamprey spinal cord in vitro. Brain Res 217:380-386.

Hidler JM, Rymer WZ (1999) A simulation study of reflex instability in spasticity: origins of clonus. IEEE Trans Rehabil Eng 7:327-340.
Hidler JM, Rymer WZ (2000) Limit cycle behavior in spasticity: analysis and evaluation. IEEE Trans Biomed Eng 47:1565-1575.
Houk JC (1979) Regulation of stiffness by skeletomotor reflexes. Annu Rev Physiol 41:99-114
Hurmuzlu Y, Basdogan C (1994) On the measurement of dynamic stability of human locomotion. J Biomech Eng 116:30-36
Hurmuzlu Y, Basdogan C, Stoianovici D (1996) Kinematics and dynamic stability of the locomotion of post-polio patients. J Biomech Eng 118:405-411
Inman V, Ralston H, Todd F (1981) Human Walking. Williams and Wilkins, Baltimore
Iooss G, Joseph DD (1990) Elementary stability and bifurcation theory. Springer-Verlag, New York, pp 324
Kirsch RF, Rymer WZ (1987) Neural compensation for muscular fatigue: evidence for significant force regulation in man. J Neurophysiol 57:1893-1910
Kuznetsov YA (1998) Elements of Applied Bifurcation Theory. In: J.E. M, L. S (eds) Applied mathematical sciences. Vol. 112. Springer-Verlag, New York, pp 591
MacKay-Lyons M (2002) Central pattern generation of locomotion: a review of the evidence. Phys Ther 82:69-83.
Masani K, Popovic MR, Nakazawa K, Kouzaki M, Nozaki D (2003) Importance of body sway velocity information in controlling ankle extensor activities during quiet stance. J Neurophysiol 90:3774-3782
McGeer T (1989) Powered flight, child's play, silly wheels, and walking machines Proceedings of the IEEE International Conference on Robotics and Automation, Piscataway, NJ, pp 1592-1597.
McGeer T (1990) Passive dynamic walking. International Journal of Robotics Research 9:62-82.
McMahon TA (1984) Muscles, reflexes, and locomotion. Princeton University Press, Princeton, New Jersey, pp 331
Mihelj M, Matjacic Z, Bajd T (2000) Postural activity of constrained subject in response to disturbance in sagittal plane. Gait Posture 12:94-104.
Morasso PG, Sanguineti V (2002) Ankle muscle stiffness alone cannot stabilize balance during quiet standing. J Neurophysiol 88:2157-2162
Schwab AL, Wisse M (2001) Basin of attraction of the simplest walking model Proceedings of ASME 2001 Design Engineering Technical Conferences and Computers and Information in Engineering Conference, Pittsburgh, Pennsylvania
Seydel R (1988) From equilibrium to chaos : practical bifurcation and stability analysis. Elsevier, New York, pp 367
Sherwood L (1997) Human physiology: from cells to systems. Wadsworth, Belmont, CA etc., pp 753
Shik ML, Severin FV, Orlovskii GN (1966) Control of walking and running by means of electrical stimulation of the mid-brain. Biophysics 11:756-765
Sinkjaer T, Toft E, Andreassen S, Hornemann BC (1988) Muscle stiffness in human ankle dorsiflexors: intrinsic and reflex components. J Neurophysiol 60:1110-1121.
Taga G (1995a) A model of the neuro-musculo-skeletal system for human locomotion. I. Emergence of basic gait. Biol Cybern 73:97-111.
Taga G (1995b) A model of the neuro-musculo-skeletal system for human locomotion. II Real-time adaptability under various constraints. Biol Cybern 73:113-121.

Taga G (1998) A model of the neuro-musculo-skeletal system for anticipatory adjustment of human locomotion during obstacle avoidance. Biol Cybern 78:9-17.

Taga G, Yamaguchi Y, Shimizu H (1991) Self-organized control of bipedal locomotion by neural oscillators in unpredictable environment. Biol Cybern 65:147-159

Thunnissen J (1993) Muscle Force Prediction During Human Gait. University of Twente, Den Haag, pp 221

Van der Helm FC, Schouten AC, de Vlugt E, Brouwn GG (2002) Identification of intrinsic and reflexive components of human arm dynamics during postural control. J Neurosci Methods 119:1-14.

Van der Helm FCT, Rozendaal LA (2000) Musculoskeletal systems with intrinsic and proprioceptive feedback. In: Winters JM, Crago P (eds) Neural control of posture and movement. Springer Verlag, New York, pp 164-174

Winter DA, Patla AE, Prince F, Ishac M, Gielo-Perczak K (1998) Stiffness control of balance in quiet standing. J Neurophysiol 80:1211-1221.

Winters JM, Stark L (1985) Analysis of fundamental human movement patterns through the use of in- depth antagonistic muscle models. IEEE Trans Biomed Eng 32:826-839.

Winters JM, Stark L (1987) Muscle models: what is gained and what is lost by varying model complexity. Biol Cybern 55:403-420

Yamaguchi GT, U. SAG, Morgan DW, Fesler MJ, Winters JM (1990) A survey of human musculotendon actuator properties. In: Winters JM, Woo SL-Y (eds) Multiple Muscle Systems: Biomechanics and Movement Organization. Springer-Verlag, New York, pp 717-773

Zehr EP, Stein RB (1999) What functions do reflexes serve during human locomotion? Prog Neurobiol 58:185-205.

Appendix A. Model equations

The musculo-skeletal model contains 6 states: the activities of both muscles, a_{ta} and a_{sol}, the length of the CEs of both muscles, $l_{ce,ta}$ and $l_{ce,sol}$, and the angle θ and angular velocity ω of the inverted pendulum.
Stretch reflexes are modeled by delayed feedback of the length of both muscles (relative to the rest lengths l_{m0}), $\Delta l_{mus,ta}$ and $\Delta l_{mus,sol}$, and the velocities of both muscles, $v_{mus,ta}$ and $v_{mus,sol}$. The lengths are fed back with gain k_p and the velocities with gain k_v. Force feedback is modeled as delayed feedback of muscle force with gain k_f.
A direct relation is assumed between the muscle lengths and velocities and the angle and angular velocity:

$$\begin{matrix} \Delta l_{mus,ta} = -\theta r \\ \Delta l_{mus,sol} = \theta r \end{matrix} \quad \text{and} \quad \begin{matrix} v_{mus,ta} = -\omega r \\ v_{mus,sol} = \omega r \end{matrix} \tag{A.1}$$

Thus, reflexive feedback is modeled as delayed feedback of angle $\theta(t-\tau)$, angular velocity $\omega(t-\tau)$, $F_{se,ta}(t-\tau)$ and $F_{se,sol}$ $(t-\tau)$. The equations of motions are:

$$\begin{aligned} \dot{a}_{ta} = \frac{1}{\tau_{ta}} \big(& u_{ss,ta} - a_{ta} - k_p c_{16} \theta (t-\tau) \\ & - k_v c_{16} \omega (t-\tau) + k_f F_{se,ta} (t-\tau) \big) \end{aligned} \tag{A.2}$$

$$\begin{aligned} \dot{a}_{sol} = \frac{1}{\tau_{sol}} \big(& u_{ss,sol} - a_{sol} + k_p c_{16} \theta (t-\tau) \\ & + k_v c_{16} \omega (t-\tau) + k_f F_{se,sol} (t-\tau) \big) \end{aligned} \tag{A.3}$$

$$\dot{l}_{ce,ta} = \begin{cases} c_4 v_{max,ta} \left(\dfrac{Fv_{ce,ta} - 1}{Fv_{ce,ta} + c_4} \right) & \text{if } Fv_{ce,ta} \le 1 \text{ (\textit{contracting})} \\ -c_6 v_{max,ta} \left(\dfrac{Fv_{ce,ta} - 1}{Fv_{ce,ta} - c_{17}} \right) & \text{else (\textit{lengthening})} \end{cases} \tag{A.4}$$

$$\dot{l}_{ce,sol} = \begin{cases} c_4 v_{max,sol} \left(\dfrac{Fv_{ce,sol} - 1}{Fv_{ce,sol} + c_4} \right) & \text{if } Fv_{ce,sol} \le 1 \text{ (\textit{contracting})} \\ -c_6 v_{max,sol} \left(\dfrac{Fv_{ce,sol} - 1}{Fv_{ce,sol} - c_{17}} \right) & \text{else (\textit{lengthening})} \end{cases} \tag{A.5}$$

$$\dot{\theta} = \omega \tag{A.6}$$

$$\dot{\omega} = c_{11} M_{\mathrm{p}} + c_{12} \left(F_{\mathrm{se,ta}} - F_{\mathrm{se,sol}} \right) + c_{13} \sin\theta \tag{A.7}$$

The force-length relationships of CEs of the muscles are:

$$Fl_{\mathrm{ce,ta}} = e^{-\left(c_2 l_{\mathrm{ce,ta}} - c_3\right)^2} \tag{A.8}$$

$$Fl_{\mathrm{ce,sol}} = e^{-\left(c_2 l_{\mathrm{ce,sol}} - c_3\right)^2} \tag{A.9}$$

The non-linear springs of the SEs of both muscles are:

$$F_{\mathrm{se,ta}} = \min\left[c_{10} a_{\mathrm{ta}} Fl_{\mathrm{ce,ta}} \,,\, c_7 \left(e^{c_8 \left(1 - c_1 - l_{\mathrm{ce,ta}}\right) - c_9 \theta} - 1 \right) \right] \tag{A.10}$$

$$F_{\mathrm{se,sol}} = \min\left[c_{10} a_{\mathrm{sol}} Fl_{\mathrm{ce,sol}} \,,\, c_7 \left(e^{c_8 \left(1 - c_1 - l_{\mathrm{ce,sol}}\right) - c_9 \theta} - 1 \right) \right] \tag{A.11}$$

The force-velocity relationships of the muscle are:

$$Fv_{\mathrm{ce,ta}} = \frac{F_{\mathrm{se,ta}}}{c_5 a_{\mathrm{ta}} Fl_{\mathrm{ce,ta}}} \tag{A.12}$$

$$Fv_{\mathrm{ce,sol}} = \frac{F_{\mathrm{se,sol}}}{c_5 a_{\mathrm{sol}} Fl_{\mathrm{ce,sol}}} \tag{A.13}$$

The maximum velocities of the muscles are:

$$v_{\mathrm{max,ta}} = c_{14} \left(1 - c_{15} \left(1 - a_{\mathrm{ta}} Fl_{\mathrm{ce,ta}} \right) \right) \tag{A.14}$$

$$v_{\mathrm{max,sol}} = c_{14} \left(1 - c_{15} \left(1 - a_{\mathrm{sol}} Fl_{\mathrm{ce,sol}} \right) \right) \tag{A.15}$$

The activation and de-activation time constants of the muscle activation dynamics are:

$$\tau_{\mathrm{ta}} = \begin{cases} \tau_{\mathrm{ac}} & \text{if } a_{\mathrm{ta}} \le u_{\mathrm{ta}} - k_{\mathrm{p}} c_{16} \theta\left(t - \tau\right) \\ & -k_{\mathrm{v}} c_{16} \omega\left(t - \tau\right) + k_{\mathrm{f}} F_{\mathrm{se,ta}}\left(t - \tau\right) \\ \tau_{\mathrm{da}} & \text{else} \end{cases} \tag{A.16}$$

$$\tau_{\mathrm{sol}} = \begin{cases} \tau_{\mathrm{ac}} & \text{if } a_{\mathrm{sol}} \le u_{\mathrm{sol}} + k_{\mathrm{p}} c_{16} \theta\left(t - \tau\right) \\ & +k_{\mathrm{v}} c_{16} \omega\left(t - \tau\right) + k_{\mathrm{f}} F_{\mathrm{se,sol}}\left(t - \tau\right) \\ \tau_{\mathrm{da}} & \text{else} \end{cases} \tag{A.17}$$

Boundary conditions on certain states and functions

$$0 \le a_{ta} \le 1 \qquad 0 \le a_{sol} \le 1$$
$$l_{ce,ta} \ge 0 \qquad l_{ce,sol} \ge 0 \qquad \text{(A.18)}$$
$$F_{se,ta} \ge 0 \qquad F_{se,sol} \ge 0$$

Constants (all positive) used in the equations of motion in terms of musculo-skeletal parameters

$$c_1 = \frac{l_t}{l_{m0}} \qquad c_2 = \frac{1}{l_{cesh}}$$
$$c_3 = \frac{l_{ce0}}{l_{cesh}} \qquad c_4 = mv_{sh}$$
$$c_5 = F_{max} \qquad c_6 = mv_{sh}mv_{shl}$$
$$c_7 = \frac{F_{max}}{e^{se_{sh}} - 1} \qquad c_8 = \frac{se_{sh}}{se_{xm}}$$
$$c_9 = \frac{se_{sh}r}{l_{m0}se_{xm}} \qquad c_{10} = F_{max}mv_{ml} \qquad \text{(A.19)}$$
$$c_{11} = \frac{1}{I} \qquad c_{12} = \frac{r}{I}$$
$$c_{13} = \frac{mgl_{com}}{I} \qquad c_{14} = mv_{vm}$$
$$c_{15} = mv_{er} \qquad c_{16} = r$$
$$c_{17} = \left(1 + mv_{sh}mv_{shl}\right)\left(mv_{ml} - 1\right) + 1$$

Musculo-skeletal parameters

m	= 80	kg	mass of male person
I	= 121.6	kgm^2	mass moment of inertia around ankles
l_{com}	= 1.0	m	length between COM and ankles
g	= 9.81	m/s^2	gravity constant
r	= 0.04	m	moment arm about ankles
l_{m0}	= 0.305	m	rest length of muscle
l_t	= 0.27	m	tendon length
l_{ce0}	= 0.1		optimum length of CE (normalized on l_{m0})
l_{cesh}	= 0.03		shape parameter determining width of Fl_{ce}
F_{max}	= 8792	N	maximum active muscle force
mv_{er}	= 0.5		scaling parameter for maximal contraction velocity
mv_{vm}	= $2l_{m0}$	1/s	maximal contraction velocity of unloaded CE
mv_{sh}	= 0.2		shape parameter of curvature of Fv_{ce}
mv_{shl}	= 0.5		shape parameter for lengthening curve of Fv_{ce}
mv_{ml}	= 1.3		maximal force gain for lengthening muscles

se_{sh} = 4.4		shape parameter of curvature of exponential slope of SE
se_{xm} = 0.043		maximal extension of SE (normalized on l_{m0})
τ_{ac} = $11.33 \cdot 10^{-3}$	s	time-constant for increased muscle activation
τ_{da} = $31.58 \cdot 10^{-3}$	s	time-constant for decreasing muscle activation

Appendix B. Approximation of discontinuity

The function $F(x)$ is defined as:

$$F(x) = \begin{cases} -x & \text{if } x < 0 \\ x & \text{else} \end{cases} \tag{B.1}$$

The function can be approximated by the following continuous function with the help of hyperbolic tangent function:

$$F_{\text{cont}}(x) = x \tanh(c_s x) \tag{B.2}$$

This way the discontinuities in the equations of motion (App. A.1) are *smoothed* into continuous functions for the performance of bifurcation analysis. The derivatives of the functions are also continuous.
The parameter c_s represents the *steepness constant*. The higher c_s is, the better the discontinuity is approached. The drawback is that a higher c_s gives a stiffer system. The steepness constant c_s is taken 1000 in all the simulations.

Appendix C. Padé approximation of time delay

For the linearized model discussed in Sect. 2.3, the time delay was modeled by a third-order Padé approximation. A Padé approximation of a time delay is based on a good approximation in the frequency domain. In the time domain the results will be less good. For the prediction of the eigenvalues associated with the equilibrium of the posture model of Sect. 2.1, a third-order Padé approximation gave good results (the higher the order, the better the approximation). The transfer function of the Padé approximation is as follows:

$$H_{\text{Pade}'} = \frac{3\tau^2 s^2 - 24\tau s + 60}{\tau^3 s^3 + 9\tau^2 s^2 + 36\tau s + 60} \tag{C.1}$$

To give an idea about the validity of the delay approximation, a comparison is made between the Padé approximation and the real delay in Laplace ($H_\tau = e^{-j\omega\tau}$) with a delay τ of 50 ms. This is shown in the Bode plot of Fig. C.1.

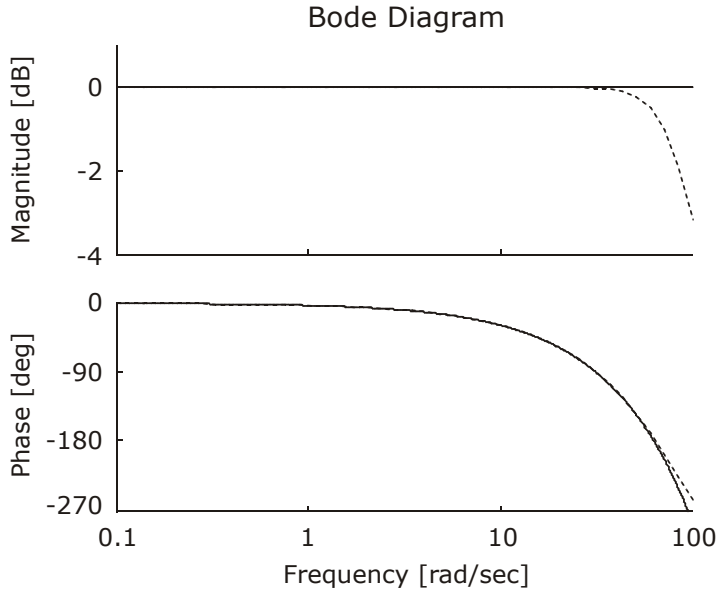

Fig. C.1 Comparision of real delay of 50 ms (*solid*) and the third-order Padé approximation (*dashed*). The approximation is good up till 50 rad/s.

The figure shows that the approximation in the frequency domain is good up till ω_u=50 rad/s. This is much larger than the open-loop (i.e. before closing the reflex loop) bandwidth of the system. Therefore, depletion of the phase and gain margin, defining the transition of linear stability to linear instability, happens at frequencies much lower than the frequency up to which the Padé approximation is valid. Thus, the approximation is at least valid up to the transition from linear stability to linear instability.
Moreover, as long as the rightmost eigenvalues $\boldsymbol{\lambda}_{\mathbf{rm}}$ of the system have an absolute value much smaller than the frequency ω_u up to which the Padé approximation is valid (i.e. $|\boldsymbol{\lambda}_{\mathbf{rm}}| << \omega_u$), the prediction of the eigenvalues by the linearized model will also be quite good in the right half plane.

As an example the eigenvalues were calculated of the equilibrium with parameter set $[u_{ss}\ k_p\ k_v\ k_f\ \tau]^T = [0.1\ 1000\ 10\ 0\ 50\cdot10^{-3}]^T$, thus way out of the stable area of the parameter space (see Fig. 4 in Sect. 3.1). The rightmost eigenvalues of the DDEs, calculated by DDE-BIFTOOL, are in this case $\boldsymbol{\lambda}_{\mathbf{rm}}$=6.88±12.31*i*. The rightmost eigenvalues, predicted by the linearized model, are in this case $\boldsymbol{\lambda}_{\mathbf{rm}}$=6.86±12.17*i*. Thus, while the absolute value of these eigenvalues, which is 14.1, is not *very* much lower than 50, the prediction by the linearized model still gives a reasonably good approximation of the most dominant eigenvalues.

Chapter 3

Energy Efficient and Robust Rhythmic Limb Movement by Central Pattern Generators

B.W. VERDAASDONK, H.F.J.M. KOOPMAN, F.C.T. VAN DER HELM

Neural Networks 19: 388-400, 2006

Abstract

Humans show great energy efficiency and robustness in rhythmic tasks, such as walking and arm swinging. In this study a mathematical model of rhythmic limb movement is presented, which shows that tight local coupling of Central Pattern Generators (CPGs) to limbs could explain part of this behavior. Afferent feedback to flexor and extensor centers of the CPG is crucial in providing energy efficiency by means of resonance tuning. Feedback of positional information provides resonance tuning above the endogenous frequency of the CPG. Integral feedback provides resonance tuning at and below the endogenous frequency. Feedback of velocity information is necessary to compensate for the time delay in the loop, coupling limb to CPG; without velocity feedback bi-stability occurs and resonance tuning is not possible at high movement frequencies. The concepts of energy efficient and robust control of rhythmic limb movements are also applicable to robotics. It is the first CPG model, which provides resonance tuning at natural limb frequencies above and below its endogenous frequency.

1. Introduction

Locomotion is a compromise between different goals such as energy efficiency, stability and maneuverability. Ballistic models of human gait show remarkable resemblances with unperturbed human gait (Kuo 2001; Mochon and McMahon 1980). This shows the importance of energy efficiency in human gait control: people exploit the natural dynamics as much as possible, just like the ballistic gait models do. However, in general the ballistic gait models possess poor stability properties, unlike human gait. The existence of neural networks on spinal level, termed Central Pattern Generators (CPGs), might contribute to the coexistence of energy efficiency and good stability properties in human gait. The CPG provides alternating motor patterns in such a way that stable gait is obtained. Proof for this originates mainly from cat studies (Amemiya and Yamaguchi 1984; Brown 1911; Shik et al. 1966).

Humans not only exploit the limb dynamics in locomotion. When people are asked to move pendulums about their wrist in the preferred frequency, this frequency scales linearly with the square root of the inverse of the pendulum's length, thus with its natural frequency (Kugler and Turvey 1987). The fact that the preferred frequency was always higher than the natural frequency of the pendulum is probably due to the joint stiffness, caused by the muscles. Hatsopoulos and Warren (1996) showed that the preferred frequency at which subjects swung their forearms in the vertical plane was equal to the natural frequency of the muscle-limb system including added mass and spring loading. Abe (2003) instructed subjects to swing their forearms rhythmically in the vertical plane under various frequency conditions. He showed that for frequencies higher then the natural limb frequency dictated by gravity, the joint stiffness is modulated in such a way that the natural frequency of the total muscle-limb system matches the instructed movement frequency. Bennett (1993) argues that even during non-rhythmical voluntary arm movements the joint stiffness is adjusted in such a way that the resonance frequency of the muscle-limb system equals the principal frequency component of the movement. These studies show that regulation of the joint stiffness determines the frequency of the rhythmical limb movements.

The above-mentioned studies indicate that CPGs are vital in performing rhythmic movements, such as walking. These movements are energy efficient and robust, but it is not known *how* this is achieved and *what* the role of the CPG and its coupling to the musculo-skeletal system might be. Furthermore, it has been shown that the frequency of rhythmical arm movements is controlled by modulation of the joint stiffness, but the underlying principles – especially the role of afferent feedback of the muscles to the CPG – are not fully understood.

The main goal of this study is to determine the roles of CPGs, afferent feedback and modulation of joint stiffness in providing energy efficient and robust rhythmic limb movement. This goal is achieved by answering the following research questions: (1) Under which conditions does the CPG *entrain* to the limb dynamics and what is the role of afferent and efferent coupling in this? (2) What is the influence of *time delay* in the loop that couples the CPG to the limb and is compensation for this delay possible? (3) Which *afferent feedback* is necessary for the CPG to obtain energy efficient rhythmic limb movement? (4) Where does the *robustness against changes in the limb dynamics* come from? These questions are answered using a model of a single limb tightly coupled to a CPG. The CPG model and methods for analyzing its coupling to a limb will be discussed in Sect. 2. The limb is represented by a mass-spring-damper model and is used for a general analysis (Sect. 3) that can also be applied in robotics (see secondary goal below).

The secondary goal of this study is to provide a method for energy efficient and robust control of rhythmic arm movements in robotics. Williamson (1998) successfully used Matsuoka's CPG model to control rhythmic movements of robot arms. The CPG model was able to tune into the robot arm's resonance frequency, which is termed *resonance tuning* and provides energy efficient arm control. However, the CPG model only showed this resonance tuning behavior in case the resonance frequency of the arm was higher than the endogenous frequency ω_{CPG} of the CPG (i.e. the frequency without sensory input). Hatsopoulos (1996) used a van der Pol oscillator as CPG model and coupled it to a mass-spring system, which represented the limb dynamics. Also in this case, resonance tuning was only possible above the endogenous frequency of the CPG. Resonance tuning below the endogenous frequency is for example useful for systems with varying stiffness. The CPG model presented in this paper provides resonance tuning below and above its endogenous frequency and is therefore able to provide energy efficient control of various types of arms with a broad range of natural frequencies.

2. Analysis of rhythmic limb movement

An overview of the model of rhythmic limb movement is shown in Fig. 1. It consists of a limb coupled to a Central Pattern Generator (CPG). The CPG model receives sensory information from the limb, which is processed and subsequently presented to the (spinal) network generating the basic rhythm. This network is represented by a half-center model (Brown 1914), whose outputs y_F and y_E control limb flexion and extension, respectively. The CPG model is discussed in detail in Sect. 2.2.

The model of the limb is kept as general and simple as possible, because this study is focused on the capability of the CPG to entrain to different types of limbs; it is not focused on the limbs themselves. A mass-spring-damper model corresponds to the limb's moment of inertia I about the joint, the joint

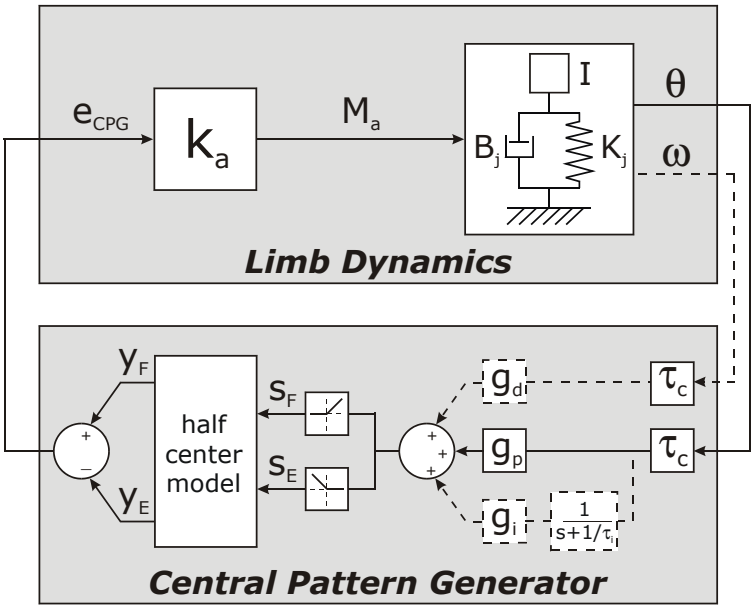

Fig. 1 Overview of the model of rhythmic limb movement, in which the limb is tightly coupled to a Central Pattern Generator (CPG). The mass-spring-damper model represents a robot arm or human limb with moment of inertia I, joint stiffness K_j and joint damping B_j. The limb's actuation is represented by gain k_a, linearly translating the CPG's output $e_{CPG}=(y_F - y_E)$ to a moment of force M_a. The half-center model of the CPG receives afferent information from the limb on its inputs s_F and s_E with time delay τ_c. The P-type CPG only has afferent feedback of limb angle θ with gains g_p (*solid lines*). The PID-type CPG has additional afferent feedback of angular velocity ω and integrated angle φ, with gains g_d and g_i, respectively (*dashed lines*). A leaking integrator with large time constant τ_i is used to obtain φ from θ.

stiffness K_j and the joint damping B_j. The spring and damper are a simplified representation of the visco-elastic joint properties composed of passive, active (e.g. monosynaptic stretch reflex in humans or state-feedback in robotics) and gravity components. Actuation is provided by muscles in human movement and is motorized in robotics. In this study actuation and efferent feedback gains are lumped together into a single actuation gain k_a, linearly translating the level of excitation $e_{CPG}=(y_F - y_E)$ to a moment of force M_a. It is noted that the applied moment of force M_a in Fig. 1 and Eq. A.2 only represents the moment of force originating from the CPG, because possible local feedback is already included in the mass-spring-damper model. If local feedback is used to change the visco-elastic joint properties, the actuator actually delivers additional moment of force. This moment of force is not explicit in this lumped model. The equations of the complete model are found in App. A.

2.1 Finding periodic solutions

Two methods are used to analyze the rhythmical limb movements. The first is an approximating method, used for physical insight in the model and prediction of its behavior. It is called *Describing Function Analysis* (DFA) and is based on frequency response methods used in linear control engineering. The second method is bifurcation analysis and is used to obtain periodic solutions and their stability, mainly to verify the approximate solutions obtained by DFA and to determine the limits of the DFA approach.

DFA can be used to approximately analyze and predict behavior of certain nonlinear systems (Slotine and Li 1991). The method can be applied to the non-linear CPG model, discussed in Sect. 2.2, because it entrains to the input; the fundamental frequency of the input and the output are the same. The higher harmonics, which are present in the CPG's output, are small in amplitude compared to the amplitude at the fundamental frequency (see Fig. 5). Moreover, the limb dynamics act as low-pass filter, which makes the limb angle an almost perfect sine wave. The method starts with the construction of Bode plots of the input-output relation of the CPG by introducing sinusoidal waves with different frequencies at the CPG's input. The single frequency Fourier transformation of the input and output is taken and the magnitude and phase between them is determined (Williamson 1998). The magnitude – and thus the gain plots of the CPG – depends strongly on the input amplitude (see Figs. 3, 4, 6 and 8), because of the non-linear characteristics of the CPG model (i.e. the 'max' operators in Eqs. 3, 4, 9 and 10). Bode plots are calculated for different input amplitudes, since the CPG's input is the limb angle θ (Fig. 1). These Bode plots represent the dynamics of the CPG at rhythmical limb movements with different angular amplitudes A rad.
When the limb is coupled to the CPG, steady state periodic solutions are expected under two necessary conditions. Firstly, since the CPG and limb are

tightly coupled, the phase difference between the input θ and output e_{CPG} of the CPG equals the phase difference between the output θ and input e_{CPG} of the limb (Williamson 1998):

$$\arg\left(H_{\text{CPG}}(j\omega)\right) = \arg\left(\frac{1}{H_{\text{limb}}(j\omega)}\right), \text{ or}$$
$$\arg\left(H_{\text{CPG}}(j\omega)\right) = -\arg\left(H_{\text{limb}}(j\omega)\right) \quad (1)$$

Secondly, a steady state periodic solution will neither grow nor shrink, so its loop gain equals 1. Thus, the magnitude of the CPG's transfer function H_{CPG} has to equal the inverse of the magnitude of the limb's transfer function H_{limb}:

$$\left|H_{\text{CPG}}(j\omega)\right| = \left|\frac{1}{H_{\text{limb}}(j\omega)}\right|, \text{ or}$$
$$\left|H_{\text{CPG}}(j\omega)\right|^{dB} = -\left|H_{\text{limb}}(j\omega)\right|^{dB} \quad (2)$$

By fulfillment of these two conditions, it is expected that DFA will provide good predictions of steady state periodic solutions for the considered type of models (Fig. 1). The obtained physical insight will be used to improve the resonance tuning behavior of the CPG (Sect. 3). It is noted that DFA does not provide knowledge about the transient behavior of the model.

The second method is bifurcation analysis. DDE-Biftool is used for the numerical bifurcation analysis (Engelborghs et al. 2001). This Matlab package can handle delay differential equations and is used in this study for the continuation of the periodic solutions and the assessment of their stability. The procedure to obtain periodic solutions is the same as in Ch. 2 (Verdaasdonk et al. 2004). Firstly a Hopf bifurcation of the equilibrium, about which the oscillation is expected, is located. This is done by parameter variation until a pair of eigenvalues cross the imaginary axis with non-zero speed. A periodic solution is obtained from this Hopf bifurcation and a branch of periodic solutions is followed in parameter space. The stability of the periodic solutions in terms of their Floquet multipliers is also calculated.

2.2 CPG model

Central patterns generators (CPGs) are neural networks on spinal level, which produce alternating bursts of motor activity, even in a completely isolated spinal cord (Nishimaru and Kudo 2000; Sqalli-Houssaini et al. 1993). Cat studies (for reviews see Barbeau et al. 1999; Burke 2001; McCrea 2001; Van de Crommert et al. 1998; Whelan 1996) suggest that at least afferent feedback from Ia and II fibers to the flexor and extensor centers are present. In our model this feedback is abstracted to feedback of limb angle θ and angular velocity ω.

The CPG model used in this study consists of a half-center model and its afferent feedback, including the time delay in the loop (lower block in Fig. 1). Two types of the CPG model are used to investigate the influence of the different types of afferent input. The *P-type CPG* only has *P*roportional feedback of the limb angle (solid lines in Fig. 1); the *PID-type* has additional feedback of the angular velocity (or *D*erivative of the angle) and the '*I*ntegral' of the limb angle to the half-center model (dashed lines in Fig. 1). The integral feedback is modeled as an internal process of the CPG. A time delay τ_c is present in the coupling of the limb with the half-center model.

The half-center model used in this section is similar to that of Matsuoka (1985; 1987) and is shown in Fig. 2. It consists of two neurons, which receive tonic input u_0 from the supra-spinal level, possess adaptation dynamics (shown by dashed paths) and inhibit each other (i.e. reciprocal inhibition). Sensory inputs to the neurons, s_F and s_E, are also shown. These inputs are used to couple the half-center model to the limb dynamics. Maximal robustness is achieved by taking the sensory inputs strictly inhibitory, because then they cannot enlarge the maximal CPG output (i.e. limb cannot swing out of bounds):

$$s_F = \max\left(0, g_p\theta(t-\tau_c) + g_d\omega(t-\tau_c) + g_i\varphi(t-\tau_c)\right) \quad (3)$$

$$s_E = \max\left(0, -g_p\theta(t-\tau_c) - g_d\omega(t-\tau_c) - g_i\varphi(t-\tau_c)\right) \quad (4)$$

in which $\theta(t-\tau_c)$ is the delayed limb angle, $\omega(t-\tau_c)$ the delayed angular velocity and $\varphi(t-\tau_c)$ the 'integral' of the delayed limb angle, which are fed to the half-center model by the afferent gains g_p, g_d and g_i respectively. For the P-type CPG the afferent feedback gains g_d and g_i are zero. The outputs of the neurons are y_F and y_E. The inputs and outputs signals represent impulse and firing rates, respectively.

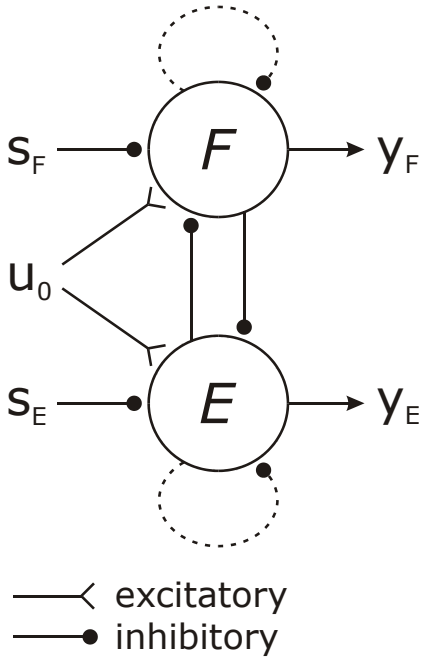

Fig. 2 Half-center model. The inputs to the neurons are the supra-spinal input u_0 and the sensory inputs s_F and s_E. The outputs are the firing rates y_F and y_E. Adaptation dynamics are shown by *dashed lines*, because it is an internal process instead of a pathway. The neuron 'F' represents the flexor center and the neuron 'E' the extensor center.

Without the sensory inputs the CPG model is equal to Matsuoka's and acts as a kind of relaxation oscillator. Both neurons receive supra-spinal tonic input u_0. However, the reciprocal inhibition between the neurons makes sure that only one neuron can fire at a time. The activity of the firing neuron goes down after a while, because of the adaptation dynamics. The other neuron then starts firing, because it is no longer inhibited and so on. Matsuoka (1985; 1987) gave necessary and sufficient conditions for the parameters to sustain oscillatory activity of the neurons.

The equations of the half-center model – including sensory inputs – are (adapted from Matsuoka (1985; 1987)):

$$\tau_r \dot{u}_F = u_0 - u_F - \beta v_F - w y_E - s_F \tag{5}$$

$$\tau_a \dot{v}_F = y_F - v_F \tag{6}$$

$$\tau_r \dot{u}_E = u_0 - u_E - \beta v_E - w y_F - s_E \tag{7}$$

$$\tau_a \dot{v}_E = y_E - v_E \tag{8}$$

$$y_F = \max(0, u_F) \tag{9}$$

$$y_E = \max(0, u_E) \tag{10}$$

The state variables of the model are u_i and v_i, where the former is related to the output y_i and the latter to the adaptation dynamics of neuron i ($i=\{E, F\}$). The constant τ_r specifies the rise time when given a step input. The strength of reciprocal inhibition is specified by w. The constant τ_a determines the time lag of the adaptation effect and β its strength. The half-center model of the CPG has the following parameter values: β=2.0; w=2.0; u_0=1.0; τ_r=0.1; τ_a=0.2. The endogenous frequency ω_{CPG} of the CPG (i.e. the frequency without sensory input) is 7.0 rad/s at these parameter settings. Changing the endogenous frequency ω_{CPG} shifts the range of input frequencies to which the CPG entrains.
The way the half-center model of the CPG entrains to high and low frequency inputs (s_F and s_E) can be seen from Eqs. 5 through 10. For input frequencies much higher than the endogenous frequency of the CPG, the input dominates the relatively slow adaptation dynamics. The *firing* neuron is being inhibited by its input before the adaptations dynamics kicks in and, therefore, shortens the time the neuron is active. Hence, the cycle time is shortened to equal the input period. For frequencies much lower than the endogenous frequency of the CPG, the *non-firing* neuron is inhibited by its input. Although the adaptation dynamics of the *firing* neuron has already set in, it can keep firing – with lower rate however – until the input stops inhibiting the non-firing neuron. In other words, the reciprocal inhibition is being slowed down by the slow input. Hence, the cycle time is lengthened to equal the input period. The larger the difference between the input frequency and the endogenous frequency, the larger the necessary input amplitude to accomplish entrainment (Williamson 1998); if the difference is too large, no entrainment can occur.

The neurons of the half-center model represent in fact groups of neurons. One group of neurons, often called the flexor center, provides alternating bursts of activity to the flexor motoneurons. The other group of neurons is called the extensor center. Half-center models are based on the work of Brown (1911; 1914). They are considered by most researchers as conceptual rather than realistic models. Nevertheless, Cheng et al. (1998) identified flexor and extensor centers for walking in the mudpuppy and their model, based on their findings, looks similar to the one used here.

3. Resonance tuning in rhythmic limb movements

In this section rhythmic limb movement resulting from the coupling between a limb and a CPG model is discussed, with the focus on energy efficiency. The most energy efficient control of rhythmic movement of a system is actuating it in its resonance frequency. The ability of the CPG to control a limb in its resonance frequency automatically is termed *resonance tuning*. Resonance tuning has advantages compared to 'normal' control strategies, such as feed-forward and feedback. Firstly, there is no need for a reference control input. The only input the CPG requires to entrain to the limb is feedback of one or several mechanical state variables (e.g. limb angle). The CPG can also entrain to feedback of force or torque (Williamson 1998), but in this paper we confine ourselves to state feedback. Secondly, resonance tuning guarantees energy efficient movement, because the limb is actuated close to its natural frequency. Thirdly, the CPG adapts to changes in limb dynamics. The latter is closely related to the second advantage and is used to control the frequency of the movement by changing the joint stiffness of the limb. In this paper joint stiffness is defined as the linearization of exerted moment of force on the limb (*not* coupled to CPG) about angular displacement in its equilibrium at zero frequency (i.e. time$\rightarrow\infty$). The stiffness can be changed by local positional feedback, which changes the natural frequency of the limb. It is noted, that humans are also able to change the joint stiffness by co-contraction, but this is very energy consuming and probably only used when necessary. The CPG will adapt to the changed natural frequency such that the movement frequency is close to it. Although the movement at this changed frequency will be the most energy efficient way of moving the limb at that particular frequency, it will of course cost more energy than moving the limb at the *mechanical* natural frequency (i.e. without local feedback). The property of the CPG to adapt to changing limb dynamics brings forth great flexibility. The same CPG can be used to control different types of limbs or limbs that have interaction with the environment (e.g. picking up a mass); all are controlled automatically in the most energy efficient way.

The energy efficient and adaptive limb control of the CPG, that is its resonance tuning capabilities, is shown for different types of afferent feedback in the next subsections. Firstly, in Sect. 3.1, only feedback of the limb angle to the half-center model is considered. The CPG with this configuration is termed *P-type CPG* (Sect. 2.2). The solutions predicted by DFA are compared to the exact periodic solutions obtained from bifurcation analysis to evaluate the validness of DFA. In Sect. 3.2, the negative influence is shown that time delay in the afferent feedback to the half-center model has on the resonance tuning behavior of the CPG. In Sect. 3.3, it is determined which afferent information the half-center model should receive

to improve its resonance tuning capabilities and the local stability of the coupled system. This is performed with the help of DFA, among others by compensation of time delay.

3.1 Rhythmic limb movement with the P-type CPG

The afferent feedback of the P-type CPG only consists of proportional feedback of the angle θ to the half-center model with gain g_p. To predict periodic solutions with DFA, first a Bode plot of the CPG is constructed. The Bode plot is subsequently used to predict periodic solutions for limbs with varying natural frequencies, when coupled to this CPG. Note that no delay is present in the system in this subsection (τ_c=0 ms).

Bode plot of the P-type CPG

In Fig. 3 Bode plots of the CPG are shown for five different input amplitudes. The angular amplitudes shown in the figure are 0.05, 0.1, 0.2, 0.4 and 0.8

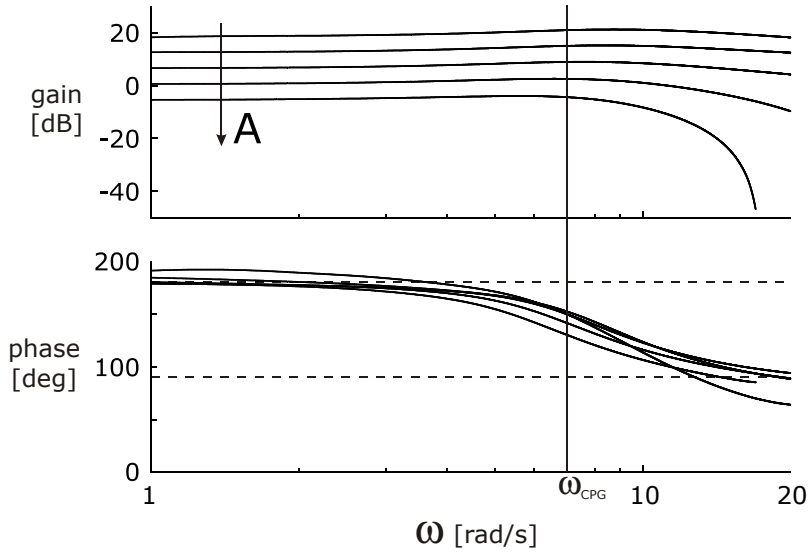

Fig. 3 Bode plots of the input-output relation of the P-type CPG model (i.e. only proportional feedback of limb angle) without delay for five different input amplitudes, namely 0.05, 0.1, 0.2, 0.4 and 0.8 rad. Larger input amplitudes *A* give lower gains, as shown by the arrow. The phase does not change much with input amplitude. *Dashed lines* in the lower graph mark 90 and 180°. The phase is about 90° for frequencies above the endogenous frequency of the CPG (ω_{CPG}=7.0 rad/s, shown by the *vertical line*), which yields resonance tuning (see text for details).

rad respectively. They are transferred to the half-center model via a gain g_p of 15. The Bode plots are determined with the DFA method described in Sect. 2.1. The resonance tuning behavior of the CPG can be seen from the *phase plots*, while the robustness of the CPG – regarding entrainment of different types of limbs – can be seen from the *gain plots (*explained below).

The *phase plots*, corresponding to different angular amplitudes (Fig. 3, lower graph), are similar for the different input amplitudes. At lower input frequencies than the endogenous frequency of the CPG, the phase lead goes up to about 180° (in fact a lag of -180°); at higher input frequencies the phase lead goes down to about 90° (in fact a lag of -270°). This difference in phase lead corresponds to the qualitatively different way the half-center model entrains to high and low frequency input (see Sect. 2.2). The limb, which is modeled as second order mass-spring-damper model, has a phase lag of 90° at its natural frequency. Since the phase of the CPG must match the phase of the inverse transfer function of the limb for a periodic solution to exist (Eq. 1, Sect. 2.1), we expect resonance tuning to occur only for limbs with resonance frequencies higher than the endogenous frequency of the CPG.
The gain plot of the inverse transfer function of the limb has to cross one of the CPG *gain plots* (Fig. 3, upper graph) at the same frequency for which the phase match occurs (Eq. 2, Sect. 2.1). The large spread in the gain plots indicates that many different types of limbs can be entrained by the CPG and shows the CPG's robustness for changing limb dynamics. At low and medium frequencies, the gain plots decrease 6 dB for each doubling of input amplitude, because the maximum output amplitude of the CPG is constant in case of inhibiting sensory inputs. If these inputs are both high frequency and high amplitude, this maximum output amplitude is not reached and thus the gain will drop dramatically (see the lower gain plot in Fig. 3, corresponding to an angular amplitude of 0.8 rad).

Coupling the limb to the CPG

A limb with a moment of inertia I of 1.0 kgm^2 and a joint damping B_j of 1.0 Nms/rad is now coupled to the P-type CPG. The stiffness of the limb joint K_j is varied to vary the limb's natural frequency and predictions of the entrained rhythmic limb movement are made at these different natural frequencies. A periodic solution is predicted when the inverse transfer function of the limb crosses one of the CPG Bode plots at a certain frequency ω_e for both phase and gain (Sect. 2.1), giving rise to a stable rhythmic limb movement with frequency ω_e and an amplitude specified by the crossed Bode plot. The gain k_a – representing the efferent feedback and actuation – is chosen 2.0 in order to ensure the crossing of the inverse transfer function with one of the Bode plots.

An example of the prediction of the frequency and amplitude of entrained rhythmic limb movement for a limb with a natural frequency of 8.0 rad/s is shown in Fig. 4.
In the figure Bode plots are shown for input angles of 0.05, 01 and 0.2 rad, respectively. The inverse transfer function of the limb is shown in gray. The intersection of the inverse transfer function with one of the Bode plots of the CPG – simultaneously for both gain and phase – is close to the Bode plot associated with 0.1 rad angular amplitude. In fact, DFA predicts the frequency and amplitude of the entrained periodic solution to be 8.55 rad/s and $9.2 \cdot 10^{-2}$ rad, respectively. This is done by calculating the Bode plots for many input amplitudes and interpolate between them to obtain a prediction of the periodic solution at the intersection. The time series and power spectral density of the *actual* entrained periodic movement is shown in Fig. 5.

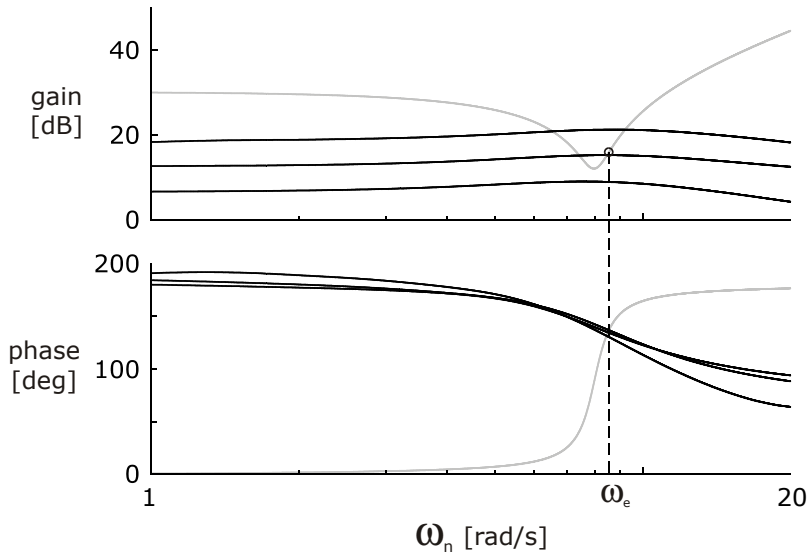

Fig. 4 Prediction of frequency and amplitude of periodic solutions. Bode plots of input-output relation of P-type CPG model for three input amplitudes *A* (0.05, 0.1, 0.2) are shown in *black*. Bode plot of inverse transfer function of the limb is shown in *gray*. The gain and phase of one of the Bode plots of the CPG has to cross simultaneously with the gain and phase of the Bode plot of the inverse transfer function (Sect. 2.1). These conditions are true only for a specific frequency ω_e and a specific CPG Bode plot, representing the amplitude of the periodic solution. In this case, the natural frequency of the limb was chosen to be 8.0 rad/s and the prediction of the frequency and amplitude of the entrained periodic solution is 8.55 rad/s and $9.2 \cdot 10^{-2}$ rad, respectively.

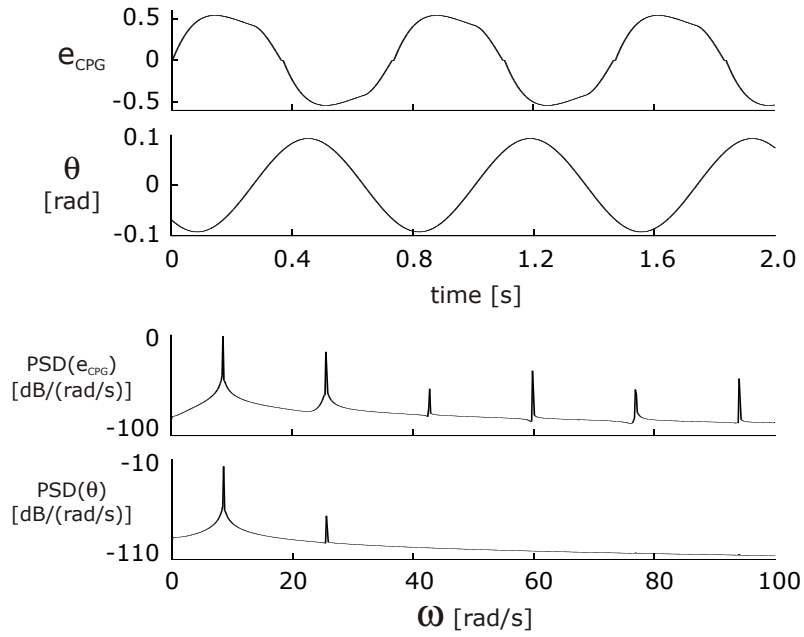

Fig. 5 Entrained periodic solution corresponding to the prediction of Fig. 4. Time series and power spectral density (PSD) plots of the CPG output e_{CPG} and the limb angle θ are shown. Higher harmonics that are present in e_{CPG} are filtered out by the limb's inertia. This way, almost perfect sinusoidal limb movement is obtained, with a frequency of 8.59 rad/s and an amplitude of $9.26 \cdot 10^{-2}$ rad.

The periodic movement has a frequency of 8.59 rad/s and an amplitude of $9.26 \cdot 10^{-2}$ rad, which is close to the values predicted by DFA.

Given the half-center model and the mechanical limb parameters (i.e. I, B_j, K_j), DFA predicts that periodic limb movement is possible within a certain range of *movement* amplitudes. Part of this of this range is shown in the gain plot of Fig. 3; the arrow indicates increasing amplitude A. The range of movement amplitudes at which entrainment occurs can be adjusted by the sensory feedback gain g_p, while the amplitude itself is adjusted by the actuation gain k_a. Increasing k_a decreases the gain of the inverse transfer function of the limb, which gives rhythmical limb movement with larger amplitude (see Fig. 4). Increasing or decreasing g_p will hardly change the gain of the CPG's Bode plots, because the output amplitude of the CPG's flexor and extensor center is almost independent of their input amplitude within a certain range of *input* amplitudes. If the input amplitude is too small, the CPG will not entrain to the limb dynamics (Williamson 1998); if the input amplitude is too large, the CPG's output amplitude will drop, especially at high frequencies (see Fig. 3). Halving of the sensory feedback gain g_p

doubles minimum and maximum possible movement amplitudes over the entire range of entrained natural limb frequencies.

Figure 6 shows both the predicted and exact entrained periodic solutions for limbs with a natural frequency ω_n of 1 up to and including 20 rad/s. This varying natural frequency is obtained by changing the joint stiffness of the limb. The upper graph shows the entrained frequency ω_e of the periodic movement, while the lower graph shows the corresponding angular amplitude *A*.
In the upper graph of Fig. 6 the predicted and exact entrained frequencies ω_e are shown in black and gray, respectively. In the lower graph the accompanying angular amplitudes of the rhythmic movements are shown. The dashed line in the upper graph, for which the entrained frequency equals the natural frequency of the limb, shows ideal resonance tuning behavior. The figure shows that resonance tuning only occurs for limbs with a natural frequency higher than the endogenous frequency of the CPG, as was already expected from Fig. 3. The entrained frequency has an asymptote of 5.54

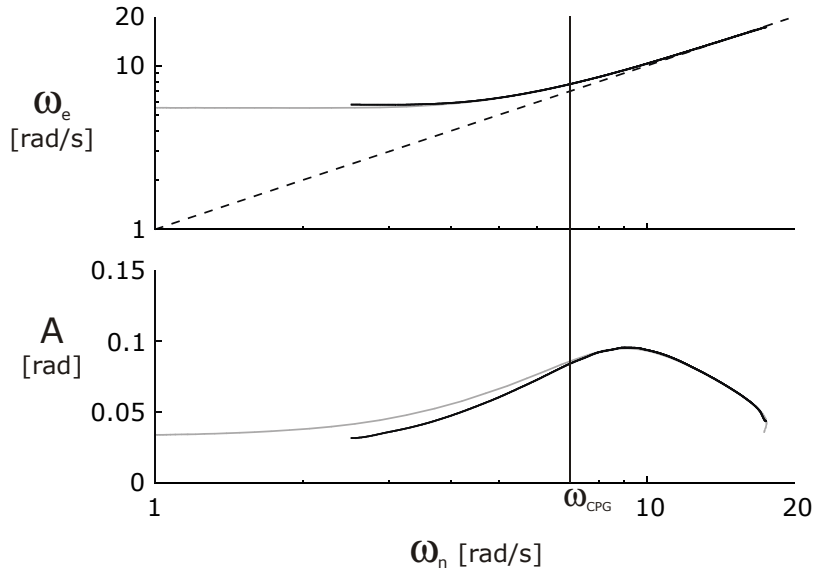

Fig. 6 Stable periodic solutions for the limb coupled to the P-type CPG, without time delay in the afferent path. The upper graph shows the natural frequency of the limb dynamics ω_n versus the entrained frequency ω_e. The lower graph shows the accompanying angular amplitudes *A*. Predictions by DFA are shown in *black*; exact solutions are shown in *gray*. Ideal resonance tuning ($\omega_e=\omega_n$) is shown by the *dashed line* and is approached for limbs with natural frequencies above the endogenous frequency of the CPG (ω_{CPG}=7.0 rad/s).

rad/s for decreasing joint stiffness ($K_j \rightarrow 0$ Nm/rad). The value of this asymptote depends on the coupling strength, but always lies between the endogenous frequency of the CPG ω_{CPG} and the natural frequency of the limb ω_n.
The predictions of entrained periodic limb movements with frequencies around and above the endogenous CPG frequency are nearly identical to the exact solutions. However, for limbs with natural frequencies ω_n higher than 17.34 rad/s the exact solutions show co-existing periodic solutions, which cannot be predicted by DFA. In fact, bi-stability is already observed at a ω_n of 17.09 rad/s (see App. B). Bi-stable solutions are undesirable for most applications, because switching between periodic solutions can occur in case of perturbations or changing conditions and so the behavior of the system becomes less predictable. Moreover, the transient behavior is worsened by the influence of the co-existing stable and unstable solutions. More information on the stability of the co-existing periodic solutions can be found in App. B.

Periodic limb movements with frequencies below the endogenous CPG frequency are entrained by inhibition of the non-firing neuron (see Sect. 2.2); the firing neuron keeps on firing until the input stops inhibiting the non-firing neuron. This causes the CPG output to resemble a square wave at low frequencies. Thus, at low frequencies, the CPG output contains more higher harmonics and this causes the predicted entrained periodic limb movements to deviate slightly from the exact solutions, especially in amplitude. DFA cannot find solutions for limbs with a natural frequency below 2.5 rad/s, because the phase lead of the CPG is more than 180° at these frequencies. Hence, intersection of the Bode plots with the inverse transfer function of the limb is not possible (the phase of the latter only goes from 0 to 180°).

3.2 Influence of time delay in the coupling loop

In Ch. 2, we showed that time delays endanger the stability of human stance (Verdaasdonk et al. 2004). In this section, the influence of a time delay on resonance tuning and the stability of periodic solutions is discussed. In Fig. 7, Bode plots of the CPG – representing the input-output relation – are plotted for different input amplitudes. The difference with Sect. 3.1 is a time delay of 50 ms in the feedback loop from limb angle to CPG (τ_c=50 ms). Comparison of Fig. 7 with Fig. 3 (without time delay) shows that the gain plots do not change. However, the phase plots show an extra phase lag increasing proportional with frequency, which agrees with the transfer function H_τ of a time delay τ ($H_\tau = e^{-j\omega\tau}$). In other words, the time delay decreases the bandwidth for which the phase lead is around 90° and resonance tuning is expected only for limbs with natural frequencies around 10 rad/s.

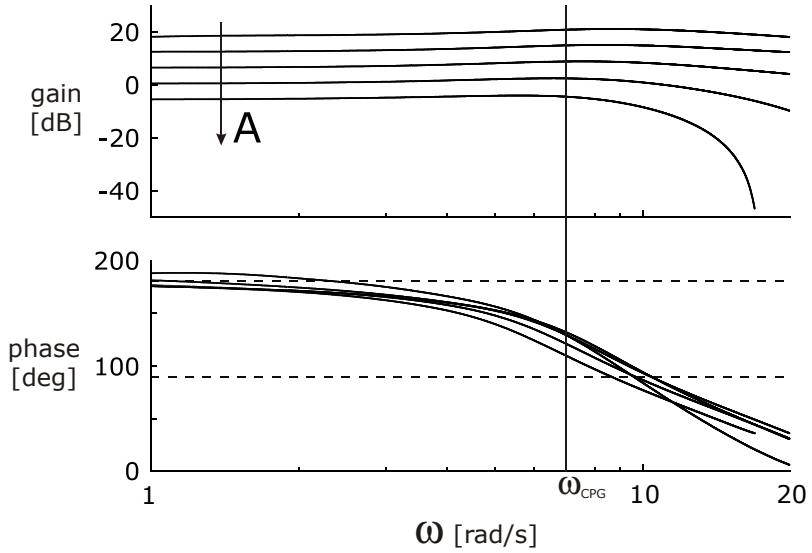

Fig. 7 Influence of 50 ms time delay τ_c on the Bode plots of the P-type CPG model for different input amplitudes (compare to Fig. 3). The phase continues to decrease and is about 90° around 10 rad/s. Therefore, the CPG is expected to only have resonance tuning capabilities when coupled to limbs with natural frequencies around 10 rad/s.

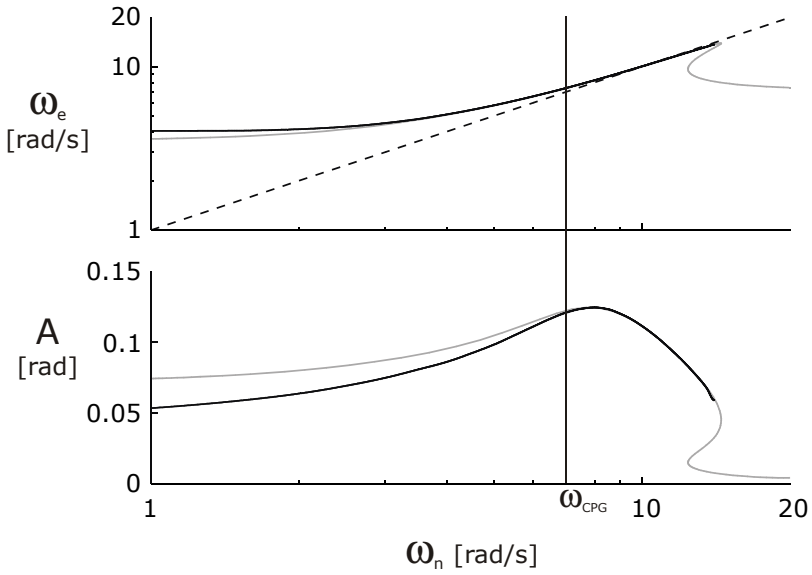

Fig. 8 Influence of time delay τ_c on the entrained periodic solutions (compare to Fig. 6). Time delay decreases the maximal natural limb frequency for which entrainment occurs (14.46 rad/s). It also causes bi-stability to occur at lower natural limb frequencies (12.39 – 14.46 rad/s), shown by the exact periodic solutions in *solid gray*. Bi-stability cannot be predicted by DFA (*black solid line*).

The upper graph of Fig. 8 shows the predicted and exact entrained frequencies ω_e in black and gray, respectively. In the lower graph the accompanying angular amplitudes of the rhythmic movements are shown. Resonance tuning only takes place for limbs with natural frequencies ω_n around 10 rad/s, as was expected from the phase plots (Fig. 7). Simultaneous intersections of the gain and phase plots of the CPG with the inverse transfer function of the limb are found with DFA for natural limb frequencies up to 14.0 rad/s. Beyond that, the frequencies at which intersection of the phase plots occurs differ from those of the gain plots for all input amplitudes (i.e. all Bode plots of the CPG). The reason is that the gain plot of the inverse transfer function of limbs with high natural frequency (i.e. large K_j) can only intersect low-input CPG gain plots, because the minimal gain of the inverse transfer function increases with joint stiffness. Thus, intersection of the gain plots can only occur at frequencies close to the natural frequency of the limb. However, the phase plots cannot intersect at these frequencies, because the time delay rendered the phase lead of the CPG well below 90° at these high frequencies.
Periodic solutions are also predicted for low natural frequencies, because the time delay adds just enough phase lag to ensure simultaneous intersection of phase and gain plots of the inverse transfer function with the CPG Bode plots (i.e. the phase plot of the CPG stays below 180°). The extra phase lag introduced by the time delay, also lowers the asymptote of the entrained frequency to 3.52 rad/s (for $K \rightarrow 0$ Nm/rad). Thus, for limbs with low natural frequency the time delay causes the CPG to entrain the limb at a frequency closer to its natural frequency. However, this has nothing to do with resonance tuning. It is noted that the lower asymptote of the entrained frequency causes larger deviation between the predicted and exact periodic solutions for low natural limb frequencies compared to feedback without time delay (see Fig. 6), because a lower entrained frequency means more higher harmonics in the CPG output (see Sect. 3.1).

The time delay lowers the highest natural frequency up to which a single periodic solution exists from 17.09 to 12.39 rad/s. Comparison of Fig. 8 with Fig. 6 shows clearly that time delay increases the region of co-existing periodic solutions at high natural limb frequencies (for details, see App. B). In conclusion, time delays narrow the bandwidth of natural limb frequencies for which resonance tuning with the P-type CPG is possible and give rise to bi-stability in limbs with high natural frequencies.

3.3 Improved resonance tuning with the PID-type CPG

The two previous subsections showed two problems concerning resonance tuning with the P-type CPG. Firstly, the entrained frequency is far from the natural limb frequency at low natural limb frequencies: the control of the CPG does not come close to resonance tuning at low natural frequencies.

Secondly, time delays enlarge the bandwidth at which multiple stable periodic solutions exist, at the expense of the usable bandwidth at which single stable periodic solutions are entrained by resonance tuning. A robust solution to these problems can be found by looking at the Bode plots of the CPG (Figs. 3 and 7). Ideal resonance tuning occurs when the phase lead of the CPG is 90° for all considered frequencies (Sect. 3.1); each limb is then actuated at –90°, so in its natural frequency. The phase plots of the CPG – not considering time delay – show a phase lead of about 180° at low frequencies and about 90° at high frequencies, with the endogenous frequency of the CPG being the transition point. Thus, a straightforward solution is to replace the proportional feedback gain g_p of the P-type CPG by a proportional-integral controller H_{PI} with the zero at the endogenous frequency of the CPG:

$$H_{PI} = \frac{g_p \left(s + \omega_{CPG}\right)}{s} \tag{11}$$

This PI controller gives a phase lag of 90° at low frequencies, but leaves higher frequencies untouched. In our model this is implemented by giving the feedback gain g_i in Eqs. 3 and 4 a value of $g_p\omega_{CPG}$. It is noted that the limb angle is integrated by a leaking integrator with a pole at –1/3 rad/s instead of an ideal one to avoid drift (see Fig. 1 and Eq. 19).

Figure 7 shows that the phase of the CPG falls well below 90° for high frequencies, because of the presence of time delay in the afferent feedback path. Derivative control (i.e. velocity feedback) is necessary to obtain resonance tuning for high natural limb frequencies, because it compensates for the phase lag caused by time delay τ_c. The necessary gain of the derivative control is $g_d=g_pc_\tau$, in which c_τ depends on the amount of time delay in the loop. In the case of τ_c=50 ms, the constant c_τ is $8.0\cdot10^{-2}$, which gives a gain g_d of 1.2 in Eqs. 3 and 4. Only a rough estimate of the time delay is necessary; a gain g_d of 1.0 or 1.4 also renders good results.

The CPG with additional integral and derivative afferent feedback is termed *PID-type CPG* (Sect. 2.2). In terms of control engineering, the proportional feedback gain g_p in the P-type CPG is replaced by the PID-controller H_{PID} in the PID-type CPG:

$$\begin{aligned} H_{PID}\left(g_p\right) &= g_p + \frac{g_p\omega_{CPG}}{s+\frac{1}{3}} + sg_d \\ &= \frac{c_t g_p s^2 + \left(1+\frac{c_t}{3}\right)g_p s + \left(\frac{1}{3}+\omega_{CPG}\right)g_p}{s+\frac{1}{3}} \end{aligned} \tag{12}$$

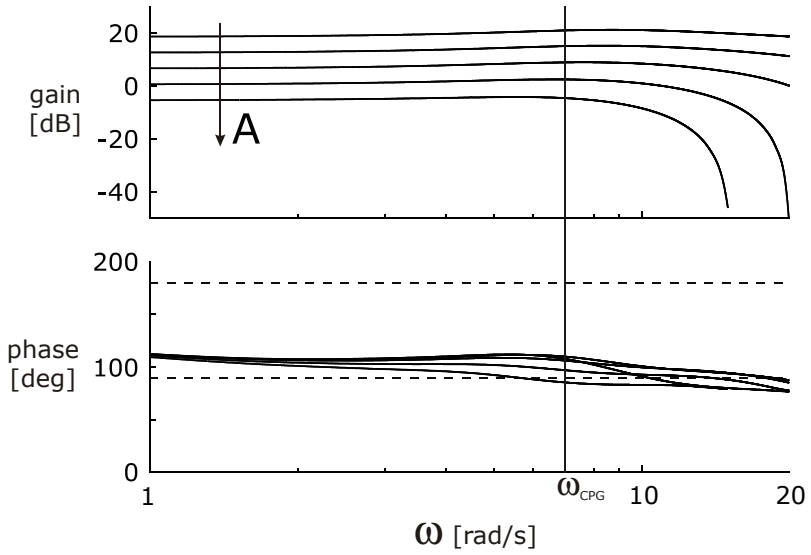

Fig. 9 Bode plots of the input-output relation of the PID-type CPG model with time delay τ_c =50 ms for different input amplitudes (compare to Fig. 7). Feedback of the integral of the limb angle to the half-center model gives 90° phase lag for low frequencies and velocity feedback compensates for the phase lag caused by time delay. This way a phase around 90° is achieved for all frequencies, which gives good resonance tuning behavior for all considered natural limb frequencies (see Fig. 10).

In applications, poles can be added at high frequencies (>>20 rad/s) without significantly changing the performance of the coupled system. This makes Eq. 12 a proper transfer function (i.e. more or equal number of poles compared to the number of zeros) and filters out high frequency noise.

Figure 9 shows the Bode plots of the PID-type CPG with a time delay of 50 ms in the feedback path. The phase plots show a phase lead close to 90° at all frequencies, while the gain plots only change slightly at high frequencies. At low frequencies the phase lead is slightly larger than 90°, because of the leaking integrator with its pole on –1/3 rad/s. Thus, good resonance tuning behavior of the PID-type CPG is expected for all considered natural limb frequencies and this is confirmed by Fig. 10. The integral control attributes to resonance tuning for frequencies lower than and around the endogenous CPG frequency. The derivative control gives resonance tuning for limbs with high natural frequency and pushes the region of co-existing stable solutions outside the range of considered limb frequencies; this region has become much smaller and exists for 20.7 up to about 22.2 rad/s (see App. B).

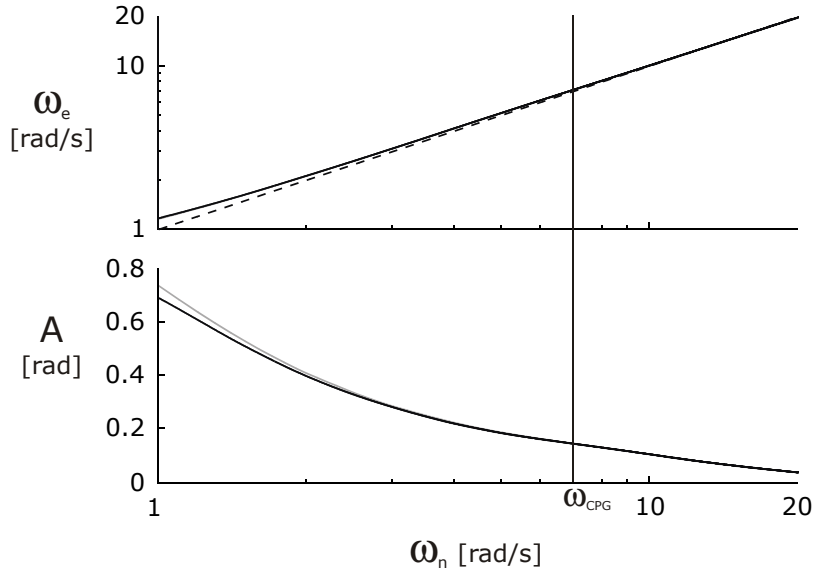

Fig. 10 Resonance tuning by the PID-type CPG is almost ideal ($\omega_e=\omega_n$, *dashed line*) for all considered natural limb frequencies. Approximations by DFA (*black solid line*) and exact solutions (*gray solid line*) agree very well. No bi-stability of stable periodic solutions is present in the considered bandwidth of natural limb frequencies.

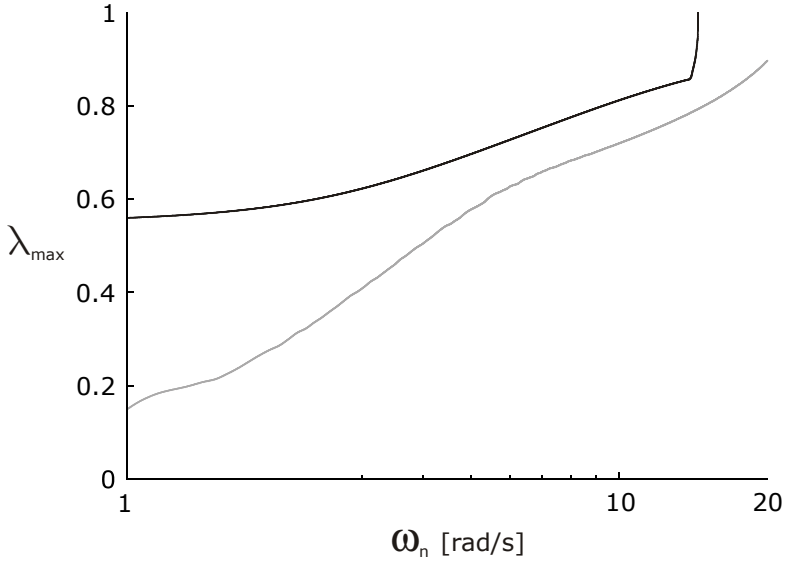

Fig. 11 Local stability of the system when the limb is coupled to the P-type CPG (*black line*) and the PID-type CPG (*gray line*). The non-trivial Floquet multiplier with the largest magnitude λ_{max} is plotted against the natural limb frequency ω_n. The time delay τ_c in the afferent path is 50 ms in both cases.

The predicted and exact entrained frequencies are nearly identical. In the accompanying amplitudes is a slight discrepancy at low frequencies, because the CPG output contains more higher harmonics at these frequencies. The deviation between predicted and exact periodic solutions is much less than for the P-type CPG, because integral control gives a much tighter coupling between the limb and the CPG at low frequency limb movements.
This tight coupling also has a positive effect on the local stability of the periodic solutions, quantified by the largest non-trivial *Floquet multiplier* (see Fig. 11). The Floquet multipliers are the eigenvalues of the mapping from cycle to cycle, termed Poincaré map (Kuznetsov 1998 pp 25-31). The Floquet multiplier with the largest magnitude, apart from the trivial one, is dominant and is an indication of the decay of small perturbations; lower values indicate faster decay from cycle to cycle. The largest non-trivial Floquet multiplier of a *stable* periodic solution has a magnitude smaller than one. Figure 11 shows the largest non-trivial Floquet multiplier for the P-type as well as for the PID-type CPG. The figure clearly shows a much faster decay of perturbations for the PID-type CPG compared to the P-type, especially for limbs with low natural frequency; this is due to the integral control. The derivative control stabilizes entrainment of limbs with high natural frequency by pushing the region of co-existing stable solutions towards higher natural limb frequencies.

This section has discussed the concept of resonance tuning for a limb coupled to a CPG. The CPG entrains to the limb if the gain and phase plot of the inverse transfer function of the limb cross the gain and phase plot of one of the Bode plots of the CPG. The amplitude of the entrained limb movement is adjusted by the efferent strength (i.e. k_a), while the range of possible movement amplitudes can be adjusted by the strength of afferent feedback (i.e. g_p). The large spread in the gain plots of the CPG provides large robustness against changing limb dynamics. Whether the entrained movement is energy efficient depends on the type of afferent feedback to the half-center model. Proportional feedback of the limb angle provides resonance tuning above the endogenous frequency of the CPG, integral feedback to the half-center model provides resonance tuning at and below the endogenous frequency and derivative feedback is necessary to compensate for the time delay τ_c in the loop that couples limb to CPG. Without derivative feedback bi-stability occurs and resonance tuning is not possible at high movement frequencies.

4. Discussion

This study has shown that tight local coupling of CPGs to limbs provides robust and energy efficient rhythmic movement. Stable rhythmic limb movement can be accomplished for a broad range of natural limb frequencies. The amplitude of the entrained limb movement is adjusted by the strength of efferent feedback, while the range of possible movement amplitudes can be adjusted by the strength of afferent feedback. The entrained frequency is adjusted by modulation of the joint stiffness.

4.1 Summary of results

Bode plots of the input-output behavior of the CPG were constructed at different angular amplitudes with the help of *Describing Function Analysis*. The large spread in the *gain plots* of the CPG (Figs. 3, 7 and 9) shows the robustness against changes in limb parameters. Feedback of different types of afferent information proved crucial in providing energy efficiency in terms of resonance tuning. This feedback shapes the *phase plots* (Fig. 9) of the CPG, such that resonance tuning is achieved for a large bandwidth of resonance frequencies of the limb (Fig. 10) and local stability is improved (Fig. 11). *Proportional* feedback of positional information – such as limb angle or muscle length – provides resonance tuning above the endogenous frequency of the CPG (Fig. 6). *Integral* feedback to the half-center model provides resonance tuning at and below the endogenous frequency. Feedback of velocity information, i.e. *derivative* feedback, is necessary to compensate for the time delay τ_c in the loop which couples limb to CPG; without velocity feedback bi-stability occurs (App. B) and resonance tuning is not possible at high movement frequencies (Fig. 8).

4.2 Application to robotics

Describing Function Analysis (DFA) predicts the periodic solutions of the coupled system well (Figs. 6, 8 and 10). It is therefore a useful 'engineering' tool, which renders fast development of robust and flexible controllers used to achieve energy efficient rhythmic arm movements in robotics with the desired frequency and amplitude. The movement frequency can be adjusted by changing the limb's resonance frequency (e.g. by local positional feedback); the CPG will subsequently entrain to the new resonance frequency of the limb. The amplitude can be adjusted by the efferent or actuation gain (e.g. by a pre-amplifier).
Williamson (1998) performed DFA on robot arms coupled to the same half-center model (Matsuoka 1985; Matsuoka 1987) as used in this study. The

DFA in this study is inspired by Williamson's work. However, Williamson did not investigate integral and derivative feedback to the half-center model.

4.3 Conclusion

In this study we investigated the roles of CPGs, afferent feedback and modulation of joint stiffness in providing energy efficient and robust rhythmic limb movement for a simple mathematical model of rhythmic limb movement. The most important finding of this study is that the type of afferent feedback to the half-center model is crucial in providing energy efficiency by means of resonance tuning.
Resonance tuning by afferent feedback to the CPG was also performed in the studies of Hatsopoulos (1996) and Williamson (1998). However, they only considered proportional feedback of the limb angle and could therefore only tune into resonance frequencies of the limb, which lie above the endogenous frequency of the CPG. They also did not consider time delays.
Most studies on CPG-controlled legged locomotion focus on the CPG itself and do not consider the interaction with the limb dynamics and environment at all (e.g.Golubitsky et al. 1998, 1999; Zielinska 1996). Taga (1995a) and Taga et al. (1991) *did* show that mutual entrainment of CPGs with the musculo-skeletal system and its environment creates stable gait which is quite robust (Taga 1995b). However, they did *not* consider energy efficiency.

The idea of achieving resonance tuning by shaping the sensory information gives insight into the way humans might control rhythmic limb movements. In a follow-up study, a neuro-musculo-skeletal model of the human forearm is proposed, using both knowledge of resonance tuning gained in this study and knowledge of the organization of CPGs from literature. Among others, the influence of time delays in the local reflex loop and the robustness against force perturbations will be investigated. In future research, the ideas of resonance tuning will also be applied to bipedal gait models.

References

Abe MO, Yamada N (2003) Modulation of elbow joint stiffness in a vertical plane during cyclic movement at lower or higher frequencies than natural frequency. Experimental Brain Research 153:394-399

Amemiya M, Yamaguchi T (1984) Fictive locomotion of the forelimb evoked by stimulation of the mesencephalic locomotor region in the decerebrate cat. Neuroscience Letters 50:91-96.

Barbeau H, McCrea DA, O'Donovan MJ, Rossignol S, Grill WM, Lemay MA (1999) Tapping into spinal circuits to restore motor function. Brain Res Brain Res Rev 30:27-51

Bennett DJ (1993) Torques generated at the human elbow joint in response to constant position errors imposed during voluntary movements. Experimental Brain Research 95:488-498

Brown TG (1911) The intrinsic factors in the act of progression in the mammal. In: Proceedings of the Royal Society of London (B). Vol. 84, London, pp 308-319

Brown TG (1914) On the nature of the fundamental activity of the nervous centres; together with an analysis of the conditioning of rhythmic activity in progression, and a theory of the evolution of function in the nervous system. Journal of Physiology 48:18-46

Burke RE (2001) The central pattern generator for locomotion in mammals. Adv Neurol 87:11-24

Burke RE, Degtyarenko AM, Simon ES (2001) Patterns of locomotor drive to motoneurons and last-order interneurons: clues to the structure of the CPG. Journal of Neurophysiology 86:447-462

Cheng J, Stein RB, Jovanovic K, Yoshida K, Bennett DJ, Han Y (1998) Identification, localization, and modulation of neural networks for walking in the mudpuppy (Necturus maculatus) spinal cord. Journal of Neuroscience 18:4295-4304

Engelborghs K, Luzyanina T, Samaey G (2001) DDE-BIFTOOL v. 2.00: a Matlab package for bifurcation analysis of delay differential equations. In. K.U. Leuven, Department of Computer Science, Heverlee, Belgium

Golubitsky M, Stewart I, Buono PL, Collins JJ (1998) A modular network for legged locomotion. Physica D. 115:56-72

Golubitsky M, Stewart I, Buono PL, Collins JJ (1999) Symmetry in locomotor central pattern generators and animal gaits. Nature 401:693-695.

Hatsopoulos NG (1996) Coupling the neural and physical dynamics in rhythmic movements. Neural Computation 8:567-581

Hatsopoulos NG, Warren Jr WH (1996) Resonance tuning in rhythmic arm movements. Journal of Motor Behavior 28:3-14

Kugler PN, Turvey MT (1987) Information, Natural law, and the self-assembly of rhythmic movement. In. Lawrence Erlbaum, Hillsdale, NJ, pp 481

Kuo AD (2001) A simple model of bipedal walking predicts the preferred speed-step length relationship. Journal of Biomechanical Engineering 123:264-269

Kuznetsov YA (1998) Elements of applied bifurcation theory. In: Marsden JE, Sirovich L (eds) Applied mathematical sciences. Vol. 112. Springer-Verlag, New York, pp 591

Matsuoka K (1985) Sustained oscillations generated by mutually inhibiting neurons with adaptation. Biological Cybernetics 52:367-376

Matsuoka K (1987) Mechanisms of frequency and pattern control in the neural rhythm generators. Biological Cybernetics 56:345-353

McCrea DA (2001) Spinal circuitry of sensorimotor control of locomotion. Journal of Physiology 533:41-50

Mochon S, McMahon TA (1980) Ballistic walking. J Biomech 13:49-57

Nishimaru H, Kudo N (2000) Formation of the central pattern generator for locomotion in the rat and mouse. Brain Research Bulletin 53:661-669

Shik ML, Severin FV, Orlovskii GN (1966) Control of walking and running by means of electrical stimulation of the mid-brain. Biophysics 11:756-765

Slotine J-JE, Li W (1991) Applied nonlinear control. In. Prentice-Hall, Englewood Cliffs, NJ, pp 459

Sqalli-Houssaini Y, Cazalets JR, Clarac F (1993) Oscillatory properties of the central pattern generator for locomotion in neonatal rats. Journal of Neurophysiology 70:803-813

Taga G (1995a) A model of the neuro-musculo-skeletal system for human locomotion. I. Emergence of basic gait. Biological Cybernetics 73:97-111.

Taga G (1995b) A model of the neuro-musculo-skeletal system for human locomotion. II Real-time adaptability under various constraints. Biological Cybernetics 73:113-21.

Taga G, Yamaguchi Y, Shimizu H (1991) Self-organized control of bipedal locomotion by neural oscillators in unpredictable environment. Biological Cybernetics 65:147-59

Van de Crommert HW, Mulder T, Duysens J (1998) Neural control of locomotion: sensory control of the central pattern generator and its relation to treadmill training. Gait Posture 7:251-263.

Verdaasdonk BW, Koopman HF, Van Gils SA, Van Der Helm FC (2004) Bifurcation and stability analysis in musculoskeletal systems: a study in human stance. Biological Cybernetics 91:48-62

Whelan PJ (1996) Control of locomotion in the decerebrate cat. Prog Neurobiol 49:481-515

Williamson MM (1998) Neural control of rhythmic arm movements. Neural Networks 11:1379-1394.

Zielinska T (1996) Coupled oscillators utilised as gait rhythm generators of a two-legged walking machine. Biol Cybern 74:263-73

Appendix A. Model equations

The model of rhythmic limb movement consists of a limb coupled to the Central Pattern Generator (CPG). The state variables are the limb angle θ and angular velocity ω, the state variables of the CPG model u_F, v_F, u_E, v_E and the 'integral' of the angle θ, denoted φ. For the latter state variable φ, integrating the angle θ is in fact performed by a leaking integrator (pole at $-1/\tau_i$, see Eq. A.7 below) to prevent infinite gain at zero frequency. The state variables associated with the flexor center of the CPG are denoted with 'F', while the state variables associated with the extensor center are denoted with 'E'. Afferent feedback to the half-center model consists of delayed limb angle $\theta(t-\tau_c)$, angular velocity $\omega(t-\tau_c)$ and the the integrated angle $\varphi(t-\tau_c)$ with gains g_p, g_d and g_i, respectively. Note that for the P-type CPG g_i and g_d are taken zero.

The delayed differential equations of the model are:

$$\dot{\theta} = \omega \tag{A.1}$$

$$\dot{\omega} = \frac{M_a - B_j\omega - K_j\theta}{I} \tag{A.2}$$

$$\dot{u}_F = \frac{1}{\tau_r}\left(u_0 - u_F - \beta v_F - w y_E - s_F\right) \tag{A.3}$$

$$\dot{v}_F = \frac{1}{\tau_a}\left(y_F - v_F\right) \tag{A.4}$$

$$\dot{u}_E = \frac{1}{\tau_r}\left(u_0 - u_E - \beta v_E - w y_F - s_E\right) \tag{A.5}$$

$$\dot{v}_E = \frac{1}{\tau_a}\left(y_E - v_E\right) \tag{A.6}$$

$$\dot{\varphi} = \frac{1}{\tau_i}\left(\tau_i\theta - \varphi\right) \tag{A.7}$$

The moment of force M_a is applied by the actuator, which has gain k_a:

$$M_a = k_a\left(y_F - y_E\right) \tag{A.8}$$

The inputs to the flexor and extensor center of the half-center-model, s_F and s_E respectively, are:

$$s_F = \max\left(0, g_p\theta\left(t-\tau_c\right) + g_d\omega\left(t-\tau_c\right) + g_i\varphi\left(t-\tau_c\right)\right) \quad \text{(A.9)}$$

$$s_E = \max\left(0, -g_p\theta\left(t-\tau_c\right) - g_d\omega\left(t-\tau_c\right) - g_i\varphi\left(t-\tau_c\right)\right) \quad \text{(A.10)}$$

The outputs y_F and y_E of the flexor and extensor centers are:

$$y_F = \max\left(0, u_F\right) \quad \text{(A.11)}$$

$$y_E = \max\left(0, u_E\right) \quad \text{(A.12)}$$

Limb parameters

I	= 1.0	kgm^2	moment of inertia of the limb about the joint
B_j	= 1.0	Nms/rad	rotational joint damping of limb
k_a	= 2.0		actuator gain between CPG output and applied moment of force M_a

CPG parameters

τ_i	= 3.0	s	time constant for leaking integrator (pole at $-1/\tau_i$)
τ_r	= 0.1	s	rise time constant
τ_a	= 0.2	s	adaptation time constant
β	= 2.0		strength adaptation effect
w	= 2.0		strength of reciprocal inhibition
u_0	= 1.0		tonic input from supra-spinal centers
c_τ	= 0.08		constant associated with velocity feedback

Variables with default values

K_j	= 0	Nm/rad	rotational joint stiffness of limb
τ_c	= $50\cdot10^{-3}$	s	time delay in feedback loop
g_p	= 15.0		feedback strength of limb angle
g_d	= $g_p c_\tau$		feedback strength of limb's angular velocity
g_i	= $g_p\omega_{CPG}$		feedback strength of 'integral' of limb angle with ω_{CPG} the endogenous frequency of the CPG, which is 7.0 rad/s for these CPG parameters

Appendix B. Stability of co-existing periodic solutions

In Figs. B.1, B.2 and B.3 the stability of a branch of 1:1 periodic solutions is shown for proportional feedback of the angle θ, delayed proportional feedback of the angle θ and delayed proportional-integral-derivative feedback of the angle θ to the half-center model, respectively. The term *1:1 periodic solutions* will be used to indicate solutions, which have one oscillation in a period for both the output of the CPG and the limb angle θ (i.e. both oscillators – the limb and CPG – oscillate at the same frequency). Stable solutions are shown by solid lines and unstable solutions by dashed lines. If an unstable 1:1 periodic solution is present for a certain ω_n, then there is also an *additional* stable solution with low amplitude in terms of the angle θ at this ω_n. These additional stable solutions, which can be periodic (*not* 1:1 though) and quasi-periodic (or have very long periods), are not shown in the figures. The additional stable *periodic* solutions seem to have periods T which are close to multiples of the natural limb period T_{limb} ($T_{limb}=2\pi/\omega_n$) and at the same time close to multiples of (slightly less than) the endogenous period of the CPG T_{CPG} ($T_{CPG}=2\pi/\omega_{CPG}$). In other words, the additional solutions will be periodic at those natural limb frequencies ω_n for which both oscillators – the limb *and* the CPG – are able to move near resonance; if this is not the case, they are found to be quasi-periodic.

Figure B.1 shows that the lowest ω_n for which an unstable 1:1 periodic solution was calculated (before the branch folds back on itself) is 17.34 rad/s. However, bi-stability is already observed at a ω_n of 17.09 rad/s, so probably – also regarding Fig. B.2 – there is at least one other branch of unstable periodic solutions, which is not connected (smoothly) to the one showed. For a ω_n of a 17.09 up to 17.14 rad/s a low-amplitude periodic solution is present with a period about 7 times T_{limb} ($T\approx7T_{limb}=2.57$ s). Beyond that, the solution becomes quasi-periodic, but for a ω_n of 20 rad/s for example, the solution is periodic again with a period of about 14 times T_{limb} ($T\approx14T_{limb}=4.40$ s). At higher ω_n the periodic solution becomes 1:1 again (not shown in figure) and has a period close to $T_{CPG.}$

Comparing Fig. B.2 to Fig. B.1, it becomes clear that time delay causes a large increase in the region of natural limb frequencies for which bi-stable periodic solutions exist, even giving rise to bi-stable 1:1 periodic solutions for natural limb frequencies ω_n of 12.39 up to 12.46 rad/s. Additional periodic solutions with the smallest multitude of T_{limb} were found for a ω_n of 12.99 up to 13.26 rad/s with a period about 4 times T_{limb} ($T\approx4T_{limb}$). Other examples of additional low-amplitude solutions are: $\omega_n=12.75$ with $T\approx16T_{limb}$, $\omega_n=12.8$ with $T\approx10T_{limb}$, $\omega_n=12.95$ with $T\approx27T_{limb}$ and $\omega_n=13.3$ with $T\approx25T_{limb}$. Quasi-periodic solutions are found between these small regions of periodic

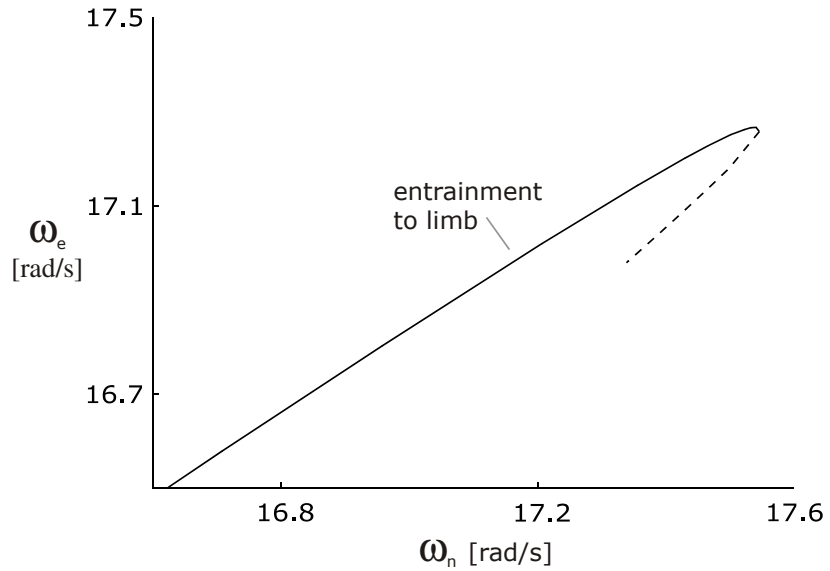

Fig. B.1 Stability of co-existing 1:1 periodic solutions for the P-type CPG (zoom-in of Fig. 6). The *solid line* shows stable solutions; the *dashed line* shows unstable solutions. On the horizontal axis the natural frequency of the limb dynamics ω_n is shown and on the vertical axis the entrained frequency ω_e is shown.

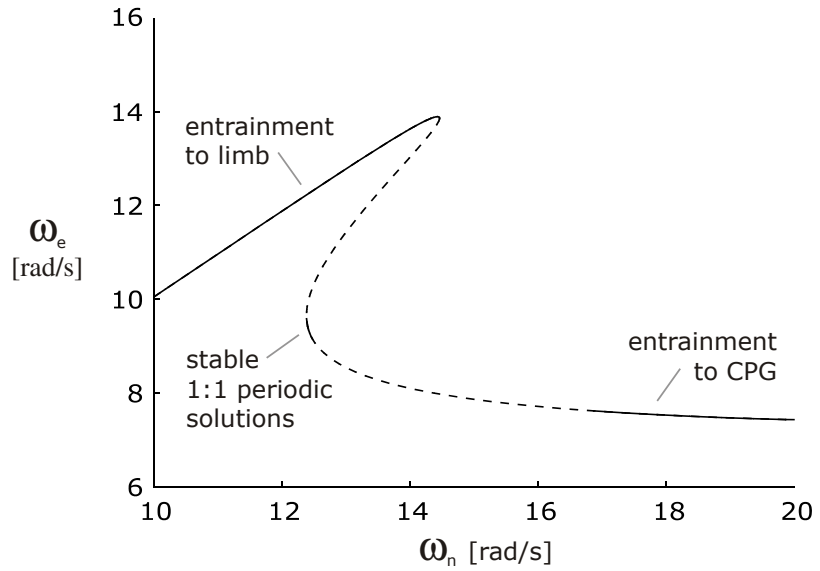

Fig. B.2 Zoom-in of Fig. 8. Time delay causes bi-stability of 1:1 periodic solutions for lower natural limb frequencies (12.39 – 12.46 rad/s), compared to the case of no time delay (Fig. B.1). The *solid lines* show stable solutions; the *dashed lines* show unstable solutions. On the horizontal axis the natural frequency of the limb dynamics ω_n is shown and on the vertical axis the entrained frequency ω_e is shown.

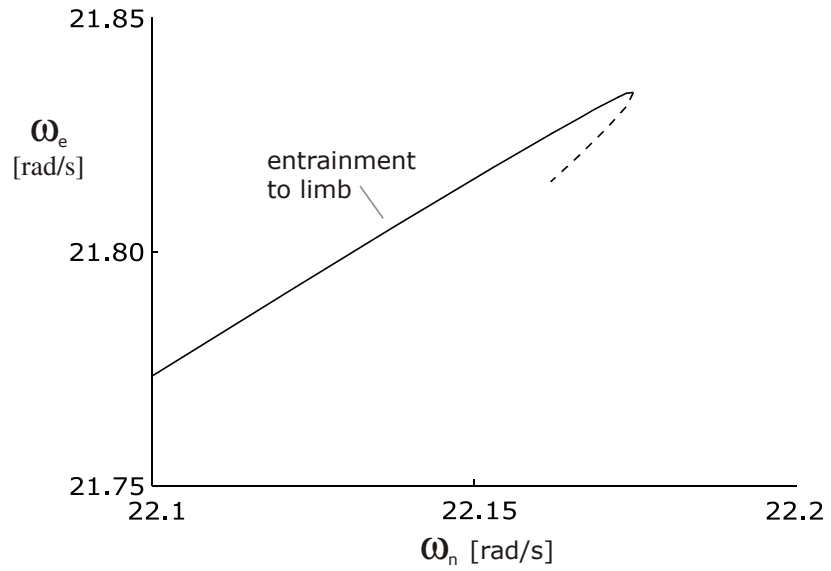

Fig. B.3 Zoom-in of Fig. 10. The region of co-existing 1:1 periodic solutions has been decreased and shifted to higher natural limb frequencies by the velocity feedback to the half-center model of the PID-type CPG, despite the time delay in the feedback path. The *solid line* shows stable solutions; the *dashed line* shows unstable solutions. On the horizontal axis the natural frequency of the limb dynamics ω_n is shown and on the vertical axis the entrained frequency ω_e is shown.

solutions. For natural limb frequencies ω_n higher than 16.8 rad/s the branch of 1:1 periodic solutions becomes stable again (Fig. B.2) and has a period close to T_{CPG} (i.e. the coupled system entrains to the CPG).

Figure B.3 shows that feedback of the angular velocity (D-control) reduces the region of natural limb frequencies for which co-existing 1:1 periodic solutions exist and pushes this region towards higher natural limb frequencies as well. Note however, that bi-stability is already observed at a ω_n of 20.7 rad/s with a period $\approx 3T_{limb}$, which slowly transforms into a stable 1:1 periodic solution with a period close to T_{CPG} at higher ω_n (not showed in the figure). No quasi-periodic solutions were found. For most applications bi-stability is unwanted and thus feedback of angular velocity renders a larger useful bandwidth (up to 20.7 rad/s) in which only one stable predictable solution exists.

Chapter 4

Resonance Tuning in a Neuro-Musculo-Skeletal Model of the Forearm

B.W. VERDAASDONK, H.F.J.M. KOOPMAN, F.C.T. VAN DER HELM

Biological Cybernetics 96: 165-180, 2007

Abstract

In rhythmic movements, humans activate their muscles in a robust and energy efficient way. These activation patterns are oscillatory and seem to originate from neural networks in the spinal cord, called Central Pattern Generators (CPGs). Evidence for the existence of CPGs was found for instance in lampreys, cats and rats. There are indications that CPGs exist in humans as well, but this is not proven yet. Energy efficiency is achieved by *resonance tuning*: the central nervous system is able to tune into the resonance frequency of the limb, which is determined by the *local reflex gains*. The goal of this study is to investigate if the existence of a CPG in the human spine can explain the resonance tuning behavior, observed in human rhythmic limb movement. A neuro-musculo-skeletal model of the forearm is proposed, in which a CPG is organized in parallel to the local reflex loop. The afferent and efferent connections to the CPG are based on clues about the organization of the CPG, found in literature. The model is kept as simple as possible (i.e. lumped muscle models, groups of neurons are lumped into half-centers, simple reflex model), but incorporates enough of the essential dynamics to explain behavior – such as resonance tuning – in a qualitative way. Resonance tuning is achieved above, at and below the endogenous frequency of the CPG in a highly non-linear neuro-musculo-skeletal model. Afferent feedback of *muscle lengthening* to the CPG is necessary to accomplish resonance tuning above the endogenous frequency of the CPG, while feedback of *muscle velocity* is necessary to compensate for the phase lag, caused by the time delay in the loop coupling the limb to the CPG. This afferent feedback of muscle lengthening and velocity represents the Ia and II fibers, which – according to literature – are inputs to the CPG. An internal process of the CPG, which integrates the delayed muscle lengthening and feeds it to the half-center model, provides resonance tuning below the endogenous frequency. Increased co-contraction makes higher movement frequencies possible. This agrees with studies of rhythmic forearm movements, which have shown that co-contraction increases with movement frequency. Robustness against force perturbations originates mainly from the CPG and the local reflex loop. The CPG delivers an increasing part of the necessary muscle activation for increasing perturbation size. As far as we know, the proposed neuro-musculo-skeletal model is the first that explains the observed resonance tuning in human rhythmic limb movement.

1. Introduction

Locomotion is one of the most obvious oscillatory activities in animal world. Walking, swimming and flying are all powered by rhythmic patterns of muscle activity. These motor patterns are oscillatory and seem to originate from neural networks on spinal level, called Central Pattern Generators (CPGs). Evidence for the existence of CPGs was found for instance in lampreys (Cohen and Wallen 1980; Grillner et al. 1981), rats (Cazalets et al. 1995; Marchetti et al. 2001; Sqalli-Houssaini et al. 1993) and cats (Amemiya and Yamaguchi 1984; Brown 1911; Shik et al. 1966). There is a growing number of observations suggesting the presence of CPGs in humans as well (reviews by Duysens and Van de Crommert 1998; MacKay-Lyons 2002). Although there is little direct evidence of CPGs in the human spine, Dimitrijevic (1998) induced alternating stance and swing phases in the lower limbs by tonic electrical stimulation of the spinal cord. CPGs have also been found to contribute to other rhythmic tasks, such as mastication (Nakamura et al. 1999), respiration (Taylor and Lukowiak 2000) and scratching (Baev et al. 1991).

Control of rhythmic arm movements by CPGs is investigated only recently, because the high number of direct corticospinal projections to the forearm muscles made the CPG an unlikely candidate for the control of arm movement. However, *rhythmic* movements are old motor behaviors and for these movements far less brain areas are used compared to *discrete* movements such as reaching and grasping (Schaal et al. 2004). Schaal et al. showed that for rhythmic movement only a few unilateral primary motor areas are used while for discrete movements additional contralateral nonprimary motor areas are used and strong bilateral activity is present in the cerebrum and cerebellum. Moreover, during rhythmic arm movement there seems to be *less* control from the primary motor cortex, because in that case the corticospinal excitability is lower compared to tonic voluntary contraction (Carroll et al. 2006). In other words, the control coming from the brain is less and simpler for rhythmic movements compared to discrete movements, which support the idea that CPGs play a crucial role in the control of rhythmic arm movement. Furthermore, reflex studies (Zehr and Chua 2000; Zehr et al. 2003; Zehr and Kido 2001) show that during rhythmic arm movement the reflex modulation in the (fore)arm muscles is similar to the reflex modulation in the leg muscles during rhythmical leg movement such as locomotion. They also point out the similarity in subcortical neural control for rhythmic movement in humans and animals for which CPGs are already discovered. Although there is no direct evidence of the existence of CPGs in humans, the archaic brain control during rhythmic arm movements together with the evidence of similar neural control in rhythmical arm and leg movement *and* the fact that CPGs are found to contribute to a large variety

of rhythmic tasks in all kinds of animals lead us to believe that in humans CPGs could play a crucial role in rhythmic arm movement. Several experimental studies (Abe and Yamada 2003; Hatsopoulos and Warren Jr 1996; Kugler and Turvey 1987; Latash 1992) have shown that in rhythmic limb movement, such as arm swinging, the limb's resonance frequency is close to the imposed movement frequency. In other words, the central nervous system is able to tune into the resonance frequency of the limb, which is termed *resonance tuning*. The limb's resonance frequency is modulated by the joint stiffness, which determines the movement frequency (Ch. 3; Verdaasdonk et al. 2006). This might indicate that local reflex gains and co-contraction levels are the parameters, which are controlled by supra-spinal centers to regulate movement frequency. Our hypothesis is that the CPG plays a key role in the observed resonance tuning behavior by entraining to the dynamical properties of the limb. Hence, the goal of this study is to investigate if the existence of spinal CPGs can explain the resonance tuning behavior, observed in human rhythmic limb movement. To achieve this goal, a neuro-musculo-skeletal model of the forearm is proposed, in which a CPG is organized in parallel to the local reflex loop (i.e. stretch reflex and reciprocal inhibition). The model is kept as simple as possible in order to investigate the plausibility of resonance tuning by entrainment of a CPG to the limb dynamics, without drowning in a sea of parameters. Moreover, a detailed model cannot be made at present, because too little is known of the exact organization and embedding of CPGs in vertebrates, let alone in humans. However, the model has enough complexity (see discussion in Sect. 4.1) to make a qualitative comparison between the simulation outcomes and the above-mentioned studies. In Ch. 3 (Verdaasdonk et al. 2006) the roles of CPGs, afferent feedback and modulation of the joint stiffness in providing energy efficient and robust rhythmic limb movement were determined for a general mass-spring-damper system. This study makes use of the knowledge gained in that study. Two important research questions, which are still unanswered, are also considered in the present study: (1) What is the influence of *time delay* in the local reflex loop and is compensation for this delay possible? (2) Where does the *robustness against force perturbations* come from and what is the role of the CPG in this?

In Sect. 2 a neuro-musculo-skeletal model of rhythmic forearm movement is proposed. Literature indicates that at least afferent feedback from Ia and II fibers to the flexor and extensor centers are present. This is translated in our model to feedback of muscle lengthening and velocity to the half-center model (*PD-type* CPG, Sect. 2.2). An internal process of the CPG, which integrates the delayed muscle lengthening and feeds it to the half-center model, is added to investigate the possibility of resonance tuning at and below the endogenous frequency of the CPG (*PID-type* CPG, Sect. 2.2). Section 3.1 discusses the resonance tuning capability of the CPG in the hanging forearm and the effect that time delay in the local reflex loop has on this capability. Robustness against force perturbations is discussed for the

forearm in upright position, because this position poses more of a challenge (Sect. 3.2).

2. Neuro-musculo-skeletal model of the forearm

A neuro-musculo-skeletal model of the human forearm is proposed, in which the local reflex loop and the CPG are organized in parallel. In this model, the afferent and efferent connections to the CPG, though fairly basic, are based on clues about the organization of the CPG, found in literature (Burke 2001; Burke et al. 2001; Butt et al. 2002; Capaday 2002; Friesen 1994; MacKay-Lyons 2002; McCrea 2001; Whelan 1996).
In Fig. 1, an overview of the model is shown. The model is divided in two blocks, namely '*Limb Dynamics*' and '*Central Pattern Generator*'. The equations of the neuro-musculo-skeletal model of the forearm can be found in App. A.

2.1 Limb dynamics

The musculo-skeletal model of the forearm consists of a pendulum with an antagonistic muscle pair, shown in Fig. 1 by the block '*Limb Dynamics*'. The pendulum represents the forearm, which the muscles can flex and extend about the elbow joint. The flexor muscle represents the flexor muscles of the forearm, mainly the Brachialis; the extensor muscle represents the extensor muscles, mainly the Triceps Brachii. The lumped Hill-type muscle model is based on the work of Winters and Stark (1985; 1987) and models both activation and contraction dynamics. It consists of a contractile element (CE) and a serial elastic element (SE), which is modeled as a non-linear spring. Both muscles are parameterized the same way for simplicity (i.e. symmetric model) and the musculo-skeletal parameters are estimated with the help of different sources (see App. A for references). The joint stiffness of the elbow is determined by the amount of co-contraction and by the positional feedback gain k_p of the local reflex loop. The local reflex loop models the stretch reflex and reciprocal inhibition and contains a time delay τ_l. It consists of feedback of muscle lengthening $\mathbf{\Delta l_{mus}}$ and velocity $\mathbf{v_{mus}}$ with gains k_p and k_v, respectively. This reflexive feedback, together with neural input from supra-spinal centers $\mathbf{u_{ss}}$ and the output from the CPG $\mathbf{u_{CPG}}$, gives the excitation of the muscles $\mathbf{e_{mus}}$. The forearm is perturbed by a moment of force M_p.
The musculo-skeletal model of the forearm is similar to the model of stance discussed extensively in Ch. 2 (Verdaasdonk et al. 2004). Thus, for detailed information about the musculo-skeletal model we refer to that chapter.

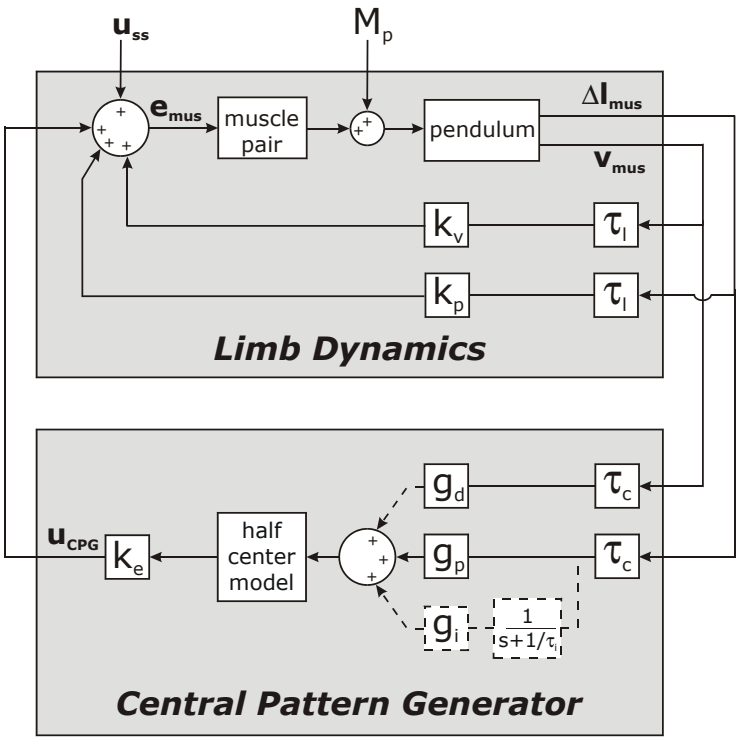

Fig. 1 Neuro-musculo-skeletal model of the forearm. The pendulum represents a forearm, which the muscles can flex and extend about the elbow joint. The local reflex loop consists of delayed (with τ_l) feedback of muscle lengthening $\mathbf{\Delta l_{mus}}$ and velocity $\mathbf{v_{mus}}$ with gains k_p and k_v, respectively. Together with supra-spinal neural input vector $\mathbf{u_{ss}}$ and the output from the CPG $\mathbf{u_{CPG}}$, it gives the excitation of the muscles $\mathbf{e_{mus}}$. The moment of force M_p perturbs the forearm. The *PD-type* CPG has afferent input of $\mathbf{\Delta l_{mus}}$ and $\mathbf{v_{mus}}$, which is fed to the half-center model with gains g_p and g_d and time delay τ_c. For the *PID-type* CPG the half-center model receives additional input from an internal process (dashed lines). The delayed muscle lengthening is integrated by a leaking integrator with large time constant τ_i and is fed to the half-center model with gain g_i. The half-center model is the basic rhythm generator; its output is coupled to the limb by efferent gain k_e.

2.2 Central Pattern Generator

The *neuro*-musculo-skeletal model of the forearm consists of the musculo-skeletal model of the forearm (Sect. 2.1) coupled to the '*Central Pattern Generator*' (see Fig. 1). The basic rhythm generator of the CPG is represented by the half-center model and is based on the work of Matsuoka (1985; 1987). The half-center model is extensively discussed in Ch. 3 (Verdaasdonk et al. 2006) and for detailed information we refer to that chapter. We choose the endogenous frequency ω_{CPG} of the half-center model

(and thus the CPG) to be 2.33 rad/s, because experimental studies of CPG activity on isolated spinal cords of rats indicate that the endogenous frequency of the CPG is below normal locomotion frequencies (Barthe and Clarac 1997; Marchetti et al. 2001; Sqalli-Houssaini et al. 1993). This was done by making the time constants τ_r and τ_a of the half-center model three times larger in comparison with Ch. 3 (Verdaasdonk et al. 2006), thereby reducing the endogenous frequency by factor three. The outputs of the flexor and extensor center of the half-center model excite the flexor and extensor muscles through efferent gain k_e.

Clues to the organization of the CPG mainly originate from cat studies (for reviews see Barbeau et al. 1999; Burke 2001; McCrea 2001; Van de Crommert et al. 1998; Whelan 1996). These suggest that at least afferent feedback from Ia and II fibers to the flexor and extensor centers are present. Afferent information from the flexor muscle (i.e. Brachialis) excites the flexor center and inhibits the extensor center, while afferent information of the extensor muscle (i.e. Triceps Brachii) excites the extensor center and inhibits the flexor center. In our model, this is translated to feedback of muscle lengthening $\mathbf{\Delta l_{mus}}$ and velocity $\mathbf{v_{mus}}$ to the half-center model with gains g_p and g_d and time delay τ_c. The CPG with this configuration is termed *PD-type* CPG.
Sqalli-Houssaini (1993) has shown that the rat's CPG is able to entrain to dorsal root stimulation with a larger period than the period of the CPG activity in case of no stimulation. In other words, the CPG is able to entrain below its endogenous frequency to a feed-forward input (i.e. in an *uncoupled* system). Moreover, the difference in phase between the stimulus input and the ipsilateral CPG output only changed roughly by about 60° when comparing the minimum entrained stimulus frequency (below endogenous frequency) to the maximum (above endogenous frequency). Although these observations are not conclusive evidence that the rat's CPG can indeed entrain below endogenous CPG frequency when it is *coupled* to the limb dynamics, the possibility is investigated in this study by adding an internal process to the CPG, which integrates the afferent input of muscle lengthening information. In fact, delayed muscle lengthening $\mathbf{\Delta l_{mus}}(t-\tau_c)$ is integrated by a leaking integrator with large time constant τ_i and is fed to the half-center model with gain g_i. The CPG with this additional feedback to the half-center model is termed *PID-type* CPG.

The model contains a total of 11 state variables (App. A): the limb angle θ relative to the vertical, the angular velocity ω, the active states of the Brachialis and the Triceps Brachii, a_B and a_T, the lengths of the CEs of both muscles, $l_{ce,B}$ and $l_{ce,T}$, the states of the half-center model u_B, v_B, u_T, v_T (Ch. 3; Verdaasdonk et al. 2006) and the leaking integral of the angle φ. The latter is only present for the PID-type CPG, *not* for the PD-type. Local reflexive feedback cause the angle and angular velocity to appear in delayed form,

$\theta(t-\tau_l)$ and $\omega(t-\tau_l)$, respectively. Additionaly, afferent feedback to the CPG cause the angle, angular velocity and the integrated angle to appear in delayed form, $\theta(t-\tau_c)$, $\omega(t-\tau_c)$ and $\varphi(t-\tau_c)$, respectively. Thus, the system is of infinite order. The muscles have different time constants for increasing and decreasing muscle activation and there is a discontinuity in the slope of the force-velocity curve of the CEs at zero velocity. These discontinuities are exactly in the equilibrium of the musculo-skeletal model of the forearm and render bifurcation analysis difficult. Therefore they have been approximated with the help of a 'sharp' tangent hyperbolic function (i.e. steep slope), in the same way as in Ch. 2 (Verdaasdonk et al. 2004). Comparing time simulations of the model with real discontinuities to solutions obtained by bifurcation analysis of the smoothed model revealed no significant change.

3. Results of numerical simulations

Tight local coupling of CPGs to limbs provides robust and energy efficient rhythmic movement for a broad band of movement frequencies if the afferent feedback to the half-center model behaves as a kind of PID-controller (Ch. 3; Verdaasdonk et al. 2006). Moreover, the movement frequency can be changed by *modulation of the joint stiffness*. In this study, we focus on the mutual observation of experimental studies (Sect. 1) that the limb's resonance frequency matches the movement frequency closely. Furthermore, we start off by assuming that the limb's resonance frequency is modulated by local reflex gains, because hardly any co-contraction was shown during rhythmic movement in above-mentioned studies. Furthermore, co-contraction is an energy consuming way of increasing the stiffness of the limb joint and probably only used when necessary. The joint stiffness during rhythmic limb movement is not quantified, because stiffness is an ambiguous concept for periodic movements; sometimes it is defined relative to the cycle (e.g. fitted on a mass-spring-damper model), while other times it is defined relative to the unstable posture (i.e. averaged).

In Ch. 3 (Verdaasdonk et al. 2006) periodic solutions were predicted with a method termed Describing Function Analysis (DFA). This method is fast if the limb dynamics are not too non-linear. However, for highly non-linear limb dynamics, such as the musculo-skeletal model of the forearm (Sect. 2.1), prediction of periodic solutions with DFA becomes a slow iterative process and is not useful anymore. Hence, all the calculations of periodic solutions in this paper were carried out by bifurcation analysis and subsequent continuation with DDE-BIFTOOL (Engelborghs et al. 2001) and checked by time simulations in Matlab. DFA was only used to initially find some afferent and efferent gains, for which stable periodic solutions were to be expected.

The resonance tuning capabilities of the PD-type and PID-type CPG in the hanging forearm is discussed in Sect. 3.1. The effect of time delay in the local reflex loop on these capabilities is also shown, as well as the influence of increased co-contraction. In Sect. 3.2, the robustness against force perturbations is discussed for the forearm in upright position, because this position poses more of a challenge in terms of stability.

3.1 Resonance tuning for the forearm in hanging position

In this subsection it is investigated to which extent the PD-type and PID-type CPG are able to entrain to a range of resonance frequencies ω_{res} of the limb dynamics of the hanging forearm. The resonance frequency ω_{res} depends on the stiffness of the elbow joint and is changed by changing the reflexive

feedback gain of the muscle lengthening k_p in the local reflex loop. Firstly, the limb dynamics are investigated without coupling the limb to the CPG (i.e. the block *Limb Dynamics* in Fig. 1). Secondly, the limb is coupled to the CPG (i.e. the block *Central Pattern Generator* in Fig. 1) to obtain rhythmic limb movement.

Limb dynamics

The joint stiffness of the elbow – and by that the resonance frequency ω_{res} – is determined by gravity, the intrinsic properties of the muscles and local reflexive feedback of muscle length. The small tonic activation, which is always present in muscles, is represented by constant supra-spinal inputs $u_{ss,B}=u_{ss,T}=0.01$ (i.e. a co-activation of the muscles of 1% of maximum). It is noted that the musculo-skeletal model of the forearm is not behaving as an ideal second order mass-spring-damper model. Muscle dynamics and the time delay τ_l of 50 ms in the local reflex loop make the limb dynamics highly nonlinear. This is especially true for high reflexive feedback gains, because then the time delay τ_l has much influence on the limb dynamics. Figure 2 shows that velocity feedback is necessary for positional feedback gains k_p

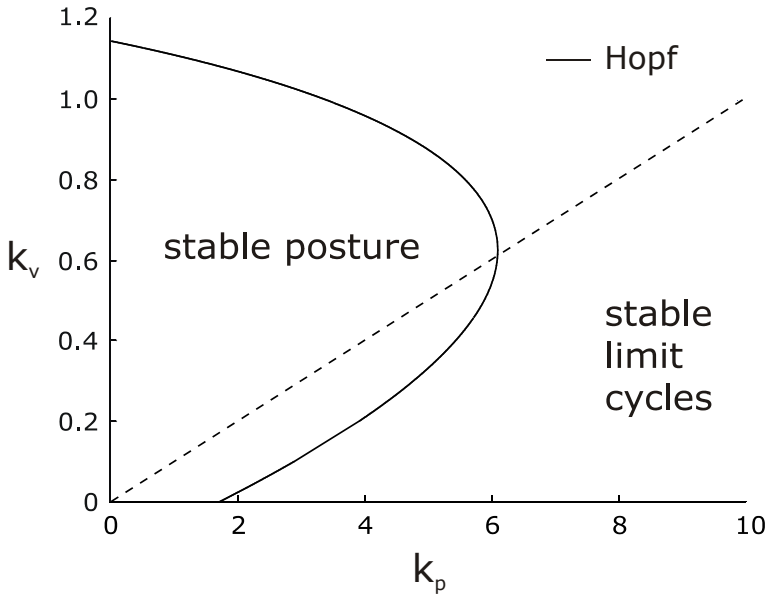

Fig. 2 A branch of Hopf bifurcations (*solid line*) divides the parameter space into areas of stable posture and stable limit cycles for the forearm, which is modeled as *hanging* pendulum with muscles. The parameters are the positional feedback gain k_p and the velocity feedback gain k_v of the local reflex loop. The *dashed line* ($k_v=k_p/10$) shows for which local reflex gains the musculo-skeletal model of the forearm is coupled to the CPG.

higher than 1.7 to obtain stable posture. It compensates for the phase lag caused by time delay τ_l in the reflex loop, muscle activation dynamics and the presence of a compliant SE (Ch. 2; Verdaasdonk et al. 2004). The Hopf branch divides the parameter space of positional gain k_p versus velocity gain k_v into regions of stable equilibria and stable limit cycles (Ch. 2; Verdaasdonk et al. 2004). The region of stable equilibria represents those reflex gains for which stable posture is obtained. In the region of stable limit cycles, the posture is unstable, but the limb exhibits periodic movement around the unstable posture. The dashed line (k_v=k_p/10) shows for which local reflex gains k_p and k_v the limb is connected to the PD-type and PID-type CPG, respectively. These local reflex gains render the limb underdamped in the region of stable posture, which is the case during rhythmic movements (Bennett et al. 1992).

Coupling the limb to the PD-type CPG

For stable periodic solutions of the total limb model (see Fig. 1), the loop gain per definition equals one and the phase between the input and output of the block *Central Pattern Generator* equals the phase between the output and input of the block *Limb Dynamics*. Therefore, the afferent and efferent coupling between limb and CPG is chosen in such a way that the gain plot of the inverse transfer function of the limb crosses one of the Bode plots of the CPG; this ensures stable rhythmic movement as explained thoroughly in Ch. 3 (Verdaasdonk et al. 2006). Afferent feedback to the half-center model of the PD-type CPG consists of delayed muscle lengths and muscle velocities with gains g_p=800 and g_d=60 respectively. The ratio between g_p and g_d is chosen in such a way that afferent feedback of muscle velocity to the CPG compensates the phase lag, caused by time delay τ_c=50 ms in the loop which couples limb to CPG. The outputs of the half-center model excite the muscles via efferent gain k_e=0.01 (see Fig. 1 and App. A).
In Fig. 3 the black solid line shows the branch of stable periodic solutions for the limb coupled to the PD-type CPG. The frequency of the entrained rhythmic movement ω_e is shown for different positional feedback gains k_p of the local reflex loop. To ascertain the resonance tuning capabilities of the PD-type CPG, the resonance frequency of the limb dynamics has to be determined and compared with the entrained frequency ω_e. The gray dashed line in Fig. 3 shows the imaginary part of the rightmost eigenvalues $\boldsymbol{\lambda}_{rm}$ of the limb dynamics, which was analytically derived. This method of linearization was carried out for a similar model in Ch. 2 (Verdaasdonk et al. 2004) and is not repeated here. The imaginary part of the rightmost eigenvalues $\boldsymbol{\lambda}_{rm}$ represent the limb's resonance frequency up to the Hopf bifurcation at k_p=6.05, beyond which the limb becomes linearly unstable (i.e. eigenvalues lie in right half plane). At first, the PD-type CPG appeared to be bad at tuning into the limb's resonance frequency, especially at high positional feedback gains k_p. However, after close examination of the limb dynamics, it became evident that the limb's resonance frequency ω_{res} is

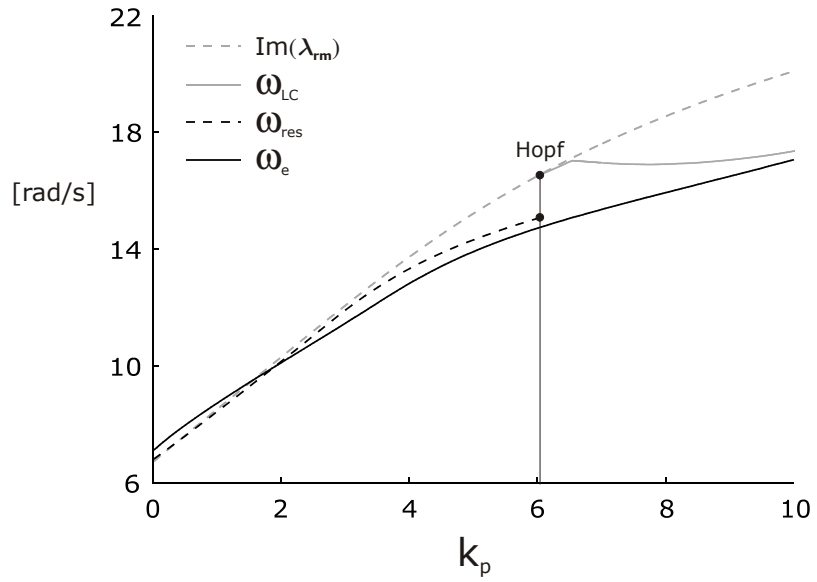

Fig. 3 Resonance tuning in the neuro-musculo-skeletal model of the forearm coupled to the PD-type CPG. The *black solid line* represents the entrained movement frequency ω_e at different positional feedback gains k_p of the local reflex loop (the velocity feedback gain $k_v=k_p/10$, see Fig. 2). The *black dashed line* shows the resonance frequency ω_{res} of the forearm (i.e. without CPG), obtained by linearizing the limb dynamics at input amplitudes associated with the entrained periodic movement at the accompanying positional feedback gain k_p. The Hopf bifurcation represents the reflex gains at which the local reflex loop becomes unstable and for higher gains limit cycles emerge (*gray solid line*). The *gray dashed line* shows the resonance frequency of the limb dynamics (i.e. the imaginary part of the rightmost eigenvalues $\boldsymbol{\lambda}_{rm}$), obtained by analytical linearization of the limb dynamics, which is only valid for very small input amplitudes. For reflex gains beyond the Hopf point, the eigenvalues lie in the right half plane.

highly dependent on the amplitude of the periodic limb movement; this is mainly due to the time delay τ_l in the local reflex loop. Therefore, a linearization of the limb dynamics was performed for input amplitudes, which are experienced during the entrained periodic limb movements. A Bode plot of the input–output relation is constructed in a similar way as it was done for the CPG in Ch. 3 (Verdaasdonk et al. 2006). The inputs of the limb dynamics in the coupled system are the alternating outputs of the CPG ($u_{CPG,B}=k_e y_B$ and $u_{CPG,T}=k_e y_T$, see Fig. 1 and app. A). These inputs resemble the halves of a sinusoidal wave. Therefore, the input in the linearization is a single sinusoidal input where the positive halves of the sinusoid are fed to the flexor muscle, while the absolute value of negative halves are fed to the extensor muscle. The output in the linearization is the length of the flexor muscle $\Delta l_{mus,B}$

relative to its rest length. Feeding the negative halves of the input sinusoid to the flexor muscle and the positive halves to the extensor muscle, while taking the extensor muscle lengthening $\Delta l_{mus,T}$ as output gives the same result. The amplitude of the sinusoidal input is chosen such that the gain between the single frequency Fourier transformations of the input during linearization and the CPG output during entrained movement (i.e. $k_e y_B$ minus $k_e y_T$) at the entrained frequency ω_e equals unity. For each positional feedback gain k_p the input amplitude is determined in this way and a Bode plot (i.e. magnitude and phase plots) is constructed for input frequencies of 1.0 up to and including 20.0 rad/s. Subsequently, the resonance frequency of the limb ω_{res} is determined by a bisection method, which converges to the frequency at which the peak amplitude of the magnitude occurs. The resonance frequency of the limb ω_{res} at different positional feedback gains k_p is shown in Fig. 3 by the dashed black line. As mentioned before, at a positional feedback gain k_p of 6.05 a Hopf bifurcation is encountered. Beyond this gain linearization with this method is not possible, because the limb dynamics possess a stable limit cycle in this region of parameter space (see Fig. 2). Although the analytical linearization is only valid for small input values, the imaginary part of its rightmost eigenvalues $\boldsymbol{\lambda}_{rm}$ almost equal ω_{res} for low k_p. This corresponds to the fact that the time delay τ_l is the main cause of the amplitude dependent resonance frequency of the limb; a higher k_p means a larger influence of the time delay.

Comparison between the entrained frequency ω_e (black solid line) and the resonance frequency of the limb dynamics ω_{res} (black dashed line) shows that the PD-type CPG actually tunes in close to the limb's resonance frequency. At low positional feedback gains k_p – and thus at low ω_{res} – the phase lead of the CPG is larger than that of the inverse transfer function of the limb and the entrained movement has a frequency ω_e higher than ω_{res} (Ch. 3; Verdaasdonk et al. 2006). At higher k_p the entrained frequency ω_e is lower than the resonance frequency ω_{res}. This is due to the time delay τ_l in the local reflex loop, which increases the phase lag of the limb (i.e. the phase lead of the inverse transfer function of the limb). The influence of the time delay increases with k_p.
The CPG is able to entrain to the limb dynamics, even when the limb is linearly unstable and possesses a stable limit cycle on its own. Beyond the Hopf bifurcation, that is for k_p>6.05 (Figs. 2 and 3), the forearm moves periodically, even *without* being coupled to the CPG. The frequency of this periodic movement is shown by the gray solid line in Fig. 3. Just beyond the Hopf bifurcation, the amplitude is very small and its frequency is close to that of the imaginary part of its rightmost eigenvalues $\boldsymbol{\lambda}_{rm}$. For increasing reflex gains, the amplitude grows towards the amplitude of the entrained periodic movement of the forearm *with* CPG and the frequency decreases towards the frequency of the entrained periodic movement. This indicates that the CPG even entrains to the linearly unstable limb in an energy efficient way.

However, for the unstable limb (i.e. beyond the Hopf bifurcation) the minimum amplitude of any entrained periodic limb movement is determined by the limit cycle of the limb dynamics. It is therefore unlikely that these periodic solutions are realistic. Hence, it can be concluded that the maximal frequency of the entrained arm movement is the frequency just before the Hopf bifurcation. For the simulation results shown in Fig. 3 – belonging to a co-contraction of 0.01 – this maximum adoptable frequency is about 2.4 Hz. Higher frequencies are possible by increasing the co-contraction of the antagonistic muscle pair. Co-contractions of 0.05, 0.1 and 0.2 give maximum frequencies of respectively 3.1, 3.6 and 4.1 Hz. Higher co-contractions give even higher maximum movement frequencies. As co-contraction is energy consuming, it seems logical that it is used only up to the level necessary to achieve the frequency of the entrained movement. This idea agrees with studies of rhythmic forearm movements, which have shown that co-contraction increases with movement frequency (Feldman 1980; Pailhous et al. 1996).

Coupling the limb to the PID-type CPG

The difference between the PID-type and PD-type CPG is that the former also has an internal process that integrates the afferent input of muscle lengthening. The entrained frequency ω_e of the limb coupled to the PID-type CPG is shown in Fig. 4 by the black solid line. At low positional feedback gains k_p the PID-type CPG, unlike the PD-type CPG (gray solid line), is able to tune into the resonance frequency of the limb ω_{res} (dashed black and gray lines). However, at medium gains k_p the resonance tuning behavior of the PID-type CPG is worse compared to the PD-type, because the integrative action undoes part of the compensatory action of the velocity feedback to the CPG, necessary to cope with the nonlinear characteristics of the forearm (especially the muscle dynamics and the time delay in the local reflex loop). An explanation of this worse behavior together with a solution by phase compensation is stated in App. B and discussed in Sect. 4.1. At high k_p the PID-type CPG behaves the same as the PD-type, because integral feedback to the half-center model has no significant influence at high movement frequencies. Note that the resonance frequency of the limb in case of coupling to the PD-type CPG and PID-type CPG are almost equal for given reflex gains (compare black with gray dashed line), because the entrained amplitude is similar in both cases.

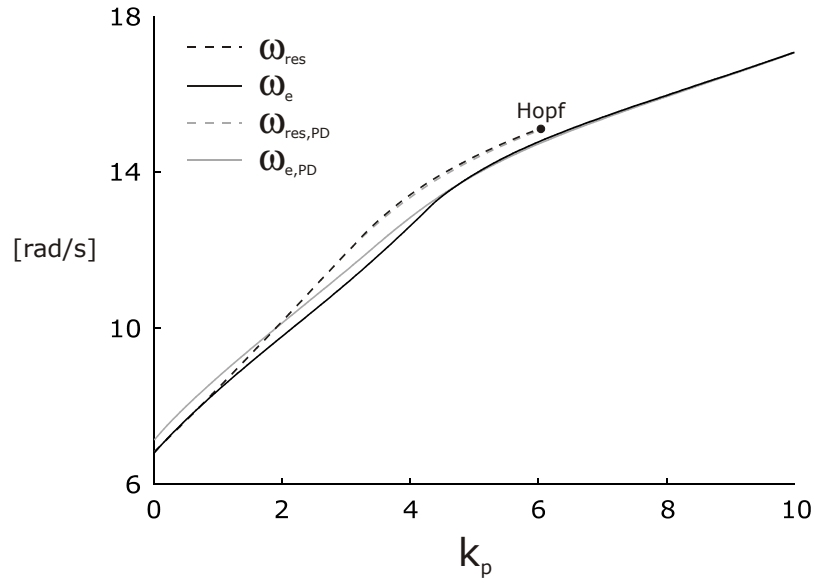

Fig. 4 Resonance tuning in the neuro-musculo-skeletal model of the forearm coupled to the PID-type CPG. The *black solid line* represents the entrained movement frequency ω_e at different positional feedback gains k_p of the local reflex loop. The *black dashed line* shows the resonance frequency ω_{res} of the forearm (i.e. without CPG), obtained by linearizing the limb dynamics at input amplitudes associated with the entrained periodic movement. For comparison with the PD-type CPG, the entrained movement frequencies and resonance frequencies of Fig. 3 are redrawn in *gray solid* ($\omega_{e,PD}$) and *dashed lines* ($\omega_{res,PD}$), respectively.

3.2 Resonance tuning for the forearm in upright position

Resonance tuning of the forearm by the CPG is not only possible in hanging position, but in fact around every posture. However, robustness against force perturbations becomes more of a challenge in these cases. In this subsection the forearm is put in upright position for two reasons. The first is to determine if the PID-type CPG is able to tune into natural limb frequencies below the CPG's endogenous frequency. This could not be assessed from simulations in the hanging forearm (Sect. 3.1), because gravity provides a minimum resonance frequency far above the endogenous frequency of the CPG (see Figs. 3 and 4). The second reason is to determine the robustness against force perturbations. It is a bit trivial to do this in case of a hanging forearm, because in that case gravity helps to stabilize the movement. For the upright forearm, gravity acts as a destabilizing force. This way, the

robustness of the coupled system can be determined as well as to which extent the local reflex loop and the CPG help in stabilizing the movement.

Figure 5 shows a fold and Hopf branch in the parameter space spanned by local reflex gains k_p and k_v of the musculo-skeletal model of the upright forearm (i.e. without CPG). The vertical fold line represents the minimal positional feedback gain $k_{p,min}$ of 1.54 necessary to obtain stable posture; it compensates for the negative gravitational stiffness (i.e. negative stiffness due to the gravitational forces). Velocity feedback is also necessary for most positional feedback gains k_p. The fold and Hopf branches divide the parameter space into three regions: unstable, stable posture and stable limit cycles. For more information on fold and Hopf bifurcations in musculo-skeletal systems, see Ch. 2 (Verdaasdonk et al. 2004). Entrainment of the limb by the CPG is only possible when the posture of the limb is stable, thus for positional feedback gains $k_p > k_{p,min}$. For all the simulations in the remainder of this subsection, the velocity feedback gain k_v is defined by the dashed line

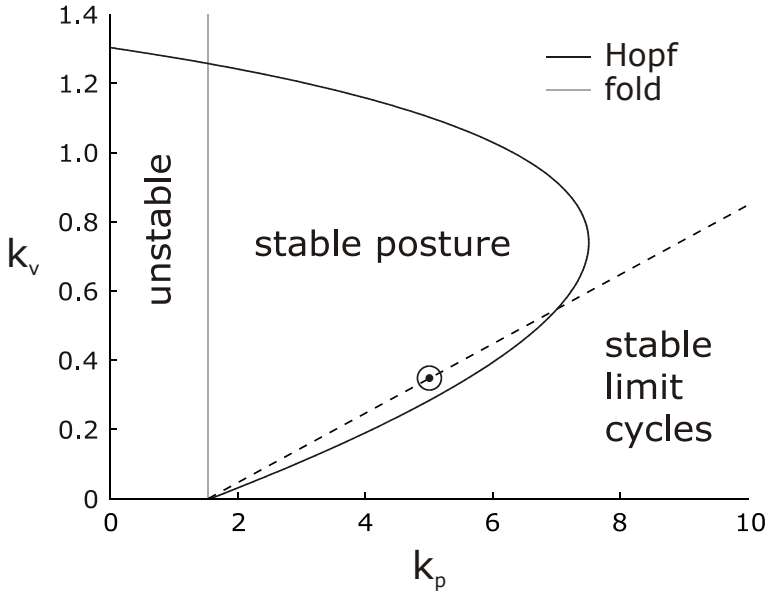

Fig. 5 Branches of Hopf (*black solid line*) and fold (*gray solid line*) bifurcations divide the parameter space into areas of stable posture, unstable posture and stable limit cycles for the forearm, which is modeled as *inverse* pendulum with muscles. The parameters are the positional feedback gain k_p and the velocity feedback gain k_v of the local reflex loop. The *dashed line* ($k_v=(k_p-1.54)/10$) shows for which local reflex parameters the musculo-skeletal model of the forearm is coupled to the PID-type CPG. The *marked point* ($k_p=5.0$) is used for time simulation in Fig. 6.

$k_v=(k_p-k_{p,min})/10$, which renders the limb underdamped (as for hanging pendulum, Sect. 3.1).

Besides the upright posture of the forearm, all the parameters of the model are the same as in Sect. 3.1, except for the efferent gain k_e. There is *not* one efferent gain k_e for which the coupled system is stable for all considered gains k_p. The maximal range of gains k_p, for which the coupled system is stable for a single k_e, is from 3.0 up till and including 10.0 and occurs for an efferent gain k_e of $2.5\cdot10^{-3}$. This range corresponds to entrained movement frequencies of 3.58 up till 13.85 rad/s. For lower k_p the efferent gain k_e has to be lowered as well for the following reason. The total joint stiffness of the elbow (i.e. negative gravitational stiffness plus intrinsic and reflexive joint stiffness) goes to zero when k_p approaches $k_{p,min}$, i.e. the fold bifurcation (Ch. 2; Verdaasdonk et al. 2004). This decreases the gain of the inverse transfer function of the limb dynamics tremendously. Therefore, the efferent gain k_e has to be decreased to make sure the gain plot of the inverse transfer function of the limb crosses one of the gain plots of the CPG (Sect. 3.1). For the results discussed in the remainder of this section the efferent gain k_e was chosen in such a way that the periodic limb movement has angular amplitude of 0.1 rad.

To determine if the PID-type CPG is able to tune into resonance frequencies below its endogenous frequency, the CPG is coupled to the limb with a positional feedback gain k_p of 1.6 (i.e. very close to the fold bifurcation). This gives a resonance frequency of the limb ω_{res} of 1.20 rad/s (determined in the same way as in Sect. 3.1). The entrained frequency ω_e of 1.28 rad/s is close to the resonance frequency ω_{res}: the PID-type CPG is indeed able to tune into resonance frequencies of the limb below its endogenous frequency of 2.33 rad/s. It is noted that a very small efferent gain k_e of $4.17\cdot10^{-5}$ is necessary to obtain this stable periodic solution. Without the CPG's internal integration process, i.e. for the PD-type CPG, the entrained frequency ω_e is 2.14 rad/s and *not* close to the resonance frequency ω_{res} of 1.20 rad/s. Instead, it is close to the endogenous frequency of 2.33 rad/s. In other words, feedback of the integrated muscle lengthening to the half-center model is necessary for resonance tuning below the endogenous frequency of the CPG. The PID-type CPG also tunes into the limb's resonance frequency for other positional gains k_p. For example, for a k_p of 5.0, the resonance frequency ω_{res} is 8.64 rad/s and the entrained frequency ω_e is 8.45 rad/s.

The neuro-musculo-skeletal model of the forearm in upright position is subjected to perturbations to assess its robustness. Perturbations were applied during the flexion phase by exerting a constant external flexion moment M_p between a limb angle θ of -0.05 and 0.05 rad; a positive angle θ means flexion of the arm. In Fig. 6 three perturbations with increasing intensity are subjected to the limb with a local reflex gain k_p of 5.0. Perturbation moments M_p of 10, 20 and 40 Nm are exerted, corresponding

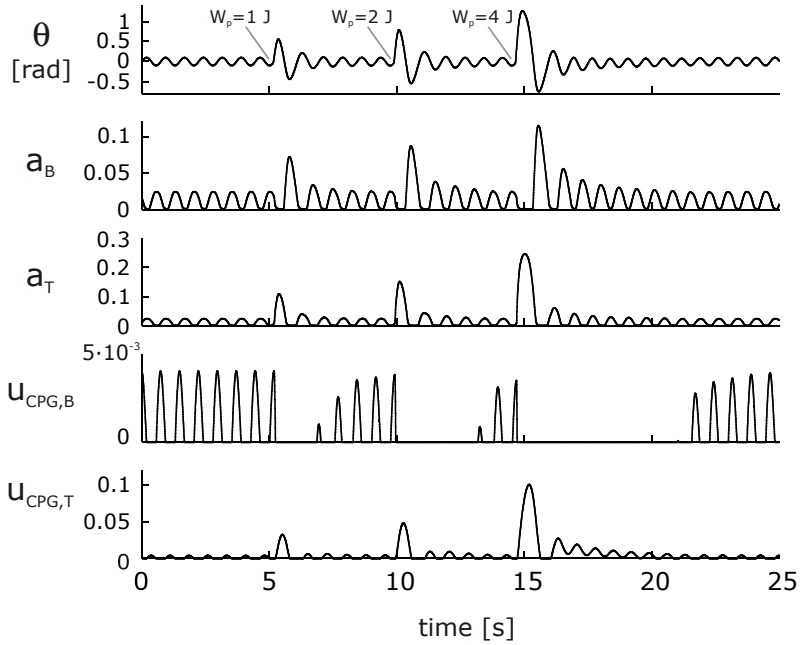

Fig. 6 Force perturbations during periodic movement of the neuro-musculo-skeletal model of the forearm in upright position with local reflex gains $[k_p\ k_v]^T = [5.0\ 0.35]^T$. On the horizontal axis the time is displayed and on the vertical axis from top to bottom: the limb angle θ relative to the vertical (positive for flexion), the muscle activation of the Brachialis a_B (flexor) and the Triceps Brachii a_T (extensor), and the neural inputs $u_{CPG,B}$ and $u_{CPG,T}$ from the CPG to the muscles. Three perturbations were applied with energy content W_p of 1.0, 2.0 and 4.0 J, respectively. These perturbations were applied between an angle θ of -0.05 and 0.05 rad by exerting an external flexion moment M_p of 10, 20 and 40 Nm, respectively.

with energy contents W_p of 1.0, 2.0 and 4.0 J, respectively; they are indicated in the top graph. On the horizontal axis the time is displayed and on the vertical axis from top to bottom: the limb angle θ relative to the vertical, the muscle activation of the flexor (i.e. Brachialis) a_B and the extensor (i.e. Triceps Brachii) a_T, and the neural inputs $u_{CPG,B}$ and $u_{CPG,T}$ from the CPG to the muscles (beware of difference in scale). A striking result is that only very low muscle activation is necessary to sustain steady-state periodic movement (2.4% of maximal activation).

The figure shows that immediately after the onset of the perturbation (in fact time delay τ_l after the onset), the extensor muscle is highly activated to oppose the perturbation. Part of this muscle activation originates from the extensor center of the CPG, namely the neural input $u_{CPG,T}$. A small part is due to the tonic activation of the muscles (0.01) and the rest originates from

the local reflex loop. For perturbations with higher intensity, the CPG delivers a larger part of the total muscle activation used to return to the limit cycle of the entrained periodic movement. The CPG delivers a part of 29.8, 31.8 and 41.0% of the maximal activation of the extensor muscle for perturbations of 1.0, 2.0 and 4.0 J, respectively (Fig. 6). The CPG has no part in the peak of the flexor muscle activation that follows half a period after the perturbation. Moreover, the flexor center of the CPG has *no* output at that time.
After perturbation, it takes about four cycles to return to the limit cycle of the periodic movement, except for sub-maximal perturbations (the last one in Fig. 6). The maximal perturbation the neuro-musculo-skeletal model can handle during periodic movements depends on the gain k_p of the local reflexive feedback of muscle length. The maximal perturbations were calculated for the following vector of feedback gains $\mathbf{k_p}$ = [1.6 2.0 3.0 4.0 5.0 6.0 8.0 10.0]^T. The accompanying vector of maximum perturbations is $\mathbf{W_p}$ = [$6.6\cdot10^{-4}$ $3.4\cdot10^{-2}$ 0.9 2.5 4.3 6.1 9.3 12.0]^T in Joule. Thus, the maximum perturbation the forearm can handle is very small for low reflexive feedback gains k_p and very large for high k_p. For low k_p the destabilizing force of gravity is initially high relative to the restoring force of the compliant limb (i.e. low joint stiffness of the elbow). This results in a large angular displacement from which the forearm cannot recover. For high k_p the opposite is true.

4. Discussion

4.1 Neuro-musculo-skeletal model

Structure and embedding of the central pattern generator

Information of the structure of the CPG and its embedding in the central nervous system mainly comes from cat and rat studies and can partly be extrapolated to humans (Duysens et al. 2000; Duysens and Van de Crommert 1998), but to which extent is uncertain (Capaday 2002). A large difference between locomotion in cats and humans is that cats have quadrupedal gaits, while humans have bipedal gaits. Therefore, humans depend more on their vestibular and visual system for keeping their balance. Dietz (2002) proposed that quadrupedal coordination is still used by humans in locomotion, but that a task dependent switch to direct cortical-motoneuronal control allows for skilled hand movements. Hence, we believe humans use the evolutionarily old system of coupled CPGs for 'automated' rhythmic tasks, such as locomotion and arm swinging.

The CPGs are embedded in the central nervous system in a complex and flexible way (Barbeau et al. 1999; Burke 2001; Burke et al. 2001; Rossignol et al. 2002; Whelan 1996). Inputs to the CPG originate among others from muscle afferents and supra-spinal centers. Moreover, various neurotransmitters can change CPG activity. The CPG outputs to a complex network of interneurons, which finally converges onto the motoneurons. This pre-motor network also receives information from supra-spinal centers and muscle afferents and is fed back to the CPG. Hence, it would be an illusion to think that an exact hard-wired model could be discovered for the CPG and its organization within the central nervous system. The wiring is probably dependent on the task at hand. Even for a predefined task, such as 'unperturbed' walking, there is still too little information on the structure of the CPG and its wiring to develop a detailed model. For this reason and for the reason of clarity, the neuro-musculo-skeletal model presented in this paper is descriptive in nature (i.e. lumped muscle models, groups of neurons are lumped into half-centers, simple reflex model), but incorporates enough of the essential dynamics to explain behavior – such as resonance tuning – in a qualitative way. Moreover, integration processes and phase compensation (see App. B) might be performed by one of the above-mentioned polysynaptic pathways, but there is no direct evidence of such feedback yet. Phase dependent modulation of reflexes (Brooke et al. 1997; Zehr et al. 2003) has not been taken into account in the present model. However, muscle dynamics (force-length and force-velocity relationships), which play a critical role in the functional significance of the stretch reflex during rhythmic movement (Kearney et al. 1999), *have* been taken into account.

Integral feedback of muscle length information

The influence of integral feedback of muscle length information on resonance tuning is seen by comparing the simulations with the PID-type CPG to those with the PD-type CPG. These are shown in Fig. 4 and the differences are explained in App. B. For low resonance frequencies of the limb, the PID-type CPG is better than the PD-type CPG at resonance tuning. For medium frequencies it is vice versa and for high frequencies the resonance tuning behavior of the two CPG types is the same. It would seem that a price has to be paid to be able to tune into resonance frequencies below the endogenous frequency of the CPG, namely a poor performance at mid-frequencies. However, there are two possible solutions to circumvent this deficiency. The first is simply to use integral feedback only when the movement frequency is below the endogenous frequency of the CPG. In the simulations performed in this study all the feedback gains were kept constant to show the adaptability of the model to a broad range of resonance frequencies of the limb. In humans, these gains could and probably are dynamically changed as circumstances require. For example, integral feedback could be modulated by pre-synaptic inhibition. The second solution is phase compensation. Theoretically, it is possible to obtain perfect resonance tuning when the extra phase lag induced by the time-delayed local reflex is compensated by additional feedback dynamics (see App. B). In humans this phase matching of limb to CPG might be learned by or imprinted in the neural pathways (e.g. spinal interneurons) in the loop coupling CPG to limb, or in the CPG itself. Whether such phase compensation is plausible with respect to resonance tuning in humans is not known at this time.

Local reflex gains and robustness

We considered the local reflex gains in this study of rhythmic arm movements to be linear and constant during the cycle. Consequently, the robustness against perturbations is very small in case the upright forearm is entrained to low resonance frequencies of the limb (Sect. 3.2), which does not seem very realistic. Non-linear reflex gains – being larger when further away from the cycle – could improve the robustness as well as the speed of recovery, while leaving the limit cycle of the rhythmic movement – and thus the corresponding energy efficiency – intact.

Difference in CPG model with respect to previous study

The major difference between the CPG model in this chapter and the one in Ch. 3 is that for this CPG model afferent feedback can *excite* and *inhibit* the flexor and extensor center of the half-center model, while for the CPG model of Ch. 3 the centers could only be inhibited. The latter has more robustness against variations in limb parameters compared to the former (i.e. larger spread in gain plots), while the former has more robustness against external force perturbations. This higher robustness against force perturbations is

achieved, because the CPG is only able to participate in counteracting perturbations when it receives excitatory afferent input. It delivers an increasing part of the necessary muscle activation for increasing perturbation size (see Fig. 6).

4.2 Rhythmic movement below resonance frequency of the limb

In the hanging forearm the minimal resonance frequency is determined by gravity (about 6.8 rad/s, depending on inertia of arm). Abe (2003) has shown that for rhythmic arm movements with frequencies below the minimal resonance frequency, the joint stiffness hardly changes; it even increases a little for decreasing frequency. He had no explanation for this behavior. It is important to note that Abe and Yamada calculated joint stiffness by fitting the deviations from the nominal movement cycle – caused by applying perturbations – on a mass-spring damper model with separate gravity component. In other words, their definition of joint stiffness excludes gravity, but includes other components – besides intrinsic and reflexive ones – such as the influence of a CPG. Hence, a possible explanation of the observed behavior is that for movement frequencies below the minimal resonance frequency, 'feed-forward' signals from supra-spinal centers input to the CPG, while leaving the feedback loop with the muscles afferents intact to provide good stability properties (e.g. robustness against perturbations and speed of recovery). We applied this idea to our neuro-musculo-skeletal model. As long as the feed-forward input dominates the afferent feedback of the muscles in amplitude, the CPG could indeed be entrained to feed-forward input with frequencies below the minimal resonance frequency of the limb. Furthermore, the maximal displacement after perturbation was smaller compared to the case of no afferent feedback from the muscles to the CPG, which represents a higher joint stiffness according to Abe and Yamada's definition of joint stiffness. This indicates that 'feed-forward' input to the CPG – while keeping the loop coupling limb to CPG intact – might indeed play an important role in the observed behavior that the joint stiffness (i.e. Abe and Yamada's definition) slightly increases with decreasing frequency below the minimal resonance frequency of the limb.

4.3 Conclusion

This study has discussed resonance tuning in the hanging and upright forearm. It was shown that resonance tuning is possible above, at and below the endogenous frequency of the CPG in a highly non-linear neuro-musculo-skeletal model. Resonance tuning is achieved above the endogenous frequency by afferent feedback of muscle lengthening and velocity to the CPG, in which the latter is necessary for compensation of the time delay

present in the loop. This feedback represents the convergence of Ia and II fibers onto the CPG. Resonance tuning at and below the endogenous frequency is accomplished by integrating the delayed muscle lengthening, after which it is fed to the half-center model; this is assumed to be an internal process of the CPG. Increased co-contraction will allow for higher maximum movement frequency, which is in agreement with studies of rhythmic forearm movements that show increased co-contraction as the movement frequency becomes higher. Excitatory afferent input enables the CPG to actively counteract force perturbations. It delivers an increasing part of the necessary muscle activation for increasing perturbation size; the other part originates mainly from the local reflex loop. As far as we know, the proposed neuro-musculo-skeletal model is the first that is able to explain the observed resonance tuning in human rhythmic limb movement, such as arm swinging.

References

Abe MO, Yamada N (2003) Modulation of elbow joint stiffness in a vertical plane during cyclic movement at lower or higher frequencies than natural frequency. Exp Brain Res 153:394-399

Amemiya M, Yamaguchi T (1984) Fictive locomotion of the forelimb evoked by stimulation of the mesencephalic locomotor region in the decerebrate cat. Neurosci Lett 50:91-96.

Baev KV, Esipenko VB, Shimansky YP (1991) Afferent control of central pattern generators: experimental analysis of scratching in the decerebrate cat. Neuroscience 40:239-256

Barbeau H, McCrea DA, O'Donovan MJ, Rossignol S, Grill WM, Lemay MA (1999) Tapping into spinal circuits to restore motor function. Brain Res Brain Res Rev 30:27-51

Barthe JY, Clarac F (1997) Modulation of the spinal network for locomotion by substance P in the neonatal rat. Exp Brain Res 115:485-492

Bennett DJ, Hollerbach JM, Xu Y, Hunter IW (1992) Time-varying stiffness of human elbow joint during cyclic voluntary movement. Exp Brain Res 88:433-442

Brooke JD, Cheng J, Collins DF, McIlroy WE, Misiaszek JE, Staines WR (1997) Sensori-sensory afferent conditioning with leg movement: gain control in spinal reflex and ascending paths. Prog Neurobiol 51:393-421

Brown TG (1911) The intrinsic factors in the act of progression in the mammal. In: Proc Royal Soc. Vol. B84, London, pp 308-319

Burke RE (2001) The central pattern generator for locomotion in mammals. Adv Neurol 87:11-24

Burke RE, Degtyarenko AM, Simon ES (2001) Patterns of locomotor drive to motoneurons and last-order interneurons: clues to the structure of the CPG. J Neurophysiol 86:447-462

Butt SJ, Lebret JM, Kiehn O (2002) Organization of left-right coordination in the mammalian locomotor network. Brain Res Brain Res Rev 40:107-117

Cannon SC, Zahalak GI (1982) The mechanical behavior of active human skeletal muscle in small oscillations. J Biomech 15:111-121

Capaday C (2002) The special nature of human walking and its neural control. Trends Neurosci 25:370-376

Carroll TJ, Baldwin ER, Collins DF, Zehr EP (2006) Corticospinal excitability is lower during rhythmic arm movement than during tonic contraction. J Neurophysiol 95:914-921

Cazalets JR, Borde M, Clarac F (1995) Localization and organization of the central pattern generator for hindlimb locomotion in newborn rat. J Neurosci 15:4943-4951

Cohen AH, Wallen P (1980) The neuronal correlate of locomotion in fish. "Fictive swimming" induced in an in vitro preparation of the lamprey spinal cord. Exp Brain Res 41:11-18

Dietz V (2002) Do human bipeds use quadrupedal coordination? Trends Neurosci 25:462-467

Dimitrijevic MR, Gerasimenko Y, Pinter MM (1998) Evidence for a spinal central pattern generator in humans. Ann N Y Acad Sci 860:360-376.

Duysens J, Clarac F, Cruse H (2000) Load-regulating mechanisms in gait and posture: comparative aspects. Physiol Rev 80:83-133.

Duysens J, Van de Crommert HW (1998) Neural control of locomotion; The central pattern generator from cats to humans. Gait Posture 7:131-141.
Engelborghs K, Luzyanina T, Samaey G (2001) DDE-BIFTOOL v. 2.00: a Matlab package for bifurcation analysis of delay differential equations. Technical Report TW-330, Department of Computer Science, K.U. Leuven, Leuven
Feldman AG (1980) Superposition of motor programs--I. Rhythmic forearm movements in man. Neuroscience 5:81-90
Friesen WO (1994) Reciprocal inhibition: a mechanism underlying oscillatory animal movements. Neurosci Biobehav Rev 18:547-553
Grillner S, McClellan A, Perret C (1981) Entrainment of the spinal pattern generators for swimming by mechano- sensitive elements in the lamprey spinal cord in vitro. Brain Res 217:380-386.
Hatsopoulos NG, Warren Jr WH (1996) Resonance tuning in rhythmic arm movements. J Mot Behav 28:3-14
Hayes KC, Hatze H (1977) Passive visco-elastic properties of the structures spanning the human elbow joint. Eur J Appl Physiol Occup Physiol 37:265-274
Kearney RE, Lortie M, Stein RB (1999) Modulation of stretch reflexes during imposed walking movements of the human ankle. J Neurophysiol 81:2893-2902.
Kugler PN, Turvey MT (1987) Information, Natural law, and the self-assembly of rhythmic movement. In. Lawrence Erlbaum, Hillsdale, NJ, pp 481
Latash ML (1992) Virtual trajectories, joint stiffness, and changes in the limb natural frequency during single-joint oscillatory movements. Neuroscience 49:209-220
MacKay-Lyons M (2002) Central pattern generation of locomotion: a review of the evidence. Phys Ther 82:69-83.
Marchetti C, Beato M, Nistri A (2001) Alternating rhythmic activity induced by dorsal root stimulation in the neonatal rat spinal cord in vitro. J Physiol 530:105-112
Matsuoka K (1985) Sustained oscillations generated by mutually inhibiting neurons with adaptation. Biol Cybern 52:367-376
Matsuoka K (1987) Mechanisms of frequency and pattern control in the neural rhythm generators. Biol Cybern 56:345-353
McCrea DA (2001) Spinal circuitry of sensorimotor control of locomotion. J Physiol 533:41-50
Nakamura Y, Katakura N, Nakajima M (1999) Generation of rhythmical ingestive activities of the trigeminal, facial, and hypoglossal motoneurons in in vitro CNS preparations isolated from rats and mice. J Med Dent Sci 46:63-73
Pailhous J, Bonnard M, Coyle T (1996) Autonomy versus forcing in the organization of human rhythmic forearm movements. C R Acad Sci III 319:773-777
Perreault EJ, Crago PE, Kirsch RF (2000) Estimation of intrinsic and reflex contributions to muscle dynamics: a modeling study. IEEE Trans Biomed Eng 47:1413-1421
Rossignol S, Bouyer L, Barthelemy D, Langlet C, Leblond H (2002) Recovery of locomotion in the cat following spinal cord lesions. Brain Res Brain Res Rev 40:257-266
Schaal S, Sternad D, Osu R, Kawato M (2004) Rhythmic arm movement is not discrete. Nat Neurosci 7:1136-1143
Shik ML, Severin FV, Orlovskii GN (1966) Control of walking and running by means of electrical stimulation of the mid-brain. Biophysics 11:756-765
Sqalli-Houssaini Y, Cazalets JR, Clarac F (1993) Oscillatory properties of the central pattern generator for locomotion in neonatal rats. J Neurophysiol 70:803-813
Taylor BE, Lukowiak K (2000) The respiratory central pattern generator of Lymnaea: a model, measured and malleable. Respir Physiol 122:197-207

Van de Crommert HW, Mulder T, Duysens J (1998) Neural control of locomotion: sensory control of the central pattern generator and its relation to treadmill training. Gait Posture 7:251-263.

Verdaasdonk BW, Koopman HF, Helm FC (2006) Energy efficient and robust rhythmic limb movement by central pattern generators. Neural Netw 19:388-400

Verdaasdonk BW, Koopman HF, Van Gils SA, Van Der Helm FC (2004) Bifurcation and stability analysis in musculoskeletal systems: a study in human stance. In: Biol Cybern. Vol. 91, pp 48-62

Whelan PJ (1996) Control of locomotion in the decerebrate cat. Prog Neurobiol 49:481-515

Winters JM, Stark L (1985) Analysis of fundamental human movement patterns through the use of in- depth antagonistic muscle models. IEEE Trans Biomed Eng 32:826-839.

Winters JM, Stark L (1987) Muscle models: what is gained and what is lost by varying model complexity. Biol Cybern 55:403-420

Winters JM, Stark L (1988) Estimated mechanical properties of synergistic muscles involved in movements of a variety of human joints. J Biomech 21:1027-1041

Zehr EP, Chua R (2000) Modulation of human cutaneous reflexes during rhythmic cyclical arm movement. Exp Brain Res 135:241-250

Zehr EP, Collins DF, Frigon A, Hoogenboom N (2003) Neural control of rhythmic human arm movement: phase dependence and task modulation of hoffmann reflexes in forearm muscles. J Neurophysiol 89:12-21

Zehr EP, Kido A (2001) Neural control of rhythmic, cyclical human arm movement: task dependency, nerve specificity and phase modulation of cutaneous reflexes. J Physiol 537:1033-1045

Zhang LQ, Rymer WZ (1997) Simultaneous and nonlinear identification of mechanical and reflex properties of human elbow joint muscles. IEEE Trans Biomed Eng 44:1192-1209

Appendix A. Neuro-musculo-skeletal model

The neuro-musculo-skeletal model of the forearm consists of a pendulum with an antagonistic muscle pair; the local reflex loop and the CPG are organized in parallel. Except for the CPG, this model is similar to the musculo-skeletal model presented in Ch. 2 (Verdaasdonk et al. 2004); details of the muscle model and its intrinsic and reflexive feedback are described in that chapter.

The model contains a total of 11 state variables. The state variables associated with the flexor muscle are denoted with a 'B' of Brachialis; the state variables associated with the extensor muscle are denoted with a 'T' of Triceps Brachii. The state variables are: the activities of both muscles, a_B and a_T, the length of the CEs of both muscles (normalized on muscle rest length l_{m0}), $l_{ce,B}$ and $l_{ce,T}$, the angle θ and angular velocity ω of the forearm, the state variables of the CPG model u_B, v_B, u_T and v_T and the integrated angle θ, denoted φ. For the latter state variable φ, the integration of the angle θ is in fact performed by a leaking integrator (pole at $-1/\tau_i$, see Eq. B.11) to prevent infinite gain at zero frequency.

Stretch reflexes are modeled by delayed feedback of the length of both muscles relative to the rest lengths l_{m0}, $\Delta l_{mus,B}$ and $\Delta l_{mus,T}$, and the velocities of both muscles, $v_{mus,B}$ and $v_{mus,T}$. The lengths are locally fed back with gain k_p and the velocities with gain k_v. Feedback to the half-center model consists of delayed muscle lengths, muscle velocities and the (leaking) integral of the muscle length changes with gains g_p, g_d and g_i respectively. Note that for the PD-type CPG g_i is taken zero.

A direct relation is assumed between the muscle lengths, velocities and the integrated muscle length changes and the angle, angular velocity and integrated angle, respectively:

$$\begin{matrix} \Delta l_{mus,B} = -\theta r \\ \Delta l_{mus,T} = \theta r \end{matrix} \quad , \quad \begin{matrix} v_{mus,B} = -\omega r \\ v_{mus,T} = \omega r \end{matrix} \quad \text{and} \quad \begin{matrix} \int_{leak} \Delta l_{mus,B} = -\varphi r \\ \int_{leak} \Delta l_{mus,T} = \varphi r \end{matrix} \tag{A.1}$$

in which $\int_{leak}$ represents the leaking integral and r is the constant moment arm about the elbow.

Thus, reflexive feedback is modeled as delayed feedback of angle $\theta(t-\tau_l)$ and angular velocity $\omega(t-\tau_l)$. Feedback to the half-center model is modeled as delayed feedback of angle $\theta(t-\tau_c)$, angular velocity $\omega(t-\tau_c)$ and the integrated angle $\varphi(t-\tau_c)$. The CPG outputs $u_{CPG,B}$ and $u_{CPG,T}$ (see Sect. 2.2 for details) excite the muscle activations a_B and a_T, respectively.

The equations of motions are:

$$\dot{a}_{\mathrm{B}} = \frac{1}{\tau_{\mathrm{B}}}\left(u_{\mathrm{ss,B}} - a_{\mathrm{B}} - k_{\mathrm{p}} c_{16}\theta\left(t-\tau_{\mathrm{l}}\right) - k_{\mathrm{v}} c_{16}\omega\left(t-\tau_{\mathrm{l}}\right) + u_{\mathrm{CPG,B}}\right) \tag{A.2}$$

$$\dot{a}_{\mathrm{T}} = \frac{1}{\tau_{\mathrm{T}}}\left(u_{\mathrm{ss,T}} - a_{\mathrm{T}} + k_{\mathrm{p}} c_{16}\theta\left(t-\tau_{\mathrm{l}}\right) + k_{\mathrm{v}} c_{16}\omega\left(t-\tau_{\mathrm{l}}\right) + u_{\mathrm{CPG,T}}\right) \tag{A.3}$$

$$\dot{l}_{\mathrm{ce,B}} = \begin{cases} c_4 v_{\max,\mathrm{B}}\left(\dfrac{Fv_{\mathrm{ce,B}} - 1}{Fv_{\mathrm{ce,B}} + c_4}\right) & \text{if } Fv_{\mathrm{ce,B}} \le 1 \text{ (\textit{contracting})} \\ -c_6 v_{\max,\mathrm{B}}\left(\dfrac{Fv_{\mathrm{ce,B}} - 1}{Fv_{\mathrm{ce,B}} - c_{17}}\right) & \text{else (\textit{lengthening})} \end{cases} \tag{A.4}$$

$$\dot{l}_{\mathrm{ce,T}} = \begin{cases} c_4 v_{\max,\mathrm{T}}\left(\dfrac{Fv_{\mathrm{ce,T}} - 1}{Fv_{\mathrm{ce,T}} + c_4}\right) & \text{if } Fv_{\mathrm{ce,T}} \le 1 \text{ (\textit{contracting})} \\ -c_6 v_{\max,\mathrm{T}}\left(\dfrac{Fv_{\mathrm{ce,T}} - 1}{Fv_{\mathrm{ce,T}} - c_{17}}\right) & \text{else (\textit{lengthening})} \end{cases} \tag{A.5}$$

$$\dot{\theta} = \omega \tag{A.6}$$

$$\dot{\omega} = c_{11} M_{\mathrm{p}} + c_{12}\left(F_{\mathrm{se,B}} - F_{\mathrm{se,T}}\right) - c_{18}\omega - c_{13}\sin\theta \tag{A.7}$$

$$\begin{aligned} \dot{u}_{\mathrm{B}} = \frac{1}{\tau_{\mathrm{r}}}\big(u_0 - u_{\mathrm{B}} - \beta v_{\mathrm{B}} - w y_{\mathrm{T}} - c_{16} g_{\mathrm{p}}\theta\left(t-\tau_{\mathrm{c}}\right) \\ - c_{16} g_{\mathrm{d}}\omega\left(t-\tau_{\mathrm{c}}\right) - c_{16} g_{\mathrm{i}}\varphi\left(t-\tau_{\mathrm{c}}\right)\big) \end{aligned} \tag{A.8}$$

$$\dot{v}_{\mathrm{B}} = \frac{1}{\tau_{\mathrm{a}}}\left(y_{\mathrm{B}} - v_{\mathrm{B}}\right) \tag{A.9}$$

$$\begin{aligned} \dot{u}_{\mathrm{T}} = \frac{1}{\tau_{\mathrm{r}}}\big(u_0 - u_{\mathrm{T}} - \beta v_{\mathrm{T}} - w y_{\mathrm{B}} + c_{16} g_{\mathrm{p}}\theta\left(t-\tau_{\mathrm{c}}\right) \\ + c_{16} g_{\mathrm{d}}\omega\left(t-\tau_{\mathrm{c}}\right) + c_{16} g_{\mathrm{i}}\varphi\left(t-\tau_{\mathrm{c}}\right)\big) \end{aligned} \tag{A.10}$$

$$\dot{v}_{\mathrm{T}} = \frac{1}{\tau_{\mathrm{a}}}\left(y_{\mathrm{T}} - v_{\mathrm{T}}\right) \tag{A.11}$$

$$\dot{\varphi} = \frac{1}{\tau_{\mathrm{i}}}\left(\tau_{\mathrm{i}}\theta - \varphi\right) \tag{A.12}$$

The force-length relationships of CEs of the muscles are:

$$Fl_{\mathrm{ce,B}} = e^{-\left(c_2 l_{\mathrm{ce,B}} - c_3\right)^2} \tag{A.13}$$

$$Fl_{\mathrm{ce,T}} = e^{-\left(c_2 l_{\mathrm{ce,T}} - c_3\right)^2} \tag{A.14}$$

The force in the non-linear springs of the SEs of both muscles are:

$$F_{\mathrm{se,B}} = \min\left[c_{10} a_{\mathrm{B}} Fl_{\mathrm{ce,B}},\ c_7\left(e^{c_8\left(1 - c_1 - l_{\mathrm{ce,B}}\right) - c_9\theta} - 1\right)\right] \tag{A.15}$$

$$F_{\mathrm{se,T}} = \min\left[c_{10} a_{\mathrm{T}} Fl_{\mathrm{ce,T}},\ c_7\left(e^{c_8\left(1 - c_1 - l_{\mathrm{ce,T}}\right) - c_9\theta} - 1\right)\right] \tag{A.16}$$

The momentary values of the force-velocity relationships of the muscle, which are used to calculate the CE velocities in Eqs. A.4 and A.5, are:

$$Fv_{\mathrm{ce,B}} = \frac{F_{\mathrm{se,B}}}{c_5 a_{\mathrm{B}} Fl_{\mathrm{ce,B}}} \tag{A.17}$$

$$Fv_{\mathrm{ce,T}} = \frac{F_{\mathrm{se,T}}}{c_5 a_{\mathrm{T}} Fl_{\mathrm{ce,T}}} \tag{A.18}$$

The maximum velocities of CEs of the muscles are:

$$v_{\mathrm{max,B}} = c_{14}\left(1 - c_{15}\left(1 - a_{\mathrm{B}} Fl_{\mathrm{ce,B}}\right)\right) \tag{A.19}$$

$$v_{\mathrm{max,T}} = c_{14}\left(1 - c_{15}\left(1 - a_{\mathrm{T}} Fl_{\mathrm{ce,T}}\right)\right) \tag{A.20}$$

The activation and de-activation time constants of the muscle activation dynamics are:

$$\tau_{\mathrm{B}} = \begin{cases} \tau_{\mathrm{ac}} & \text{if } a_{\mathrm{B}} \le u_{\mathrm{B}} - k_{\mathrm{p}} c_{16}\theta\left(t - \tau_{\mathrm{i}}\right) - k_{\mathrm{v}} c_{16}\omega\left(t - \tau_{\mathrm{i}}\right) + k_{\mathrm{e}} y_{\mathrm{B}} \\ \tau_{\mathrm{da}} & \text{else} \end{cases} \tag{A.21}$$

$$\tau_{\mathrm{sol}} = \begin{cases} \tau_{\mathrm{ac}} & \text{if } a_{\mathrm{T}} \le u_{\mathrm{T}} + k_{\mathrm{p}} c_{16}\theta\left(t - \tau_{\mathrm{i}}\right) + k_{\mathrm{v}} c_{16}\omega\left(t - \tau_{\mathrm{i}}\right) + k_{\mathrm{e}} y_{\mathrm{T}} \\ \tau_{\mathrm{da}} & \text{else} \end{cases} \tag{A.22}$$

The perturbation moment M_{p} is zero for most simulations shown in this paper (except Sect. 3.2, see Fig. 6).

The outputs of the flexor and extensor centers are:

$$y_B = \max(0, u_B) \tag{A.23}$$

$$y_T = \max(0, u_T) \tag{A.24}$$

The CPG outputs equal the half-center outputs multiplied by the efferent gain k_e:

$$u_{CPG,B} = k_e y_B \tag{A.25}$$

$$u_{CPG,T} = k_e y_T \tag{A.26}$$

Boundary conditions on certain state variables and functions

$$0 < a_B \le 1 \qquad 0 < a_T \le 1$$
$$l_{ce,B} > 0 \qquad l_{ce,T} > 0 \tag{A.27}$$
$$F_{se,B} > 0 \qquad F_{se,T} > 0$$

Constants (all positive) used in the equations of motion in terms of musculo-skeletal parameters

$$c_1 = \frac{l_t}{l_{m0}} \qquad c_2 = \frac{1}{l_{cesh}}$$
$$c_3 = \frac{l_{ce0}}{l_{cesh}} \qquad c_4 = mv_{sh}$$
$$c_5 = F_{max} \qquad c_6 = mv_{sh} mv_{shl}$$
$$c_7 = \frac{F_{max}}{e^{se_{sh}} - 1} \qquad c_8 = \frac{se_{sh}}{se_{xm}}$$
$$c_9 = \frac{se_{sh} r}{l_{m0} se_{xm}} \qquad c_{10} = F_{max} mv_{ml} \tag{A.28}$$
$$c_{11} = \frac{1}{I} \qquad c_{12} = \frac{r}{I}$$
$$c_{13} = \frac{mgl_{com}}{I} \qquad c_{14} = mv_{vm}$$
$$c_{15} = mv_{er} \qquad c_{16} = r$$
$$c_{17} = (1 + mv_{sh} mv_{shl})(mv_{ml} - 1) + 1 \qquad c_{18} = \frac{B_j}{I}$$

CPG parameters

τ_i	= 9.0	s	time constant for leaking integrator (pole at $-1/\tau_i$)
τ_r	= 0.3	s	rise time constant
τ_a	= 0.6	s	adaptation time constant

β	= 2.0		strength adaptation effect
w	= 2.0		strength of reciprocal inhibition
u_0	= 1.0		tonic input to CPG from supra-spinal centers
τ_c	= $50 \cdot 10^{-3}$	s	time delay in the loop coupling limb to CPG

Musculo-skeletal parameters

m	= 2.0	kg	mass of forearm including hand
I	= 0.1	kgm^2	mass moment of inertia about elbow joint
B_j	= 0.1	Nms/rad	joint damping of the elbow
l_{com}	= 0.2	m	length between COM and elbow joint
r	= 0.025	m	moment arm about elbow
g	= 9.81	m/s^2	gravity constant
l_{m0}	= 0.245	m	rest length of muscle
l_t	= 0.18	m	tendon length
l_{ce0}	= 0.3		optimum length of CE (normalized on l_{m0})
l_{cesh}	= 0.09		shape parameter determining width of Fl_{ce}
F_{max}	= 2000	N	maximum active muscle force
mv_{er}	= 0.5		scaling parameter for maximal contraction velocity
mv_{vm}	= 3.0 l_{m0}	1/s	maximal contraction velocity of unloaded CE
mv_{sh}	= 0.36		shape parameter of curvature of Fv_{ce}
mv_{shl}	= 0.5		shape parameter for lengthening curve of Fv_{ce}
mv_{ml}	= 1.3		maximal force gain for lengthening muscles
se_{sh}	= 2.6		curvature shape parameter of exponential slope of SE
se_{xm}	= 0.047		maximal extension of SE (normalized on l_{m0})
τ_{ac}	= $7.0 \cdot 10^{-3}$	s	time-constant for increased muscle activation
τ_{da}	= $35 \cdot 10^{-3}$	s	time-constant for decreasing muscle activation
τ_l	= $50 \cdot 10^{-3}$	s	time delay in local reflex loop

These values of the musculo-skeletal parameters could not be derived from one source. That is why multiple sources were used. The parameter values l_{m0}, l_t, se_{sh}, τ_{ac} and τ_{da} are from Winters and Stark (1988). The parameter values l_{cesh}, l_{ce0}, mv_{er}, mv_{vm}, mv_{sh}, mv_{shl}, mv_{ml} and se_{xm} are estimated by the methods of Winters and Stark (1985; 1987). The parameter values of I, r and F_{max} are from Cannon and Zahalak (1982); m and l_{com} are estimated; a joint damping B_j of 0.1 Nms/rad is a plausible value (Hayes and Hatze 1977). The values found in literature for the time delay τ_l of the elbow joint's reflex loop range from 11 ms (Cannon and Zahalak 1982) to 50 ms (Perreault et al. 2000; Zhang and Rymer 1997); in this study the worse case, that is 50 ms, is chosen. The time delay τ_c in the loop coupling the limb's afferents and efferents to the CPG is chosen as 50 ms; this seems a plausible value, for this loop exists on spinal level.

Appendix B. Achieving perfect resonance tuning by phase compensation

Effect of the local reflex loop on resonance tuning

The half-center model of the CPG has a phase lead between the output and input of 180° for low frequencies and 90° for high frequencies, with the CPG's endogenous frequency ω_{CPG} as turning point. Integral feedback to the half-center model with gain $g_i=g_p\omega_{CPG}$ causes the *phase lead* of the CPG (i.e. half-center model *and* integral feedback) to be close to 90° for all frequencies. As mentioned in Sect. 3.1, entrainment occurs at that frequency for which the phase lead of the CPG equals the phase lag of the limb dynamics. Figure B.1 shows that for low resonance frequencies ω_{res} the limb acts almost as a second order mass-spring-damper model with a *phase lag* close to 90° (gray solid line, left vertical axis). The mechanical properties of the limb are dominant for low resonance frequencies, because these resonance

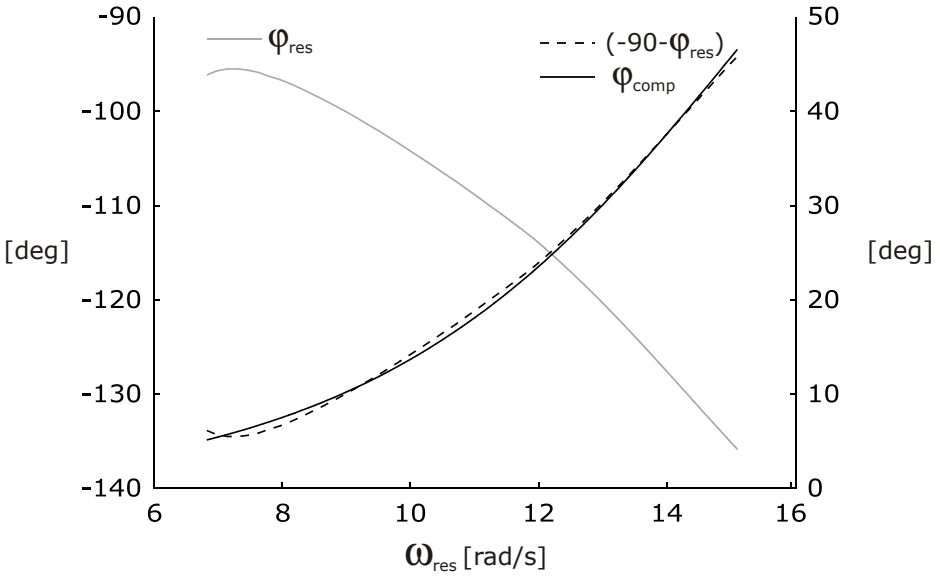

Fig. B.1 *Left axis*: Phase difference between the input and output of the forearm φ_{res} (i.e. without CPG) at the resonance frequencies ω_{res} (*gray solid line*). *Right axis*: The difference in phase between an ideal second order limb at resonance (i.e. –90°) and the phase of the forearm φ_{res} is shown by the *dashed line*. Additional afferent feedback dynamics H_{comp} approximately compensates for this difference in phase (*black solid line*).

frequencies are obtained by small local reflex gains (see Fig. 4). Therefore, the PID-type CPG achieves almost perfect resonance tuning behavior at *low movement frequencies*, unlike the PD-type CPG.

For *high movement frequencies* the dynamics of the local reflex loop become significant and the limb does not behave as a simple mechanical pendulum anymore. This is caused by the time delay in the local reflex loop together with the muscle dynamics and becomes more significant when the local reflex gains become higher, as is the case for higher resonance frequencies of the limb. This is shown by the phase difference φ_{res} of the input-output relation of the limb dynamics at its resonance frequency in Fig. B.1 (gray solid line, left vertical axis), which is far from -90° for high frequencies. At these frequencies, feedback of muscle velocity to the CPG compensates most of the extra phase lag caused by the local reflex loop. This causes the resonance tuning behavior of the CPGs to be good for both the PD-type and PID-type CPG, because the integral feedback has no influence at high movement frequencies.

At *medium movement frequencies* (i.e. medium local reflex gains) the integral feedback still brings the CPG's phase lead towards 90°, while at these frequencies the local reflex loop has already significant influence on the behavior of the limb: the limb is not acting as a second-order mass-spring-damper system with a 90° phase lag at its resonance frequency. This actually causes the resonance tuning behavior of the PID-type CPG to be worse at medium movement frequencies compared to the PD-type (see Fig. 4). In other words, at medium frequencies integral feedback counteracts the compensatory work of velocity feedback.

Phase compensation improves resonance tuning

Theoretically, perfect resonance tuning can be achieved by making the phase lead of the CPG equal to the phase lag of the limb (Ch. 3; Verdaasdonk et al. 2006). Hence, the resonance tuning behavior of the PID-type CPG can be greatly improved when the extra phase lag caused by the local reflex loop is compensated by additional feedback dynamics. Figure B.1 shows the extra phase lag (-90 - φ_{res}) by the dashed line (right axis).
In order to demonstrate that phase compensation actually improves resonance tuning, the following transfer function H_{comp} is added to the feedback dynamics (e.g. directly before the half-center model in Fig. 1):

$$H_{comp} = \frac{280\ (s^2 + 11.51s + 263.7)}{(s + 31.57)\ (s^2 + 11.51s + 1812)} \qquad \text{(B.1)}$$

Note that this function has no physical meaning, but is merely chosen in such a way that it approximately compensates for the extra phase lag introduced by the local reflex loop. In Fig. B.1 this approximation is shown by

the black solid line (right axis). In Fig. B.2 the results are shown for the CPG coupled to the limb.

The gray solid line in Fig. B.2 represents the entrained movement frequency $\omega_{e,comp}$ in case H_{comp} is added to the feedback dynamics. It shows a significant overall improvement in the ability to tune into the resonance frequency of the limb ω_{res}, except for positional feedback gains k_p below 1.4. At these low k_p the phase lead of the PID-type CPG is less close to 90° than the phase lead shown by the Bode plot of the CPG with inhibitory inputs only (Ch. 3; Verdaasdonk et al. 2006); it has a maximum of 125° at k_p=1.4 for the phase plot belonging to a 0.2 rad angular movement. Thus, by making the phase of the combination of limb dynamics and H_{comp} close to an 'ideal' 90°, results are actually worsened. The compensatory dynamics H_{comp} can be changed to account for this, which will improve the resonance tuning behavior at these low k_p, but that is not the goal of this example. The example clearly shows that an approximate compensation of the extra phase lag introduced by the

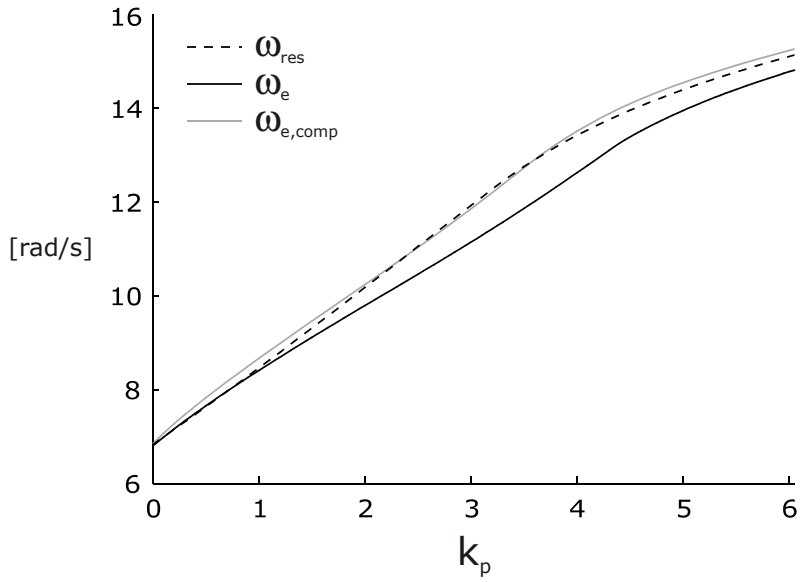

Fig. B.2 Resonance tuning in the neuro-musculo-skeletal model of the forearm coupled to a PID-type CPG. The *black solid line* represents the entrained movement frequency ω_e at different positional feedback gains k_p of the local reflex loop (compare with Fig. 4). The *dashed line* shows the resonance frequency ω_{res} of the forearm (i.e. without CPG), obtained by linearizing the limb dynamics at input amplitudes associated with the entrained periodic movement. The *gray solid line* represents the entrained movement frequency $\omega_{e,comp}$ in case additional feedback dynamics H_{comp} is present to approximately compensate the time delay in the local reflex loop τ_l (see Fig. B.1).

local reflex loop can improve resonance tuning considerably. However, whether phase compensation is plausible with respect to resonance tuning in humans is not known at this time

It is noted that for the results shown in Fig. B.2, linearization of the limb dynamics was calculated for input amplitudes experienced when coupled to the PID-type CPG *with* and *without* additional dynamics H_{comp}. However, the difference in calculated resonance frequency of the limb ω_{res} between both cases is so small that it is almost indistinguishable in a figure. Therefore, ω_{res} is only shown in Fig. B.2 for the linearization associated with the entrained periodic movements without H_{comp}.

Chapter 5

Energy Efficient Walking with Central Pattern Generators: from passive dynamic walking to biologically inspired control

B.W. VERDAASDONK, H.F.J.M. KOOPMAN, F.C.T. VAN DER HELM

Submitted to IEEE transactions on Robotics, 2007

Abstract

Like human walking, passive dynamic walking – i.e. walking down a slope with no actuation except gravity – is energy efficient by exploiting the natural dynamics. In the animal world, neural oscillators termed *Central Pattern Generators* (CPGs) provide the basic rhythm for muscular activity in locomotion. We present a CPG model, which automatically tunes into the resonance frequency of the passive dynamics of a bipedal walker, i.e. the CPG model exhibits *resonance tuning* behavior. Each leg is coupled to its own CPG, controlling the hip moment of force. Resonance tuning above the endogenous frequency of the CPG – i.e. the CPG's eigenfrequency – is achieved by feedback of both limb angles to their corresponding CPG, while integration of the limb angles provides resonance tuning at and below the endogenous frequency of the CPG. Feedback of the angular velocity of both limbs to their corresponding CPG compensates for the time delay in the loop coupling each limb to its CPG. The resonance tuning behavior of the CPG model allows the gait velocity to be controlled within a large range by a single parameter, while retaining the energy efficiency of passive dynamic walking.

1. Introduction

Walking is an important function of the human movement apparatus. Healthy people are not aware of the complexity of walking; they walk with little effort, without consciously thinking about it. During the stance phase, the stance leg acts as an inverted pendulum with a mass on top. Therefore, human walking is statically unstable. Thus, an interesting question is how human gait can be dynamically stable, robust and energy efficient at the same time. In this study we focus on the energy efficiency of walking.

Observations of human walking show that most of the muscles are only highly active at the beginning and end of the stance and swing phase (Inman et al. 1981). Ballistic gait models are based on these observations. They exploit their natural dynamics: the legs behave as a jointed pendulum, moving passively through the swing phase under the action of gravity (Mochon and McMahon 1980). Therefore, ballistic gait models are very energy efficient. However, the lack of control during the swing phase gives them poor robustness against perturbations. Even small perturbations can accumulate during the swing phase into large foot placement errors at heel strike. Hence, control is necessary during the entire gait cycle to obtain *robust gait*, but should leave the natural dynamics intact as much as possible to obtain *energy efficient gait*. The latter is *not* the mainstream starting-point of bipedal gait control: path-following control and control based on keeping the COP (center of pressure) within the foot base of support are common in robotics. However, this kind of control will force the *actual* walking cycle to differ from the *natural* walking cycle. This costs a lot of energy and is therefore unlikely to be used in human gait. Neural oscillators in the spinal cord, termed *Central Pattern Generators* (CPGs), *are* likely to play a key role in providing energy efficient human gait, for the following reasons. Firstly, many animals use CPGs to control gait. CPGs excite the muscles in a periodic fashion, giving rise to stable locomotion. Most evidence of the existence of CPGs in vertebrates comes from lamprey (e.g. Grillner et al. 1981), rats (e.g. Cazalets et al. 1995; e.g. Sqalli-Houssaini et al. 1993) and cats (e.g. Amemiya and Yamaguchi 1984; e.g. Shik et al. 1966); for reviews see MacKay-Lyons (2002), Whelan (1996) and Grillner et. al. (1998). Secondly, it has been shown that a simple model of a CPG is able to provide energy efficient rhythmic single limb movement (Ch. 3 and 4; Verdaasdonk et al. 2006; Verdaasdonk et al. 2007b). Although no direct evidence of CPGs in the human body is found yet, indications of their existence are present (e.g. Dimitrijevic et al. 1998).

It has been shown in bipedal gait models (Taga 1995a; Taga et al. 1991; Verdaasdonk et al. 2007a (Ch. 6); Verdaasdonk et al. 2004b) that mutual entrainment of the CPGs with the musculo-skeletal system and its environment creates a stable limit cycle which is quite robust against perturbations (Taga 1995b; Verdaasdonk et al. 2007a (Ch. 6)). The

robustness is caused by the coupling between CPGs and musculo-skeletal system, which continuously cause perturbed state variables to be pulled back towards the limit cycle during the entire gait cycle.
The *energy efficiency* of CPG controlled gait has not been considered up to now. In Ch. 3 and 4 (Verdaasdonk et al. 2006; Verdaasdonk et al. 2007b) it was shown that CPGs are very suitable for energy efficient and robust rythmic *single limb* movement. The CPGs entrain to reflexive inputs, such as muscle length and velocity. This means that the CPGs adapt their outputs (i.e. frequency and amplitude) to the 'mechanical oscillator' in such a way that stable rhythmic movement is obtained, which is robust and energy efficient. The *energy efficiency* is obtained by tuning into the resonance frequency of the musculo-skeletal system. The type of afferent feedback to the flexor and extensor centers of the CPG plays a crucial role in obtaining this *resonance tuning* behavior of the CPG. In this study the 'mechanical oscillator' is a simple gait model and we investigate whether the principles of CPG-controlled energy efficient and robust rhythmic limb movement (Ch. 3 and 4; Verdaasdonk et al. 2006; Verdaasdonk et al. 2007b) also apply to walking.
Passive dynamic walking (McGeer 1990) – i.e. walking down a slope with no actuation except gravity – is an extreme form of ballistic walking (Mochon and McMahon 1980) and is very energy efficient. Drawbacks of passive dynamic walking are the poor robustness, as shown by the small size of its basin of attraction (Schwab and Wisse 2001), and of course the lack of controllability. The goal of this study is to control the quality of bipedal gait in terms of stride length, stride period and thus velocity, while keeping the energy efficient behavior of passive dynamic walking intact. To achieve this goal, we start off with a passive dynamic walking model and subsequently add biologically inspired control. This control consists of a CPG tightly coupled to each hip joint.

2. Methods

To investigate if central pattern generators (CPGs) are able to maintain the energy efficiency of passive dynamic walkers, we start off with a passive dynamic walking model (Sect. 2.1). Subsequently, each leg is locally coupled to its own CPG at the hip joint (Sect. 2.2). This coupling is afferent and efferent, associated with sensory feedback and motor control, respectively. The total bipedal walker can be seen as two coupled oscillators. One oscillator is the passive dynamic walker (Fig. 1) and the other oscillator is the neural oscillator, which consists of one CPG per hip joint (Fig. 2). By coupling these two oscillators tightly, the combined system will oscillate at one frequency and result in stable gait. The energy efficiency of the CPG-controlled gait model is discussed in Sect. 2.3 and depends on two factors. The first is the ability of the neural oscillator to tune into the resonance frequency of the passive dynamic walker, which is termed *resonance tuning* ability. The second is the energy losses by damping, mainly caused by impact during heel strike.

2.1 The Passive Dynamic Walker

The passive dynamic walking model consists of two rigid legs (Fig. 1). The legs are connected at the hip by a frictionless hinge joint and have point feet. The model only has three point masses: one point mass m_h at the hip and two smaller point masses m_f located at the feet. Since the walker does not have knees, ground-clearance during swing phase is provided artificially (App. A). The passive dynamic walker is able to walk passively down a small slope α. In that case, gravity provides exactly as much energy during the gait cycle as is lost by damping (mainly at heel strike). The stride frequency of this walker – its 'resonance frequency' – is changed by adding rotational hip stiffness K_h.

The model without hip stiffness (i.e. K_h=0) resembles minimalistic models of passive dynamic walking, such as the 'The simplest walking model' (1998) and the 'compass gait model' (Goswami et al. 1997). The major difference between our model and most other passive dynamic walking models (Borzova and Hurmuzlu 2004; Garcia et al. 1998; Goswami et al. 1997; McGeer 1990; van der Linde 1999) is the way foot-ground contact is described. The ground reaction force is modeled by viscous damping in both *x*- and *y*-direction and stiffness only in *y*-direction (see App. A for details). This makes investigation of walking on different types of ground (e.g. slippery) possible (although not done in this study). Most other models make use of impact equations at heel strike, after which the legs are switched and a new swing phase starts (e.g. Schwab and Wisse 2001). Our model is a continuous-time model, able to walk 'for ever' instead of one step at the time. The approach of Lagrange was used to derive the equations of motion (see App. B). The equations of motion

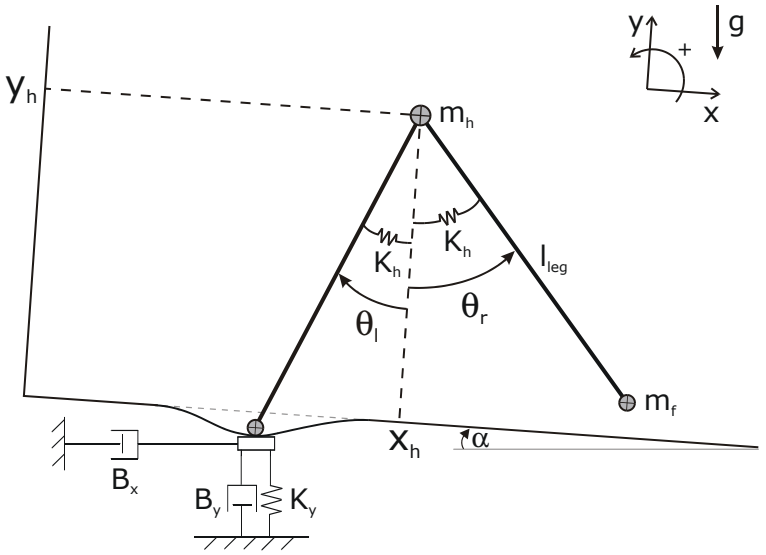

Fig. 1 The passive dynamic walker. The model has a large hip mass m_h relative to the mass of the feet m_f. The legs have length l_{leg} and the hips have rotational stiffness K_h. The model is able to walk passively down a slope α, for which gravity g supplies all the energy needed to overcome impact losses. Foot-ground contact is modeled by damping B_x in the x-direction and by damping B_y and stiffness K_y in the y-direction. The generalized coordinates are the hip angles θ_r and θ_l and the coordinates of the hip mass x_h and y_h.

are expressed in four generalized coordinates $\mathbf{q} = [x_h\ y_h\ \theta_r\ \theta_l]^T$, in which x_h and y_h are the coordinates of the hip mass m_h parallel and perpendicular to ground level, respectively, and θ_r and θ_l are the angles of respectively the right and left leg relative to the perpendicular of the ground.

2.2 Coupling the Legs to Central Pattern Generators

Central patterns generators (CPGs) are neural networks in the spinal cord, which output periodic excitation to the muscles, even in a completely isolated spinal cord (Nishimaru and Kudo 2000; Sqalli-Houssaini et al. 1993). The CPG model used in this study is similar to the 'PID-type' CPG, discussed in Ch. 3 (Verdaasdonk et al. 2006). The CPG model features *Positional, Integral* and *Derivative* feedback of the limb angle to the flexor and extensor centers of the CPG. Previous studies (Verdaasdonk et al. 2006; Verdaasdonk et al. 2007b) have shown that this type of afferent feedback is crucial in providing energy efficient control in rhythmic single limb movement. In these studies, feedback of *positional* information was shown to provide resonance tuning above the CPG's endogenous frequency f_{CPG} (i.e. the natural frequency at

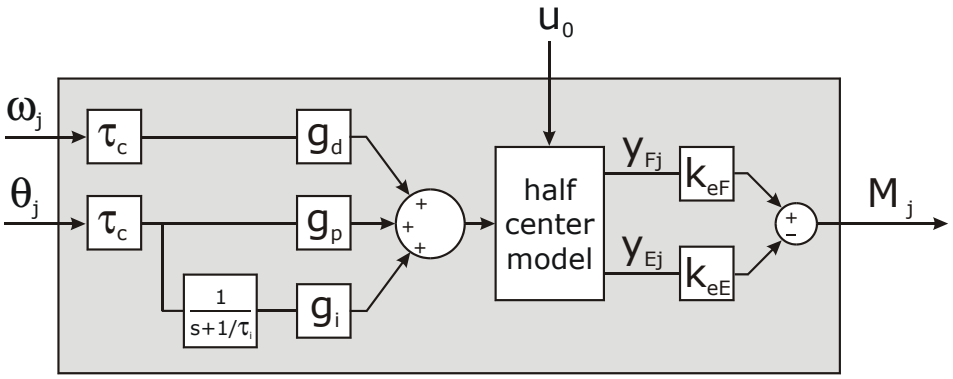

Fig. 2 The CPG model for leg j (j={r,l}). It has supra-spinal input u_0 and afferent input of leg angle θ_j and angular velocity ω_j, which is fed to the half-center model with gains g_p and g_d and time delay τ_c. The leg angle is integrated by a leaking integrator with large time constant τ_i and is fed to the half-center model with gain g_i. The half-center model is the basic rhythm generator, which outputs y_{Fj} and y_{Ej} are coupled to the limb by efferent gains k_{eF} and k_{eE} to provide a hip moment of force M_j from the torso.

which the uncoupled CPG oscillates). *Integral* feedback was shown to provide resonance tuning at and below f_{CPG}. Feedback of *velocity* information (i.e. derivative feedback) was shown necessary to compensate for the time delay in the loop coupling limb to CPG, else resonance tuning is not possible at high movement frequencies (Ch. 3; Verdaasdonk et al. 2006).

The CPG model is shown in Fig. 2 and its equations are stated in App. C. The basic rhythm generator of the CPG is a half-center model. It is based on the work of Matsuoka (1985; 1987) and was discussed at length in Ch. 3 (Verdaasdonk et al. 2006). Literature (Barbeau et al. 1999; Burke 2001; McCrea 2001; Van de Crommert et al. 1998; Whelan 1996) suggests feedback from Ia and II fibers to the flexor and extensor centers are present during walking. This is abstracted in our model as delayed feedback of the leg's angle θ_j and angular velocity ω_j (j={r,l}) to the half-center model with gains g_p and g_d and time delay τ_c. An internal process of the CPG 'integrates' the delayed leg angle θ_j (t-τ_c) by a leaking integrator with large time constant τ_i, which is subsequently fed to the half-center model with gain g_i. The hip joint of each leg j is locally coupled to its own CPG.

Our passive dynamic walker has no trunk, which has little effect on the motion of the legs (McGeer 1990). To still be able to control the hips separately, as humans do, a *virtual* torso is introduced: the torso is considered perpendicular to the ground level and immovable. The output of the flexor center y_F and extensor center y_E are amplified by the respective efferent gains k_{eF} and k_{eE} to form the *motor signals* to the muscles which provide hip flexion and extension. The 'muscles' are modeled most simple,

translating the motor signals linearly to a hip moment of force M_j relative to the torso ($j=\{r,l\}$). Supra-spinal input u_0 to the CPG can be changed to increase or decrease the outputs of the flexor and extensor center, and thus the hip moments of force.

2.3 Energy Efficiency Analysis

In engineering the energy efficiency of a system is often defined as the ratio between the amount of total performed work (i.e. the sum of positive and negative work) and the energy expenditure needed to achieve this work. The efficiency η of the CPG-controlled actuation at the hips can be determined during one gait cycle:

$$\eta = 100\frac{W}{E_{\text{exp}}} \qquad \% \qquad (1)$$

with W the total amount of work performed by the hip muscles during one gait cycle and E_{exp} the accompanying energy expenditure. The work W is necessary to compensate for the damping losses, which are mainly caused by impact at heel strike. The hip muscles of our gait model do not store energy; performing positive as well as negative work costs energy. Thus, the energy expenditure E_{exp} is calculated as follows:

$$E_{\text{exp}} = \sum_j \left(\int_0^T \left| (M_j \omega_j) \right| dt \right) \qquad \text{J} \qquad j=\{r,l\} \qquad (2)$$

with E_{exp} the energy expended during one gait cycle, T the period of the gait cycle, M_j the muscle moment of force about hip joint j relative to the torso, and ω_j the angular velocity of leg j. When the signs of M_j and ω_j are equal, positive work is done; else negative work is done. The energy efficiency ratio η is 100% if only positive work is performed by the hip muscles during the gait cycle. Note that for perfect resonance tuning in a mass-spring system with spring extension x and sinusoidal actuation force F, the energy efficiency ratio η is 100%, because the phase of the transfer function $H(s)=x(s)/F(s)$ is -90° at the resonance frequency, i.e. the force F and velocity $v=dx/dt$ are in phase and only positive work is performed. In a similar way, an energy efficiency ratio η of 100% is obtained for our CPG-controlled gait model if the stride frequency equals the 'resonance frequency' of the passive dynamic walker. Resonance tuning leaves the natural exchange between potential and kinetic energy intact: no active braking of the legs is necessary and thus only positive work is performed by the hip muscles. Forcing the gait model to walk slower or faster then its natural frequency at given gait velocity, would imply a control that actively brakes and thus performs negative work.

The efficiency ratio η is a good measure of the resonance tuning capabily of the CPGs. However, it gives an *incomplete* view on the energy efficiency of walking. Even if the efficiency η of the hip muscles is 100%, a certain distance can be walked with different energy expenditures. For our simple gait model, this is caused by different collision losses at heel strike (i.e. the negative work done by the dampers B_x and especially B_y) for different gait qualities (i.e. different stride length S and/or stride period T). Therefore, the energy expenditure per unit distance walked E_m is also determined (normalized to mass). In the field of bio-mechanics this is a widely used measure for the energy efficiency of walking (Koopman 1989; McMahon 1984). The energy E_{exp} expended during one gait cycle is divided by the stride length S and total mass ($2m_f + m_h$) of the gait model to yield E_m:

$$E_m = \frac{E_{exp}}{S\left(2m_f + m_h\right)} \qquad \text{J/(kgm)} \qquad (3)$$

To perform the above-mentioned energy efficiency analysis, periodic cycles of the gait model have to be found and analyzed. This is done with help of Poincaré mapping as discussed thoroughly in Ch. 6 (Verdaasdonk et al. 2007a).

3. Results

3.1 Passive Dynamic Walking

The gait model (Fig. 1) is able to walk down certain slopes α without any control, i.e. it is a passive dynamic walker (Sect. 2.1). The gravitational energy received by the passive dynamic walker – i.e. the work W_g performed by gravity – is proportional to the slope α and equals $(2m_f+m_h)\,g\sin(\alpha)$ Joule per meter walked. Figure 3 shows the stride length S, stride period T and gait velocity v against downward slope α for all stable gait solutions. Since the stride period T is almost invariant with regard to the slope, which was also shown by Kuo (Kuo 2002) and Garcia et al. (Garcia et al. 1998), increasing gait velocity $v=S/T$ implies increasing stride length S. A larger stride length means more mechanical work has to be done by gravity to redirect the hip mass velocity at heel strike (Donelan et al. 2002), which corresponds to a

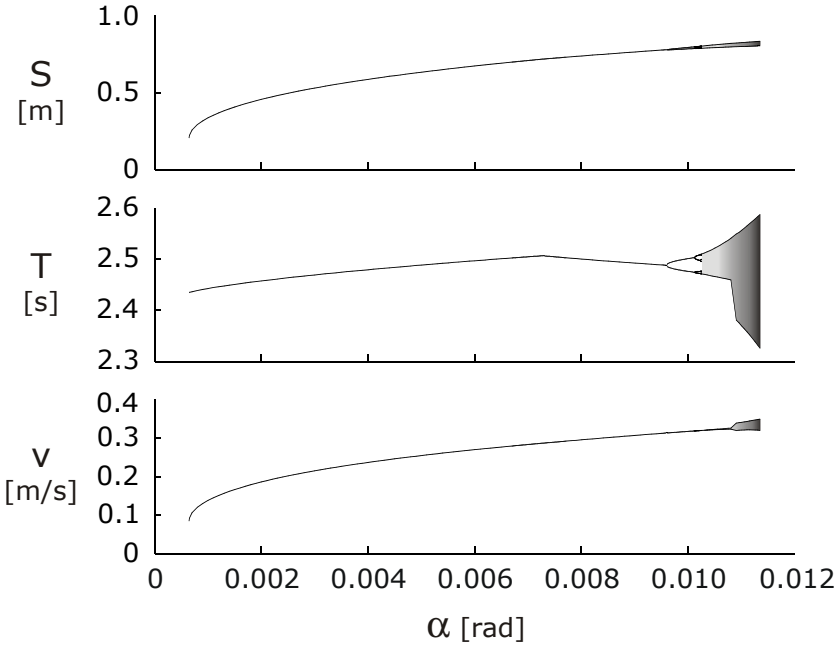

Fig. 3 Passive dynamic walking for increasing slope α. The top graph shows the stride length S, the middle graph shows the stride period T, and the bottom graph shows the gait velocity v. At steep slopes there is a route to chaos, which is depicted in Fig. 4. Beyond slopes of 0.0114 stable walking is not possible.

steeper slope in passive dynamic walking. Hence, the gait model walks faster down a steep slope than a shallow one.
Stable passive dynamic walking is not possible for slopes below $6.44 \cdot 10^{-4}$ rad, because in our model the foot of the stance leg sinks a little into the ground, which is modeled as a spring-damper. For very small stride lengths this sinking depth is relative large compared to the angle between both legs at heel strike. Therefore, after heel strike, the foot of the former stance leg does not lift above ground level and the walker stumbles and falls. For higher values of the slope the walker undergoes a series of bifurcations, which eventually lead to chaotic gait. Stable gait is not possible beyond slopes of 0.0114 rad.
Figure 4 shows the route to chaos in terms of the maximal segment angle of the right leg θ_r during one gait cycle. This route to chaos resembles the ones in (Garcia et al. 1998) and (Goswami et al. 1998), except that it starts of with a pitchfork bifurcation instead of a period doubling bifurcation. This is due to the different way in which gait is modeled in this study. Our model is a continuous-time model in which a complete stride (i.e. two steps) corresponds to the smallest possible recurrent period, while for the models in (Garcia et al. 1998) and (Goswami et al. 1998) one step is the smallest

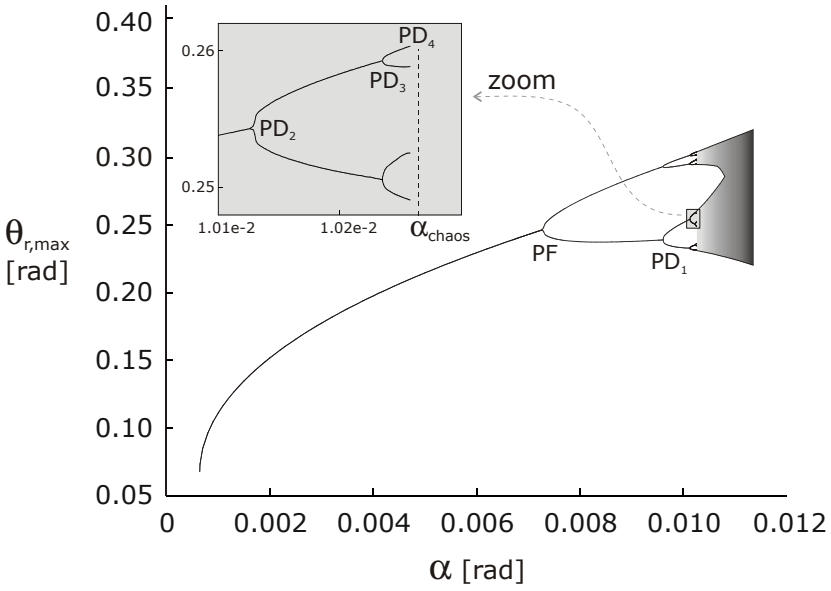

Fig. 4 Route to chaos. The passive dynamic walker initially exhibits a pitchfork bifurcation – marked PF – and subsequently period doubling bifurcations – marked PD_n – for increasing slope α. The zoom-in in the upper-left corner shows up to the fourth period doubling bifurcation and the estimated slope α_{chaos} at which chaotic gait begins (for $n \to \infty$).

possible recurrent period, as they swap the indices of the legs after each heel strike (i.e. right becomes left and vice versa). Thus, the pitchfork bifurcation in the bifurcation diagram corresponds to the slope beyond which asymmetrical gait, i.e. a limping gait, emerges. Figure 4 shows a zoom-in up to the fourth period doubling bifurcation. The onset of chaos can be estimated with the help of Feigenbaum's universal scaling law (Feigenbaum 1978), which is shown in Eq. 4.

$$\lim_{n\to\infty} \frac{\alpha_{PD,n} - \alpha_{PD,n-1}}{\alpha_{PD,n+1} - \alpha_{PD,n}} = \delta \tag{4}$$

in which $\alpha_{PD,n}$ is the slope at which the n^{th} period doubling bifurcation occurs and δ is the Feigenbaum constant, which has a value of 4.6692….
From Eq. 4 the asymptotic value of the slope where infinite period doubling bifurcations have occurred can be derived. This is the slope α_{chaos} beyond which chaos emerges (Eq. 5).

$$\alpha_{chaos} = \alpha_{PD,\infty} = \frac{\alpha_{PD,n} - \alpha_{PD,n-1}}{\delta - 1} \tag{5}$$

By filling in Eq. 5 for n=4 a rough estimate of α_{chaos}=0.0103 rad is obtained.
Since the stride frequency of the passive dynamic walker $f_{PDW}=1/T$ is almost constant for all slopes, the walker can be thought of having a kind of 'resonance frequency'. Adding rotational hip stiffness K_h increases this resonance frequency, as is shown in Fig. 5. The stride frequency f_{PDW} increases with increasing K_h, while the stride length S decreases. The graph shows that the gait model walks faster for a higher K_h, while the energetic input from gravity remains the same (α=-2.6·10^{-3} rad). The reason for this more energy efficient gait is that energy is buffered in the hip springs, thereby decreasing the stride length and accompanying collision costs.
The resonance frequency

$$f_{pend} = \frac{1}{2\pi}\sqrt{\left(\frac{g}{l_{leg}} + \frac{K_h}{m_f l_{leg}^2}\right)}$$

of the swing leg – that is, if it is swinging freely as a single hanging pendulum – is higher than the stride frequency f_{PDW} (see Fig. 5), because the swing leg covers more than half a period during the swing phase. The swing leg starts with a negative angular velocity to clear the ground, subsequently becomes positive to swing forward and becomes negative again just before heel strike (see Fig. 6). Actually, half a period (i.e. from zero angular velocity to zero angular velocity) of the swing phase is *shorter* than half a period of the free hanging pendulum. This higher 'resonance frequency' of the swing leg during

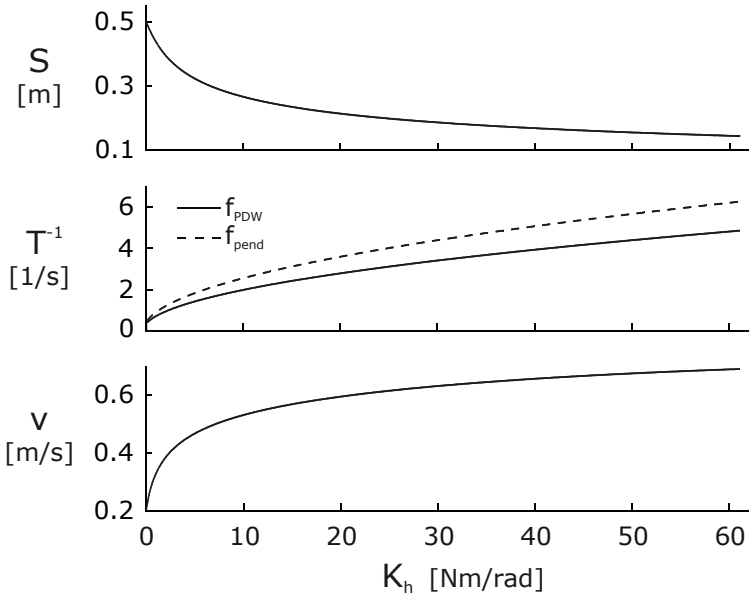

Fig. 5 Passive dynamic walking for increasing hip stiffness K_h. The top graph shows the stride length S, the middle graph shows the stride frequency f_{PDW} (*solid line*) versus the resonance frequency of the swing leg f_{pend} as free hanging pendulum (*dashed line*), and the bottom graph shows the gait velocity v.

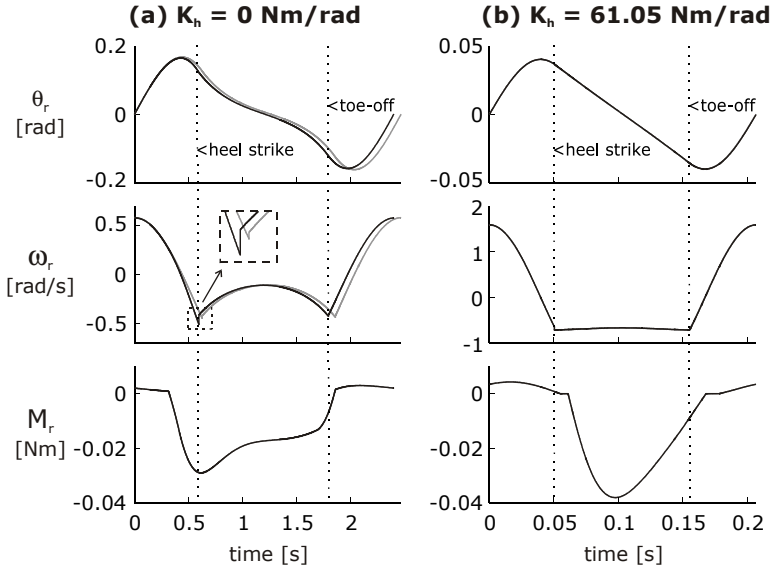

Fig. 6 Comparison of CPG-controlled walking (*black lines*) with passive dynamic walking (*grey lines*) for (a) no hip springs (K_h = 0 Nm/rad) (b) maximal spring constant (K_h = 61.05 Nm/rad). Time series of the angle θ_r, angular velocity ω_r and the muscle moment of force M_r of the right leg are shown during one gait cycle.

gait is caused by the gravity-induced initial deceleration and subsequent acceleration of the hip mass to which the swing leg is hinged. The 'resonance frequency' of the swing leg during gait becomes closer to the resonance frequency of the free hanging pendulum if hip springs are added, because the exchange of energy between the hip springs and the large hip mass (i.e. the potential energy in the springs is in counter-phase with that of the hip mass) flattens the velocity profile of the stance leg (compare angular velocity ω_r in Fig. 6a with that in Fig. 6b), and thereby decreases the deceleration and acceleration of the hip mass.

3.2 Energy Efficient CPG-Controlled Walking by Resonance Tuning

In this section the ability of the CPG to provide energy efficient gait by tuning into the resonance frequency of the passive walker is investigated. CPG-controlled walking at level ground is compared to the stable gait solutions of passive dynamic walking, shown in the previous section (see Fig. 5), for the same range of hip stiffness values K_h. The strength of afferent feedback g_p – and by that g_d and g_i (see App. C) – is adapted for all gait solutions, in such a way that the gait velocity matches that of passive dynamic walking for all values of K_h. This is done to dispose of the weak dependence of the stride frequency on gait velocity. Figure 7 compares the stride frequency $1/T$ of CPG-controlled walking (solid line) to that of passive dynamic walking (dotted line) for the above-mentioned range of K_h values, while Fig. 8 plots the accompanying energy efficiency. The two most extreme cases are depicted in Fig. 6, which compares the time series of one gait cycle of CPG-controlled walking (black lines) with passive dynamic walking (grey lines) in case of no hip stiffness (Fig. 6a) and maximal hip stiffness (Fig. 6b). Below we discuss the results in detail.

Figure 7 shows the entrained stride frequency $1/T$ to equal the frequency of passive dynamic walking f_{PDW} very well. However, for stride frequencies below the endogenous frequency f_{CPG} – i.e. the eigenfrequency of the CPG, which is 0.62 1/s for the parameter settings in this study – there are slight deviations (best visible in Fig. 7 by looking at S, as $v=S/T$ is constant for given f_{PDW}). The top graph of Fig. 8 shows that this slight deviation from perfect resonance tuning at low stride frequencies causes the energy expenditure E_m of the CPG-controlled muscles (black solid line) to be somewhat higher than the work W_m (grey solid line) they perform. This is expressed by the efficiency η (see (1), Sect 2.3) in the bottom graph of Fig. 8, which has its minimum of 96.9% at the lowest stride frequency (i.e. K_h=0 Nm/rad). The accompanying time series of one gait cycle of CPG-controlled walking in Fig 6a (black lines) shows that just before heel strike and just after toe-off, the moment of force M_r is indeed a short period of time out of phase with the angular velocity ω_r, thus performing negative work. Figure 6b shows that for the highest considered stride frequency (i.e. K_h=61.05

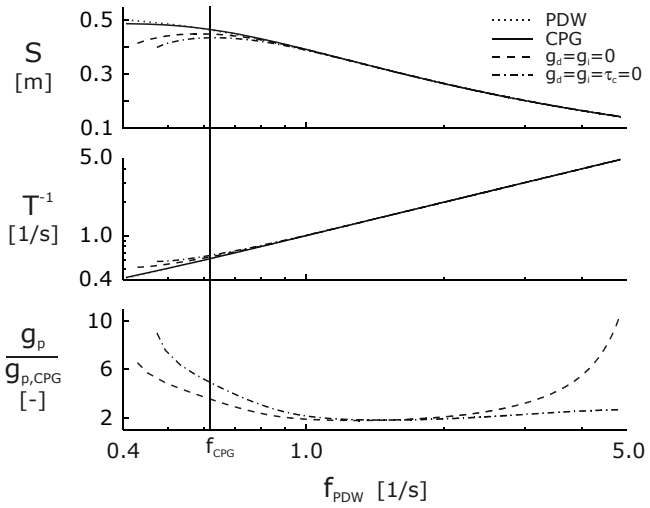

Fig. 7 Resonance tuning for same speed as passive dynamic walker (Fig. 5). The top graph shows the stride length *S*, the middle graph shows the stride frequency 1/*T*, and the bottoms graph shows the afferent strength necessary to maintain speed, relative to the default CPG.

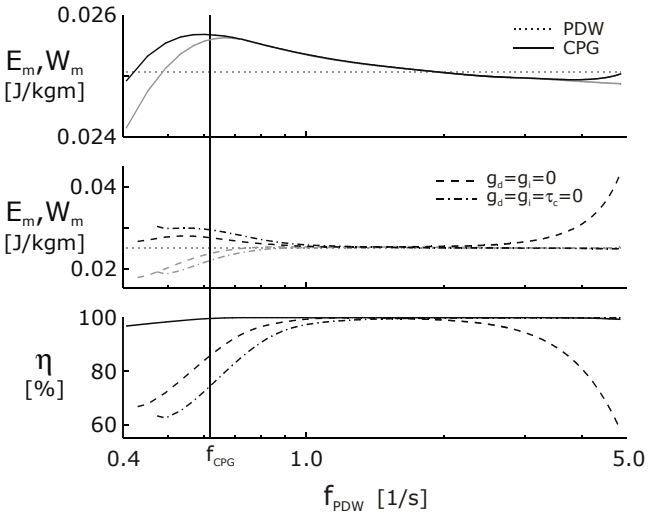

Fig. 8 Energy and work for the gait solutions shown in Fig. 7. The top graph shows the energy expenditure E_m of the muscles (*solid black line*) and their performed work W_m (*solid grey line*) versus the work W_g done by gravity in case of passive dynamic walking (*dotted grey line*). The middle graph shows E_m and W_m in case of no derivative and integral feedback to the half-center model (*dashed black and grey lines*, respectively) and in case of – besides the lack of integral and derivative feedback – the absence of time delay τ_c (*dashed-dot black and grey lines*, respectively); both are plotted versus W_g (*dotted grey line*). The bottom graph shows the accompanying efficiency η of the muscles in CPG-controlled walking (same legend applies as in top and middle graph). The endogenous frequency f_{CPG} is shown by a vertical line.

Nm/rad), M_r is only a *very* short period of time – just before heel strike – out of phase with ω_r, giving a η of 99.4%. The small differences in work W_m performed by the CPG-controlled muscles (solid grey line) and work W_g performed by gravity for passive dynamic walking (dotted grey line) – shown in the top graph of Fig. 8 – can be explained by small differences in the stride length S and the swing leg's angular velocity at heel strike. At low stride frequencies, the foot mass looses more kinetic energy at heel strike in CPG-controlled walking than in passive dynamic walking (see zoom-in of ω_r in Fig. 6a), while it is vice versa at high frequencies. This causes W_m to be smaller than W_g for high stride frequencies and higher than W_g for low frequencies, with the exception of the lowest frequencies. At the lowest stride frequencies the smaller stride length in CPG-controlled walking means smaller collision losses, which cause W_m to be smaller than W_g.

Above-mentioned results show that the CPG is able to control gait in an energy efficient way by resonance tuning. The type of afferent feedback to the half-center model is important in achieving this. To show the influence of integral and derivative feedback of the legs' angles to the half center model, we also performed simulations without these types of feedback. The dashed line in Fig. 7 shows the entrained gait solutions when there is no feedback of angular velocity or the integrated angle (i.e. $g_d=g_i=0$), again with the afferent strength adapted to match the passive dynamic walking velocities. The influence of integral feedback shows at low frequencies. Without it, the stride frequency $1/T$ deviates substantially from f_{PDW} below f_{CPG}. Walking without hip stiffness is no longer possible (the minimal K_h for stable gait is 0.05). Even at and beyond f_{CPG} small deviations are present. This poor resonance tuning behavior causes to drop the efficiency η of the muscles to a minimum of 66.8% for the lowest stride length (bottom graph, Fig. 8). Although W_m is smaller than W_g at low frequencies – merely due to smaller stride lengths – the bad efficiency causes E_m to be larger than W_g (middle graph, Fig. 8). The influence of derivative feedback shows at high frequencies. Although without derivative feedback $1/T$ is only slightly lower than f_{PDW} at high frequencies (top graph, Fig. 7), the efficiency η goes down to 58.3% for the highest stride frequency. This shows that η is a better measure for resonance tuning than the entrained stride frequency itself. By increasing the afferent strength significantly (bottom graph, Fig. 7), the entrained frequency comes close to f_{PDW}, giving a false sense of good resonance tuning behavior, while in fact the energy expenditure is very high (middle graph, Fig. 8). The dashed-dot lines in Fig. 7 and 8 show simulations for which – besides the integral and derivative afferent feedback – the time delay τ_c in the loop coupling the CPGs to the limbs is absent (i.e. $g_d=g_i=\tau_c=0$). These show almost perfect resonance tuning at high stride frequencies with a minimum efficiency η of 99.97% at the highest stride frequency. Hence, these results clearly show that velocity feedback is necessary to compensate for the time delay in the loop, just as in rhythmic single limb movement (Ch. 3 and 4; Verdaasdonk et al. 2006; Verdaasdonk et al. 2007b). At low stride frequencies, the absence of time delay makes the

resonance tuning worse with a minimum efficiency η of 62.5% at the lowest stride frequency. Moreover, a minimum K_h of 0.15 Nm/rad is necessary to obtain stable gait.

The performance at low stride frequencies is worse, because absence of time delay means absence of extra phase lag in the feedback loop to the half-center model. Extra phase lag is necessary for frequencies below the CPG's endogenous frequency to obtain resonance tuning (for a detailed explanation, see Ch. 3). In fact, this is the reason that integral feedback is necessary for achieving energy efficient walking at low stride frequencies.
Figure 9 shows the gait solutions for increasing time delay in case there is no velocity feedback (i.e. g_d=0), default velocity feedback (i.e. g_d=0.08g_p) and velocity feedback for which the strength is linearly dependent on the size of the delay (i.e. g_d=0.08$g_p\tau_c$/50·10^{-3}). We start off with the gait solution of

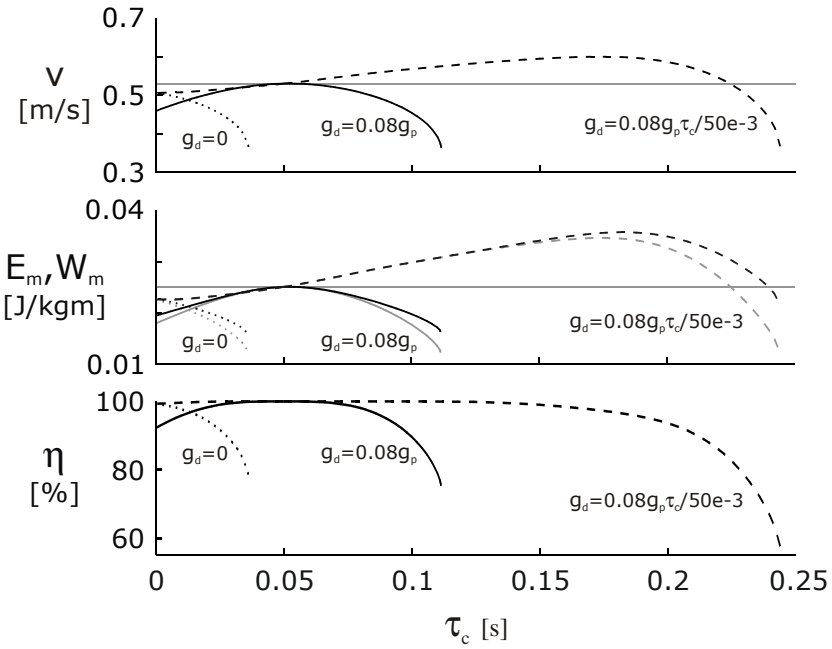

Fig. 9. Compensation of time delay by velocity feedback. The top graph shows the gait velocity v, the middle graph shows the muscles' energy expenditure E_m and their performed work W_m (*black and grey lines*, respectively), and the bottom graph shows the muscle efficiency η. The *dotted lines* represent gait solutions obtained without derivative feedback to the half-center model (i.e. g_d = 0), the *solid lines* represent gait solutions for the default velocity feedback (i.e. g_d = 0.08g_p), and the *dashed lines* represent gait solutions for velocity feedback with strength proportional to the time delay τ_c in the loop (i.e. g_d=0.08$g_p\tau_c$/ 50·10^{-3}).

Figs. 7 and 8 belonging to a stride frequency f_{PDW} of 2.0 1/s (i.e. K_h is 10 Nm/rad) and leave the accompanying afferent positional gain g_p at the constant value of 19.0 for all simulations. The default velocity feedback (solid lines) shows that the value of g_d relative to g_p is laid out to compensate phase lags of time delays around 50 ms. The efficiency η is close to 100% and the gait velocity v is close to that of passive dynamic walking as long as the time delay is close to 50 ms. Much lower and much higher time delays will cause bad resonance tuning behavior, with accompanying bad efficiency and lower gait velocities. The energy expenditure in these cases is less, because the stride length S diminishes with v, which means lower collision costs. No velocity feedback (dotted lines) causes the efficiency η to be near 100% only in case of no delay. Even in that case the gait velocity v is lower than in passive dynamic walking, because the afferent gain g_p is not adapted to match the latter velocity. Hence, the CPG gets less total afferent input (as there is no velocity feedback) and will walk with the same stride frequency, but with lower stride length S and therefore with less energy expenditure E_m.
The combination of positional and velocity feedback is similar to a PD-controller and gives maximal 90° phase lead. As the phase lag of the time delay increases with frequency ($H_\tau=e^{-j\omega\tau}$), there is a limit to the time delay, which can be compensated. The maximal time delay for which stable walking is possible is 0.244 s and is shown by the dashed lines in Fig. 9, which represent velocity feedback for which the strength is linearly dependent on the size of the delay. The efficiency η shows that for time delays up to 0.15 s very good resonance tuning behavior – and by that, energy efficient walking – is achieved by velocity feedback to the CPG.
It is noted that – based on a vast amount of simulations, many not discussed in this paper – the route to chaos is not encountered for CPG-controlled walking. The CPG seems to prevent or retard this route to chaos. Stable symmetric gait solutions exist for a certain parameter space and become unstable almost immediately after leaving this parameter space, sometimes preceded by asymmetric gait and one or two period doubling bifurcations. Thus, it could be that the route to chaos *is* present, but is compressed by the CPG into a very small area of the parameter space.

3.3 Velocity Control

For a given hip stiffness K_h, increasing gait velocity v of the CPG-controlled walker is achieved by increasing the energy expenditure of the muscles. This can be done by increasing the afferent gain g_p, the efferent gain k_{eE}, or the supra-spinal input u_0. Figure 10 shows the range of hip stiffness values K_h at which stable gait is possible for afferent strengths of 2, 20, 60, and 100. For a given hip stiffness K_h, the velocity v is increased by increasing g_p (top graph). The increasing gait velocity is achieved by increasing the stride length S (second graph), because the CPG tunes into the resonance frequency of the walker regardless of the afferent strength g_p (within certain

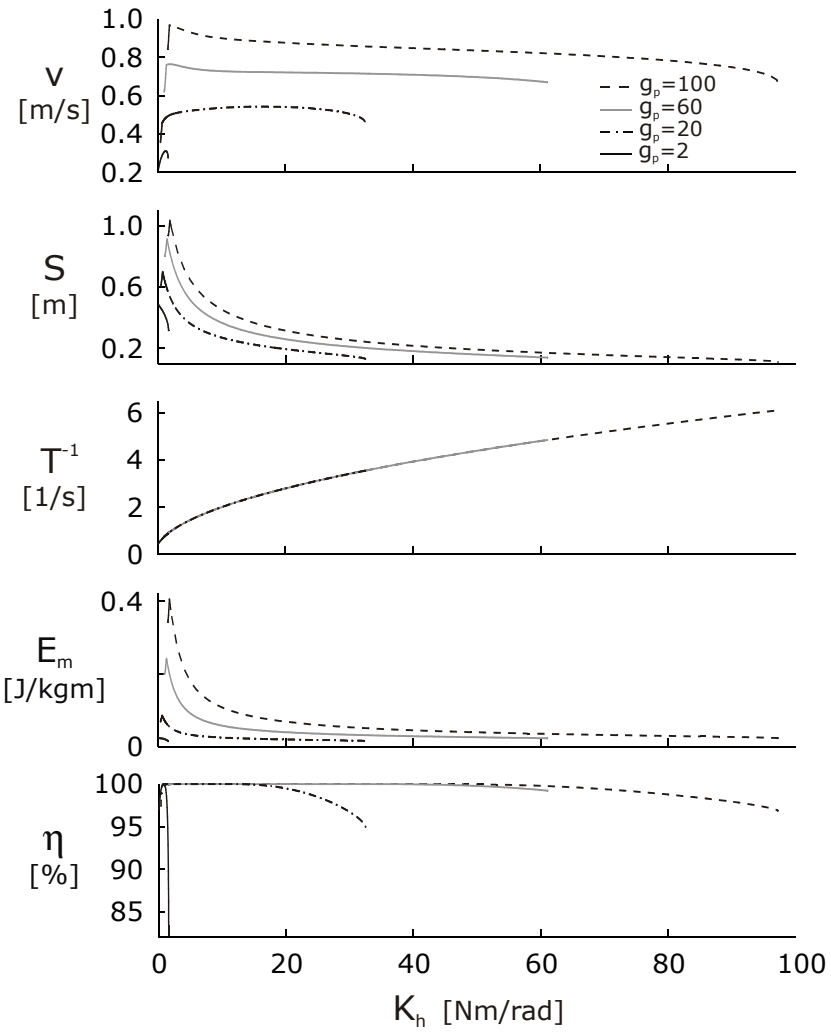

Fig. 10 Changing gait velocity by adaptation of afferent strength g_p for a range of hip stiffness values K_h. Shown are from top to bottom graph: gait velocity v, stride length S, stride frequency $1/T$, energy expenditure E_m, and muscle efficiency η. The gait solutions are shown for an afferent strength g_p of 2 (*solid black lines*), 20 (*dashed-dot black lines*), 60 (*solid grey lines*), and 100 (*dashed black lines*).

limits), and is accompanied by a higher energy expenditure E_m (fourth graph). The fact that the CPG tunes into the walker's resonance frequency for all afferent strengths g_p is shown by the overlapping plots of the stride frequency $1/T$ versus the hip stiffness K_h (middle graph). This good resonance tuning behavior is also shown by the muscle efficiency η (bottom graph). The range of resonance frequencies (i.e. range of values of K_h) for which stable walking is possible increases with increasing g_p, although the lowest possible stride frequency becomes somewhat higher. For given afferent strength g_p, higher hip stiffness K_h does not affect the gait velocity v much (top graph), as long as K_h is in the range where resonance tuning behavior is almost perfect, i.e. η close too 100% (bottom graph). However, the energy expenditure E_m is much less for higher K_h, because of the lower collision costs associated with smaller stride lengths S.
Hence, the stride length S is increased or decreased by increasing or decreasing the afferent gain g_p, the efferent gain k_{eE}, or the supra-spinal input u_0, while the stride frequency $1/T$ stays close to the mechanical resonance frequency of the walker due to the resonance tuning behavior of the CPG. This

way, a range of gait velocities v can be achieved by changing only one parameter. For example, for given g_p of 20 and K_h of 5, a range of gait velocities is achieved from 0.28 up to 0.75 m/s – with accompanying range of stride lengths from 0.20 to 0.54 m – by changing the supra-spinal input u_0 from 0.12 to 8.19.
The range of velocities, for which stable gait is possible, can be made much larger by increasing and decreasing the walker's resonance frequency with gait velocity. The resonance frequency can be increased by increasing the hip stiffness K_h by a local positional feedback, just as a stretch reflex can increase the muscle stiffness (Ch. 2; Verdaasdonk et al. 2004a) and by that the resonance frequency of a limb (Ch. 4; Verdaasdonk et al. 2007b). Thus, by making the local positional feedback gain dependent (e.g. proportionally) on g_p, k_{eE}, or u_0, a large range of gait velocities can be obtained by controlling only one parameter (g_p, k_{eE}, or u_0). It is noted that controlling K_h in this way costs energy, as the obtained resonance frequency differs from the real mechanical resonance frequency. This additional energy expenditure is not taken into account in the results of this study, where K_h is considered to be an energy conserving spring.

4. Discussion

4.1 Robustness

In this study we have focused on the energy efficiency of CPG-controlled walking. CPGs also play an important role in the recovery from small and medium-sized perturbations, and even from large perturbations, as was shown for a model of rhythmic arm movement in Ch. 4 (Verdaasdonk et al. 2007b). In Ch. 6 (Verdaasdonk et al. 2007a) we discuss the trade-off between energy consumption and robustness for a CPG-controlled bipedal walking model with 'human-like' mass distribution.

4.2 Conclusion

This study has shown that the principles of energy efficient rhythmic single limb movement by CPGs also apply to walking. The CPG achieves to control gait energy efficiently by tuning into the resonance frequency of the passive dynamics of the walker. Our CPG model on the one hand might elucidate how humans achieve energy efficient walking, and on the other hand can be used as (part of a) gait controller in applications such as walking robots or powered walking orthoses.

References

Amemiya M, Yamaguchi T (1984) Fictive locomotion of the forelimb evoked by stimulation of the mesencephalic locomotor region in the decerebrate cat. Neurosci Lett 50:91-96.

Barbeau H, McCrea DA, O'Donovan MJ, Rossignol S, Grill WM, Lemay MA (1999) Tapping into spinal circuits to restore motor function. Brain Res Brain Res Rev 30:27-51

Borzova E, Hurmuzlu Y (2004) Passively walking five-link robot. Automatica 40:621-629

Burke RE (2001) The central pattern generator for locomotion in mammals. Adv Neurol 87:11-24

Cazalets JR, Borde M, Clarac F (1995) Localization and organization of the central pattern generator for hindlimb locomotion in newborn rat. J Neurosci 15:4943-4951

Dimitrijevic MR, Gerasimenko Y, Pinter MM (1998) Evidence for a spinal central pattern generator in humans. Ann N Y Acad Sci 860:360-376.

Donelan JM, Kram R, Kuo AD (2002) Mechanical work for step-to-step transitions is a major determinant of the metabolic cost of human walking. J Exp Biol 205:3717-3727

Feigenbaum MJ (1978) Quantitative universality for a class of non-linear transformations. J. Stat. Phys. 19:25-52

Garcia M, Chatterjee A, Ruina A, Coleman M (1998) The simplest walking model: stability, complexity, and scaling. J Biomech Eng 120:281-288.

Goswami A, Espiau B, Keramane A (1997) Limit cycles in a passive compass gait biped and passivity-mimicking control laws. Autonomous Robots 4:273-286

Goswami A, Thuilot B, Espiau B (1998) A study of the passive gait of a compass-like biped robot: Symmetry and chaos. International Journal of Robotics Research 17:1282-1301

Grillner S, Ekeberg, El Manira A, Lansner A, Parker D, Tegner J, Wallen P (1998) Intrinsic function of a neuronal network – a vertebrate central pattern generator. Brain Res Brain Res Rev 26:184-197

Grillner S, McClellan A, Perret C (1981) Entrainment of the spinal pattern generators for swimming by mechano- sensitive elements in the lamprey spinal cord in vitro. Brain Res 217:380-386.

Inman V, Ralston H, Todd F (1981) Human Walking. In. Williams and Wilkins, Baltimore

Koopman HFJM (1989) The three-dimensional analysis and prediction of human walking. In: Department of Mechanical Engineering. University of Twente, Enschede, The Netherlands

Kuo AD (2002) Energetics of actively powered locomotion using the simplest walking model. J Biomech Eng 124:113-120

MacKay-Lyons M (2002) Central pattern generation of locomotion: a review of the evidence. Phys Ther 82:69-83.

Matsuoka K (1985) Sustained oscillations generated by mutually inhibiting neurons with adaptation. Biol Cybern 52:367-376

Matsuoka K (1987) Mechanisms of frequency and pattern control in the neural rhythm generators. Biol Cybern 56:345-353

McCrea DA (2001) Spinal circuitry of sensorimotor control of locomotion. J Physiol 533:41-50

McGeer T (1990) Passive dynamic walking. International Journal of Robotics Research 9:62-82.

McMahon TA (1984) Muscles, reflexes, and locomotion. In. Princeton University Press, Princeton, New Jersey, pp 331

Mochon S, McMahon TA (1980) Ballistic walking. J Biomech 13:49-57

Nishimaru H, Kudo N (2000) Formation of the central pattern generator for locomotion in the rat and mouse. Brain Res Bull 53:661-669

Schwab AL, Wisse M (2001) Basin of attraction of the simplest walking model. In: Proceedings of ASME 2001 Design Engineering Technical Conferences and Computers and Information in Engineering Conference, Pittsburgh, Pennsylvania

Shik ML, Severin FV, Orlovskii GN (1966) Control of walking and running by means of electrical stimulation of the mid-brain. Biophysics 11:756-765

Sqalli-Houssaini Y, Cazalets JR, Clarac F (1993) Oscillatory properties of the central pattern generator for locomotion in neonatal rats. J Neurophysiol 70:803-813

Taga G (1995a) A model of the neuro-musculo-skeletal system for human locomotion. I. Emergence of basic gait. Biol Cybern 73:97-111.

Taga G (1995b) A model of the neuro-musculo-skeletal system for human locomotion. II Real-time adaptability under various constraints. Biol Cybern 73:113-121.

Taga G, Yamaguchi Y, Shimizu H (1991) Self-organized control of bipedal locomotion by neural oscillators in unpredictable environment. Biol Cybern 65:147-159

Van de Crommert HW, Mulder T, Duysens J (1998) Neural control of locomotion: sensory control of the central pattern generator and its relation to treadmill training. Gait Posture 7:251-263.

van der Linde RQ (1999) Passive bipedal walking with phasic muscle contraction. Biol Cybern 81:227-237

Verdaasdonk BW, Koopman HF, Helm FC (2006) Energy efficient and robust rhythmic limb movement by central pattern generators. Neural Netw 19:388-400

Verdaasdonk BW, Koopman HF, Van Der Helm FC (2007a) Achieving energy efficient and robust bipedal gait with a CPG-controlled bipedal walker: Tuning the neural coupling gains. In: Williams TO (ed) Biological Cybernetics Research Trends. Nova Science Publishers, Hauppauge NY

Verdaasdonk BW, Koopman HF, Van der Helm FC (2007b) Resonance tuning in a neuro-musculo-skeletal model of the forearm. Biol Cybern 96:165-180

Verdaasdonk BW, Koopman HF, Van Gils SA, Van Der Helm FC (2004a) Bifurcation and stability analysis in musculoskeletal systems: a study in human stance. Biol Cybern 91:48-62

Verdaasdonk BW, Koopman HFJM, Van Gils SA, Van Der Helm FC (2004b) Stable walking with central pattern generators. In: Proceedings of the European Society of Biomechanics Congress, Eindhoven University of Technology, 's-Hertogenbosch, The Netherlands

Whelan PJ (1996) Control of locomotion in the decerebrate cat. Prog Neurobiol 49:481-515

Appendix A. Ground reaction forces

The ground reaction force for a foot standing on the ground, F_{Gjd}, is modeled by viscous damping in both *x*- and *y*-direction and stiffness only in *y*-direction:

$$F_{Gjx} = -B_x \dot{x}_{fj},$$
$$F_{Gjy} = \begin{cases} -B_y \dot{y}_{fj} - K_y y_{fj} & \text{if } \dot{y}_{fj} < 0 \\ -K_y y_{fj} & \text{else} \end{cases} \quad (A.1)$$

with B_x, B_y and K_y constant damping and stiffness factors, chosen such that an overdamped contact with negligible slip is obtained, x_{jf} and y_{jf} the coordinates of the feet relative to a base point on the ground. The indices *j* and *d* have the following meaning:

$j = \{r,l\}$ leg index
$d = \{x,y\}$ direction ground reaction force

Since our walker does not have knees, ground-clearance during swing phase must be provided artificially. This is accomplished by a ground reaction force G_{fjd} at foot *j*, stated as follows:

$$G_{fjd} = \begin{cases} F_{Gjd} & \text{if leg } j \text{ in Stance Phase} \\ 0 & \text{else} \end{cases} \quad (A.2)$$

A leg is said to be in stance phase when its foot is below ground level and its angular velocity is below a threshold value ω_G=0.1 (y_{fj}<0 & ω_j<ω_G). The threshold value ω_G is used because at very low speeds, heel strike (the beginning of stance phase) can occur at slightly positive angular velocity.

Appendix B. Lagrange's equations for the passive dynamic walker

The indices j, n and d in this appendix have the following meaning:

j = {r,l}	*leg index*
n = {1,2,3,4}	*generalized coordinate index*
d = {x,y}	*direction ground reaction force*

The generalized coordinates **q** are defined as the position of the hip mass m_h in the global system, (x_h, y_h), and the angles of the right and left leg relative to the vertical (i.e. segment angles), θ_r and θ_l:

$$\mathbf{q} = \begin{bmatrix} x_h & y_h & \theta_r & \theta_l \end{bmatrix}^T \tag{B.1}$$

The positions of the feet $\mathbf{x_f} = \begin{bmatrix} x_{fr} & y_{fr} & x_{fl} & y_{fl} \end{bmatrix}^T$ are expressed in **q** as follows:

$$\begin{aligned} x_{fj}(\mathbf{q}) &= x_h + l_{leg}\sin(\theta_j) \\ y_{fj}(\mathbf{q}) &= y_h - l_{leg}\cos(\theta_j) \end{aligned} \tag{B.2}$$

The scalar kinetic energy function $T(\mathbf{q})$ is given by:

$$\begin{aligned} T(\mathbf{q},\dot{\mathbf{q}}) &= \frac{1}{2}m_h\dot{x}_h^{\,2} + \frac{1}{2}m_h\dot{y}_h^{\,2} \\ &+ \sum_j \left(\frac{1}{2}m_f\dot{x}_{fj}^2(\mathbf{q}) + \frac{1}{2}m_f\dot{y}_{fj}^2(\mathbf{q}) \right) \end{aligned} \tag{B.3}$$

The scalar gravitational potential energy function $V_g(\mathbf{q})$ is given by:

$$\begin{aligned} V(\mathbf{q}) &= m_h g\left(\sin(-\alpha)x_h + \cos(-\alpha)y_h\right) + \sum_j \frac{1}{2}K_h\theta_j^2 \\ &+ \sum_j m_f g\left(\sin(-\alpha)x_{fj}(\mathbf{q}) + \cos(-\alpha)y_{fj}(\mathbf{q})\right) \end{aligned} \tag{B.4}$$

The foot-ground contact forces Eq. A.2 are written as vector $\mathbf{G_f}(\mathbf{x_f}) = \begin{bmatrix} G_{frx} & G_{fry} & G_{flx} & G_{fly} \end{bmatrix}^T$, which is expressed in local foot coordinates $\mathbf{x_f}$ and must be transformed to an expression in generalized coordinates before entering Lagrange's equations of motion:

$$\mathbf{G}_n(\mathbf{q},\dot{\mathbf{q}}) = \sum_{k=1}^{4} \mathbf{G}_{\mathbf{f}k}(\mathbf{x_f}) \frac{\partial \mathbf{x}_{\mathbf{f}k}}{\partial q_n} \tag{B.5}$$

Lagrange's equations of motion are now:

$$\frac{d}{dt}\left(\frac{\partial T}{\partial \dot{q}_n}\right) - \frac{\partial T}{\partial q_n} + \frac{\partial V}{\partial q_n} = \mathbf{M}_n + \mathbf{G}_n \qquad \text{(B.6)}$$

with **M** the vector of generalized forces, comprising the CPG-controlled hip moments of force (Eq. C.8): $\mathbf{M}=[0\ 0\ M_r\ M_l]^T$.

Parameters

m_h	= 1.0	kg	hip mass
m_f	= 0.04	kg	foot mass
l_{leg}	= 1.0	m	leg length
g	= 9.81	m/s^2	gravity constant
K_y	= 1·10^5	N/m	ground stiffness in y-direction
B_y	= 1·10^4	Ns/m	ground damping in y-direction
B_x	= 1·10^6	Ns/m	ground damping in x-direction

Variables with default values

α	= 2.6·10^{-3}	rad	ground slope
K_h	= 0	Nm/rad	rotational stiffness of the hip

Appendix C. Central pattern generator

The dynamics for the CPG coupled to leg j ($j=\{r,l\}$) are given by the following equations:

$$\dot{u}_{Fj} = \frac{1}{\tau_r}\left(u_0 - u_{Fj} - \beta v_{Fj} - w y_{Ej} - g_p \theta_j (t-\tau_c) - g_d \omega_j (t-\tau_c) - g_i \varphi_j (t-\tau_c)\right) \quad \text{(C.1)}$$

$$\dot{v}_{Fj} = \frac{1}{\tau_a}\left(y_{Fj} - v_{Fj}\right) \quad \text{(C.2)}$$

$$\dot{u}_{Ej} = \frac{1}{\tau_r}\left(u_0 - u_{Ej} - \beta v_{Ej} - w y_{Fj} + g_p \theta_j (t-\tau_c) + g_d \omega_j (t-\tau_c) + g_i \varphi_j (t-\tau_c)\right) \quad \text{(C.3)}$$

$$\dot{v}_{Ej} = \frac{1}{\tau_a}\left(y_{Ej} - v_{Ej}\right) \quad \text{(C.4)}$$

$$\dot{\varphi}_j = \frac{1}{\tau_i}\left(\tau_i \theta_j - \varphi_j\right) \quad \text{(C.5)}$$

in which u_{Fj}, v_{Fj}, u_{Ej} and v_{Ej} are the state variables of the flexor ('F') and extensor ('E') centers and φ_j is the integral of the angle θ_j. Integration of the angle θ_j is assumed to be performed by an internal process of the CPG, which is modeled as leaking integrator (pole at $-1/\tau_i$ see Eq. 18).

The outputs of the flexor and extensor centers, y_{Fj} and y_{Ej}, are given by:

$$y_{Fj} = \max(0, u_{Fj}) \quad \text{(C.6)}$$

$$y_{Ej} = \max(0, u_{Ej}) \quad \text{(C.7)}$$

The actuation moments of force of our CPG-controlled hip muscles are then given by:

$$M_j = k_{eE} y_{Ej} - k_{eF} y_{Fj} \quad \text{(C.8)}$$

Parameters

τ_r	= 0.18	s	rise time constant
τ_a	= 0.36	s	adaptation time constant
τ_i	= 10.0	s	time constant for leaking integrator

β	= 2.0	strength adaptation effect
w	= 2.0	strength of reciprocal inhibition
k_{eE}	= 0.04	efferent gain associated with extensor center
k_{eF}	= $0.1\,k_{eE}$	efferent gain associated with flexor center

Variables with default values

u_0	= 1.0	tonic input from supra-spinal centers
g_p	= 2.0	feedback strength of limb angle
g_d	= $0.08\,g_p$	feedback strength of limb's angular velocity
g_i	= $2\pi f_{CPG} g_p$	feedback strength of integrated limb angle
τ_c	= $50 \cdot 10^{-3}$ s	time delay in feedback loop

Chapter 6

Achieving energy efficient and robust bipedal gait with a CPG-controlled bipedal walker: Tuning the neural coupling gains

B.W. VERDAASDONK, H.F.J.M. KOOPMAN, F.C.T. VAN DER HELM

Biological Cybernetics Research Trends, pp. 165-199, 2007
ISBN 1-60021-568-8

Abstract

Human gait is at the same time energy efficient and robust against all sorts of perturbations (e.g. stumbling, getting pushed). For decades, biomechanical engineers try to model human gait by roughly two different approaches. The static approach is based on maintaining a kind of postural stability (i.e. static) by keeping the center of mass above the foot support area of the stance leg at all times. These bipedal walking mechanisms are robust for predefined perturbations, but in general consume a lot of energy. The dynamic approach is based on exploiting the natural dynamics of the biped as in ballistic walking. These walkers are energy efficient, but in general not robust. The goal of this study is to investigate to which extent a Central Pattern Generator (CPG) can attribute to the reconciliation of high energy efficiency and high robustness, seen in human walking. To achieve this goal, the limits regarding energy efficiency and robustness against perturbations are explored for a bipedal walking model. The model consists of two rigid legs with human-like mass distribution and is controlled by a Central Pattern Generator (CPG). The CPG is tightly coupled to the legs through sensory afferents and motor efferents and as such is able to generate stable locomotion. The exploration is carried out by optimizing the afferent and efferent gains with respect to energy efficiency and robustness. For the latter, our walker is subjected to two types of perturbations: its swing leg is pulled backwards during midswing and it encounters sudden ground level changes. With this approach gaits are found that are almost three times as efficient as human walking, as well as gaits that enable recovery when the swing leg is deprived of 70% of its angular velocity during midswing. Symmetry-breaking bifurcations, i.e. pitchfork bifurcations, are present throughout the parameter space and represent transitions from symmetric to asymmetric gait. For both symmetric and asymmetric walking, solutions with large stability regions are found. A strict trade-off between energy efficiency and robustness exists, which is most evident for the symmetric solutions. It could be that humans 'choose' the strength of the afferent and efferent pathways to and from the CPG as circumstances may require. That way, one would employ a more robust but less energy-efficient gait solution for uneven terrain compared to flat terrain.

1. Introduction

In everyday life, walking is something we do unconsciously. That is, we are not continuously aware of all that goes on in our body when we take a next step. Yet, we seem perfectly able to establish an energy efficient gait and maintain it while withstanding a wide range of perturbations. Unraveling the way nature achieves such a high-quality gait has been a research topic for many years, and will be for many years to come. From an anatomical point of view, several parts play a role in locomotion. Mechanically, the skeleton with its segments and joints defines the possible movements, while the muscles supply the power to move. For the nervous system, a distinction is made between the Central Nervous System (CNS) and the Peripheral Nervous System (PNS). The human CNS consists of the brain and spinal cord. The PNS is further divided into the neural pathways leading *to* the CNS, *the sensory afferents*, and pathways leading *from* the CNS, *the motor efferents*. As such, the sensory afferents are said to feed back information about the mechanical state and the environment to the CNS, whereas the motor efferents carry signals from the CNS to the muscles.

The way information is processed by the CNS and the PNS is still open to debate. Inspired by the obvious oscillatory nature of locomotion, a promising line of research suggests a Central Pattern Generator (CPG), for the legs located in the lower part of the spinal cord, as a crucial part of the CNS. The CPG is often described by the *half-center model* (Brown 1911): two reciprocally inhibiting groups of neurons, together generating an oscillating signal by firing alternatingly. Through the motor efferents, one group induces activity in the flexor muscles and the other in the extensor muscles. Information about the resulting motion is fed back through the sensory afferents to the CPG.

Various researchers have provided evidence for the existence of a locomotor CPG, mostly by experiments on cats (for review, see MacKay-Lyons 2002). Most of these studies built upon the pioneering work of Brown (1911), whose experiments showed that cats with a transected spinal cord and with cut dorsal roots still showed rhythmic alternating contractions in ankle flexors and extensors. MacKay-Lyons concluded that the existence of locomotor CPGs in animals has been established beyond reasonable doubt, but the relative importance of CPG activity – if any – in the control of human locomotion remains to be elucidated.

In the field of biomechanical engineering, several model studies have shown that it is indeed possible to generate stable bipedal gait using a CPG (e.g. Taga 1995a; Taga et al. 1991; Verdaasdonk et al. 2004). The CPG model used for these bipedal walkers is based on the work of Matsuoka (1985;

1987), who constructed a mathematical model of a neural oscillator. This model incorporates key neural features like the buildup of the neuron's membrane potential – causing the neuron to fire – and a fatigue effect that decreases the neuron's firing rate in time. Taga (1995b) and Taga et al. (1991) restricted their research to an assessment of stability. We will investigate the gait's energy efficiency as well, regarding both energy efficiency and robustness against perturbations as two key determinants of the quality of gait (Sect. 2.3).

Most attempts to model human gait focus on robustness against perturbations *or* on energy efficiency. The *former* approach is based on maintaining a kind of postural stability (i.e. static) by keeping the center of mass above the foot support area of the stance leg at all times. Based on trajectory control, these *static* bipedal walking mechanisms are robust for predefined perturbations, but are *not* fast and *nor* energy efficient: forcing a system far from its natural motion costs a lot of energy (e.g. compare the energy cost of moving a pendulum in its eigenfrequency with moving it in a higher or lower frequency). Nowadays, a lot of bipedal gait robots are based on a stability criterion termed Zero Moment Point (ZMP). The ZMP concept (Vukobratovic and Borovac 2004) is an extension of the static walking concept towards a more dynamic gait solution. However, these bipeds are still trajectory controlled and therefore in most cases not energy efficient: the chance that the trajectory, calculated on basis of the ZMP criterion, comes close to the natural motion of the biped is very slim indeed. The *latter* approach *is* based on exploiting the natural dynamics. These *ballistic* walkers (e.g. Mochon and McMahon 1980) use gravity to their advantage by making use of the natural exchange of potential and kinetic energy of their body with pendulum-like limbs; the swing leg acts as a hanging pendulum, while the stance leg (with the body mass on top) acts as an inverse pendulum. This way, energy efficient gait is obtained, but the lack of control in these bipeds results in poor stability properties; only small perturbations are needed to make the biped fall. The most extreme type of *ballistic* walking is passive dynamic walking (Garcia et al. 1998; McGeer 1990). These walking mechanisms only need a small slope to sustain their walking cycle, but have such poor stability properties (Schwab and Wisse 2001) that getting them started is a science on its own.

The goal of this paper is to investigate if Central Pattern Generators (CPGs) can provide the control that ballistic walkers lack, giving high robustness against perturbations, but without sacrificing much of the energy efficiency that characterizes ballistic walking. It is investigated for our CPG-controlled gait model if high energy efficiency and high robustness can coexist as in human walking, and if a trade-off between the two exists. To achieve this goal, it is investigated how the energy efficiency of CPG-controlled bipedal gait and its robustness against perturbations depend on the choice of afferent and efferent coupling strengths. We explicitly use the term robustness to

stress our interest in how the walker recovers from large perturbations, for which linear stability analysis no longer holds. Local stability will be assessed as well, but solely as a necessary condition for gait.

The methods necessary to achieve this goal are discussed in Sect. 2. The gait model (Sect. 2.1) is a two-segment sagittal walker with point feet, with a CPG closely coupled to each leg. This coupling models the *peripheral* nerves: *motor efferents* translate the CPG-outputs into hip moments of force, and *sensory afferents* feed information about the state of the legs (e.g. angle) back to the CPG. The dynamics of motor efferents and sensory afferents are together addressed as *coupling dynamics*. In this study, the coupling dynamics are modeled as proportional gains. By varying these coupling gains different gaits result, for example gaits with different step length, step frequency, walking speed, energy expenditure or stability. An optimization routine (Sect. 2.4) is used to find settings of the coupling gains that give (local) optimums of energy efficient gait, robust gait, or a compromise between them throughout the parameter space in order to reflect the great variety of possible 'high quality' gaits. Thus, the goal of the optimizations is *not* to find the global optimum for energy efficient and robust gait, but to obtain an understanding of the diversity of possible gaits in terms of energy efficiency and robustness and the possible trade-off between these gait qualities. The results are shown in Sect. 3 and discussed in Sect. 4.

2. Methods

The bidepal walking model is described in Sect. 2.1. Subsequently, the gait cycle analysis is treated (Sect. 2.2), necessary to calculate the quality criteria of gait (Sect. 2.3). Gait is considered to have two important quality determinants: its energy efficiency, giving an idea of how costly it is for a walker to maintain a certain gait, and its robustness against perturbations. We will restrict ourselves to two specific perturbations, namely a swing leg pull and a change in ground level. For both, a robustness measure is formulated that expresses the largest perturbation from which the walker can still recover. Here recovery is seen as returning to the local region of a limit cycle, after having been perturbed from it (see Sect. 2.2). The quality criteria are combined in an object function. The optimization routine is discussed in Sect. 2.4 for five different object function cases. These cases are aimed at giving gait that is energy efficient, robust, or a trade-off between energy efficiency and robustness.

2.1 The bipedal walking model

The bipedal walker is modeled as two coupled oscillators (Fig. 1). One oscillator is the musculo-skeletal part of our walker and is inherently

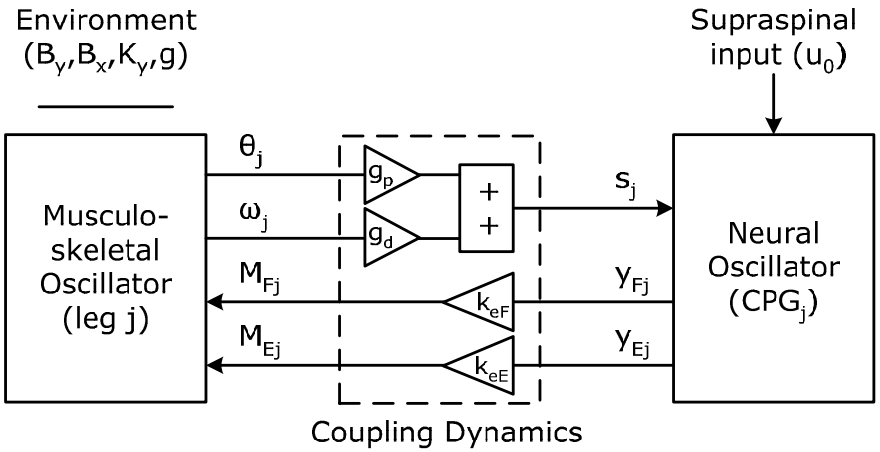

Fig. 1 The two oscillators coupled via afferent and efferent coupling gains, illustrated for leg j (j={r,l}). Coupling dynamics are identical for both legs. The CPG has afferent input s_j, which consists of feedback of limb angle θ_j and angular velocity ω_j with gains g_p and g_d, respectively. The motor signals for the hip flexor and extensor muscles M_{Fj} and M_{Ej} consists of the outputs of the flexor and extensor center y_{Fj} and y_{Ej} multiplied by the efferent gains k_{eF} and k_{eE}, respectively.

unstable. The other oscillator is the Central Pattern Generator (CPG), which is robust for a broad range of input frequencies. By closely coupling these two oscillators, the combined system will oscillate at one frequency and result in stable gait. The coupling of these two oscillators is given by the gains of the sensory afferents and motor efferents, the neural pathways associated with sensory feedback and motor control.

The musculo-skeletal part

The body of our walker consists of two rigid legs (Fig. 2). The legs are pin-jointed at the hip and have point feet. The head, arms and trunk of the body (HAT) are reduced to one point mass m_h, located at the hip. The inertia of the legs is represented by their center of mass (m_r, m_l) and mass moments of inertia around these centers of mass (I_r, I_l), and agree with human-like inertial properties (Chandler et al. 1975). The value for the rotational hip joint damping (B_{hr}, B_{hl}) has been taken from Thunnissen (1993). Note that

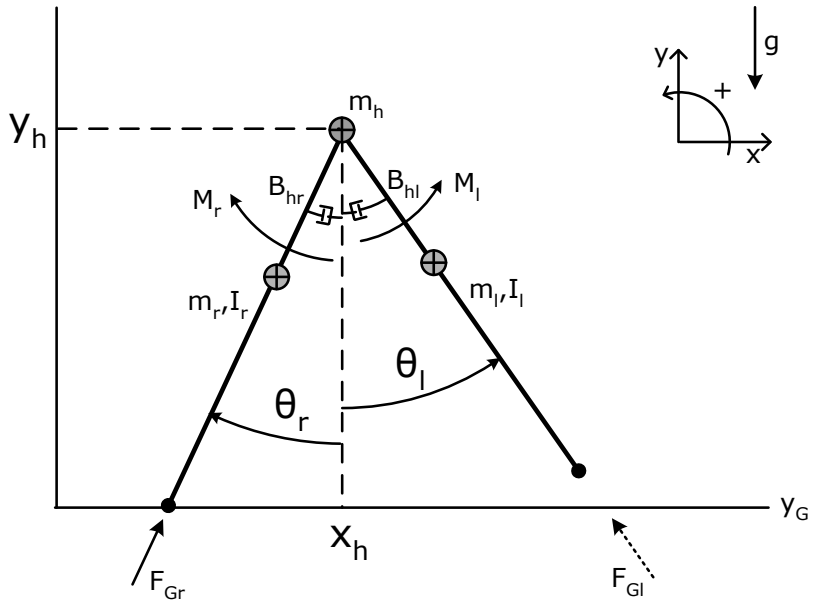

Fig. 2 The musculo-skeletal part of the walker. The generalized coordinates are the coordinates of the HAT mass m_h in horizontal and vertical direction, x_h and y_h respectively, and the angles of the right and left leg relative to the vertical, θ_r and θ_l respectively. The legs have mass m_j and moments of inertia I_j ($j=\{r,l\}$). The hip muscles actuate the legs by applying moments of force M_r and M_l on the right and left leg, respectively. F_{Gr} and F_{Gl} are the ground reaction forces. Note that F_{Gl} is indicated with a striped arrow to illustrate that this ground reaction force is zero during swing phase, even when the swing foot is below ground level.

for this segment model, stable passive dynamic walking (McGeer 1990) is not possible. Hence, controlled actuation is indispensable for our walker even when walking down a slope.

Humans have control of each of their hips. To make separate hip control possible in such a simple model, it is necessary to introduce a *virtual* torso (*not* shown in Fig. 2): the torso is considered perpendicular to the ground level and immovable. The actuators in our model are the hip muscles, acting on the legs by applying a moment of force around the hip joint. For each leg, one muscle supplies the flexion moment of force between hip and torso while another, its antagonist, supplies the extension moment of force. A muscle is modeled as a most simple actuator, linearly translating the level of actuation to a moment of force.

In deriving the equations of motion, the approach of Lagrange is used (see App. A). The equations of motion are expressed in four generalized coordinates, $\mathbf{q} = [x_h\ y_h\ \theta_r\ \theta_l]^T$, in which x_h and y_h are the coordinates of HAT mass m_h in horizontal and vertical directions, respectively, and θ_r and θ_l are the angles of respectively the right and left leg relative to the vertical. The contact of the walker's feet with the ground deserves some more attention. The ground reaction force for a foot standing on the ground, F_{Gjd}, is modeled by viscous damping in both *x*- and *y*-direction and a stiffness only in *y*-direction (Fig. 3 and Eq. 1).

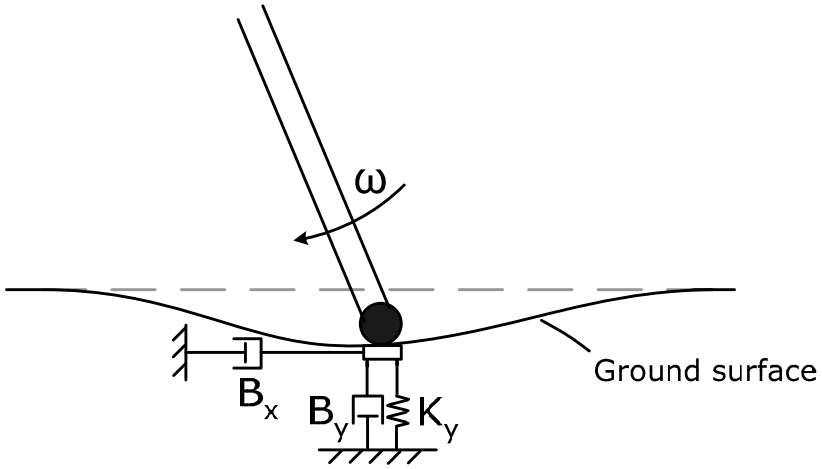

Fig. 3 Model of foot-ground contact during stance. The ground reaction force for a foot standing on the ground is modeled by damping B_x in the *x*-direction and by damping B_y and stiffness K_y in the *y*-direction (see Eq. 1).

$$F_{Gjx} = -B_x \dot{x}_{fj},$$
$$F_{Gjy} = \begin{cases} -B_y \dot{y}_{fj} - K_y(y_{fj} - y_{Gj}) & \text{if } \dot{y}_{fj} < 0 \\ -K_y(y_{fj} - y_{Gj}) & \text{else} \end{cases} \qquad j=\{r,l\} \tag{1}$$

Here B_x, B_y and K_y are constant damping and stiffness factors, chosen such that an overdamped contact with negligible slip is obtained. The coordinates of the feet in horizontal and vertical direction are x_{fj} and y_{fj}, respectively. Damping forces in vertical (y-) direction are only present when movement of the foot is downwards ($\dot{y}_{fj} < 0$). Since our walker does not have knees, ground-clearance during swing phase must be provided artificially. This is accomplished by a ground reaction force G_{fjd} at foot j, stated as follows:

$$G_{fjd} = \begin{cases} F_{Gjd} & \text{if leg } j \text{ in Stance Phase} \\ 0 & \text{else} \end{cases} \qquad j=\{r,l\},\ d=\{x,y\} \tag{2a}$$

For example, F_{Grx} is the ground reaction force in x-direction for the right leg. A leg is said to be in stance phase when its foot is below ground level y_{Gj} and its angular velocity is below a threshold value ω_G=0.01 ($y_{fj}<y_{Gj}$ & $\omega_j<\omega_G$). The threshold value ω_G is used because at very low speeds, heel strike (the beginning of stance phase) can occur at slightly positive angular velocity. To reduce calculation time, the numerical stiffness of the system is reduced by smoothing the discrete condition in Eq. 2a:

$$G_{fjd} = F_{Gjd}\left\{\left(\tfrac{1}{2} - \tfrac{1}{2}\tanh(c_s(y_{fj} - y_{Gj}))\right)\left(\tfrac{1}{2} - \tfrac{1}{2}\tanh(c_s(\omega_j - \omega_G))\right)\right\} \tag{2b}$$

with 'tanh' the hyperbolic tangent function. The constant c_s determines the steepness of tanh and is chosen high (c_s=10^5) to prevent a significant difference in simulation results when using Eq. 2b instead of Eq. 2a for the ground reaction force. The ground reaction force G_{fjd} is expressed in local foot coordinates and must be transformed to an expression in generalized coordinates before it can be used in the equations of motions (see Eq. A.5 of App. A).

The central pattern generator (CPG)

Our CPG is based on the work of Matsuoka (1985; 1987). Matsuoka showed that a group of neurons can achieve a stable oscillating output signal, when they are arranged in a mutually inhibiting network and each neuron is subject to fatigue. Moreover, Matsuoka gave necessary and sufficient conditions for the neurons to sustain this oscillatory activity. The dynamics of the CPG are governed by a set of first-order differential equations (see App. A).

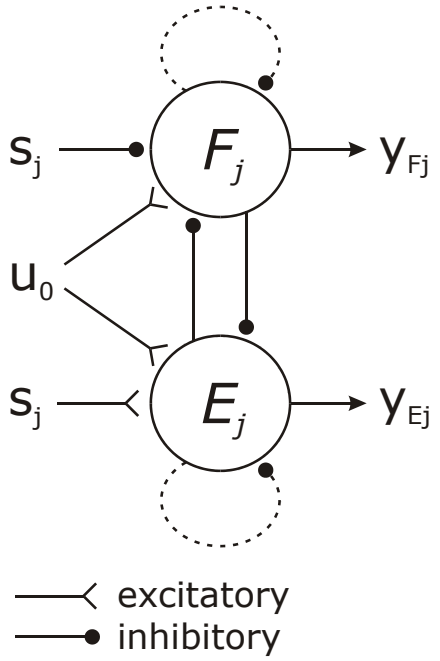

Fig. 4 CPG-model for leg j ($j=\{r,l\}$). The inputs to the neurons are the supra-spinal input u_0 and the sensory inputs s_j. The outputs are the firing rates y_{Fj} and y_{Ej}. Adaptation dynamics are shown by *dashed lines*, because it is an internal process instead of a pathway. The neuron 'F_j' represents the flexor center and the neuron 'E_j' the extensor center.

In our walker, each leg is controlled separately by one CPG, consisting of two neurons (Fig. 4). Its activity is initiated by a supra-spinal input signal u_0. From the moment a neuron starts firing, it starts to fatigue. This fatigue results in a decreasing firing rate, and accordingly in a decreasing inhibitory influence on the other neuron. When this inhibitory signal has reached a certain threshold value, the other neuron takes over and starts firing. This sequence repeats itself indefinitely when a (constant) $u_0>0$ is applied, and will occur even when no sensory input s_j is present. In the latter case, this CPG oscillates in its *endogenous* frequency with an amplitude proportional to u_0. When s_j is a nonzero periodic signal with a frequency within the *entrainment region* of the CPG, the CPG will adapt its own frequency to that of the input signal. The CPG is then said to be entrained by its input.

The coupling dynamics

Information about the state of the legs and the environment, i.e. proprioceptive and exteroceptive information, consists of the legs' angles and

angular velocities relative to a vertical axis. These are denoted by θ_j and ω_j, respectively. From a physiological point of view, one could say that the sensory apparatus of our walker consists of muscles spindles and a vestibular organ. For each leg, the states θ_j and ω_j are amplified by their respective gains g_p and g_d and directly fed back to the CPG as one combined sensory input signal s_j:

$$s_j = g_p\theta_j + g_d\omega_j \qquad j=\{r,l\} \tag{3}$$

The CPG processes this signal and forms two appropriate output signals for each leg, aimed at driving the musculo-skeletal part. These signals are denoted y_{Fj} and y_{Ej}, implicitly stating whether they are expected to contribute to a flexion or an extension of the leg. Both signals are amplified by the respective gains k_{eF} and k_{eE} to form the efferent *motor signals* for the flexion and extension hip muscles, M_{Fj} and M_{Ej}:

$$\begin{aligned} M_{Ej} &= k_{eF}y_{Ej} \\ M_{Fj} &= k_{eF}y_{Fj} \end{aligned} \qquad j=\{r,l\} \tag{4}$$

Following from the intrinsic properties of the CPG, these signals are never negative. In this paper the coupling dynamics will be characterized by the settings for the coupling gain vector $\mathbf{P_{cg}} = [g_p\ g_d\ k_{eE}\ k_{eF}]^T$.

2.2 Gait cycle analysis

Definition of gait

Let $\mathbf{X} = \{(x, \mathbf{W}) \in \Re^1 \times \Re^{n-1}\}$ be the n-dimensional state vector of the bipedal walker, in which:

x = state variable indicating distance traveled by the walker in direction of gait.
W= (n-1)-dimensional state vector containing all periodic state variables of **X**.

Furthermore, let Z be the (n-1)-dimensional state space spanned by the (n-1) periodic state variables given by **W**.

Then, *gait* is considered a periodic orbit $\Omega(\mathbf{W})$ in Z for which $\dot{x} \neq 0$, that in time approaches an attracting limit cycle Γ (i.e. locally stable). The time associated with one period gait cycle is termed the gait cycle period T. The distance traveled in one gait cycle is termed the stride length S and equals the time integral of x over a complete gait cycle.

Poincaré mapping

In determining the quality of gait, we will not follow the walker in time. Instead we observe its behavior only once per cycle, and take actions accordingly. Mathematically, a fixed one-sided Poincaré section Σ is set up that is transverse to the flow, and gait is analyzed each time it crosses this Poincaré section (Nayfeh and Balachandran 1995). This section gives a stroboscopic view on the system dynamics. The following section is chosen:

$$\Sigma = \left\{ \mathbf{W} \in \Re^{n-1} \mid \theta_r = 0, \omega_r > 0 \right\} \tag{5}$$

In words, this section is located at midswing of the right leg. It is suitable since a walker will pass this section once for each gait cycle. Note that by fixing θ_r and only taking periodic state variables given by **W** into account, the dimension of the section is (n-2).

Only regarding the crossings of Poincaré section reduces the system dynamics to a discrete Poincaré mapping P, which maps the system's state from the k-th crossing to the next:

$$\mathbf{Y}_{k+1} = P(\mathbf{Y}_k) \tag{6}$$

in which **Y** denotes the reduced state vector giving the system's coordinates on this Poincaré section. The limit cycle of a certain gait is identified on the Poincaré section as the fixed point $\mathbf{Y}^*$ of the Poincaré map, since it is mapped exactly onto itself:

$$\mathbf{Y}^* = P(\mathbf{Y}^*) \tag{7}$$

Gait approaches its limit cycle in time. On the Poincaré section this means that within the limits of robustness, for $k \to \infty$, $\mathbf{Y}_k$ approaches $\mathbf{Y}^*$. The Poincaré mapping is implemented using Matlab's event functions. A crossing of a Poincaré section is defined as an event taking place, at which it exits numerical integration.

Local stability of gait

By the definition of gait given above, it is a necessary condition for the limit cycle Γ to be an attractor, or in other words, to be at least locally asymptotically stable in the sense of Poincaré. This means that the magnitude of all eigenvalues of the linearized Poincaré map around its fixed point $\mathbf{Y}^*$ should be less than one (Eq. 8):

$$\lambda_{max} = \max_i \left(\left| \boldsymbol{\lambda}_i \right| \right) < 1 \qquad i=\{1,..,n\text{-}2\} \tag{8}$$

These eigenvalues can be shown to equal the non-trivial Floquet multipliers $\boldsymbol{\lambda}$, which are the eigenvalues of the monodromy map (Seydel 1994, pp 257-261). Locally the value of λ_{max} indicates the speed of convergence to the fixed point. The smaller its value, the faster the limit cycle is approached (Kuznetsov 1998; Seydel 1994).

Strictly speaking, locally stable gait approaches its limit cycle in time but will never actually reach it. In practice the fixed point $\mathbf{Y}^*$ is approximated when determining local stability:

$$\hat{\mathbf{Y}}^* \approx \mathbf{Y}^* \tag{9}$$

This approximation $\hat{\mathbf{Y}}^*$ is found by evaluating the (Euclidean) distance on the Poincaré section between the current crossing point $\mathbf{Y}_k$ and the previous one, $\mathbf{Y}_{k-1}$. This distance indicates how closely the gait has approached its limit cycle. If it remains below the threshold value δ_a=0.001 for five subsequent crossings, *the walker is said to have reached its limit cycle.* The approximation of the fixed point becomes the value of the last crossing point $\mathbf{Y}_k$ (when $|\mathbf{Y}_k-\mathbf{Y}_{k-1}|<\delta_a$, the walker is inside the local region of the limit cycle where linearization is valid. In comparison, typical values for $|\mathbf{Y}_k-\mathbf{Y}_{k-1}|$ right after perturbation are around 1.0). *Recovery* from a perturbation is defined as reaching the concerning limit cycle afterwards (i.e. $|\mathbf{Y}_k-\mathbf{Y}_{k-1}|<\delta_a$ for five subsequent gait cycles).

Let $\hat{P}$ be the linearization of the Poincaré map P around the approximated fixed point $\hat{\mathbf{Y}}^*$. Then, the limit cycle represented by the fixed point $\mathbf{Y}^*$ is said to be locally stable in the sense of Poincaré, if the magnitudes of all eigenvalues of the Jacobian of $\hat{P}$ are less than one. This Jacobian is constructed by a numerical perturbation method: one by one, the (n-2) state variables that span Σ are lightly perturbed to determine their first-order partial derivatives. To make $\hat{\mathbf{Y}}^*$ a valid approximation of $\mathbf{Y}^*$, and accordingly $\hat{\boldsymbol{\lambda}}_i$ a valid approximation of $\boldsymbol{\lambda}_i$, the threshold value δ_a is kept ten times as small as the perturbation size. Concludingly, the necessary stability condition for gait translates into the following practical condition:

$$\hat{\lambda}_{max} = \max_i \left(\left| \hat{\boldsymbol{\lambda}}_i \right| \right) < 1 \qquad i=\{1,..,n\text{-}2\} \tag{10}$$

During optimization $\hat{\lambda}_{max}$ is not calculated to reduce calculation time; it is assumed that the condition in Eq. 10 is met when locally stable gait is found. Explicit calculation of $\hat{\lambda}_{max}$ is used in the end to validate results found.

Failure mechanisms

Besides local stability, correct *ground-clearance* is also a necessary condition for *valid* gait. In each cycle, starting at the Poincaré section where the right leg is at midswing and below ground level, the correct order for the feet to come above ground level is *right-left-left-right.* When a foot fails to come above ground during the swing phase, or when this happens in a different order, the gait is invalid. Cases in which this type of failure can occur are those for which the angular velocity of the swing leg is too low, either because of low energy levels or large perturbations. In the simulation, an error handle is defined using event functions to make sure these cases are detected. Other failure mechanisms are easier to detect since gait will not be periodic afterwards. For instance, a walker could fall when the swing leg is not fast enough to take over the stance phase, or when the extension moment of force is not large enough to turn the stance leg forward. These cases are dealt with by an error handle that stops calculation if it takes more than 60 seconds (calculation time) to finish a gait cycle.

2.3 Quality of gait

This subsection shows how the quality of gait belonging to a certain set of neural coupling gains is measured. The quality of gait is measured by its energy efficiency and robustness and these measures are used as criteria in the object function (Sect. 2.4). The energy efficiency of gait is defined as the forward distance the walker can travel on a certain amount of energy expended. As for robustness, we are interested in how well our walker can recover from realistic perturbations during gait. A well-known mathematical stability region is the basin of attraction, defined as the set of all initial conditions from which a system will return to the attractor (Arrowsmith and Place 1990). Disadvantages of this stability measure are the long calculation times and the often difficult interpretation of results. For instance, a larger basin of attraction does not guarantee a higher robustness against a certain perturbation. Therefore, robustness is not expressed in limits on state variables, but in maximal 'real-life' perturbations from which the walker can recover. Two scalar measures are introduced: robustness against a swing leg pull R_{SLP} and robustness against a change in ground level R_{CGL}.

Energy efficiency

A widely used measure for energy efficiency in walking literature (e.g. Koopman 1989; McMahon 1984) is the energy expenditure per unit distance walked E_m [J/(kgm)], which is normalized on body weight. As a criterium for energy efficiency in our optimization, we use the non-normalized version of E_m, that is, the energy expenditure per unit distance walked E_d [J/m]. This is merely done to ensure large enough results of the object function (Eq. 15) for our optimization routine to work with (i.e. avoid rounding errors).

For a high quality gait, the aim is to achieve high energy efficiency and thus a low E_d. In the optimization the expended energy E_{exp} and traveled distance S (i.e. stride length) during one gait cycle are evaluated to yield E_d:

$$E_d = \frac{E_{exp}}{S} \qquad \text{J/m} \tag{11a}$$

In the simulation results (Sect. 3), we will show the normalized efficiency measure E_m next to or instead of E_d to make comparison to human walking and other bipedal gait models easier (Sect. 4.1):

$$E_m = \frac{E_d}{m_h + 2m_j} \qquad \text{J/(kgm)} \tag{11b}$$

The only actuators in our walker are the hip muscles, accounting for all the energy expended by the walker through the work they do on the legs. Since our muscles do not store energy, performing positive as well as negative work costs energy:

$$E_{exp} = \sum_j \left(\int_0^T \left| (M_j \omega_j) \right| dt \right) \qquad \text{J} \qquad j=\{r,l\} \tag{12}$$

with E_{exp} the energy expenditure from $t=0$ to $t=T$, T the period of the gait's limit cycle (i.e. stride period), M_j the muscle moment of force around joint j, and ω_j the angular velocity of leg j. When the signs of M_j and ω_j are equal, positive work is done; else negative work is done.

Robustness

Robustness against a Swing Leg Pull (R_{SLP})

The first method of perturbation is adapted from Forner Cordero (2003). Forner Cordero researched the recovery behavior of human individuals while walking on a treadmill, when their swing leg was suddenly pulled via a cord connected to the leg. He identified that perturbations applied at midswing were difficult to recover from. The force Forner Cordero applied through the cord is translated in our setup to a perturbation moment of force M_p around the hip joint. It is varied in amplitude and applied at the right leg at midswing. Where Forner Cordero stated the duration as a period of time, we apply the perturbation over a fixed angular distance ($0 \le \theta_r \le \theta_p$, see Fig. 5a). This way, the work done by the perturbing moment of force is independent of the swing leg's angular velocity. The angular distance is set to 0.1 rad,

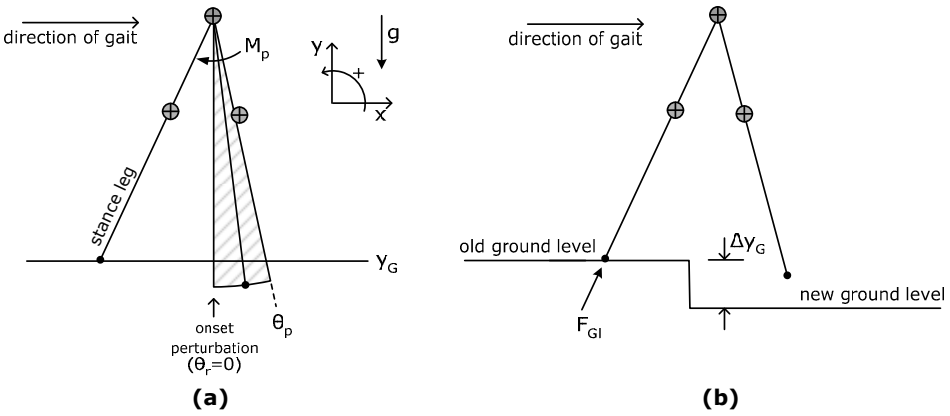

Fig. 5 Types of perturbation applied to gait model. **(a)** Swing leg pull: the right swing leg is perturbed by applying a perturbation moment M_p over an angle range $0 \leq \theta_r \leq \theta_p$. **(b)** Change in ground level: the walker is confronted by a sudden change Δy_G in ground level.

chosen as a compromise between a challenging perturbation and giving the walker time to act on it. (Forner Cordero (2003) identified longer time durations of perturbations as more difficult to recover from).

As measure for the robustness against a swing leg pull R_{SLP}, we use the maximal amount of work done by the perturbation from which the walker can still recover:

$$R_{SLP} = \int_{t(\theta_r=0)}^{t(\theta_r=\theta_p)} \left| M_{p,max} \omega_r(t) \right| \, dt = \left| M_{p,max} \theta_p \right| \qquad \text{J} \tag{13}$$

in which $M_{p,max}$ is the maximal constant perturbation moment of force the walker can handle. The robustness is determined during evaluation of the object function. Perturbations start with an M_p of 0 Nm and are increased until the walker fails to recover.

Robustness against a Change in Ground Level (R_{CGL})

The second method of perturbation is a sudden change in ground level Δy_G (Fig. 5b). The robustness margin for this type of perturbation is the maximal change in ground level from which a walker can still recover:

$$R_{CGL} = \Delta y_{G,max} \qquad \text{mm} \tag{14}$$

Only a decrease in ground level was applied ($\Delta y_G<0$). The ground level is decreased in two phases, by first lowering the right ground level when the right leg is at midswing, and then lowering the left ground level when the left leg is at midswing.

2.4 Finding energy efficient and robust gaits

To find a variety of 'high quality' gaits throughout the parameter space and discover a possible trade-off between energy efficiency and robustness, five different cases of an object function will be optimized for three sets of optimization parameters. Thus, as mentioned in the introduction (Sect. 1), the goal of this optimization is not to find a global optimum. This is reflected in the settings of the optimization parameters (see App. B), which allow for a relative fast search for sub-optimal solutions throughout the parameter space.

Since trade-off between energy efficiency and robustness is one of our primary concerns, these quality criteria (Sect. 2.3) are combined in one object function. Robustness is measured by either R_{SLP} or R_{CGL}:

$$J(\sigma, R_T) = \min\left(\frac{E_d^{1-\sigma}}{R_T^{\sigma}}\right) \qquad R_T=\{R_{SLP} \text{ ór } R_{CGL}\} \tag{15}$$

in which the weighing factor σ can be seen as a level of caution ($0 \le \sigma \le 1$): for $\sigma=1$ only robustness counts, while for $\sigma=0$ only energy efficiency counts. In between 0 and 1, both energy efficiency and robustness count and a compromise is expected.

With a parameter setting – weighing factor c and coupling gain vector $\mathbf{P_{cg}} = [g_p\ g_d\ k_{eE}\ k_{eF}]^T$ – and a state vector given as initial conditions, evaluation of the object function starts with finding the corresponding gait's limit cycle. When the gait is close enough to its limit cycle, the energy expenditure per unit distance E_d [J/m] is calculated over the last cycle (Sect. 2.3). The last crossing of the Poincaré section gives the starting point for the second part of the object function evaluation: determining the gait's robustness against a perturbation. The maximal perturbation from which the walker can recover is found by a trial-and error method: starting with a perturbation *stepsize* (=1 J or 1 mm depending on type of perturbation), the perturbation is increased until the walker fails to recover. Then a smaller stepsize is taken, and the loop starts again from the last perturbation at which recovery was successful. This way, the maximal perturbation will be found in the least amount of trials, with an accuracy of 0.1 J or 0.1 mm. Evaluation(s) of the object function results in one iteration step of the optimization routine.

Our optimization routine will search the optimal gain settings for five different object function cases, each given by a different combination of weighing factor σ and type of perturbation τ:

$$J(\sigma,R_T) = \{J(0,-),\ J(0.5,R_{SLP}),\ J(0.5,R_{CGL}),\ J(1,R_{SLP}),\ J(1,R_{CGL})\} \tag{16}$$

Three different sets of coupling gains (i.e. $\mathbf{P_{cg}}$ or a subset of $\mathbf{P_{cg}}$) are used as optimization parameters to minimize each of the object function cases given in Eq. 16:

a) only sensory afferents $\{g_p, g_d\}$,
b) only motor efferents $\{k_{eE}, k_{eF}\}$, (17)
c) all four coupling gains $\{g_p, g_d, k_{eE}, k_{eF}\}$.

Details on the optimization routine – including a flowchart of the evaluation of the object function – are stated in App. B.

3. Results

Firstly, a preparatory analysis is carried out to obtain suitable *starting points* for the optimization routine (Sect. 3.1). These starting points are chosen to be far apart in parameter space, and yield very different results for energy efficiency and robustness. Secondly, the optimization results are shown (Sect. 3.2). Optimization has been performed for each of the five object function cases (Eq. 16), varying both the starting points (Sect. 3.1, Table 1) and the set of the neural coupling gains used to optimize the gait quality (Eq. 17). Section 3.3 discusses the transformation from symmetric to asymmetric gait (i.e. limping) under variation of the neural coupling gains, including the corresponding change in energy expenditure and robustness. The large variation in energy efficiency of different gait solutions is explained in Sect. 3.4. Finally, the robustness against large perturbations is discussed (Sect. 3.5).

3.1 Preparatory analysis

Finding starting points is not a trivial task. Even assuming correct initial conditions, gait is unstable for a large number of gain combinations. Three suitable starting points for the optimization routine are shown in Table 1. Starting point *I* and *II* have relatively low energy expenditure (E_d), but also low robustness against a Swing Leg Pull (R_{SLP}). In contrast, starting point *III* has a much higher R_{SLP} but also relatively high energy expenditure. The robustness against a Change in Ground Level (R_{CGL}) differs less significantly. Note that although *I* and *II* are similar in their energy efficiency and robustness, their gain settings differ greatly.

3.2 Optimization results

The three starting points (Table 1) together with the three options for gains to optimize (Eq. 17), yield 3·3=9 optimizations carried out for each *object function case* (Eq. 16). Inherent to fmincon's search algorithm, each of these 9 optimizations will generally lead to a different local optimum. Thus, in total 9·5=45 optimizations were carried out.

Table 2 gives the best local optimums found for each of the five object function cases, and indicates which of the 9 local optimizations led to that result. The results are divided in three parts. The first part contains the gain settings g_p, g_d, k_{ee} and k_{ef} corresponding to the optimums found. The second part shows the values of the three quality measures E_d, R_{SLP} and R_{CGL} at the optimum. The normalized energy expenditure E_m is shown for reasons of comparison and is shown in italic. The third part shows four important gait

Table 1 The starting points for the main optimization round, following from the preparatory analysis. They are suitable since they differ considerably in gain settings as well as in results for energy efficiency and robustness. The results are divided in three parts: the suitable initial gain settings found, the values of the three quality measures E_d, R_{SLP} and R_{CGL} for these gain settings (E_m, the normalized version of E_d, is shown in italic) and four important gait cycle characteristics: the maximal Floquet multiplier λ_{max} indicating local stability (see Sect. 2.2.3), the stride length S, the time period of the gait cycle T and the walking velocity v.

	Starting Point	***I***	***II***	***III***
Initial Gains	g_p	13.0	20.0	20.0
	g_d	0.4	0.8	0.4
	k_{ee}	20	15	30
	k_{ef}	7.0	6.0	6.0
Quality scores	E_d [J/m]	24.5	25.0	62.2
	E_m [J/kgm]	*0.33*	*0.33*	*0.83*
	R_{SLP} [J]	0.5	0.7	3.5
	R_{CGL} [mm]	1.9	2.2	2.4
Gait cycle Results	Max Floquet multiplier λ_{max}	0.81	0.97	0.72
	Stride length S [m]	0.65	0.59	1.12
	Time period of cycle T [s]	1.16	1.14	1.14
	Forward speed averaged over cycle v [m/s]	0.56	0.52	0.99

cycle characteristics: the maximal Floquet multiplier λ_{max} indicating local stability (see Sect. 2.2), the stride length S (i.e. distance walked per gait cycle), the time period of the gait cycle T and the walking velocity v. Optimum A is the energy efficiency optimum, D and E are robustness optimums, and B and C are the optimums for a compromise between energy efficiency and robustness.

Results show large differences in energy efficiency and robustness, scoring considerably better than the starting points (compare Table 2 to Table 1). Figure 6 illustrates the gait cycles of the optimums found by showing the phase diagrams for each optimum, plotting angle versus angular velocity for both legs. Perturbations were only applied on one side: it is always the right

Table 2 The (local) optimums found in the main optimization round, for five different object function cases. The results are divided in three parts: the optimized gain settings found, the values of the three quality measures E_d, R_{SLP} and R_{CGL} at the optimums (E_m, the normalized version of E_d, is shown in italic) and four important gait cycle characteristics: the maximal Floquet multiplier λ_{max} indicating local stability (see Sect. 2.2), the stride length S, the time period of the gait cycle T and the walking velocity v.

Settings	Optimums found	***A***	***B***	***C***	***D***	***E***
	Object function case $J(\sigma,R_T)$					
	Weighing factor (E vs R) σ	0	0.5	0.5	1	1
	Robustness measure R_T	-	R_{SLP}	R_{CGL}	R_{SLP}	R_{CGL}
	Starting point used	I	II	I	II	II
	Corresponding set of optimized parameters (see Eq. 17)	c	c	a	a	c
Optimized gains	g_p	14.9	19.9	12.5	30.0	20.0
	g_d	0.34	0.46	0.26	0.62	0.8
	k_{ee}	16.4	20.8	20.0	15.0	24.8
	k_{ef}	5.7	10.0	7.0	6.0	15.8
Quality scores	E_d [J/m]	21.8	77.8	27.3	68.9	107
	E_m [J/(kgm)]	*0.29*	*1.04*	*0.36*	*0.92*	*1.43*
	R_{SLP} [J]	0.5	9.0	1.2	7.5	1.6
	R_{CGL} [mm]	1.8	2.2	3.8	1.8	6.0
Gait cycle Results	Max Floquet multiplier λ_{max}	0.95	0.53	0.62	0.62	0.53
	Stride length S [m]	0.61	0.86	0.73	0.90	0.82
	Time period of cycle T [s]	1.21	1.08	1.20	1.10	0.96
	Forward speed averaged over cycle v [m/s]	0.51	0.80	0.60	0.82	0.86

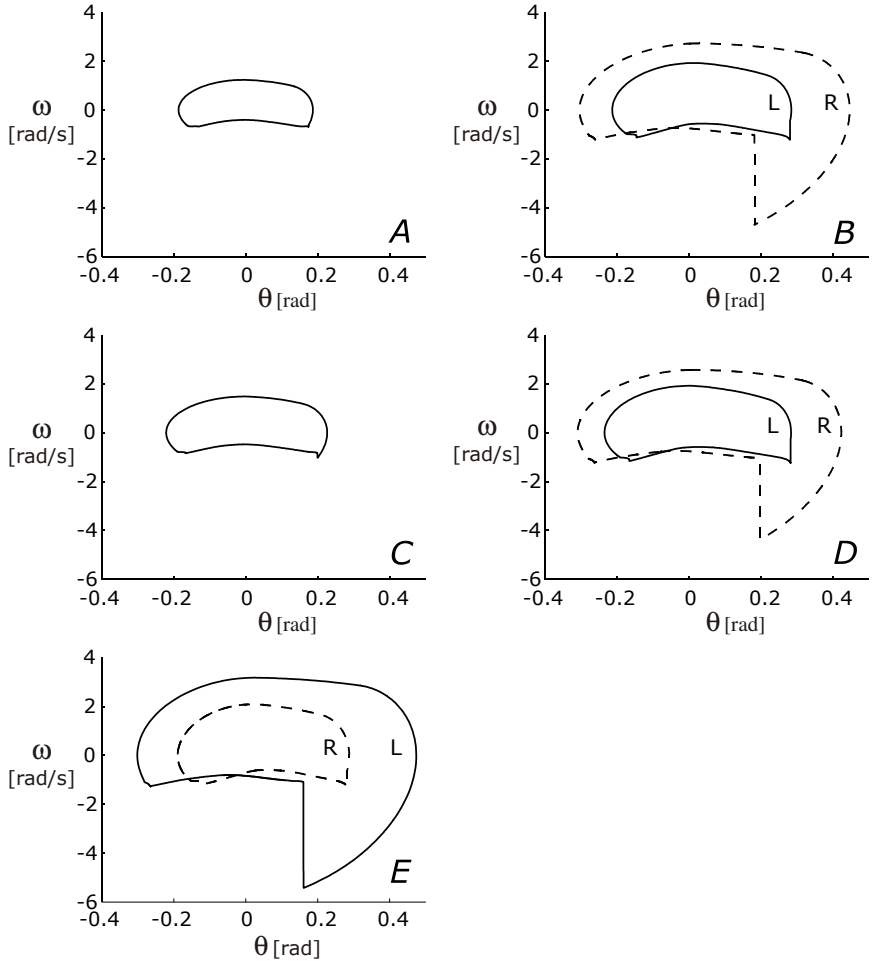

Fig. 6 Phase plane plots of the optimized gaits shown in Table 2; symmetric (*A* and *C*) as well as asymmetric gaits (*B*, *D* and *E*) are found. For asymmetric gaits, the limit cycle of the right leg is dashed and denoted '*R*'; the limit cycle of the left leg is solid and denoted '*L*'.
optimum *A*: only optimized for energy expenditure per unit distance walked (E_m).
optimum *B*: optimized for both E_m and $R_{SLP.}$
optimum *C*: optimized for both E_m and $R_{CGL.}$
optimum *D*: only optimized for robustness against a *Swing Leg Pull* (R_{SLP})
optimum *E*: only optimized for robustness against a *Change in Ground Level* (R_{CGL})

leg that is pulled and it is always the right leg that takes the first step down the change in ground level. The results show that the most robust gaits to cope with these one-sided perturbations are *asymmetric* gaits. For the R_{SLP}-optimum (*D*) the right leg swings much faster than the left leg, for the R_{CGL}-optimum (*E*) the left leg swings much faster than the right leg.

The results also show that optimization is difficult for this highly non-linear gait model: R_{SLP} at optimum *D* is lower than R_{SLP} at optimum *B* (7.5 mm versus 9.0 mm), while the highest value of R_{SLP} is expected at optimum *D*. Furthermore, optimums C and D are found by optimizing only the afferent gains g_p and g_d, while the best results are expected when optimizing *all* gains. It seems that the parameter landscape is full of local optimums, in which the gradient search algorithm can easily get stuck. Although the goal of the optimization in this study is not to find the global optimums, it is interesting to know why this happens. For this reason and for a better understanding of the trade-off between energy efficiency and robustness, the behavior of the gait model is investigated in detail in the next section by changing one parameter over the entire space while keeping all the other parameters fixed.

3.3 Symmetry-breaking bifurcations

Under the influence of changes in gain settings, gait can transform from symmetric to asymmetric gait. In terms of nonlinear system dynamics, *symmetry-breaking* or *pitchfork bifurcations* occur (Nayfeh and Balachandran 1995). When comparing optimum *D* and *E* with starting point *II* it is clear that such a transition can occur when changing two gains. In fact, these pitchfork bifurcations can be found when only one gain is changed. Typically, at a bifurcation the gait becomes linearly unstable; the way it looses local stability indicates the type of bifurcation. For a pitchfork bifurcation, the maximal Floquet multiplier leaves the unit circle through +1.

To illustrate how energy efficiency and robustness change along such a pitchfork, a bifurcation diagram was constructed (Fig. 7), starting from the previously found optimum *B*, with g_p as bifurcation parameter. On the left of the bifurcation point *Q* one stable symmetric branch exists, which becomes unstable at *Q*. Two stable asymmetric branches appear on the right of *Q*, to accompany the unstable symmetric branch (latter not shown in the figure). As an indicator of the change in system dynamics, the maximum of the angular velocity of the right leg, $\omega_{r,max}$ is chosen. Note that g_p is the only coupling parameter that is varied; the parameters g_d, k_{eE} and k_{eF} remain at 0.46, 20.8 and 10.0, respectively.

The two asymmetric solutions that exist for each g_p>16.3, are each other's exact *mirror image*: movement of the right (left) leg at the upper branch

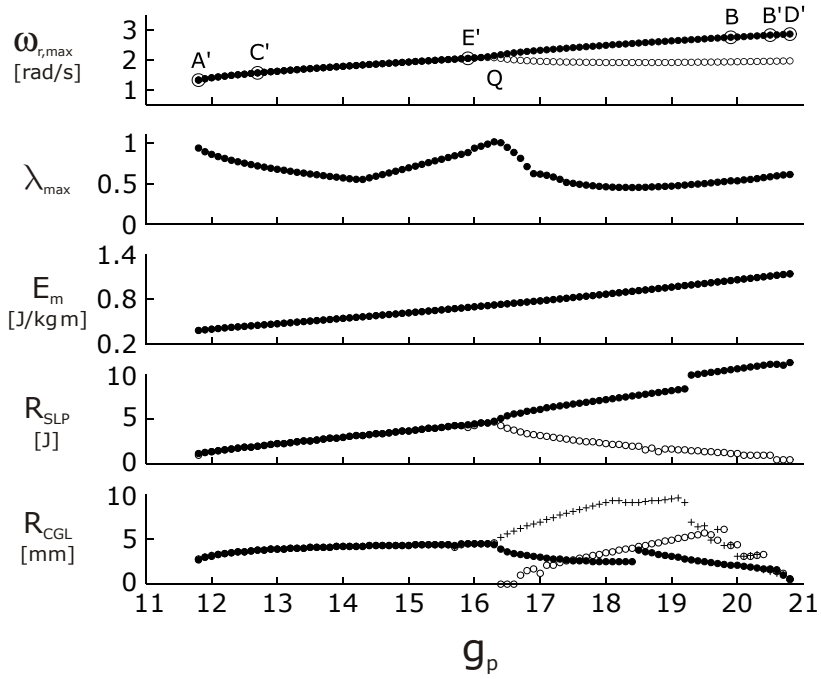

Fig. 7 Energy efficiency and robustness along a pitchfork. The data from the upper branch is marked by black dots, the data from the lower branch with white dots. The pitchfork diagram was constructed starting from optimum *B* (indicated by the circle *B* at g_p=19.9) and changing g_p with steps of 0.1. The maximal angular velocity of the right leg $\omega_{r,max}$ during a gait cycle represents the system dynamics. The maximum multiplier λ_{max} goes through 1 at the pitchfork bifurcation *Q*. For λ_{max} and the energy expenditure E_m both branches are identical, while the pitchfork *is* visible for the robustness against a swing leg pull, R_{SLP}, and for the robustness against a change in ground level, R_{CGL}. The 'plus signs' in the R_{CGL} plot show the robustness for the lower branch, if recovery to the other (upper) branch is considered valid. Local optimums along the pitchfork, for the five object function cases given by Eq. 16, are denoted *A′* - *E′* (see Table 3).

equals movement of the left (right) leg at the lower branch. Note that for gains g_p lower then 11.8 and higher then 20.8 co-existing invalid gait cycles emerge (no foot clearance). The slightest perturbation brings the walker from the valid to the invalid gait cycle. These gait cycles with no robustness are not interesting for our study and therefore not shown.

Figure 7 shows that the normalized energy expenditure per unit distance E_m rises fairly linear with increasing g_p, with almost the same slope before and after the bifurcation point *Q*. The transition from symmetric gait to asymmetric gait does *not* cause an exponential increase in energy

Table 3 The (local) optimums found when analyzing along the pitchfork of Fig. 7.

	Optimums found	***A'***	***B'***	***C'***	***D'***	***E'***
Settings	*Object function case* $J(\sigma,R_\tau)$					
	Weighing factor σ	0	0.5	0.5	1	1
	Robustness measure R_τ	-	R_{SLP}	R_{CGL}	R_{SLP}	R_{CGL}
	Branch	-	Upper	Lower	Upper	Lower
	Optimized parameter g_p	11.8	20.5	12.7	20.8	15.9
Results	E_d [J/m]	28.9	83.2	34.0	85.4	51.9
	E_m [J/kgm]	*0.39*	*1.11*	*0.45*	*1.14*	*0.69*
	R_{SLP} [J]	1.0	9.7	2.0	9.9	4.1
	R_{CGL} [mm]	2.8	1.7	3.8	0.6	4.5
	λ_{max}	0.94	0.58	0.46	0.62	0.48

expenditure. The robustness against a swing leg pull R_{SLP} is clearly higher for the upper branch than for the lower branch, and rises fairly linear with increasing g_p as well. The results for the robustness R_{CGL} against a change in ground level are less straightforward. Firstly, gait cycles on the lower branch can hardly stand any perturbation to the right of the bifurcation point, while these gait cycles should be able to resist higher perturbations than those of the upper branch from a mechanical point of view (see discussion in Sect. 4.2). This is especially true for gains adjacent to the bifurcation point. The reason is that for perturbations beyond a certain threshold, recovery is towards the other (upper!) branch, which is not regarded as a valid recovery in this study. In the plot for R_{CGL} in Fig. 7, the 'plus signs' indicate what R_{CGL} would be for the lower branch, if recovery to the other branch *would* be seen as a valid recovery. This shows a considerable increase in robustness (R_{CGL}=9.9 mm). Secondly, Fig. 7 shows a lot of irregular jumps in the maximal allowable perturbation R_{CGL} for the branches to the right of the bifurcation point *Q*. A possible explanation for the occurrence of these jumps could be that for this type of perturbation the assumption does *not* hold that if the walker can recover from a perturbation size *Δ,* it can recover from all perturbations smaller than *Δ*! To test this idea, we calculated the *actual* robustness against *all* changes in ground level for the upper branch. This is

shown in Fig. 8. The gray areas represent all the perturbations from which the walker recovers. The large gray area has a rather surprising form, with a sort of an oblique peak pointing backwards around gains 18.1-18.6. The large jump in the value for R_{CGL} around the gain g_p of 18.5 is due to this peak. Interestingly, there are also three smaller areas of high perturbations from which the walker recovers (top left corner of Fig. 8). The other two branches – the lower branch where recovery to the upper branch *is* and *is not* regarded valid – probably also have areas of recoverable perturbations with complex shapes. In conclusion, recovery from a certain change in ground level does not guarantee that the walker will recover from all smaller ground level changes.

The optimization routine finds the maximum perturbation by first trying large steps and then, if not successful, smaller steps (see Sect. 2.4). In other words, it will sometimes find high values for R_{CGL} while the walker cannot recover from smaller perturbations, because the optimization routine steps over the areas of non-recoverable perturbations in those cases. This is the reason why Fig. 7 shows many irregular jumps.

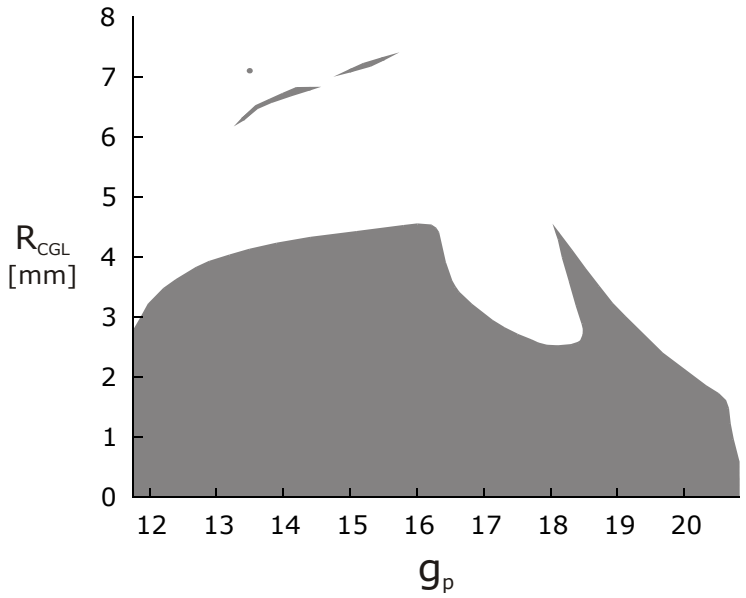

Fig. 8 The actual robustness against a change in ground level, R_{CGL}, for the upper branch of the pitchfork shown in Fig. 7. The gray areas represent the changes in ground level for which the walker recovers, plotted against the same range of positional gains g_p as in Fig. 7. Note that recovery from a certain change in ground level does not guarantee that the walker also recovers from all smaller changes in ground level.

The *local* optimums for the five object function cases (Eq. 16), when looking *along* the pitchfork where only g_p is varied*,* are indicated with *A′-E′*. They are given in Table 3 and marked in Fig. 7. The ranges for energy efficiency and robustness found along this branch are comparable to those found in the optimization results in Sect. 3.2 (Table 2). Note that optimum A′ is completely at the left of the pitchfork, representing the least energy expenditure possible; optimum D′ is completely at the right of the pitchfork, giving the largest possible robustness against swing leg pulls; optimum C′ and B′ are compromises and lie between the extremes A′ and D′; optimum E′ is stuck at a local minimum close to the bifurcation point (see Sect. 4.2 for the reason why).

The same types of pitchforks also occur when changing the value of g_d. A fundamental difference between a g_p-pitchfork and a g_d-pitchfork is their direction: the latter has two stable asymmetric branches for low values of g_d and one symmetric branch for higher values of g_d. Recall that optimum *A* is the optimum found for energy efficiency and has a symmetric gait. When choosing g_d as the bifurcation parameter and starting from optimum *A* (here g_d=0.34, Table 2), indeed a pitchfork is found: asymmetric gait is found when g_d is lowered past g_d=-0.06. Noticeably, the value of g_d can even be lowered to g_d=-0.2 along this pitchfork before becoming unstable. Apparently, stable symmetric gaits are possible without any velocity feedback. Increasing g_d from (energy) optimum *A* immediately leads to instability. Just as for the pitchfork of Fig. 7, the energy efficiency optimum lies on the outer boundary of the symmetric branch. For k_{eE} and k_{eF} no pitchforks have been found with considerable stable regions at both sides of the bifurcation point. Bifurcations only occur at the outer stability boundaries of k_{eE} and k_{eF}, where solutions become unstable almost immediately.

3.4 Explaining differences in energy expenditure

For suitable coupling gain settings, *mutual entrainment* takes place between the mechanical system and the CPG. Importantly, g_p must be chosen much higher than g_d (Table 2). In these cases, the sensory input $s_j(t)$ is dominated by the angle $\theta_j(t)$ of leg j (j={*r,l*}*).* Effect of this mutual entrainment is that both the mechanical system and the CPG oscillate in the same frequency, and the phase difference between the two is constant (i.e. phase-locked). This synchronization between actuation signals and leg movement results in steady and stable gait. By changing the coupling gain settings, the amplitude and frequency of oscillation change considerably. However, the phase difference largely remains the same and the CPG-output has a similar shape for all (stable) coupling gain settings. The actuators are active about 80% of the gait cycle, with an *extension phase* around *heel strike* and a *flexion phase* around *toe-off*. For higher frequencies, this percentage decreases. Figure 9 shows the sensory input and actuation signals normalized to the gait cycle

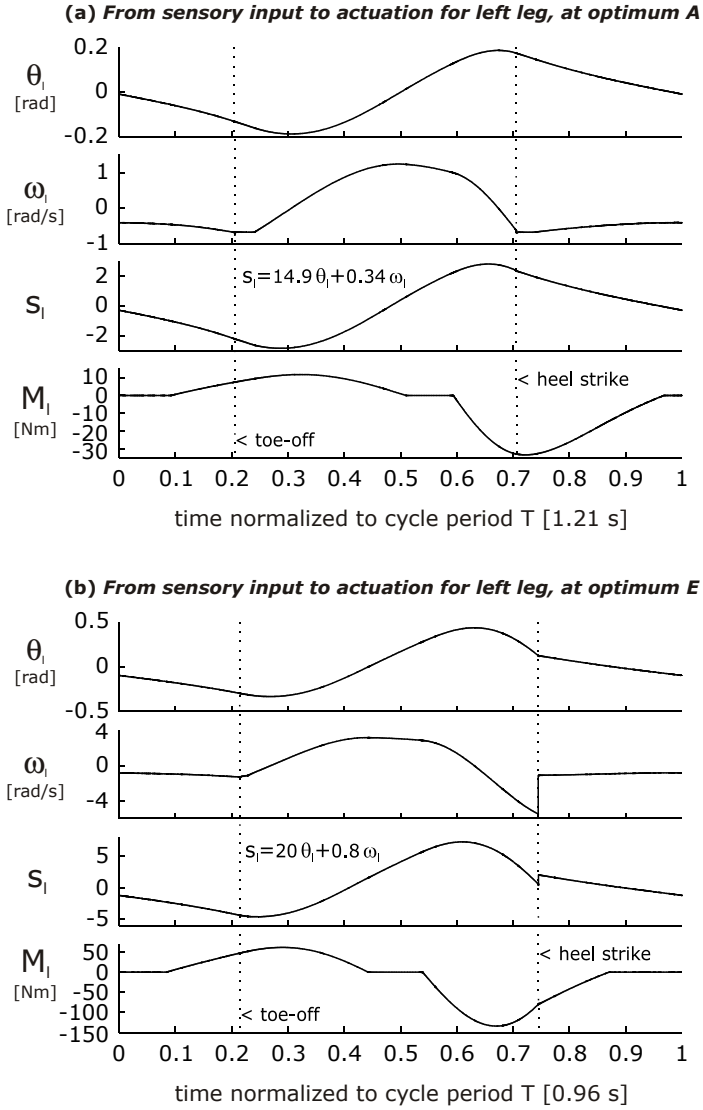

Fig. 9 Actuation and sensory signals of the left leg for (a) symmetric gait (optimum *A*) and (b) asymmetric gait (optimum *E*). The sensory input s_l to the CPG of the left leg consists of feedback of the leg angle θ_l and angular velocity ω_l weighed by their respective afferent gains g_p and g_d. The CPG output is converted to the hip moment of force M_l by efferent gains. Note that the actuation cycle in both cases is of similar shape: an extension moment of force around heel strike (swing to stance) and a flexion moment of force around toe-off (stance to swing). Due to slight changes in timing however, both gaits differ considerably in energy efficiency (see Fig. 10). The dotted lines indicate heel strike (t=0.71, 0.75) and toe-off (t=0.21, 0.22).

and compares gaits at optimum *A* (E_m=0.29 J/(kgm)) and optimum *E* (E_m=1.43 J/(kgm)).

The explanation for the large differences in energy efficiency primarily lies in the amount of energy expended during the first part of the extension phase, before *heel strike*. By starting the extension phase well before heel strike, the CPGs make sure the leg's angles remain within acceptable limits (due to this active pull during end of swing phase, θ_{max} is about 25% smaller than for a freely swinging pendulum of same inertia). However, due to large impact losses at heel strike, the energy expended during this first part of extension phase is canceled out and cannot contribute to an increase in step length and step frequency. In view of energy efficiency, the percentage of total energy expended during this first part of extension phase should be as low as possible.

For increasing swing velocities, the percentage of total energy expended during the first part of extension phase increases exponentially. This is due to the occurrence of two timing changes, shown here by comparing optimums *A* and *E*. Firstly, heel strike timing is delayed (relative to the gait cycle): t_{hs}/T=0.75 for *E* compared to 0.71 for *A*; toe-off timing remains almost constant around t_{to}/T=0.21 since changes in gait are primarily due to changes in the swing phase (i.e. swing phase determines when and where the foot is placed). Secondly, the extension phase starts earlier for the faster swinging leg: t/T=0.54 for optimum *E* compared to t/T=0.60 for *A*. Consequently, an increased and significant part of the extension phase falls before heel strike. Since this is also the part of the gait cycle where the highest angular velocities occur, the power supply and consequently the energy expenditure during this phase rises exponentially. Figure 10 shows that at optimum *E*, this phase accounts for 67% of total energy expended while at optimum *A* this is only 16%.

3.5 Perturbation size

The perturbations from which robust walkers can recover are quite large, as illustrated in Fig. 11 below for optimum *B*. It shows how the walker recovers from a Swing Leg Pull of –9.0 J, requiring 19 gait cycles to return to its limit cycle (for the naked eye however, recovery takes about 5 cycles). Figure 11 also shows that the walker is being perturbed far outside the local region of the limit cycle, where linear stability analysis is no longer valid.

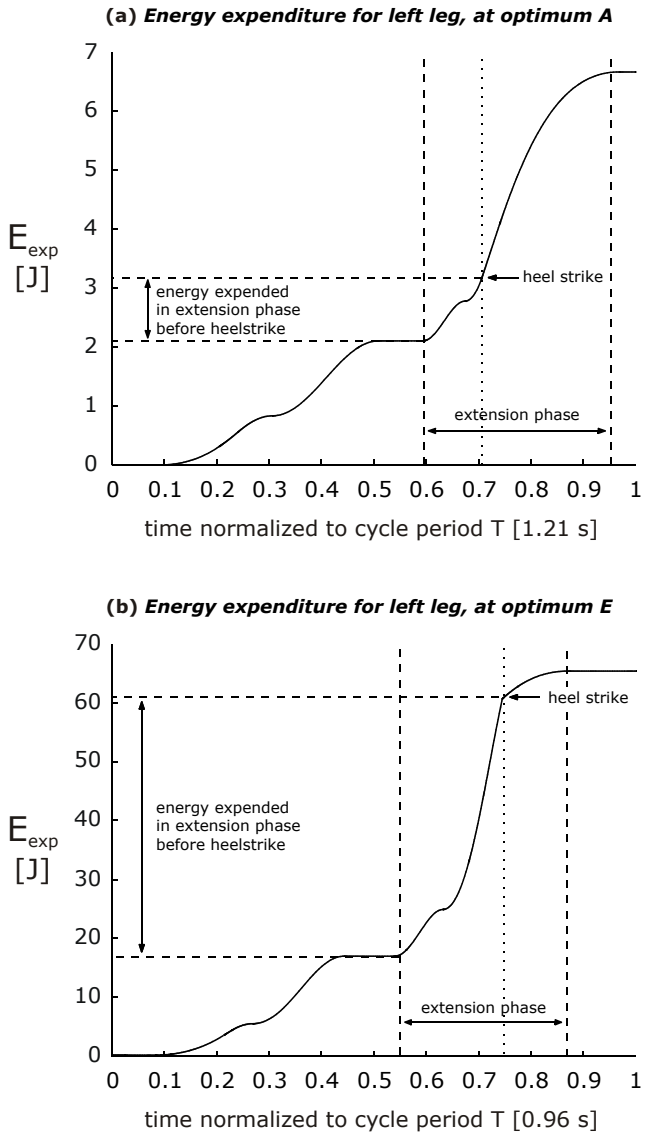

Fig. 10 Energy expenditure E_{exp} during a gait cycle for the left leg at (a) optimum *A* and (b) optimum *E*. At *A*, the optimum for energy efficiency, the first part of the extension phase up till heel strike only accounts for 16 % of the total energy expenditure. For the robustness optimum *E* however, this is about 67 %.

(a) ***Sensor signals and actuation during recovery (right leg, optimum B)***

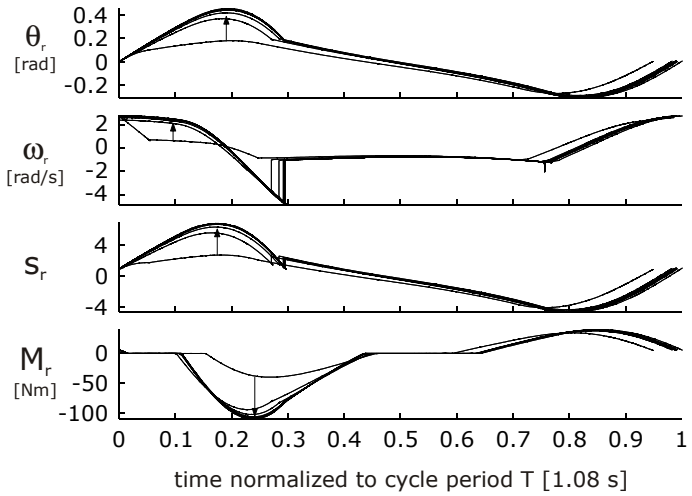

(b) ***Phase plot of recovery from a perturbation (optimum B, SLP=-9.0 J)***

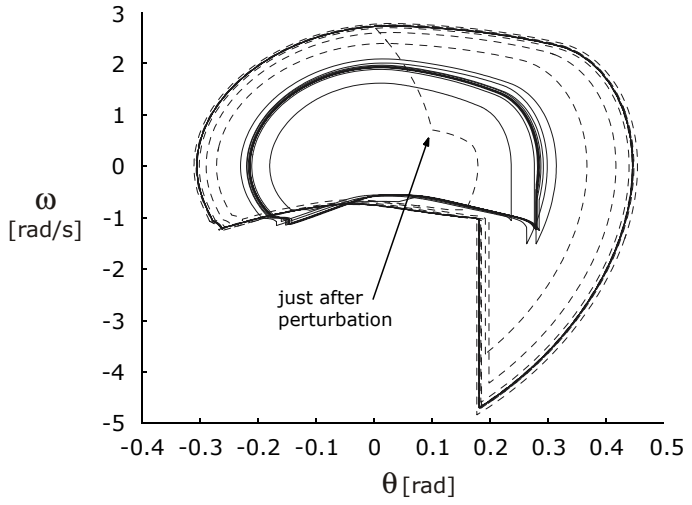

Fig. 11 Recovery from a perturbation of the right swing leg of –9.0 J. The gain settings are those of optimum *B*. (a) Actuation and sensory signals of the *right* leg during recovery (compare with Fig. 9). The arrows indicate the direction of recovery, starting from the first cycle after perturbation. (b) Phase plane plot showing two 2d-projections of the recovery towards the gait's limit cycle: the dashed line (towards large cycle) illustrates the right leg; the solid line (towards small cycle) illustrates the left leg. The arrow shows the large decrease of ω_r from 2.7 rad/s to 0.7 rad/s due to the perturbation.

4. Discussion

4.1 Energy efficiency

Energy efficiency of walking is defined in this study as the forward distance a walker travels on a certain amount of energy expended. This definition in itself does not explicitly take the walker's speed into account. By defining gait as having a non-zero speed, the trivial result of a 'standing' walker expending zero energy is excluded. In practice, since stable gait is only found for considerable walking speeds (>0.5 m/s), optimizations were not influenced by this trivial result. Best scores on energy efficiency *were* obtained at lowest walking speeds, but a higher energy expenditure per unit distance did not always correspond with a higher walking speed (compare results in Table 2). Aside from raised kinetic energy levels, other factors had a larger influence on energy efficiency. The most important cause of decreased efficiency is the delayed heel strike for higher angular velocities of the swing leg (Sect. 3.4), because more energy is lost at impact in this case (Fig. 10).

It was shown that very energy efficient gait is achieved for a CPG-controlled bipedal walker by a suitable choice of coupling gains. An optimum for the energy expenditure per unit distance walked, E_d, was found at 22 J/m, which amounts to a normalized energy expemditure E_m of 0.29 J/(kgm) for our 75 kg walker (Table 2, optimum *A*). The walking velocity at this energy level is 0.51 m/s. Our walker is able to achieve higher walking speeds as well. For instance, with gain settings from starting point *III* (Table 1) walking speed is 0.99 m/s at an energy expenditure of 0.83 J/(kgm). Below, the energy efficiency of our walking model is compared with that of humans as well as some other bipedal walking models.

Compared to human walking

Humans are generally considered to walk very energy efficient, as shown by various experiments with human subjects. Waters and Mulroy (1999) measured oxygen uptake of their subjects, and found that *metabolic* energy expenditure for young adults is around 3.1 J/(kgm) when walking at their customary walking speed (around 1.3 m/s). Van der Kooij et al. (2003) performed an inverse dynamics analysis on data obtained from a human subject (80 kg, 1.9 m), walking at 1.28 m/s, and showed that the *positive mechanical work done* by joint muscles for this subject is around 0.8 J/(kgm). When the metabolic efficiency of human muscular labor is chosen at an accepted value of 30%, these two studies yield comparable results for the amount of *mechanical* energy expended.

Since our walker is actuated by lossless moments of force, only its mechanical energy expenditure can be calculated. It is therefore most fair to compare its energy expenditure with the mechanical energy expended by humans, which is, according to the two sources mentioned above, about 0.8 J/(kgm). Hence, our CPG-controlled model can walk almost three times as energy efficient as humans can. Note however, that our model is a 2D model without a trunk, while humans need energy to maintain stability in a 3D environment (e.g. actively swinging the arms and balancing the trunk costs energy). Moreover, when our model is compared with humans when both walking at around 1.3 m/s, our model is expected to be slightly less efficient than humans, though exact data for these higher walking speeds is not yet available.

In real life, power consumption is just as important as energy efficiency. Our most energy efficient walker (optimum *A*, Table 2) has a maximal power consumption of about 20 W, but for the walker that is most robust against changes in ground level (optimum *E*) this is 400 W. For human walking, the latter would mean more than 1200 W (i.e. 16 W/kg) *metabolic* power and would be very exhausting. These amounts of power consumption are only used by humans for running, but not for normal walking (McMahon 1984).

Compared to other bipedal walking models

In *passive dynamic walkers*, only gravitational energy is used for actuation by walking down a slope (McGeer 1990). Although often seen as being energy efficient, this is only true for low slopes, with correspondingly low speeds. For the test biped of McGeer (3.5 kg), stable gait was found at a slope α of 0.025 rad with (low) corresponding speed of 0.1 m/s. At low slopes, the (gravitational) energy expenditure is proportional to the slope and in this case equals $g\sin(\alpha)$=0.24 J/(kgm). At higher slopes, and correspondingly higher speeds, stable gait is not possible.
For the *simplest walking model* – the most simple passive dynamic walker – Garcia et al. (1998) have suggested scaling laws relating slope to walking speed and energy expenditure. They give a prediction of energy expenditure for a 50 kg, 1m-legged person walking at 1 m/s, resulting in E_m=1.2 J/(kgm). Note though, that this walking speeds calls for a slope at which stable passive dynamic walking is not possible! The stability region for the simplest walker is given by α<0.015 rad, stated by Garcia et al. (1998) and verified by Schwab and Wisse (2001).
Van der Linde (1999) simulated a bipedal walking model, whose pneumatic muscles were activated by reflex-like trigger signals. He found an optimum for energy expenditure of E_m=0.33 J/(kgm) at a walking speed of 0.47 m/s, while maximal stable speed achieved was 0.7 m/s (at which E_m=0.55 J/(kgm)). Note that considerable rotational hip stiffness is present in Van der Linde's model (walking speed is varied by varying this stiffness), whereas in

our model the only elastic (i.e. energy storing) parts are in the foot-ground contacts in vertical direction.

We conclude that our walker is among the most energy efficient walkers for all but the lowest walking speeds (<0.1 m/s). Furthermore, it can achieve speeds that are far outside the stable region of the passive dynamic walker, and are higher than the speeds found by Van der Linde as well.

4.2 Robustness

In this study we perturbed the walker in two ways, and expressed robustness as the maximal perturbation the walker can recover from. These perturbations were applied on the *right side* only. The optimums found for robustness were asymmetric gaits. The reason why such an asymmetric gait is optimal for one-sided perturbations is explained below.

Robustness against a Swing Leg Pull

When the swing leg is pulled backwards at midswing, it looses speed. Subsequently, it will fail if its foot does not come above ground at the end of the swing phase (see Sect. 2.2). The best way to cope with this perturbation is to make the angular velocity ω_j at midswing as high as possible. As illustrated in the previous section, angular velocities above a certain threshold value ($=\omega_j$ at a bifurcation point) are only achieved with asymmetric gaits. The branch is chosen where $\omega_r > \omega_l$, as seen for optimum *B* and *D*, because that branch represents the gait solutions for which the perturbed leg has largest angular velocities at the onset of the perturbation.

Forner Cordero et al. (2003); (2005) showed for swing leg perturbations that the most challenging perturbations often trigger a *lowering strategy* in humans, meaning that the perturbed leg is put to the ground as quickly as possible. Smaller perturbations are met by an *elevating strategy*, consisting of an elevation of the swing leg. Thus, the elevating strategy is a more energy efficient, but less robust way of facing perturbations compared to the lowering strategy. Our gait model will always face a perturbation by the elevating strategy, because of the lack of knees in our model. In the future it would be interesting to see if additional knees and corresponding neural control could also trigger the lowering strategy, thereby increasing the robustness against perturbations even further.

Robustness against a Change in Ground Level

When the ground level is suddenly lowered and the right leg is the first leg to encounter this change in ground level, the walker must have the left leg in place fast enough to take over the stance phase from the right leg. Failure occurs when either the left leg is not swinging fast enough, or when the

stance phase of the right leg (following the change in ground level) is too short. Again an asymmetric gait can be seen as the best way to cope with this type of perturbation. In this case it is most favorable to choose the *opposite* branch where $\omega_r<\omega_l$. This asymmetric gait is the best solution for two reasons: Firstly, the left leg's angular velocity in swing phase is much higher than that of the right leg; Secondly, the angle between the legs is higher than for symmetric gaits (0.6 rad versus 0.4 rad when comparing Figs. 6e and 6c, respectively). The latter makes sure that stance phase duration right after perturbation is still considerable.

However, the results found for R_{CGL} along the pitchfork of Fig. 7 seem to disagree with the generality of the mechanical explanation given here. They show that the local robustness optimum *E'* is a symmetric instead of an asymmetric gait. These results are explained by the following two observations: Firstly, at higher perturbations on the lower branch, recovery is towards the other (upper!) branch, which is not regarded as a valid recovery in this study; Secondly, for this type of perturbation the assumption does *not* hold that if the walker can recover from a perturbation size Δ, it can recover from all perturbations smaller than Δ! Both phenomena lead to jumps in the robustness measure R_{CGL} along the parameter axis, which causes the optimization routine to get stuck at local optimum *E'*. Whether asymmetric gait is in general more robust than symmetric gait against this change in ground level, remains to be elucidated. The location in parameter space probably determines if the perturbed asymmetric gait returns to its own or the opposite branch. When recovery to the opposite branch *is* considered valid, the most robust gaits against (one-sided) changes in ground level are probably always found to be asymmetric. However, it is outside the scope of this study to completely analyze the whole parameter space to verify this.

The maximum step-down from which a walker can recover is sometimes used as measure of robustness in gait robots (e.g. Wisse and Van Frankenhuyzen 2003). However, the results of this study show that the ability to recover from a large change in ground level does not guarantee recovery from smaller perturbations. Hence, when using this measure to quantify robustness, careful consideration must be given to whether the walker can recover from all smaller perturbations as well.

4.3 Trade-off between energy efficiency and robustness

The optimums found in this study suggest that a trade-off exists between energy efficiency and robustness. This idea is supported by calculations of the energy expenditure, robustness against swing leg pulls and robustness against ground level changes for gait cycles along a pitchfork (Fig. 7). For symmetric gait a strict trade-off exists for which robustness against both

types of perturbations (i.e. R_{SLP} and R_{CGL}) can simultaneously be increased by expending more energy. For the asymmetric gaits expending more energy results in an increase of one specific type of robustness, while the other decreases.

Applying only one-sided perturbations offered some fundamental insight that would not have been achieved if perturbations were applied on both sides: for a large part of the parameter space, *asymmetric* gaits are the only stable solutions found. Symmetry-breaking bifurcations occur: under the influence of changes in (mainly) g_p and g_d, gait changes from symmetric to asymmetric and vice versa. However, in real life perturbations are most likely to occur on both left and right legs. Moreover, the results in this study (see Fig. 7) show that for symmetric gait increased robustness against swing leg pulls goes hand in hand with increased robustness against changes in ground level, while for asymmetric gait these are inversely related. The energy efficiency of symmetric gait is also found to be higher compared to asymmetric gait. Thus, in an unpredictable environment (i.e. real life situations) a compromise between robustness and energy efficiency will always result in a symmetric gait. This applies to humans as well as bipedal walking robots, as long as the dynamics are symmetric over the sagittal plane (i.e. same inertial properties of the legs, same leg lengths, same neural controller for each leg, etc.). Small asymmetries found in human gait are probably due to small asymmetries in the body.

4.4 Symmetry-breaking bifurcations

The occurrence of bifurcations in itself is not new to bipedal walking research. For passive dynamic walkers, various researchers have identified cascades of period-doubling bifurcations as the mechanism of loosing (local) stability, termed *route to chaos* (Garcia et al. 1998; Thuilot et al. 1997). This route to chaos is perhaps the most well-known and described in many studies (Nayfeh and Balachandran 1995). The symmetry-breaking bifurcations, found in this study, would in fact present themselves as period-doubling bifurcations instead of pitchfork bifurcations if our Poincaré mapping would map a step – and change legs after each step like above-mentioned studies – instead of a stride. Thus, the asymmetric gaits found here are qualitatively similar to the 'limping' gaits found in other gait studies. Therefore, the route to chaos might also exist for our gait model, although it was not encountered. The CPG might prevent or retard this route to chaos. This view is supported by two observations. Firstly, stable asymmetric gaits were found in large parts of the (coupling gains') parameter space, without encountering additional period doubling bifurcations. Secondly, gait becomes unstable almost immediately after leaving this parameter space.

The bifurcation diagram (Fig. 7) provides some fundamental insight in the *relation between local stability and robustness*. It shows that the Floquet multipliers do not predict robustness. Only for small perturbations, after which the gait cycle stays close to the limit cycle, Floquet multipliers are a valid measure for gait stability. From observations during this study it became clear that the Floquet multipliers predict recovery correctly for (Swing Leg Pull) perturbations up to 0.3 J (on a kinetic energy level of 15 J).

4.5 Concluding remarks

Our approach of changing the coupling gains was successful in finding gaits with large differences in energy efficiency and robustness. This great variety of gaits is possible by mutual entrainment between the Central Pattern Generator (CPG), the musculo-skeletal system (i.e. two actuated legs with a large mass on top) and the environment (i.e. ground reaction forces). The skeletal part on its own can *not* walk stably down a slope passive-dynamically, because our gait model possesses human-like inertial properties. The CPG plays a key role in the sense that it not only stabilizes the unstable oscillator, comprising the skeletal system and foot-ground contact, but also allows for a great variety of different gaits in terms of energy efficiency, robustness, velocity, step frequency and stride length. In this study we focused on energy efficiency, robustness and the trade-off between them. Our walking model is found to be very energy efficient when compared to humans as well as to other bipedal walking machines. Very robust gaits are found as well: the walker can even recover when its swinging leg is deprived of 70% of its angular velocity. For the perturbations used in this study, a strict trade-off between energy efficiency and robustness exists, especially for symmetric gait (see Fig. 7). For both types of perturbations – swing leg pulls and changes in ground level – large velocities of the swing leg are necessary to cope with large perturbations. This agrees with the statement of Wisse et al. (2005) that you will never fall forward if the swing leg is put fast enough in front of the stance leg. The asymmetric gait solutions found in this study clearly show that the swing leg velocity of the *perturbed* leg needs to be high enough to cope with large swing leg pulls, while for large changes in ground levels the swing leg velocity of the *unperturbed* leg needs to be high enough in order to guarantee recovery. An important finding for bipedal walking machines similar to our gait model is that recovery from a certain change in ground level does *not* guarantee recovery from all smaller changes in ground level, not even in symmetric gait (see the three small gray areas in Fig. 8). Thus, if the maximal change in ground level is taken as the measure to represent the robustness of a bipedal walking machine, one has to make sure that it also recovers from all smaller ground level changes. The gait model presented in this study achieves a fairly large range of speeds, though not as large as humans, which is probably due

to the lack of knees and feet in our gait model. For large speeds the swing leg is forcefully swung forward (see Fig. 9b) and actively decelerated at the end of the swing phase (see Fig. 10b). This agrees with the suggestion of Forner Cordero (2003) that the ability to swiftly swing the leg plays a key role in determining the maximum walking speed in humans.

References

Arrowsmith DK, Place CM (1990) An introduction to dynamical systems. In. Cambridge University Press, Cambridge, pp 423

Brown TG (1911) The intrinsic factors in the act of progression in the mammal. In: Proc Royal Soc. Vol. B84, London, pp 308-319

Chandler RF, Clauser CE, McConville JT, Reynolds HM, Young JW (1975) Investigation of the inertial properties of the human body. In. Aerospace Medical Research Laboratories, Wright-Patterson Air Force Base, Ohio

Forner Cordero A (2003) Human gait, stumble and. fall? Mechanical limitations of the recovery from a stumble. In: Faculty of Engineering Technology. University of Twente, Enschede, pp 196

Forner Cordero A, Koopman HF, van der Helm FC (2003) Multiple-step strategies to recover from stumbling perturbations. Gait Posture 18:47-59

Forner Cordero A, Koopman HJ, van der Helm FC (2005) Energy analysis of human stumbling: the limitations of recovery. Gait Posture 21:243-254

Garcia M, Chatterjee A, Ruina A, Coleman M (1998) The simplest walking model: stability, complexity, and scaling. J Biomech Eng 120:281-288.

Inman V, Ralston H, Todd F (1981) Human walking. In. Williams and Wilkins, Baltimore

Koopman HFJM (1989) The three-dimensional analysis and prediction of human walking. In: Department of Mechanical Engineering. University of Twente, Enschede, The Netherlands

Kuznetsov YA (1998) Elements of applied bifurcation theory. In: Marsden JE, Sirovich L (eds) Applied mathematical sciences. Vol. 112. Springer-Verlag, New York, pp 591

MacKay-Lyons M (2002) Central pattern generation of locomotion: a review of the evidence. Phys Ther 82:69-83.

Matsuoka K (1985) Sustained oscillations generated by mutually inhibiting neurons with adaptation. Biol Cybern 52:367-376

Matsuoka K (1987) Mechanisms of frequency and pattern control in the neural rhythm generators. Biol Cybern 56:345-353

McGeer T (1990) Passive dynamic walking. International Journal of Robotics Research 9:62-82.

McMahon TA (1984) Muscles, reflexes, and locomotion. In. Princeton University Press, Princeton, New Jersey, pp 331

Mochon S, McMahon TA (1980) Ballistic walking. J Biomech 13:49-57

Nayfeh AH, Balachandran B (1995) Applied nonlinear dynamics: analytical, computational, and experimental methods. In: Wiley series in nonlinear science. Wiley, New York, pp 685

Schwab AL, Wisse M (2001) Basin of attraction of the simplest walking model. In: Proceedings of ASME 2001 Design Engineering Technical Conferences and Computers and Information in Engineering Conference, Pittsburgh, Pennsylvania

Seydel R (1994) Practical bifurcation and stability analysis: from equilibrium to chaos. In: Interdisciplinary Applied Mathematics. Vol. 5. Springer-Verlag, New York, pp 407

Taga G (1995a) A model of the neuro-musculo-skeletal system for human locomotion. I. Emergence of basic gait. Biol Cybern 73:97-111.

Taga G (1995b) A model of the neuro-musculo-skeletal system for human locomotion. II Real-time adaptability under various constraints. Biol Cybern 73:113-121.

Taga G, Yamaguchi Y, Shimizu H (1991) Self-organized control of bipedal locomotion by neural oscillators in unpredictable environment. Biol Cybern 65:147-159

Thuilot B, Goswami A, Espiau B (1997) Bifurcation and chaos in a simple passive bipedal gait. In: Proceedings of IEEE International Conference on Robotics and Automation. Vol. 1, pp 792-798 vol.1

Thunnissen J (1993) Muscle force prediction during human gait. In. University of Twente, Den Haag, pp 221

van der Kooij H, Jacobs R, Koopman B, van der Helm F (2003) An alternative approach to synthesizing bipedal walking. Biol Cybern 88:46-59

van der Linde RQ (1999) Passive bipedal walking with phasic muscle contraction. Biol Cybern 81:227-237

Verdaasdonk BW, Koopman HFJM, Van Gils SA, Van Der Helm FC (2004) Stable walking with central pattern generators. In: Proceedings of the European Society of Biomechanics Congress, Eindhoven University of Technology, 's-Hertogenbosch, The Netherlands

Vukobratovic M, Borovac B (2004) Zero-moment point – Thirty five years of its life. International Journal of Humanoid Robots 1:157-173

Waters RL, Mulroy S (1999) The energy expenditure of normal and pathologic gait. Gait Posture 9:207-31

Wisse M, Schwab AL, van der Linde RQ, van der Helm FCT (2005) How to keep from falling forward: elementary swing leg action for passive dynamic walkers. Robotics, IEEE Transactions on [see also Robotics and Automation, IEEE Transactions on] 21:393-401

Wisse M, Van Frankenhuyzen J (2003) Design and construction of Mike; a 2D autonomous biped based on passive dynamic walking. In: Proceedings of 2nd International Symposium on Adaptive Motion of Animals and Machines, Kyoto, Japan

Appendix A. Model equations

The indices j, n and d in this appendix have the following meaning:
j = {r,l} *leg index*
n = {1,2,3,4} *generalized coordinate index*
d = {x,y} *direction ground reaction force*

This appendix treats the (mechanical) equations of motion as well as the (neural) oscillator dynamics of the CPG (for the latter, see Eq. A.9). Our walker is modeled by a point mass m_h representing the HAT (Head-Arms-Trunk) of the walker, and two rigid legs that each have a mass m_j of 12.2 kg and a mass moment of inertia I_j around the centers of mass.

The approach of Lagrange is followed in deriving the equations of motion. The generalized coordinates vector **q** is defined as the position of one base-point and the two angles of the legs. As a base-point we've chosen the location of m_h:

$$\mathbf{q} = \begin{bmatrix} x_h & y_h & \theta_r & \theta_l \end{bmatrix}^T \tag{A.1}$$

Expressed in **q**, the positions of the legs' centers of mass (m_r,m_l) are given by:

$$\begin{aligned} x_{mr}(\mathbf{q}) &= x_h + l_{com}\sin(\theta_r) \\ y_{mr}(\mathbf{q}) &= y_h - l_{com}\cos(\theta_r) \\ x_{ml}(\mathbf{q}) &= x_h + l_{com}\sin(\theta_l) \\ y_{ml}(\mathbf{q}) &= y_h - l_{com}\cos(\theta_l) \end{aligned} \tag{A.2}$$

The scalar kinetic energy function $T(\mathbf{q})$ is given by:

$$\begin{aligned} T(\mathbf{q},\dot{\mathbf{q}}) = {} & \frac{1}{2}J_r\dot{\theta}_r^2 + \frac{1}{2}J_l\dot{\theta}_l^2 + \frac{1}{2}m_r\dot{x}_{mr}(\mathbf{q})^2 + \\ & \frac{1}{2}m_r\dot{y}_{mr}(\mathbf{q})^2 + \frac{1}{2}m_l\dot{x}_{ml}(\mathbf{q})^2 + \frac{1}{2}m_l\dot{y}_{ml}(\mathbf{q})^2 + \frac{1}{2}m_h\dot{x}_h^2 + \frac{1}{2}m_h\dot{y}_h^2 \end{aligned} \tag{A.3}$$

The scalar gravitational potential energy function $V_g(\mathbf{q})$ is given by:

$$V_g(\mathbf{q}) = m_r g y_{mr}(\mathbf{q}) + m_l g y_{ml}(\mathbf{q}) + m_h g y_h \tag{A.4}$$

Recall that the foot-ground contact forces, consisting of both conservative and nonconservative forces, are $\mathbf{G_f} = \begin{bmatrix} G_{frx} & G_{fry} & G_{flx} & G_{fly} \end{bmatrix}^T$ (see Sect. 2.1). $\mathbf{G_{feet}}$ is expressed in foot coordinates and must be transformed to an expression in generalized coordinates:

$$\mathbf{G}_{\mathrm{n}}(\mathbf{q},\dot{\mathbf{q}}) = \sum_{k=1}^{4} \mathbf{G}_{\mathbf{f}\mathrm{k}}(\mathbf{x}_{\mathbf{f}}) \frac{\partial \mathbf{x}_{\mathbf{f}\mathrm{k}}}{\partial \mathrm{q}_{\mathrm{n}}} \tag{A.5}$$

in which the positions of the feet $\mathbf{x}_{\mathbf{f}} = \left[x_{\mathrm{fr}}\ y_{\mathrm{fr}}\ x_{\mathrm{fl}}\ y_{\mathrm{fl}}\right]^{T}$ are given by:

$$\begin{aligned} x_{\mathrm{mr}}(\mathbf{q}) &= x_{\mathrm{h}} + l_{\mathrm{leg}} \sin(\theta_{\mathrm{r}}) \\ y_{\mathrm{mr}}(\mathbf{q}) &= y_{\mathrm{h}} - l_{\mathrm{leg}} \cos(\theta_{\mathrm{r}}) \\ x_{\mathrm{ml}}(\mathbf{q}) &= x_{\mathrm{h}} + l_{\mathrm{leg}} \sin(\theta_{\mathrm{l}}) \\ y_{\mathrm{ml}}(\mathbf{q}) &= y_{\mathrm{h}} - l_{\mathrm{leg}} \cos(\theta_{\mathrm{l}}) \end{aligned} \tag{A.6}$$

The hip damping moments of force are given by:

$$\mathbf{D}(\dot{\mathbf{q}}) = \begin{bmatrix} 0 \\ 0 \\ -B_{\mathrm{hr}}\omega_{\mathrm{r}} \\ -B_{\mathrm{hl}}\omega_{\mathrm{l}} \end{bmatrix} \tag{A.7}$$

The actuation moments of force of our CPG-controlled hip muscles are given by:

$$\mathbf{M}(\mathbf{q},\dot{\mathbf{q}}) = \begin{bmatrix} 0 \\ 0 \\ k_{\mathrm{eE}} y_{\mathrm{Er}} - k_{\mathrm{eF}} y_{\mathrm{Fr}} \\ k_{\mathrm{eE}} y_{\mathrm{El}} - k_{\mathrm{eF}} y_{\mathrm{Fl}} \end{bmatrix} \tag{A.8}$$

in which y_{Ej} and y_{Fj} are the outputs of the two CPG-neurons per leg j determined by the following set of differential equations. This model incorporates key neural features like the buildup of the neuron's membrane potential – causing the neuron to fire – and a fatigue effect that decreases the neuron's firing rate in time (Matsuoka 1985):

$$\begin{aligned} &\text{flexion neuron } j\text{:} && \begin{cases} \tau_{\mathrm{r}}\dot{u}_{\mathrm{Fj}} = u_0 - u_{\mathrm{Fj}} - \beta v_{\mathrm{Fj}} - w y_{\mathrm{Ej}} - s_{\mathrm{j}} \\ \tau_{\mathrm{a}}\dot{v}_{\mathrm{Fj}} = -v_{\mathrm{Fj}} + y_{\mathrm{Fj}} \end{cases} \\ &\text{extension neuron } j\text{:} && \begin{cases} \tau_{\mathrm{r}}\dot{u}_{\mathrm{Ej}} = u_0 - u_{\mathrm{Ej}} - \beta v_{\mathrm{Ej}} - w y_{\mathrm{Fj}} + s_{\mathrm{j}} \\ \tau_{\mathrm{a}}\dot{v}_{\mathrm{Ej}} = -v_{\mathrm{Ej}} + y_{\mathrm{Ej}} \end{cases} \end{aligned} \tag{A.9}$$

$$\begin{aligned} y_{\mathrm{Fj}} &= \max(0, u_{\mathrm{Fj}}) \\ y_{\mathrm{Ej}} &= \max(0, u_{\mathrm{Ej}}) \end{aligned}$$

With zero sensory input s_j, these equations lead to alternating outputs of $y_{Fj}(t)$ and $y_{Ej}(t)$ in the *endogenous* frequency of the CPG. This oscillation is due to the adaptation or fatigue effect in each neuron given by the state variables v_{Fj} and v_{Ej}, respectively, and the reciprocal coupling of the two neurons given by wy_{Fj} and wy_{Ej}, with w the degree of inhibition. The state variables directly related to the output of the neurons are given by u_{Fj} and u_{Ej}. The constants τ_r and τ_a are the rise time constant and adaptation time constant, respectively. To resemble biological neurons, outputs are always positive, hence the max-operation ($y_{Fj}=\max(0,u_{Fj})$; $y_{Ej}=\max(0,u_{Ej})$). When s_j is a periodic signal, oscillation of the CPG will adapt to the frequency of s_j. The sensory input s_j is as given by Eq. 3:

$$s_j(\mathbf{q},\dot{\mathbf{q}}) = g_p\theta_j + g_d\omega_j \tag{A.10}$$

Together these terms lead to Lagrange's equations of motion:

$$\frac{d}{dt}\left(\frac{\partial T}{\partial \dot{q}_n}\right) - \frac{\partial T}{\partial q_n} + \frac{\partial V}{\partial q_n} = \mathbf{M}_n + \mathbf{D}_n + \mathbf{G}_n \tag{A.11}$$

Parameters used in the equations of motion

m_h	= 50.6	kg	mass of HAT
m_j	= 12.2	kg	leg mass
I_j	= 1.19	kgm^2	moments of inertia around centers of mass
B_{hj}	= 1.09	Nms/rad	joint damping of the hip joints
l_{com}	= 0.38	m	Length between COM and hip of each leg
l_{leg}	= 1.0	m	leg length
g	= 9.81	m/s^2	gravity constant
K_y	= $1\cdot10^5$	N/m	ground stiffness in y-direction
B_y	= $1\cdot10^4$	Ns/m	ground damping in y-direction
B_x	= $1\cdot10^7$	Ns/m	ground damping in x-direction
τ_r	= 0.12	s	rise time constant
τ_a	= 0.6	s	adaptation time constant
β	= 2.5		strength adaptation effect
w	= 2.0		strength of reciprocal inhibition
u_0	= 1.0		tonic input from supra-spinal centers

Appendix B. Optimization routine

The optimization is based on Matlab's constrained minimization routine *fmincon*, which is a gradient search method. During optimization towards the minimum of the object function, fmincon will only vary its optimization parameters, in this case the coupling gains. However, for our specific problem, the initial state vector should be changed as well. After all, our walker has a different limit cycle for each setting of coupling gains. When changing the coupling gains without changing the initial state vector, the walker has to walk from the old limit cycle to the new one, but will often fail to reach it. Therefore, fmincon will only find stable solutions in the neighborhood of its starting position, resulting in a very local and often poor solution. By using a *mediator* function between the fmincon function call and the function that evaluates the object function, much better results are achieved. The mediator function maintains a look-up table for stable solutions, which contains the gain settings and corresponding initial state vectors.

Hence, one iteration cycle of the optimization routine goes as follows. The mediator function receives a new set of coupling gains from fmincon, compares it with gain settings already available in the look-up table and picks out the initial state vector that is closest by. It then calls the file that evaluates the object function (see Fig. B.1) with the coupling gains from fmincon and the new initial state vector. When the walker achieves stable gait, the value of the object function $J(c)$ is passed to fmincon and the look-up table is updated with the newly found values. Otherwise, a penalty value of 1000 is returned for $J(c)$ (see Sect. 2.2 for possible failure mechanisms).

The evaluation of the object function is shown in Fig. B.1. It starts in the upper left corner. It then goes down on the left to calculate the energy expenditure for the given walker. It continues with the loop in the right part of the flow diagram to calculate its robustness against perturbations. This is expressed as the maximal perturbation the walker can recover from. To find this maximum, the perturbation applied is increased with stepsize *dpert* each loop. When the maximum is found, the evaluation of the object function is complete.

The settings used for the optimization were such that sub-optimal solutions could be found throughout the parameter space in a relative short time. The fmincon-specific options used are *DiffMinChange=0.1* and *MaxFunEvals=80*. This leads to a satisfactory detail in gain settings tried, and greatly improves overall calculation times. To make sure all four optimization parameters in the coupling gain vector $\mathbf{P_{cg}}$ are in the same order of magnitude, $10g_d$ was used during optimization instead of g_d. Furthermore, boundaries for all four

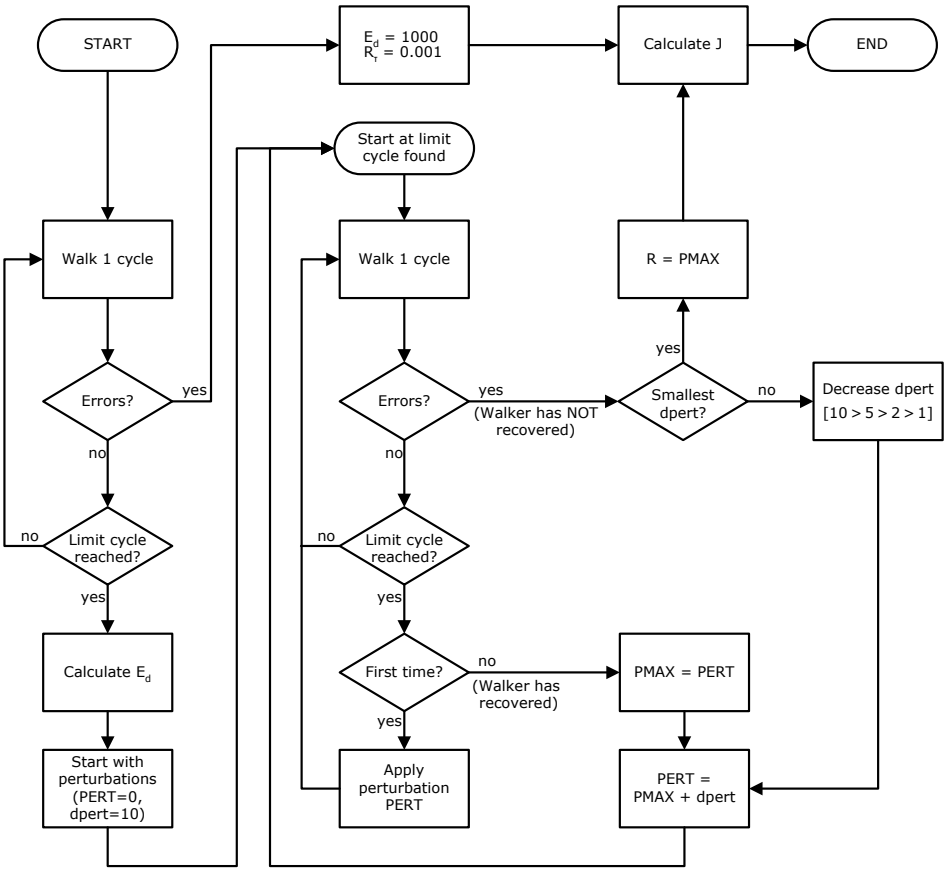

Fig. 12 Flowchart illustrating the evaluation of the object function *J*. The energy expenditure E_d and the robustness R_T (R_{SLP} or R_{CGL}) are calculated subsequently and result in a value for *J* (see Eq. 15).

optimization parameters in $\mathbf{P_{cg}}$ were chosen: for each the lower bound is set to 0 and the upper bound to 30. These boundaries keep calculation times acceptable. Note that for starting point *III* (Table 1), k_{eE} is already at its boundary value. Most other gain settings found in this first phase were much lower however. If an optimum found has one or more gains set at its boundary value, an optimization is repeated with a higher upper bound.

Optimizations were performed on two PCs: an Intel P4 1.80 GHz with 256 MB RAM and an Intel P4 3.0 GHz with 1 GB RAM. Although above-mentioned settings allowed for relative short calculation times, the necessary time to recalculate the total optimization is estimated to be still around 400 hours for the second PC.

Chapter 7

Conclusions

1. Discussion

1.1 Is the paradox solved?

The goal of the research presented in this thesis was to find the principles of neural control that make human walking both efficient and robust. Being simultaneously efficient and robust at the level displayed by human walking seems contradictory. Research in the fields of biomechanics and robotics *has* provided us with models of bipedal walking that display either great efficiency (Collins et al. 2005; Garcia et al. 1998; McGeer 1990) or robustness (Hirai et al. 1998; Sakagami et al. 2002). However, a model that incorporates gait control that reconciles both qualities to the standard of human walking is lacking. The *efficient* gait control of the models is mostly based on *ballistic walking* (Mochon and McMahon 1980), which compensates for the energy lost at heelstrike by a push-off at the end of the stance phase. Efficiency is achieved by letting the natural exchange between potential and kinetic energy of the pendulum-like legs determine the gait movement: the natural dynamics of the walker are exploited. However, the intermittent control allows perturbations to accumulate during the swing phase into a large foot placement error from which the walker cannot recover. Hence, this type of gait control lacks robustness against perturbations. *Robust* control of bipedal gait models is often *trajectory-based* (e.g. Azevedo et al. 2004; e.g. Hirai et al. 1998; Mu and Wu 2003; Park and Chung 2000; Tzafestas et al. 1996). By forcing the joints to follow a predefined trajectory, a robust gait is obtained, which can *look* quite natural (e.g. by copying the joint trajectories of normal human walking). However, the chances that the predefined trajectory comes close to the natural movement of the walker are very small indeed. As actuating a system outside its natural movement costs a lot of energy (e.g. compare the energy costs of moving a mass-spring-damper system in its resonance frequency with moving it far below or above the resonance frequency), trajectory-based gait control is generally not efficient.

Has the research presented in this thesis brought us closer to solving the paradox of human walking being both efficient and robust? Our analysis has shown at least that in principle the existence of central pattern generators (CPGs) in the human spine can contribute to the reconciliation of robustness and efficiency in walking. Given the proper types of afferent feedback, the CPGs entrain to the musculo-skeletal part of the walker and its environment in such a way that it exploits the natural dynamics, leaving the natural motion of the walker almost untouched. Just as in ballistic walking, this guarantees efficiency. However, unlike ballistic walking, perturbations cannot accumulate to produce large foot placement errors, because the CPGs will continuously pull the perturbed system back to the limit cycle of walking. This continuous control accounts for the increased robustness against

perturbations when compared to the intermittent control in ballistic gait models. Although human walking is much more intricate than the CPG-controlled gait models presented in thesis, our research has shown that CPGs and their embedding in the central nervous system could play a key role in solving the paradox of human walking being both efficient and robust.

1.2 Limitations

The models developed in this thesis are deliberately very basic in nature. Their goal was to illuminate the influence of low-level spinal control and come to an understanding of how it is possible that human walking is both efficient and robust. Therefore, these models cannot be used for prediction, but only to explain certain behavior on a qualitative level. Control of human stance and walking is much more complex than considered in this thesis. Besides spinal control, sensory information from vision, the vestibular system and mechanorecepors in muscles and skin is integrated in the human brain to contribute to a better balance. Furthermore, phasic modulation of spinal reflexes during walking (Brooke et al. 1997; Stein and Capaday 1988; Zehr and Stein 1999), such as the stumble correction reflex and reflex reversal, is not included in our models. Mechanically, our gait models lack knees and feet, which makes them much more vulnerable for perturbations. It is therefore not surprising that the human resilience against perturbations still surpasses that of our gait models. Finally, our models are simulated in a two-dimensional space, while real-life three-dimensional space brings along additional challenges regarding balance, such as lateral stability.

1.3 Applications

Given the proper sensory information, the CPG model presented in this thesis is a highly adaptive, efficient and robust controller for rhythmic movements, including walking. The mathematical compactness of the model (four first order low-pass filters per CPG) do not ask for great computing power nor memory. In other words, the CPG model is ideal for implementation in real-time microprocessor applications. Coupling between CPGs and CPGs with more than two neurons can give rise to more complex rhythmical patterns (Matsuoka 1985; Matsuoka 1987).
Possible applications fields are rehabilitation, bionics and robotics. In active knee-joint prostheses for example, the CPG controller could act as basic rhythm generator that entrains to the walker to provide the actuation signals on the right time. Reflex-like local feedback could be added to increase the robustness (see Ch. 4). The gait could be adapted to the user's intention by supplying sensory information of the healthy leg to the CPG. If the user makes larger or fasters steps with his healthy leg, the CPG will adapt to this information and faster or larger steps of the actuated leg – and thus a faster gait – will be obtained. Another way for the user to influence the gait quality

could be by providing the controller with EMG information of the muscles above the knee prostheses. The EMG information could be used as feedforward signal for the controller, or the user could change the knee joint stiffness by giving certain pulses of muscle activity. In the latter case the CPG will adapt to the changed knee joint stiffness; higher joint stiffness will result in a faster swing. The CPG could also entrain to the gait of people with a hip-knee-ankle-foot orthosis, acting as timing device for functional electrical stimulation. In bipedal walking robots, CPGs could act as basic gait controllers, providing efficient and robust control (see Ch. 5 and 6). Another example where these controllers could be used is in industrial robots that have to perform repetitive rhythmical tasks.

It is noted that in most applications, the CPGs alone are not sufficient. In applications regarding gait, CPGs provide robustness against perturbations in the sagital plane. However, walking in three-dimensional space adds two degrees of freedom – yaw and roll – that cannot be easily stabilized by CPGs. In bipedal robots, yaw and roll can be stabilized mechanically (Wisse et al. 2001). An alternative that could also be applied for active prostheses and orthoses is to add a kind of equilibrium controller for keeping balance in the frontal plane. The CPG would then effectively see a two-dimensional walker that can be controlled efficiently and robustly, as shown in this thesis. For active prostheses and orthoses safety is of the utmost importance and has to be guaranteed. Knee buckling, for example, has to be prevented. Moreover, functions like switching from posture to gait and back have to be added and possibly feedback to the user is wanted.

In summary, the CPGs' ability to adapt to the dynamics of the total system including environment will allow it to be used as a basic rhythm generator or timing device in a larger system controller, thereby playing a key role in the efficient and robust control of rhythmic movements such as walking.

2. Conclusions and future directions

2.1 Conclusions

To get towards an understanding of efficient and robust control of bipedal walking, as displayed by human beings, a bottom-up approach gave rise to three research questions. The research reported in this thesis is an effort to find answers to these questions. The findings are stated below.

- What is the influence of different components of reflexive feedback on postural stability and associated dynamical behavior?

  To obtain a stable posture the total stiffness of the joints should be positive. Gravity causes a negative stiffness in joints that need to uphold a body part with a center of mass above the joint position. Examples of this are the ankle joints in a standing person (Ch. 2) and the elbow joint in an upright forearm (Ch. 4). The negative gravitational stiffness needs to be compensated by the muscles in order to remain standing. Co-contraction is the most straightforward way to increase joint stiffness, but consumes a lot of energy. Reflexive feedback of muscle lengthening is a much more efficient way to increase joint stiffness, but time delays – and in lesser part activation dynamics and visco-elastic tendon dynamics – add considerable phase lag to the reflex loop, endangering the stability of posture. Reflexive feedback of muscle velocity adds phase lead and is necessary to compensate for time delays in the reflex loop (Ch. 2).
  The two ways in which reflexive feedback can become unstable are associated with bifurcations. Zero joint stiffness is associated with the fold bifurcation, while postural instability by a combination of high reflex gains and phase lag is associated with a Hopf bifurcation. Beyond the latter stable periodic movement emerges that corresponds to a neural deficiency, termed clonus. Branches of fold and Hopf bifurcations divide the parameter space of reflex gains in areas of stable and unstable posture. Within the area of stable posture, dynamical properties such as damping, stiffness and resonance frequency depend on the reflex gains (Ch. 2). These dynamical properties are also important for rhythmic movement. For example, to achieve efficiency in arm swinging (Ch. 4), people 'choose' their reflex gains in such a way that low joint damping is obtained.

- Can the co-existence of CPGs and reflexes explain observed efficient and robust rhythmic limb movement?

  CPGs are able to entrain to the limb dynamics in such a way that efficient and robust rhythmic limb movement is obtained. The efficiency is achieved by resonance tuning: the CPG tunes into the resonance frequency of the limb. Chapter 3 explains which types of afferent input are necessary and sufficient for the CPG to obtain this resonance tuning behavior. Feedback of positional information provides resonance tuning above the endogenous frequency of the CPG. Integral feedback provides resonance tuning at and below the endogenous frequency. Analogous to the local reflex loop, feedback of velocity information is necessary to compensate for the time delay in the loop that couples the CPG to the limb muscles. The non-linear properties of the CPG make it very robust against changes in limb parameters. Chapter 3 shows that this non-linearity results in a dependence of the gain of the CPG's transfer functions on input amplitude and that the CPG is therefore able to entrain to a broad range of different limb dynamics. Chapter 4 presents a model of the forearm in which the CPG loop co-exists with the local reflex loop. The CPG entrains to the limb dynamics, which are shaped by the local reflex loop. Efficiency is also achieved by resonance tuning in this highly non-linear neuro-musculo-skeletal model, just like observed in human arm swinging. Force perturbations on the forearm in upright position show that both reflex loop and CPG take part in counteracting environmental perturbations.

- Can both efficiency and robustness be achieved in CPG-controlled walking or is there a trade-off between these gait qualities?

  In chapter 5 it is shown that a neural oscillator – consisting of one locally coupled CPG per hip joint – achieves efficiency comparable to passive dynamic walking. Efficiency is obtained by positional, derivative and integral feedback, similar to the models of rhythmic limb movement in chapter 3 and 4. This way, the CPGs hardly affect the natural limit cycle of passive dynamic walking, but add robustness against perturbations (this was observed during simulations for chapter 5, though not shown here; robustness is treated in chapter 6) and controllability of gait velocity (see Ch. 5). The adaptability of the CPGs to changing dynamic properties of the walker's mechanical oscillator (i.e. the passive walker) is shown by adding hip stiffness: resonance tuning enables the CPGs to entrain to the gait's new natural limit cycle, which has shorter stride length and period. Although in human walking the gait velocity is not changed by

a change in hip joint stiffness, reflexes (e.g. the hamstring and quadriceps reflexes) could be modulated to change the dynamical properties of the musculo-skeletal part to which the CPGs are coupled. The CPGs will adapt to this and a new gait cycle is obtained, for example with increased velocity. Chapter 6 shows that CPGs are able to stabilize gait models that are inherently unstable due to human mass distribution (i.e. it is unable to walk passively down a slope, as displayed by passive dynamic walkers). Although stable gait cycles that are both efficient and robust are obtained for many combinations of afferent and efferent coupling gains, a clear trade-off is visible between efficiency and robustness against perturbations, especially for normal symmetrical gait.

2.2 Future directions

The goal of the research presented in this thesis was to find the principles of neural control that make human walking both efficient and robust. The outcome of the performed modeling and simulations suggest that CPGs could play a key role in achieving such robust and efficient gait. However, the research of this thesis is qualitative in nature. To progress towards models can be evaluated quantitatively, I would recommend adding complexity in a bottom-up way, extending the gait model step by step. The first step would be to add knees and feet. Without knees, it is impossible to overcome large obstacles and feet add robustness (McGeer 1990; Wisse and Van Frankenhuyzen 2003). Muscle dynamics, cutaneous (i.e. related to the skin) and load (i.e. related to force) reflex mechanisms, and reflex modulation – such as the stumble correction reflex and reflex reversal – should be incorporated next. Ultimately, a three-dimensional gait model including supraspinal control and integration of all sensory information would be desirable, but this would require a lot more physiological data than is currently available. More physiological information of the embedding of CPGs and reflexes in the CNS, supraspinal gait control and sensory integration is necessary to develop valid gait models. At present, modeling and experimental physiology are more or less separate disciplines, while they need each other to progress. More collaboration between these fields is necessary to extent our knowledge of human walking in the future.

With respect to active orthoses and lower-limb prostheses, it has to be investigated how the CPG models can be incorporated in a controller that is safe and can be utilized – besides gait – in posture and more complex tasks such as initiating and stopping gait, turning corners and stair climbing. Another point of investigation is the sensory information that has to be supplied to the CPGs to obtain the best adaptive gait behavior. Besides local coupling to the actuated joint, sensory information of the healthy leg is probably necessary to obtain a more robust and adaptive gait pattern.

Another idea is to entrain a CPG model to the healthy leg as well and couple it to the CPG model of the affected leg.

Not many bipedal gait robots have been built that use CPGs to generate locomotion. In most of them, the CPGs are used as trajectory generators with merely phase resetting of the CPG oscillators to ensure entrainment between the CPGs and the robot's mechanics (e.g. Morimoto et al. 2006; Righetti and Ijspeert 2006). This approach still 'forces' the robot to entrain to a desired trajectory and is not likely to exploit the natural dynamics of the robot. Only a few bipedal gait robots use sensory feedback to obtain stable walking by entrainment between the CPGs and the robot's mechanics (Endo et al. 2004; Tenore et al. 2007). However, as far as I know, none were developed with the right sensory feedback to provide not only robust and adaptive, but also energy efficient gait. A promising new line of research could be the incorporation of CPG and reflex-like control in gait robots based on ballistic walking. The CPG controller would entrain to the efficient mechanics of the gait robot to provide efficient walking that is also highly controllable and robust against perturbations.

References

Azevedo C, Andreff N, Arias S (2004) BIPedal walking: From gait design to experimental analysis. Mechatronics 14:639

Brooke JD, Cheng J, Collins DF, McIlroy WE, Misiaszek JE, Staines WR (1997) Sensori-sensory afferent conditioning with leg movement: gain control in spinal reflex and ascending paths. Prog Neurobiol 51:393-421

Collins S, Ruina A, Tedrake R, Wisse M (2005) Efficient bipedal robots based on passive-dynamic walkers. Science 307:1082-5

Endo G, Morimoto J, Nakanishi J, Cheng G (2004) An empirical exploration of a neural oscillator for biped locomotion control. In: Proceedings - IEEE International Conference on Robotics and Automation. Vol. 2004: Proceedings- 2004 IEEE International Conference on Robotics and Automation, New Orleans, LA, pp 3036

Garcia M, Chatterjee A, Ruina A, Coleman M (1998) The simplest walking model: stability, complexity, and scaling. J Biomech Eng 120:281-8.

Hirai K, Hirose M, Haikawa Y, Takenaka T (1998) The development of Honda humanoid robot. In: Robotics and Automation, 1998. Proceedings. 1998 IEEE International Conference on. Vol. 2, pp 1321-1326 vol.2

Matsuoka K (1985) Sustained oscillations generated by mutually inhibiting neurons with adaptation. Biol Cybern 52:367-76

Matsuoka K (1987) Mechanisms of frequency and pattern control in the neural rhythm generators. Biol Cybern 56:345-53

McGeer T (1990) Passive dynamic walking. International Journal of Robotics Research 9:62-82.

Mochon S, McMahon TA (1980) Ballistic walking. J Biomech 13:49-57

Morimoto J, Endo G, Nakanishi J, Hyon SH, Cheng G, Bentivegna D, Atkeson CG (2006) Modulation of simple sinusoidal patterns by a coupled oscillator model for biped walking. In: Proceedings - IEEE International Conference on Robotics and Automation. Vol. 2006: 2006 IEEE International Conference on Robotics and Automation, ICRA 2006, Orlando, FL, pp 1579

Mu X, Wu Q (2003) Synthesis of a complete sagittal gait cycle for a five-link biped robot. Robotica 21:581

Park JH, Chung H (2000) Hybrid control of biped robots to increase stability in locomotion. Journal of Robotic Systems 17:187

Righetti L, Ijspeert AJ (2006) Programmable central pattern generators: An application to biped locomotion control. In: Proceedings - IEEE International Conference on Robotics and Automation. Vol. 2006: 2006 IEEE International Conference on Robotics and Automation, ICRA 2006, Orlando, FL, pp 1585

Sakagami Y, Watanabe R, Aoyama C, Matsunaga S, Higaki N, Fujimura K (2002) The intelligent ASIMO: system overview and integration. In: Intelligent Robots and System, 2002. IEEE/RSJ International Conference on. Vol. 3, pp 2478-2483 vol.3

Stein RB, Capaday C (1988) The modulation of human reflexes during functional motor tasks. Trends Neurosci 11:328-32

Tenore F, Vogelstein RJ, Etienne-Cummings R (2007) Sensor-based dynamic control of the central pattern generator for locomotion. In: Proceedings - IEEE International Symposium on Circuits and Systems: 2007 IEEE International Symposium on Circuits and Systems, ISCAS 2007, New Orleans, LA, pp 613

Tzafestas S, Raibert M, Tzafestas C (1996) Robust sliding-mode control applied to a 5-link biped robot. Journal of Intelligent and Robotic Systems: Theory and Applications 15:67

Wisse M, Schwab AL, Linde RQV (2001) A 3D passive dynamic biped with yaw and roll compensation. Robotica 19:275

Wisse M, Van Frankenhuyzen J (2003) Design and construction of Mike; a 2D autonomous biped based on passive dynamic walking. In: Proceedings of 2nd International Symposium on Adaptive Motion of Animals and Machines, Kyoto, Japan

Zehr EP, Stein RB (1999) What functions do reflexes serve during human locomotion? Prog Neurobiol 58:185-205.

Summary

Walking is a very important function of the human movement apparatus. The question how walking is controlled by the central nervous system is yet to be answered. A number of reasons lead us to believe that neural oscillators in the spinal cord, termed Central Pattern Generators (CPGs), have a major contribution to human gait control. Firstly, CPGs play a key role in locomotion of many animals by providing the basic rhythm for muscular activity and by interacting with the reflex system. Secondly, normal walking does not require attention: it goes automatically. Finally, a growing number of observations indicate the presence of CPGs in the human spine. A convincing example of the latter is the fact that anencephalic babies – having a brain stem but no cerebellum or cerebrum – are able to 'walk' on a treadmill and display coordinated stepping movements when their feet touch the ground.

At present, no bipedal gait model combines efficiency and robustness up to the level of human walking. The main motivation for the research in this thesis is to obtain fundamental knowledge of the principles that account for this reconciliation of efficiency and robustness in human walking. Other motivations come from the fields of rehabilitation and bipedal gait robots.

The goal of the conducted research is to find the basic principles of neural control that make human walking both efficient and robust. To achieve this goal, a bottom-up approach was chosen that started with analyzing the behavior and stability of posture under reflexive control and concluded with an efficient and robust spinal control of bipedal gait. This led to the following research questions that needed answering for the goal to be reached:

- What is the influence of different components of reflexive feedback on postural stability and associated dynamical behavior?

- Can the co-existence of CPGs and reflexes explain observed efficient and robust rhythmic limb movement?

- Can both efficiency and robustness be achieved in CPG-controlled walking or is there a trade-off between these gait qualities?

The first research question is addressed in chapter 2. The influence of reflexive feedback gains and delays on the behavior and stability in postural tasks is examined using a musculo-skeletal model of human stance. Bifurcation analysis is used to ascertain the boundaries of postural stability in terms of reflex parameters. A bifurcation represents a change to a qualitative different behavior of the system under parameter change. Linearization of the model links the bifurcations to bio-mechanical concepts.
We started off by investigating the influence of the stretch reflex, which is modeled by feedback of muscle lengthening and velocity with a typical delay of 50 ms. Branches of fold and Hopf bifurcations are calculated in a parameter space constructed by the positional and velocity feedback gains and divide the parameter space into regions of unstable posture, stable posture and stable limit cycles. The fold bifurcation represents zero ankle joint stiffness and is associated with the minimal positional feedback gain required for stable posture. Both increased co-contraction and positive force feedback lower the necessary minimal positional feedback gain, as they both increase the joint stiffness. The Hopf bifurcation represents an unstable reflex loop; beyond it stable limit cycles emerge that lead to oscillatory movement, which is associated with the pathology termed clonus. To prevent oscillatory movement a certain minimal velocity feedback gain is necessary to compensate for the phase lag caused by muscle activation dynamics, the presence of compliant tendons, and most of all the time delay in the reflex arcs. The latter has a profound effect on postural stability as increasing time delay shrinks the Hopf branch – and by that the region of stable posture – considerably. Oscillatory movement also occurs if the combined reflexive feedback – composed of muscle lengthening, velocity and positive force – is too large for a given co-contraction level. Higher co-contraction levels allow a higher combined reflexive feedback. Within the region of stable posture, the combination of co-contraction, reflex gains and delay determine dynamic characteristics such as natural frequency and relative damping. Areas of reflex gains used by healthy subjects in quiet and perturbed stance were estimated by fitting the model to the dynamic characteristics shown in data from literature. The overlap of these areas could indicate that stretch reflexes are important not only in perturbed, but also in quiet stance.

The second research question is answered in chapters 3 and 4. Both chapters discuss CPG-controlled single limb movement. In chapter 3 the limb including reflexes is represented by a general mass-spring-damper model, while in chapter 4 a neuro-musculo-skeletal model of the forearm is introduced.
Recent studies indicate the use of CPGs in human rhythmic limb movement. Firstly, reflex modulation experienced during arm and leg cycling is similar to that in animals with CPG-controlled rhythmic limb movement. Secondly, brain control is less and simpler for rhythmic arm movements compared to discrete movements: a major part of the control comes from spinal level. Other studies show that rhythmic arm movement is achieved by ‘resonance tuning’, that is, by actuating the arm in its resonance frequency automatically. The

preferred frequency in which people like to swing their arms matches the arm's resonance frequency, while the latter is changed to match a *desired* movement frequency by adjusting the limb's joint stiffness. This 'resonance tuning' behavior ensures maximal efficiency, as moving a system in its resonance frequency requires a minimal amount of energy.
In chapter 3 is investigated if the 'resonance tuning' behavior could be reproduced by a model of a limb coupled to a CPG. The limb's resonance frequency is varied between 1 to 20 rad/s by changing the joint stiffness. The type of afferent feedback to the CPG proves crucial for its resonance tuning capability. According to literature, at least afferent feedback from Ia and II fibers to the CPG's flexor and extensor centers is present. This is modelled by positional and velocity feedback of the limb's angle. Integral feedback is also investigated. The influence of the different types of afferent feedback is analyzed by DFA (i.e. describing function analysis) and checked by numerical simulations (i.e. bifurcation analysis and continuation of periodic solutions). Feedback of positional information provides resonance tuning above the endogenous frequency of the CPG (i.e. eigenfrequency of the CPG). Integral feedback provides resonance tuning at and below the endogenous frequency. Feedback of velocity information is necessary to compensate for the time delay in the loop, coupling limb to CPG; without it bi-stability occurs and resonance tuning is not possible at high movement frequencies. DFA showes that robustness against changes in limb parameters originates from the CPG's non-linear characteristics: the large spread in the CPG's gain plots – associated with different angular movement amplitudes – ensures entrainment between limb and CPG for a wide range of limb parameters. The PID-type afferent feedback shapes the phase coupling between CPG and limb to ensure that this entrainment leads to periodic movement in the limb's resonance frequency. This CPG model is the first to provide resonance tuning at natural limb frequencies above and below its endogenous frequency.
In chapter 4, besides the CPG's resonance tuning capability, the CPG's contribution in counteracting perturbations is investigated for a more realistic limb model. In a highly non-linear neuro-musculo-skeletal model of the forearm, for which the CPG is organized in parallel with the stretch reflexes, the limb's resonance frequency is varied by changing the reflex gain associated with feedback of muscle lengthening. To maintain a realistic damping ratio of the limb, the reflexive velocity feedback gain is adjusted accordingly. Integral feedback is thought of as an internal process of the CPG. The results show the CPG's ability to tune into a broad range of resonant frequencies of the forearm in hanging and inverse position. Increased co-contraction allows for higher maximum movement frequency, which is in agreement with studies of rhythmic forearm movements. The efficiency was shown by the very low muscle activation necessary to sustain steady-state periodic movement (even in inverse position only a few percent). The robustness of the CPG control was tested by applying force perturbations to the forearm in the most challenging, inverse position. The CPG delivers an increasing part of the necessary counteracting muscle

activation (up to 41%) for increasing perturbation size. The other part mainly originates from the local reflex loop. As far as we know, the proposed neuro-musculo-skeletal model is the first to explain the observed resonance tuning in human rhythmic arm movement.

The third research question is treated in chapters 5 and 6. In chapter 5 the efficiency of CPG-controlled walking is evaluated and in chapter 6 the trade-off between robustness and efficiency is investigated.
Like human walking, passive dynamic walking – i.e., walking down a slope with no actuation except gravity – is energy efficient by exploiting the natural dynamics of the limbs that act as inverse (stance leg) and hanging (swing leg) pendulums. In chapter 5 the efficiency of level-ground CPG-controlled walking is compared with passive dynamic walking. Each leg of the passive walker is locally coupled to its own CPG that controls the hip moment of force. The CPG achieves to control gait efficiently by tuning into the resonance frequency of the passive dynamics of the walker. Positional, integral and derivative (PID) afferent feedback of the limb angle play the same crucial role as in rhythmic single limb movement (chapters 4 and 5): resonance tuning above the CPG's endogenous frequency, resonance tuning at and below the endogenous frequency and compensation for time delay, respectively. The resonance tuning behavior of the CPG model allows the gait velocity to be controlled within a large range by a single parameter, while retaining the energy efficiency of passive dynamic walking.
In chapter 6 the limits regarding energy efficiency and robustness against perturbations are explored for a bipedal walking model with human-like mass distribution. A CPG is tightly coupled to each leg through sensory afferents and motor efferents. A great variety of different gaits in terms of energy efficiency, robustness, velocity, stride frequency and stride length are found by optimizing the afferent and efferent gains to different cost functions regarding energy efficiency and robustness. For the latter, our walker is subjected to two types of perturbations: its swing leg is pulled backwards during midswing and it encounters sudden ground level changes. The CPG-controlled walking model is found to be energy efficient compared to humans as well as to other bipedal walking machines. Robust gaits are found as well: the walker can even recover when its swinging leg is deprived of 70% of its angular velocity during midswing. Symmetry-breaking bifurcations, i.e. pitchfork bifurcations, are present throughout parameter space and represent transitions from symmetric to asymmetric gait. A strict trade-off between efficiency and robustness exists and is most evident symmetric walking.

In conclusion, we showed that CPGs could play a key role in reconciling energy efficiency and robustness in human rhythmic movement, such as arm swinging and walking. Reflexes shape the limb dynamics to which the CPGs entrain, while both reflexes and CPGs contribute in the recovery from perturbations. In the future, the CPG model can be used as part of a gait controller in applications such as walking robots or powered walking orthoses.

Samenvatting

Lopen is een belangrijke functie van het menselijk bewegingsapparaat. De vraag hoe lopen geregeld wordt door het centrale zenuwstelsel is nog onbeantwoord. Er zijn belangrijke aanwijzingen dat oscillatoren in de wervelkolom, genaamd Centrale Patroon Generatoren (CPGs), een grote bijdrage leveren aan de menselijke loopregeling. Ten eerste spelen CPGs een sleutelrol bij de voortbeweging van veel dieren door de verzorging van het basisritme van spieractiviteit en door interactie met het reflex systeem. Ten tweede is lopen geen bewuste beweging: het gaat automatisch. Ten slotte wijzen een groeiend aantal waarnemingen op het bestaan van CPGs in de menselijke wervelkolom. Een overtuigend voorbeeld hiervan is dat anencephalische baby's – met een hersenstam, maar zonder grote en kleine hersenen – gecoördineerde stappen maken wanneer hun voeten de grond raken en kunnen 'lopen' op een loopband.

Tot op heden is er geen model van tweebenig lopen dat zich kan meten aan menselijk lopen qua energetische efficiëntie en stabiliteit. De belangrijkste motivatie voor dit onderzoek is het begrijpen hoe efficiëntie en robuustheid in menselijk lopen samengaan. Andere motivaties komen uit het veld van rehabilitatie en tweebenige looprobots.

Het doel van het onderzoek is het vinden van de basis principes qua neurale regelingen, die menselijk lopen zowel efficiënt als robuust maken. Om dit doel te bereiken is voor een bottum-up aanpak gekozen. De eerste stap bestaat uit het analyseren van de invloed van reflexen op het gedrag en de stabiliteit van houdingstaken. De laatse stap moest een efficiënte en robuuste spinale regeling voor tweebenig lopen opleveren. Deze aanpak resulteerde in de volgende onderzoeksvragen die beantwoord moesten worden om het doel te bereiken:

- Wat is de invloed van verschillende componenten van reflexieve terugkoppeling op de stabiliteit en bijbehorend gedrag in houdingstaken?

- Kan de co-existentie van CPGs en reflexen de waargenomen efficiëntie en robuustheid in ritmische arm- en beenbewegingen verklaren?

- Kan zowel efficiëntie als robuustheid worden bereikt in CPG-geregeld lopen of is er een afweging tussen beide kwaliteiten?

De eerste onderzoeksvraag wordt uitgewerkt en beantwoord in hoofdstuk 2. De invloed van reflexieve terugkoppelfactoren en tijdsvertragingen op het gedrag en de stabiliteit in houdingstaken is onderzocht met behulp van een musculo-skeletair model van staan. Bifurcatie analyse is gebruikt om de grenzen van stabiliteit te bepalen in termen van reflex parameters. Een bifurcatie representeert een verandering naar een kwalitatief ander gedrag door parameterverandering. Linearisatie van het model koppelt de bifurcaties aan bio-mechanische concepten.
Het onderzoek is begonnen met de bepaling van de invloed van de monosynaptische reflex, die gemodelleerd is als terugkoppeling van de spierverlenging en spiersnelheid met een typische tijdvertraging van 50 ms. Curven van fold en Hopf bifurcaties zijn berekend in een parameterruimte opgespannen door de positie- en snelheidsterugkoppelfactoren. Deze curven verdelen de parameterruimte in gebieden van instabiliteit, stabiel staan en limiet cycli. De fold bifurcatie representeert het punt waarvoor er geen stijfheid in het enkelgewricht aanwezig is. Het is geassocieerd met de minimale positieterugkoppeling, die nodig is om stabiel te staan. Zowel verhoogde co-contractie als positieve krachtterugkoppeling verlagen de benodigde minimale positieterugkoppeling, omdat ze beiden leiden tot een verhoogde enkelstijfheid. De Hopf bifurcatie representeert een instabiele reflexboog. Na een Hopf bifurcatie ontstaat een stabiele limiet cyclus, die leidt tot periodieke beweging welke gerelateerd is aan het ziektebeeld clonus. Om dit te voorkomen is een bepaalde minimale snelheidsterugkoppeling nodig om de faseachterstand – veroorzaakt door spieractivatie dynamica, compliante pezen, maar vooral door de tijdvertraging in de reflexbogen – te compenseren. De tijdvertraging heeft een grote invloed op de stabiliteit van houdingstaken, aangezien de Hopf curve – en dus het gebied van stabiel staan – snel kleiner wordt voor grotere tijdvertraging. Voor een gegeven hoeveelheid co-contractie leidt een te grote totale reflexieve terugkoppeling, bestaande uit terugkoppeling van spierverlenging, snelheid en positieve kracht, ook tot periodieke beweging. Hogere co-contracties laten een hogere reflexieve terugkoppeling toe. Voor stabiel staan bepaalt de combinatie van co-contractie, reflexieve terugkoppelfactoren en tijdvertraging de dynamische eigenschappen zoals natuurlijke frequentie en relatieve demping. De dynamische eigenschappen tijdens normaal en geperturbeerd staan, afgeleid van data uit de literatuur, zijn als input gebruikt om de bijbehorende gebieden van reflexieve terugkoppelfactoren, die mensen normaal gebruiken, te schatten. Het feit dat deze twee gebieden overlappen, zou kunnen betekenen dat reflexen niet alleen in geperturbeerd staan, maar ook in normaal staan van groot belang zijn.

De tweede onderzoeksvraag wordt beantwoord in hoofdstukken 3 and 4. Beide hoofdstukken gaan over CPG-geregelde ritmische bewegingen van

armen en benen. In hoofdstuk 3 wordt een algemeen massa-veer-demper systeem als model voor een ledemaat met reflexen gebruikt, terwijl in hoofdstuk 4 een meer realistisch neuro-musculo-skeletair model van de onderarm wordt geïntroduceerd.
Uit recente studies komen aanwijzingen naar voren, die duiden op het gebruik van CPGs voor ritmische arm- en beenbewegingen in mensen. Ten eerste blijkt dat de reflex modulatie tijdens ritmische arm- en beenbewegingen in de mens gelijksoortig is aan die van dieren, waarvoor het gebruik van CPGs is aangetoond. Ten tweede is sturing vanuit het brein voor ritmische arm- en beenbewegingen veel minder en simpeler in vergelijking met discrete bewegingen: een groot deel van de sturing vindt dus plaats op spinaal niveau. Andere studies laten zien dat voor ritmische armbewegingen 'resonance tuning' wordt gebruikt. Resonance tuning wil zeggen dat een systeem automatisch in zijn resonantiefrequentie wordt aangestuurd. Wanneer aan mensen wordt gevraagd om met hun arm te zwaaien, dan doen ze dat in de resonantiefrequentie van de arm. Wanneer echter wordt gevraagd om de arm met een bepaalde voorgeschreven frequentie te zwaaien, dan wordt de resonantiefrequentie van de arm aan deze voorgeschreven frequentie aangepast door de gewrichtsstijfheid te veranderen. Dit 'resonance tuning' gedrag zorgt voor een maximale efficiëntie, aangezien het bewegen van een systeem in zijn resonantiefrequentie het minst energie kost.

In hoofdstuk 3 is onderzocht of het 'resonance tuning' gedrag zou kunnen worden gereproduceerd door een model van een ledemaat, die gekoppeld is aan een CPG. De resonantiefrequentie van de ledemaat is hierbij gevarieerd tussen 1 tot en met 20 rad/s door verandering van de gewrichtsstijfheid. Het type afferente terugkoppeling naar de CPG blijkt van cruciaal belang om het resonance tuning gedrag te bewerkstelligen. Volgens de literatuur is er mimimaal sprake van afferente terugkoppeling van de spieren naar de flexie en extensie centra van de CPG via Ia en II vezels. Deze is gemodelleerd door positie -en snelheidsterugkoppeling van de ledemaat's hoek. Integrale terugkoppeling is ook onderzocht. De invloed van deze PID-achtige afferente terugkoppelingen is geanalyseerd door DFA (i.e. describing function analysis) en gecontroleerd door numerieke simulaties (i.e. bifurcatie analyse en continuering van periodieke oplossingen). Terugkoppeling van positionele informatie geeft resonance tuning voor frequenties, die boven de endogene frequentie van de CPG (i.e. eigenfrequentie van de CPG) liggen. Integrale terugkoppeling geeft resonance tuning rondom en beneden de endogene frequentie. Snelheidsterugkoppeilng is nodig om de tijdsvertraging in de terugkoppellus tussen ledemaat en CPG te compenseren; anders ontstaat bi-stabiliteit en is resonance tuning niet mogelijk voor hoge bewegingsfrequenties. DFA laat ook zien dat de robuustheid tegen veranderende ledemaat parameters voortkomt uit de niet-lineariteit van de CPG: de grote spreiding in de CPG's modulus grafieken – geassocieerd met verschillende zwaai amplitudes – zorgt ervoor dat entrainment tussen

ledemaat en CPG plaats vindt voor een groot bereik van ledemaat parameters, zoals massa en stijfheid. Het PID-type afferente terugkoppeling bepaalt de fasekoppeling tussen CPG en ledemaat zodanig dat deze entrainment leidt tot periodieke beweging in de resonantiefrequentie van de ledemaat. Dit CPG model is de eerste, die zowel boven als onder de CPG's endogene frequentie resonance tuning laat zien.
In hoofdstuk 4 wordt, naast het resonance tuning vermogen van de CPG, ook de bijdrage van de CPG aan het tegengaan van perturbaties onderzocht. Hiervoor is een meer realistisch, hoogst niet-lineair, neuro-musculo-skeletair model van de onderarm gebruikt, waarbij de CPG en lokale reflexen parallel georganiseerd zijn. De resonantie frequentie van de onderarm is gevarieerd door de reflexieve terugkoppelfactor van spierverlenging te veranderen. De reflexieve snelheidsterugkoppelingsfactor is daarbij zodanig aangepast dat de arm een realistische relatieve demping behield. Integrale terugkoppeling wordt gezien als intern proces van de CPG. De resultaten laten zien dat de CPG de onderarm aanstuurt in zijn resonantie frequentie voor een groot bereik van resonantiefrequenties in zowel hangende als staande positie. Hogere co-contractie laat hogere maximum bewegingsfrequenties toe, wat in overeenstemming is met studies naar ritmische onderarm bewegingen. De efficiëntie is getoond aan de hand van de zeer lage spieractivatie, die nodig is om voortgaande periodieke beweging te bewerkstelligen (zelfs in staande positie slechts een paar procent). De robuustheid van de CPG regeling is getest door middel van kracht perturbaties op de onderarm in de meest uitdagende, staande positie. De CPG levert hierbij een toenemend aandeel van de spieractivatie (tot 41%) – nodig om de perturbaties tegen te gaan – bij toenemende perturbatie grootte. De rest van de spieractivatie komt grotendeels van de lokale reflexen. Voor zover wij weten, is dit voorgestelde neuro-musculo-skeletaire model het eerste, dat het resonance tuning gedrag in ritmische armbewegingen van mensen kan verklaren.

De derde onderzoeksvraag wordt behandeld in hoofdstukken 5 en 6. In hoofdstuk 5 wordt de energetische efficiëntie van CPG-geregeld lopen geëvalueerd en in hoofdstuk 6 wordt de afweging tussen robuustheid en efficiëntie onderzocht.
Passief dynamisch lopen – dat wil zeggen, over een kleine hoek naar beneden lopen zonder enige actuatie behalve de gravitatie – is net als menselijk lopen efficiënt door het uitbuiten van de natuurlijke dynamica van de benen, die dienst doen als staande (standfase) en hangende (zwaaifase) pendulums. In hoofdstuk 5 wordt de efficiëntie van CPG-geregeld lopen op vlakke vloer vergeleken met passief dynamisch lopen. Elk been van de passieve loper is hierbij lokaal gekoppeld aan zijn eigen CPG welke het heupmoment bepaald. De CPG bereikt energie efficiënt lopen door de passieve loper in de resonantie frequentie aan te sturen. Afferente terugkoppeling van heuphoek, hoeksnelheid en de geïntegreerde hoek (dat wil zeggen, PID terugkoppeling van de heuphoek) spelen dezelfde cruciale rol als in ritmisch armzwaaien (hoofdstukken 3 and 4). Terugkoppeling van de heuphoek geeft resonance

tuning boven de CPG's endogene frequentie, terwijl terugkoppeling van de hoek's integraal resonance tuning rondom en onder de endogene frequentie geeft. Terugkoppeling van de hoeksnelheid compenseert voor tijdvertragingen. Het resonance tuning gedrag van het CPG model zorgt ervoor dat de loopsnelheid binnen een groot bereik gecontroleerd kan worden met een enkele parameter, terwijl de efficiëntie van passief dynamisch lopen behouden blijft.
In hoofdstuk 6 worden de grenzen qua efficiëntie and robuustheid tegen perturbaties verkend voor een tweebenig loopmodel met menselijke massaverdeling. Aan elk heup is een CPG gekoppeld via sensorische afferenten and motorische efferenten. Veel verschillende looppatronen wat betreft energieverbruik, robuustheid, snelheid, stapfrequentie en stapgrootte zijn gevonden door middel van optimalisatie van de grootte der afferente en efferente koppelingen naar verschillende kostfuncties in termen van energie efficiëntie en robuustheid. Wat robuustheid betreft, onderging onze loper twee typen perturbaties: er werd aan zijn zwaaibeen getrokken gedurende het midden van de zwaaifase en hij onderging plotselinge veranderingen in de hoogte van de grond. Het CPG-geregelde loopmodel is energiezuinig bevonden vergeleken met zowel mensen als andere tweebenige loopmechanismen. Robuuste looppatronen zijn ook gevonden: het loopmodel kan zijn balans zelfs herstellen, nadat het zwaaibeen 70% van zijn hoeksnelheid was afgenomen. Symmetriebrekende bifurcaties – dat wil zeggen, pitchfork bifurcaties – zijn veelvuldig aanwezig in de parameterruimte and geven de overgang van symmetrisch naar asymmetrisch lopen weer. Een strikte afweging tussen efficiëntie and robuustheid bestaat wel degelijk en is het meest duidelijk aanwezig in symmetrisch lopen.

In deze studie hebben we laten zien dat CPGs een sleutelrol kunnen spelen in het samengaan van efficiëntie and robuustheid voor ritmische bewegingen van de mens, zoals armzwaaien en lopen. Reflexen veranderen de dynamica van armen en benen, naar welke de CPGs entrainen. Na perturbaties participeren zowel de reflexen als de CPGs in het herstel van de ritmische beweging. In de toekomst kan het CPG model gebruikt worden als onderdeel van een loopregeling in applicaties zoals looprobots en geactueerde orthesen.

Dankwoord

Tijd is relatief. Voor mij lijkt de tijd de laatste tijd zelfs tegelijkertijd langzaam en snel te zijn verlopen. Ik kan me haast niet voorstellen dat het al twee en een half jaar geleden is dat ben ik bij Nefit begon te werken en parallel daaraan mijn proefschrift moest afronden. De tijd vloog om, waarschijnlijk door gebrek aan vrije tijd, of misschien eerder nog, het idee of besef van dit gebrek, waardoor ik mezelf geen vrije tijd gunde, maar stiekem af en toe toch toebedeelde, al was het maar uit pure noodzaak (heerlijk lange zin, hier mag het ;-)). Aan de andere kant leek het schrijven van het proefschrift niet vooruit te branden. Het was soms zelfs alsof ik terug in de tijd ging. Echter, door niet te strak te plannen kon ik mezelf meestal voor de gek houden door te zeggen dat alles 'volgens plan' verliep.

Buiten bovenstaand geneuzel wil ik hier vooral de mensen bedanken, die het mede mogelijk gemaakt hebben dat dit proefschrift nu daadwerkelijk voor u open ligt. Allereerst wil ik mijn promotoren Bart Koopman en Frans van der Helm bedanken. Frans, bedankt voor je inspiratie en motivatie. Als je ooit nog ander werk zou willen – al geloof ik daar niks van – dan kun je altijd nog als 'professional motivator' aan de slag. Sorry, dat ik niet door had dat je niet bij Twente weg mocht totdat ik gepromoveerd was. Bart, jou wil ik graag bedanken voor je nuchtere blik en toewijding. Je stond altijd klaar als ik er om vroeg. Speciaal voor jou heb ik zo lang gewacht met promoveren, dat je als professor in de commissie kon plaatsnemen. Ik wil hier ook Stephan van Gils bedanken voor zijn wiskundige assistentie gedurende de beginperiode van mijn project. Al zaten we niet altijd in dezelfde toestandsruimte tijdens discussies (jij zat soms al in 'Riemann space', terwijl ik nog op planeet aarde zat), we hebben wel samen een mooi eerste artikel geschreven.
Vervolgens wil ik mijn kamergenoten op chronologische volgorde bedanken. De eerste twee jaar zat ik op de kamer met Hendrik-Jan Boven. Al waren veel van onze discussies over muziek, whiskey, wetenschap en vage ideeën omtrent energie-extractie uit zwarte gaten niet altijd goed voor de voortgang van mijn onderzoek, ze waren het wel voor mijn humeur! De laatste jaren heb ik op de kamer doorgebracht met Miguel Aznar Alonso en Martijn Klein Horsman. Aan mijn Spaanse vriend zijn glazige ogen kon ik altijd goed aflezen dat mijn tekst nog een tikkeltje onbegrijpelijk was. Martijn – die pas geleden en dus voor mij gepromoveerd is (shame on me) – fungeerde ook

als klankbord, maar dan vooral op het gebied van muziek en wereldbeeld. Verder wil ook alle collega's en (oud)studenten van de vakgroep Biomedische Werktuigbouwkunde, alsmede enkele van de BSS groep, bedanken voor de goede sfeer en medewerking. Vele gezellige koffiepauzes, vakgroepuitjes, café bezoekjes en niet te vergeten het squashen en zaalvoetbal, droegen bij aan een plezierige werkomgeving de afgelopen jaren. Van de vakgroep wil ik nog even Herman van der Kooij en Anton Sanders apart noemen. Met Herman heb ik veel discussies gehad over de controle van balans in staan en lopen. Ook al waren we het lang niet altijd eens, de werklust waarmee hij zich op een onderwerp kan storten moet bewonderd worden. Met Anton heb ik het vaak gehad over toepassingen van mijn CPG model in de revalidatie. Ik heb veel waardering voor zijn praktische en pragmatische blik op dit gebied en hoop dat er in de toekomst nog wat gedaan wordt met onze ideeën. Van de vier studenten die ik begeleid heb tijdens hun afstuderen waren Hendrik-Jan Boven en Koen Mulder al bezig toen ik begon. Door de uitgebreide literatuur studies die zij al hadden gedaan kreeg ik een 'head start'. Daarna heb ik slechts twee studenten kunnen vinden die zo gek waren om op dit gebied, of met mij als begeleider, af te studeren, namelijk Sita Drost en Arnout van den Broeke. Arnout wil ik speciaal bedanken voor de hoeveelheid tijd en werklust, die hij in zijn afstudeerwerk heeft gestoken. Dit heeft hem het mede-auteurschap van een boekartikel (hoofdstuk 6) opgeleverd.
Verder wil ik ook mensen bedanken, die geen directe wetenschappelijke bijdrage aan het proefschrift hebben geleverd, maar wel hebben gezorgd voor de nodige afleiding en ondersteuning. Allereerst wil ik Jos Aarninkhof en Dennis van Heijningen van Nefit B.V. bedanken voor de mogelijkheid mijn uren flexibel in te zetten wanneer dat nodig was.
Belangrijker dan het promoveren zelf zijn natuurlijk vrienden en familie. Matthias van Ardenne wil ik bedanken voor zijn onuitputtelijke motivatie, al werd deze meestal al hijgend op de fiets via een mobiele telefoon mijn kant op gestraald. Arno de Jong wil ik bedanken voor de vele avonden 'supper with gaming entertainment'. Ik ben blij dat je me altijd laat winnen met PES, zodat ik me weer onoverwinnelijk voel als ik huiswaarts keer ;-) Matthias en Arno, bedankt dat jullie mijn paranimf willen zijn! Verder heeft het spelen in een band voor jaren plezierige afleiding gezorgd. De muziekstijl is gegroeid van simpele pop en rock naar uitdagende jazz en funk, wat mij veel voldoening geeft. Daarvoor wil ik de bandleden, Erik-Jan de Hoon, Pieter Lerou, Joost van Ingen, Marjolein Hilgerink en oud-bandgenoot alsmede oud-huisgenoot Alex Hendriks bedanken. Ook het biertje na de repetitie met bijbehorend geouwehoer is erg relaxed. Pa en ma, jullie zijn letterlijk het begin van mij. Voor dat en jullie eeuwige zorg en toewijding, bedankt! Mijn zus Nadja wil ik bedanken voor het feit dat ze altijd zichzelf is, en dat je kunt komen en gaan wanneer je wilt. En last but not least, wil ik mijn vriendin Gea bedanken voor haar 'moral support'. Ze moet ondertussen wel moe zijn van mijn moe zijn en ik denk dat ik haar nog moet overtuigen dat ik vanaf heden niet meer zo vaak 'te druk' zal zijn.